TECHNICAL DIGEST

MPLP-2018

The VIII International Symposium

“MODERN PROBLEMS OF LASER PHYSICS”

Novosibirsk, Russia, 25 August – 01 September, 2018

mplp2018.laser.nsc.ru

Organized by:

Institute of Laser Physics, SB RAS, Novosibirsk, Russia

Novosibirsk State University, Novosibirsk, Russia

Institute of Spectroscopy, RAS, Troitsk, Moscow, Russia

Federal State Unitary Enterprise "VNIIFTRI", Mendeleevo, Moscow region, Russia

Supported and Sponsored by:

Federal Agency for Scientific Organizations

Russian Academy of Sciences

Russian Foundation for Basic Research

The Nauchnoe Oborudovanie Group of Companies

INTERNATIONAL ADVISORY COMMITTEE

Sergei Arakelian	*Vladimir State University, Vladimir, Russia*
Nicolò Beverini	*Dipartimento di Fisica, Universita' di Pisa, Italy*
Elizabeth Donley	*National Institute of Standards and Technology, Boulder, USA*
Martial Ducloy	*Laboratoire de Physique des Lasers, Universite Paris-Nord, France*
John Kitching	*National Institute of Standards and Technology, Boulder, USA*
Nikolai Kolachevsky	*P.N. Lebedev Physics Institute RAS, Moscow, Russia*
Sergei Kulik	*Lomonosov Moscow State University, Russia*
Leong Chuan Kwek	*Centre for Quantum Technologies, National University of Singapore*
Gerhard Leuchs	*Max Planck Institute for the Science of Light, Erlangen-Nuremberg, Germany*
Kyung Hyun Park	*Electronics and Telecommunications Research Institute, Korea*
Ekkehard Peik	*Physikalisch-Technische Bundesanstalt, Braunschweig, Germany*
Hélène Perrin	*Université Paris 13, Villetaneuse, France*
Ernst Rasel	*Institute of Quantum Optics, Hanover, Germany*
Igor Ryabtsev	*Rzhanov Institute of Semiconductor Physics SB RAS, Novosibirsk, Russia*
Anatoly Shalagin	*Institute of Automation and Electrometry SB RAS, Novosibirsk, Russia*
Alexander Shkurinov	*Lomonosov Moscow State University, Russia*
Feng Song	*Nankai University, Tianjin, China*
Aleksei Taichenachev	*Institute of Laser Physics SB RAS, Novosibirsk, Russia*
Andrey Turlapov	*Institute of Applied Physics RAS, Nizhny Novgorod, Russia*
Ken-ichi Ueda	*Institute for Laser Science, University of Electro Communications, Tokyo, Japan*
Antoine Weis	*University of Fribourg, Fribourg, Switzerland*
Victor Zadkov	*Institute of Spectroscopy RAS, Troitsk, Russia*
Ming-Sheng Zhan	*Wuhan Institute of Physics and Mathematics, Chinese Academy of Sciences, Wuhan, Cnina*
Alexey Zheltikov	*Lomonosov Moscow State University, Russia*

Symposium Chair: Prof. Sergei N. Bagayev, *Institute of Laser Physics, SB RAS*

Symposium Secretary: Dr. Oleg N. Prudnikov, *Institute of Laser Physics, SB RAS*

Table of Contents

Oral Presentations

1. New trends in laser physics

2. High-resolution spectroscopy and fundamental metrology

3. Physics of ultracold atoms, ions, and molecules

4. Atom interferometers, magnetometers and other quantum sensors

5. Quantum optics and quantum information

6. Ultrahigh laser fields and attoscience

7. Nonlinear optics and novel phenomena

8. Nano- and femto- photonics: Foundations and applications

9. Fiber optics and fiber lasers

10. Applications of laser radiation from THz to UV in biomedicine, technology and other fields

Poster Sessions

Quantum information science: State of art and perspectives

S. Kulik[1,2]
[1]*Faculty of Physics, M.V. Lomonosov Moscow State University, 119991, Moscow, Russia*
[2]*Quantum Technologies Centre, M.V. Lomonosov Moscow State University, 119991, Moscow, Russia*
E-mail: sergei.kulik@physics.msu.ru

The talk reports the current state and prospects of the interdisciplinary field of knowledge - Quantum Information Processing and Computation (QIPC).

Basically, QIPC includes three large sections: quantum computation, quantum communications, and quantum information science.

The report will consider general and some special issues related to the theoretical and experimental aspects of QIPC mainly related to quantum computation, quantum communications.

The focus is on the main technologies of QIPC developed in the world, and especially in the Russian Federation, which potentially lead or have already led to the creation in the near future of quantum simulators and quantum communication systems.

In the field of quantum computation/simulators, these are technologies that exploit neutral atoms and ions in traps as working physical systems, superconducting systems, impurity structures, and linear optical systems.

In the field of quantum communication - is the creation of a global network based on fiber-optic, atmospheric and space channels.

Separately, the main problems of the implementation of certain nodes/elements of the systems of quantum simulators and quantum coupling are considered.

In the second part of the talk I will present an overview of the experimental results in the field of quantum computation and quantum coupling, which are held at the Faculty of Physics, within the framework of the Center for Quantum Technologies of the Moscow State University. Prospects for the development of these two areas will be considered in the context of the rapid growth of interest in the world in quantum technologies. On the example of two physical systems - photonic chips and neutral atoms in optical traps, the principles of quantum computation and the main stages in the construction of quantum computers will be presented.

In the final part, three particular projects will be presented. These large complex projects are carried out at the MSU Faculty of Physics together with number of partners:

- Optical Quantum Simulators;
- Development and creation of high-speed quantum encoders;
- "Quantum telephone".

Atom interferometry for high sensitivity in inertial measurements

A. Landragin, X. Alauze, M. Altorio, A. Bonnin,
R. Geiger, A. Imanaliev, R. Karcher, S. Merlet,
F. Pereira Dos Santos, D. Savoie, L. Sodorenkov
LNE-SYRTE, Observatoire de Paris, Université PSL, CNRS, Sorbonne Université,
61 avenue de l'Observatoire, 75014, Paris, France
E-mail: arnaud.landragin@obspm.fr

Since the pioneering experiments of 1991, atom interferometry has established as a unique tool for precision measurements of fundamental constants and of gravito-inertial effects. Atom interferometry covers multiple applications in metrology, inertial navigation, geophysics, tests of fundamental physics, and has been proposed for gravitational wave detection. Indeed, atom interferometry combines both intrinsic high sensitivity and accuracy thanks to the high level of control of the atom-laser interaction. Beyond the proof of principle, the main difficulties lie on the development of the methods and the high level of control in order to fulfill these expectations.

One of the first major achievements so far in term of application is the realization of absolute atomic gravimeters, which already compete with the state of the art absolute gravimeters. After a first period of development and validation of their performances, including participations to international key comparisons, we will show that recent developments based on the use of ultra-cold atom sources allows reaching record-breaking accuracies at the level of 10^{-8} m.s^{-2} [1].

If most of the results have been demonstrated in laboratory environment, some significant developments have been done in order to achieve field measurements [2] and even onboard mobile carrier. In particular, we have demonstrated the ability of performing measurements in a plane and in weightless with two different species of atoms, which constitutes a fundamental test of the equivalence principle [3]. This result is an important step in order to prepare both a test of the equivalence principle in a dedicated space mission [4] and inertial navigation applications.

Two important limitations of cold atom interferometers are the low bandwidth when using long interaction time for high sensitivity and dead times between successive measurements, corresponding to the preparation of the atom source prior to the injection in the interferometer. We present a matter-wave gyroscope with 11 cm^2 Sagnac area operating without dead times [5] and at a sampling frequency of 3.75 Hz. This is achieved by interleaving the atom laser-cooling step and the interrogation of the atoms. We demonstrate a record short term sensitivity of 32 nrad.s^{-1}.Hz$^{-1/2}$, which allows us to characterize and stabilize systematic effects below 3×10^{-10} rad.s^{-1} after 15 000 seconds of integration time. Such level of stability competes with best long term stabilities obtained with fiber-optics gyroscopes, and paves the way for applications of cold-atom sensors in inertial navigation or geoscience.

Beyond the developments of cold atom interferometers using free falling atoms, significant efforts are carried out in order to propose and demonstrate alternative methods based on trapped or guided atoms with dipole [6] and/or magnetic traps [7]. Such interferometers benefit from the possibility of extending the interrogation time and might lead to the realization of more compact sensors. As they keep the atom better localized, they are also promising candidates for applications to inertial navigation and local force measurements. We will present our latest results on an interferometer based on trapped atoms in an optical lattice [6], which features a state of the art force sensitivity, of 7.10^{-30} N/Hz$^{1/2}$, and an excellent spatial resolution of 2.5 µm. This sensor will be used to probe local (1-10µm) forces and perform fundamental tests of the short range atom-surface interactions.

In conclusion, atom interferometry is an active field both in term of sensors and in term of applications. The increasing knowledge in the domain leads to new projects as onboard gardiometry [8] and gravitational wave detector [9].

References

[1] R. Karcher, et al. arXiv:1804.04909 (2018).
[2] B Fang, et al. *J. Phys.: Conf. Ser.* **723** 012049 (2016).
[3] B. Barrett, et al. Nature Communications **7**, 13786 (2016).
[4] D. Aguilera, et al. , Class. Quantum Grav. **31**, 115010 (2014).
[5] I. Dutta, et al. Phys. Rev. Lett. **116,** 183003 (2016).
[6] M-K. Zhou, et al. Phys Rev A **88**, 013604 (2013).
[7] C. L. Garrido Alzar, Phys. Rev. A 97, 033405 (2018).
[8] K. Douch, et al. Advances in Space Research **61**, 1307-1323 (2018).
[9] W. Chaibi, et al. Phys. Rev. D 93, 021101 (2016).

Trapped ion optical clocks and tests of the equivalence principle

E. Peik
Physikalisch-Technische Bundesanstalt, 38116, Braunschweig, Germany
E-mail: ekkehard.peik@ptb.de

Optical clocks based on different atoms and ions with systematic uncertainties in the low 10^{-18} range allow for frequency comparisons and precise measurements of frequency ratios [1]. These can be used in tests of fundamental physics, especially quantitative tests of relativity and searches for violations of the equivalence principle [2]. The $^{171}Yb^{+}$ optical clock that is based on the extremely narrow S-F electric octupole transition possesses a favorable combination of small systematic uncertainty [3] and high sensitivity for such tests because of the strongly relativistic character of the excited state. In comparisons of two $^{171}Yb^{+}$ single-ion clocks, a ^{87}Sr optical lattice clock and primary Cs clocks at PTB we perform tests for temporal variations of the fine structure constant, the proton-to-electron mass ratio and for violations of local Lorentz invariance and obtain improved limits on possible violations of the equivalence principle in these cases. A future nuclear clock based on the low-energy transition in Th-229 may further increase the sensitivity of such tests. Recent results from hyperfine spectroscopy of the Th-229 isomer provide experimental data on fundamental nuclear properties of this unusual system [4].

References

[1] A. D. Ludlow, M. M. Boyd, Jun Ye, E. Peik, P. O. Schmidt, Rev. Mod. Phys. **87**, 637 (2015).
[2] M. S. Safronova, D. Budker, D. DeMille, Derek F. Jackson Kimball, A. Derevianko and C. W. Clark, arXiv 1710.01833, Rev. Mod. Phys. (in print).
[3] N. Huntemann, C. Sanner, B. Lipphardt, Chr. Tamm, and E. Peik, Phys. Rev. Lett. **116**, 063001 (2016).
[4] J. Thielking, M. V. Okhapkin, P. Glowacki, D. M. Meier, L. v. d. Wense, B. Seiferle, C. E. Düllmann, P. G. Thirolf, E. Peik, Nature **556**, 321 (2018).

Recent advances in high-precision optical clocks based on ultracold atoms and ions

S. Bagayev[1,2], A. Taichenachev[1,2], and V. Yudin[1-3]
[1]*Institute of Laser Physics SB RAS, Novosibirsk, Russia*
[2]*Novosibirsk State University, Novosibirsk, Russia*
[3]*Novosibirsk State Technical University, Novosibirsk, Russia*
E-mail: taichenachev@laser.nsc.ru

Presently, laser spectroscopy and fundamental metrology are among the most important and actively developed directions in modern physics. Frequency and time are the most precisely measured physical quantities, which, apart from practical applications (in navigation and information systems), play critical roles in tests of fundamental physical theories (such as QED, QCD, unification theories, and cosmology) [1,2]. Now, laser metrology is confronting the challenging task of creating an optical clock with fractional inaccuracy and instability at the level of 10^{-18} and better. Indeed, considerable progress has already been achieved along this path for both ion-trap [3,4] and atomic-lattice-based [5,6] clocks.

Work in this direction has stimulated the development of novel spectroscopic methods such as spectroscopy using quantum logic [7], magnetically induced spectroscopy [8], hyper-Ramsey spectroscopy [9], spectroscopy of "synthetic" frequency [10] and others [11,12]. Part of these methods was developed in order to excite and detect strongly forbidden optical transitions. The other part fights with frequency shifts of various origins. In the present talk we will review both parts with a special emphasis on methods developed and studied in Institute of Laser Physics SB RAS, Novosibirsk. The history and present status of experimental works devoted to the optical frequency standards will be discussed.

This work was supported by the Russian Scientific Foundation (projects No. 16-12- 00052 and No. 16-12- 00054).

References

[1] S.N. Bagayev et al., Appl. Phys. B 70, 375 (2000).

[2] S.A. Diddams et al., Science 306, 1318 (2004).

[3] T. Rosenband et al., Science 319, 1808 (2008); C.W. Chou et al., Phys. Rev. Lett. 104, 070802 (2010).

[4] N. Huntemann et al., Phys. Rev. Lett. 116, 063001 (2016).

[5] T. Akatsuka,M. Takamoto, and H. Katori, Nature Physics 4, 954 (2008).

[6] N. Hinkley et al., Science 341, 1215 (2013); B.J. Bloom et al., Nature 506, 71 (2014).

[7] P.O. Schmidt et al., Science 309, 749 (2005).

[8] A.V. Taichenachev et al., Phys. Rev. Lett. 96, 083001 (2006); Z. Barber et al., Phys. Rev. Lett. 96, 083002 (2006).

[9] V.I. Yudin et al., Phys. Rev. A 82, 011804(R) (2010); N. Huntemann et al., Phys. Rev. Lett. 109, 213002 (2012); T. Zanon-Willette et al., Phys. Rev. A 96, 023408 (2017).

[10] V.I. Yudin et al., Phys. Rev. Lett. 107, 030801 (2011); V.I. Yudin et al., Phys. Rev. A 94, 052505 (2016).

[11] V.I. Yudin et al., Phys. Rev. Lett. 113, 233003 (2014).

[12] Ch. Sanner et al., Phys. Rev. Lett. 120, 053602 (2018); V.I. Yudin et al. Phys. Rev. Applied 9, 054034 (2018).

An optical clock using $^{176}Lu^{+}$

M.D. Barrett[1,2], K.J. Arnold[1,2], R. Kaewuam[1,2], T.R. Tan[1,2]
[1]*Department of Physics, National University of Singapore, 119077*
[2]*Center for Quantum Technologies, Singapore, 117543*
E-mail: phybmd@nus.edu.sg

Singly ionized lutetium ($^{176}Lu^{+}$) is an optical clock candidate with three available clock transitions: a highly forbidden M1 transition at 848nm ($^1S_0$-$^3D_1$), a spin-forbidden E2 transition at 804nm ($^1S_0$-$^3D_2$), and an E2 transition at 577nm ($^1S_0$-$^1D_2$), [1,2,3]. A technique of hyperfine averaging eliminates shifts arising from the electronic angular momentum [1], which realizes an effective J=0 to J=0 transition in each case. This provides reference frequencies with low sensitivity to electric and magnetic fields. In particular, the 848-nm transition has the lowest blackbody radiation shift of all clock candidates under active consideration, and the 804-nm transition has a negative differential scalar polarizability allowing micromotion shifts to be cancelled for a judiciously chosen trap drive frequency [4]. Additionally, a narrow electric dipole transition provides suitable detection and a low Doppler cooling limit.

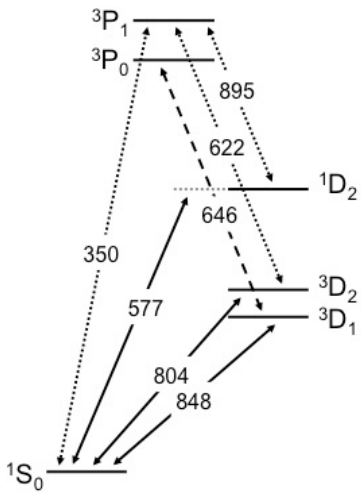

Fig. 1 Level structure of Lu^{+} showing the relevant clock (solid), detection (dashed) and repump (dashed) transitions.

The level structure and relevant transitions are illustrated in Fig. 1 along with the approximate wavelengths. All lasers are diode laser based with the 577-, 622-, and 350-nm lasers being frequency doubled systems. The 577- and 622-nm lasers are frequency doubled via fiberized waveguide doublers. Where necessary multiple hyperfine levels are addressed using wideband fiberized electro-optic modulators. This offers the possibility of a highly compact laser system suitable for the development of a portable atomic clock. With the exception of the 350-nm transition, wavelengths are also suitable for chip-scale integration.

So far we have measured the differential scalar polarizabilities for the 804- and 848-nm clock transitions using a CO_2 laser (10.6um), which characterizes the blackbody radiation (BBR) shift at room temperature [4]. In addition we have measured the dynamic polarizabilities over a range of wavelengths to characterize the dynamic BBR correction. Measurements at near-resonant wavelengths of 598 ($^3D_1$-$^3P_1$) and 646nm have been carried out via two independent measurement schemes. This provides both an accurate determination of the two dominant contributions to the dynamic polarizability of the 848-nm transition and a consistency check of our experimental method. We are now working to implement sub-Doppler cooling and a clock-to-clock comparison.

References

[1] M. D. Barrett, New J. Phys., **17** (5), 053024, (2015).
[2] Eduardo Paez, et al. Phys. Rev. A, **93** (4), 042112, (2016).
[3] R. Kaewuam, A. Roy, T. R. Tan, K. J. Arnold, and M. D. Barrett, J. Mod. Opt., **65** (5-6), 592, (2017).
[4] K. J. Arnold, R. Kaewuam, A. Roy, T. R. Tan, and M. D. Barrett, Nat. Comm., **9**, 1650, (2018).

Modified primary time and frequency standard of VNIIFTRI based on the use of cooled atoms technologies

S.I. Donchenko[1], A.N. Schipunov[1], I.Yu. Blinov[1], N.B. Koshelyaevsky[1], I.B. Noretz[1], Yu.F. Smirnov[1], V.G. Palchikov[1,2]

[1]FGUP "VNIIFTRI", Mendeleevo, 141570, Moscow region, Russia

[2]National Research Nuclear University "MEPhI", Moscow, 115409, Russia

E-mail: vitpal@mail.ru

The National time scale of the Russian Federation is reproduced and maintained based on the use the primary State standard of time and frequency operated at a facility located in Mendeleevo, Moscow region, Russia. The main purpose of the VNIIFTRI system of primary frequency standards, comprising two caesium fountains, is to perform regular calibrations of the international time-scale TAI/UTC at the highest accuracy and to provide a stable reference for the construction and steering of UTC(SU), as well as the local representation of UTC in Russia. The primary frequency standards based on the use of modern laser cooling technologies, which provides the working temperature for atoms up to the level of several micro kelvin.

It is important to note, that the system of primary frequency standard can be use also for absolute frequency measurements of optical frequency standards using femto-second Comb techniques developed at VNIIFTRI. VNIIFTRI is involved substantially in the implementation of the Federal special-purpose programme GLONASS, and it is the principal metrological Institution of Russia, concerned with creation of new and upgrading of existing standard means of timing, positioning and navigation support with the aim of achieving the prescribed accuracy characteristics of GLONASS.

The UTC(SU) time scale is currently transmitted to the GLONASS Ground Control Segment using signal receivers. The UTC(SU) time scale is a representation of UTC in accordance with the BIPM requirements.

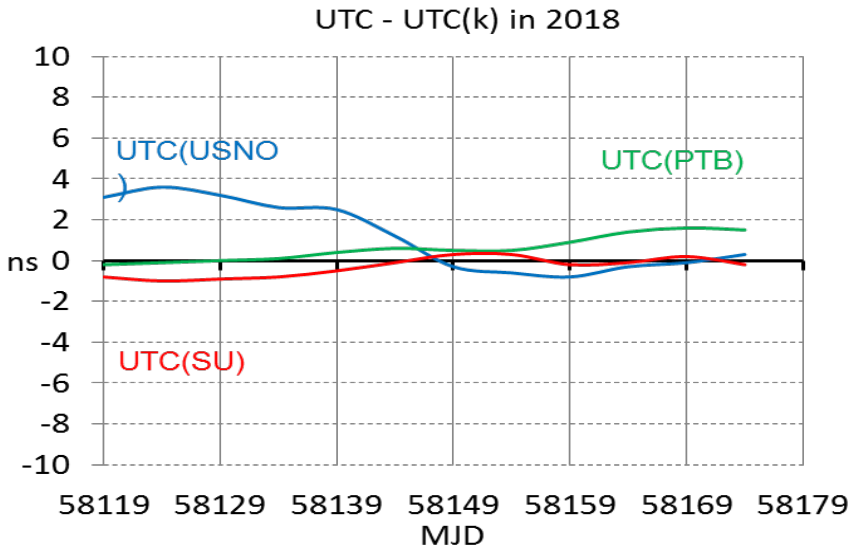

Fig. 1 National local representations of UTC (k).

As follows from the BIPM Circular T, the UTC(SU) time offset from UTC has not exceeded several ns in this year (see, for example, Fig. 1).

Progress towards a $^{40}Ca^{+}$ optical clock with a fractional uncertainty at the 10^{-18} level

K. Gao, Y. Huang, and H. Guan
Wuhan Institute of Physics and Mathematics, Chinese Academy of Sciences, Wuhan, 430071, China
E-mail: klgao@wipm.ac.cn

We recently reported a 5×10^{-17} level frequency comparison of two $^{40}Ca^{+}$ optical clocks, one of which has fractional frequency uncertainty of 3.4×10^{-17}, limited by the BBR effect. Here we present progress towards a $^{40}Ca^{+}$ optical clock with uncertainty at the 10^{-18} level. The differential static scalar polarizability $\Delta\alpha_0$ of the $^{40}Ca^{+}$ ion clock transition is obtained by precisely measuring the "*magic*" rf drive frequency. $\Delta\alpha_0$ is measured as $-7.2614(21)\times10^{-40}$ J m^2/V^2, the blackbody radiation shift is then calculated to be 0.37880(12) Hz at 300 K. The contribution of the blackbody shift coefficient to the uncertainty of the optical clock at room temperature is reduced to 5.6×10^{-19}, the excess micromotion induced clock uncertainty is also reduced to the 10^{-19} level by choosing the appropriate trap drive frequency. With a suppression of the BBR field temperature uncertainty to the sub-Kelvin level and improved clock stability, a robust, relatively low-cost $^{40}Ca^{+}$ ion clock with uncertainty at 10^{-18} level can be made.

The optical clocks with lowest fractional frequency uncertainties reported to date are the $^{171}Yb^{+}$ ion clock [1] and the ^{87}Sr optical lattice clock [2], both have reached uncertainty at the low 10^{-18} level. Since most of the clocks are running at the room temperature, the blackbody radiation effect contributes the largest frequency shift in most of state-of-artion or neutral atom optical clocks [1-4].

The blackbody radiation (BBR) shift at the room temperature is related to the differential static scalar polarizability $\Delta\alpha_0$. However, the state-of-art theoretical calculations of $\Delta\alpha_0$ only have uncertainty at the 1% level [5-8], which will contribute BBR shift uncertainty at the 10^{-17} level. $\Delta\alpha_0$ can be experimentally measured, which can give results with much higher precision. For neutral atom clocks, $\Delta\alpha_0$ of Yb [9] and Sr [10] are obtained by measuring the clock frequency shift due to applied dc electric fields, introduced by using precision parallel-plate capacitors. For the single-ion-based clocks, $\Delta\alpha_0$ of Yb^{+} is obtained by measuring clock shifts under near-infrared laser radiation with different wavelengths [1]; $\Delta\alpha_0$ of Sr^{+} is obtained by measuring the trap driving frequency at which the quadratic scalar Stark shift and the 2nd order Doppler shift due to the ion micromotion cancel each other [3].

The uncertainty of theoretically calculated $\Delta\alpha_0$ contributes 1.3×10^{-17} to our clock uncertainty. Via precisely measuring the "*magic*" trap drive frequency, $\Delta\alpha_0$ is experimentally measured with uncertainty of 0.06%, ~19 times better compared to the best atomic structure calculations with uncertainty of ~1.15% [5]. To our knowledge, our measurement of $\Delta\alpha_0$ currently has the lowest uncertainty over a variety of ion-based optical clocks.

For a $^{40}Ca^{+}$ ion trapped in a Paul trap, at drive frequency of $\Omega_0 \approx \frac{e}{mc}\sqrt{-\frac{h\nu_0}{\Delta\alpha_0}}$, the total micromotion-related shift will be zero [3]. The frequency Ω_0 is so-called the "*magic*" trap drive frequency. Based on our previous work [11], improvements have been made. First of all, the rf driving source of the two clocks, called Clock1 and Clock2, are redesigned, the two clocks can both running at the "*magic*" rf driving frequency Ω_0. A variable capacitor is added with connection in parallel to the trap, the trap driving frequency can be continuously tuned from 22 to 27 MHz by adjusting the capacitance of the capacitor. The rf driving frequency can be changed while keeping the ion trapped. The working parameter of Clock1 is kept unchanged during the whole experiment. A dc offset voltage is added to the vertical compensation electrode of Clock2, producing a static electric field that will move the mean position of the ion vertically from the *E*-field free trap saddle point (trap center) to a new equilibrium position. Taking Clock1 as a frequency reference, the micromotion shifts can be measured by the frequency comparison of the two clocks. The rf trapping frequency of Clock2 is scanned for the study of "*magic*" trap frequency

To reduce the measurement statistical uncertainty of Ω_0, the rf drive frequency of Clock2 is repeatedly and randomly scanned from 24.7~24.95 MHz. Linear fit are taken to obtain Ω_0 after each scan. After 15 of such scans, the inset shows the data taken in one of the scan and its linear fit. The corresponding weighted mean gives Ω_0=24.801(2) MHz.

To further determine $\Delta\alpha_0$ from Ω_0 with a higher accuracy, ion motions in Clock2 has to be studied [3]. By considering the motion harmonics at the frequencies of $n\Omega_0$, $\Delta\alpha_0$ is then calculated as $-7.2614(21)\times10^{-40}$ J m^2/V^2. The measurement of $\Delta\alpha_0$ reported here is in excellent agreement with the value $-7.31(8)\times10^{-40}$ J m^2/V^2 made by the recent theoretical calculations [5].

With our measured value of $\Delta\alpha_0$ and the dynamic correction calculated, from Eq. (1) the BBR shift is calculated as 0.37880(12) Hz at 300 K. The contribution of the BBR coefficient to the $^{40}Ca^+$ ion clock is then reduced from a previously limiting value of 1.1×10^{-17} to 3×10^{-19}. With a suppression of the BBR field temperature uncertainty to sub-Kelvin level, the total fractional uncertainty will reach into the 10^{-18} level. For example, a BBR temperature uncertainty of 0.1 K would give a BBR shift uncertainty of 1.5×10^{-18}. In the meantime, the precisely measured "*magic*" rf drive frequency also helps suppress the overall micromotion induced frequency shift or uncertainty. By setting the trap drive frequency at the "*magic*" frequency Ω_0, the excess micromotion induced clock uncertainty can be easily reduced to the 10^{-19} level. A simplified uncertainty budget of the $^{40}Ca^+$ optical clock is shown in Table I.

TABLE I. SIMPLIFIED UNCERTAINTY BUDGET OF THE $^{40}CA^+$ OPTICAL CLOCK

Contribution	***Fractional frequency uncertainty***
BBR field evaluation (temperaturte)	1.9×10^{-17}
BBR coefficient ($\Delta\alpha_0$)	3×10^{-19}
Excess micromotion	6×10^{-19}
Second-order Doppler (thermal)	5.5×10^{-18}
ac Stark shift	1.3×10^{-18}
Residual quadrupole	3.6×10^{-18}
Zeeman effect	1.5×10^{-18}
Servo	7.6×10^{-18}
Total	2.2×10^{-17}

The work reported here provides a significant improvement showing that the $^{40}Ca^+$ ion clock uncertainties caused by both the BBR shift coefficient and excess micromotion have been reduced to the 10^{-19} level. The servo error, primarily caused by statistical uncertainty of servo error signal data analysis, can be reduced by introducing the state preparation technique before the clock interrogations. The observed clock transition can be narrowed by using better clock lasers, smaller trap vibration, or weaker air turbulence. Narrower linewidth helps improving the clock stability thus suppressing the servo error. With a suppression of the BBR field temperature uncertainty to sub-Kelvin level, a robust, relatively low-cost $^{40}Ca^+$ ion clock with uncertainty at 10^{-18} level can be made.

References

N. Huntemann, C. Sanner, B. Lipphardt, C. Tamm and E. Peik, Phys. Rev. Lett. **116**, 063001 (2016)

T. L. Nicholson, S. L. Campbell, R. B. Hutson, et al. Nat. Commun. **6**, 6896 (2015)

P.Dubé, A. A. Madej, et al. Phys. Rev. Lett. **112**, 173002(2014)

G. P. Barwood, G. Huang, et al. Phys. Rev. A **89**, 050501(2014)

M.S. Safronova et al. Phys. Rev. A **83**, 012503 (2011)

S. G. Porsev and A. Derevianko, Phys. Rev. A **74**, 020502 (2006))

D. Jiang, B. Arora, M. S. Safronova, and C. W. Clark, J. Phys. B **42**, 154020 (2009)

S. G. Porsev, A.D. Ludlow, M.M. Boyd, and J. Ye, Phys. Rev. A **78**, 032508 (2008)

J. A. Sherman, N. D. Lemke, N. Hinkley, M. Pizzocaro, R. W. Fox, A. D. Ludlow, and C. W. Oates, Phys. Rev. Lett. **108**, 153002 (2012).

T. Middelmann, S. Falke, C. Lisdat, and U. Sterr, Phys. Rev. Lett. **109**, 263004 (2012)

Y. Huang, H. Guan, P. Liu, W. Bian, L. Ma, K. Liang, T. Li, and K. Gao, Phys. Rev. Lett.**116**, 013001 (2016)

Toward an optical frequency standard based on ultra-cold magnesium atoms

A.N. Goncharov[1-3], A.E. Bonert[1], V.I. Baraulya[1], M.A. Tropnikov[1], S.A. Kuznetsov[1], O.N. Prudnikov[1], A.V. Taichenachev[1,2], S.N. Bagayev[1,2]

[1]*Institute of Laser Physics SB RAS, prosp. Lavrentyeva 13/3, 630090, Novosibirsk, Russia*
[2]*Novosibirsk State University, st. Pirogova 2, 630090, Novosibirsk, Russia*
[3]*Novosibirsk State Technical University, pr. Karla Marksa 20, 630073, Novosibirsk, Russia*
E-mail: gonchar@laser.nsc.ru

Optical frequency standards based on cold atoms are of a great interest both for various applications in navigation and metrology and for fundamental physics [1]. Experimental studies aimed at developing optical frequency standards using cold magnesium, calcium, ytterbium, strontium, mercury, and thulium atoms are in progress. Magnesium atoms have a number of properties useful for their application in optical frequency standards [2]. Despite some complexities in the use of magnesium atoms for an optical frequency standard, related to the problem of their deep cooling to temperatures of ~10 mK [3–5] and a relatively large value of the quadratic Zeeman effect [2], encouraging results have been obtained recently, which demonstrate good prospects of magnesium atoms as a base of an optical standard with a relative uncertainty of $10^{-17} - 10^{-18}$ [6].

This paper presents the results of experimental studies aimed at the development of an optical frequency standard based on ultra-cold magnesium atoms with relative frequency uncertainty and long- term stability at the level of $\Delta\nu/\nu \sim 10^{-17}$ -10^{-18}.

The cloud of cooled Mg atoms localized in the magneto-optical trap (MOT) was interrogated with time separated laser pulses resonant to $^1S_0$-$^3P_1$ transition [7]. Narrow Ramsey-Borde fringes with the width of 390 Hz (HWHM) were detected. We stabilized the frequency of our clock laser system at 457 nm to narrow fringes. The results of stabilization were studied with femtosecond comb based on Ti:Sa laser. Long-term stability of $\sigma(\tau) \sim 5\ 10^{-15}$ at averaging time $\tau = 10^3$ was obtained [8,9]. The measured frequency stability was determined appreciably by the stability of the measurement system based on the femtosecond optical frequency synthesizer stabilized to optical frequency of the Yb:YAG/I_2 standard. Figure1 shows the results of measuring the frequency stability (Allan variance), the continuous measurement time was 1 h.

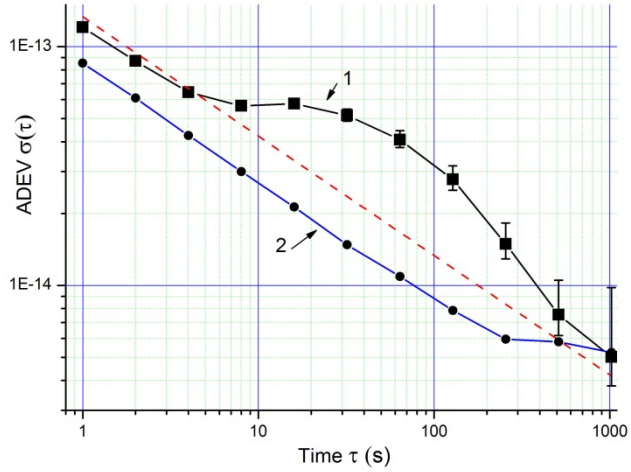

Fig. 1 (*1*) Allan variance characterizing the frequency stability of the developed Mg standard and (*2*) Allan variance of the beat signal of two Yb: YAG/I2 frequency standards, one of which was used to stabilize the parameters of femtosecond optical frequency synthesizer; the dashed line is an approximation of the measured stability by the function $f(\tau) = 1.3\times10^{-13}/\sqrt{\tau}$.

We also present our theoretical an experimental efforts [3-5, 10] to deep laser cooling of Mg atoms to a temperature of about 10-50 μK for further their localization in an «optical lattice».

As the result, we developed a radiation source with relative long-term frequency instability $\Delta\nu/\nu < 5\ 10^{-15}$ at an averaging time of 10^3 s. Frequency stabilization was performed using narrow optical resonances on the intercombination transition $^1S_0 - {}^3P_1$ in Mg atoms, which were cooled and localized in the MOT. The frequency stability can be significantly increased by improving the thermal stabilization system of the reference interferometer and increasing the signal-to-noise ratio when recording Ramsey resonances. To rise the signal-to-noise ratio, we are planning to record the absorption signal on the clock transition using the secondary MOT on the $^3P_2 - {}^3D_3$ triplet transition and reduce the temperature of the cloud of cold magnesium atoms, applying sub-Doppler cooling of atoms in the secondary MOT on the $^3P_2 - {}^3D_3$ triplet transition [3-5, 10]. In future, we are planning to implement sub-Doppler cooling of magnesium atoms to a temperature of 10–50 μK and localize atoms in a one-dimensional optical lattice in order to form an optical frequency standard based on ultra-cold magnesium atoms with a relative long-term instability and frequency uncertainty at a level of 10^{-17}–10^{-18} using the strongly forbidden $^1S_0 - {}^3P_0$ transition.

This work was supported by the Russian Science Foundation (Grant No. 16-12-00054). M.A. Tropnikov acknowledges the support of the Russian Science Foundation (Grant No. 17-72-20089) for measuring the frequency stability using a femtosecond frequency synthesizer. The metrological parameters of our "clock" laser system were measured using the equipment of the Shared Facilities Centre 'Femtosecond Laser Complex'.

References

[1] Ludlow A.D. et al., Rev. Mod. Phys., **87**, 637 (2015).
[2] Kulosa A.P. et al., Phys. Rev. Lett., **115**, 240801 (2015).
[3] Prudnikov O.N. et al., Laser Phys., **26**, 095503 (2016).
[4] Prudnikov O.N. et al., Quantum Electron. **46**, 661 (2016)
[5] Prudnikov O.N. et al., Phys. Rev. A, **92**, 063413 (2015).
[6] Jha N. et al., Proc. 2017 Joint Conf. European Frequency and Time Forum and IEEE Intern. Frequency Control Symposium (EFTF/IFC) (Besancon, France, 2017) p. 495.
[7] A. N. Goncharov et al., Quantum Electron. **44**, 521 (2014).
[8] A.N.Goncharov et al., Journal of Physics: Conf. Series **793**, 012008 (2017).
[9] A.N.Goncharov et al, Quantum Electronics **48** (5) 410 – 414 (2018).
[10] O.N. Prudnikov et al., Journal of Physics: Conference Series. **793**, 012021 (2017).

A scheme for chip scale atomic clock

H. Lin[1], Y. Tian[2], J. Chen[2], and S. Gu[1,2]
[1]*Wuhan National Laboratory for Optoelectronics, Huazhong University of Science and Technology, PR China*
[2]*Key Laboratory of Atomic Frequency Standards, Wuhan Institute of Physics and Mathematics, Chinese Academy of Sciences, PR China*
E-mail: shgu@wipm.ac.cn

The frequency stability of the present chip scale atomic clock (CSAC) product is around $2\times10^{-10}\tau^{-1/2}$, which is relative low mainly caused by the effects: 1) the strong background signal from the frequency components of the multi-chromatic light which do not participate in coherent population trapping (CPT) resonance; 2) the spin-polarized trap state atoms produced by the circularly polarized laser [1]; and 3) the FM-AM noise, the amplitude noise converted from the frequency jittering, which is relative strong with the VCSEL output laser [2]. We have exploited a CPT atomic scheme which obtains CPT signal through differentially detecting the magneto-optically-rotated light to reduce the three effects [3] and considerably improve the frequency stability. However, the scheme is not suitable for implementing CSAC due to the difficulty of stablizing laser frequency. In this work, we explore a modified scheme [4], which basically keeps the advantages of ref [3] scheme, while it stabilizes laser frequency with the same spectral line as the conventional CPT atomic clock so that it is not the obstacle for applying in CSAC.

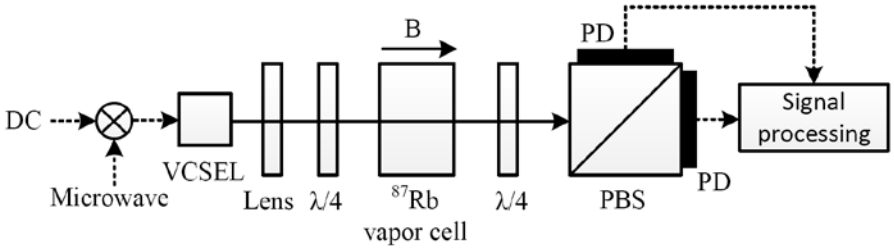

Fig. 1 Schematic of the experimental apparatus

The experimental setup as Fig. 1, linearly polarized multi-chromatic laser beam is turned into elliptically polarized one by a λ/4, the quarter wavelength plate, which interacts with ^{87}Rb atoms in the vapor cell as right and left polarized superimposed lights with different amplitudes. The transmitted elliptically polarized beam is turned back to linearly polarized one by the second λ/4, and it is then split into equal intensity beams by the polarizing beam splitter (PBS). Then the beams are detected separately by two PDs, photo-detectors.

The Doppler broaden spectral line for stabilizing laser frequency is obtained by summing the PDs' outputs, and the CPT spectral line is extracted by subtracting two PDs' outputs. If there is no interaction with atoms, the laser beam is split by the PBS into equal intensity beams and ideally, the outcome of the subtraction is zero. However, the magneto-optically-rotated effect makes the light, which interacts with atoms, rotate its polarization direction. Therefore, teh PBS's outputs are not equal intensity beams and a differential signal is obtained by subtracting the outputs of two detectors when the bi-chromatic components interact with atoms when the multi-chromatic beam goes through the cell. The CPT signal can be extracted from the differential signal, although the amplitude of the obtained CPT signal is reduced, as the strong background signal from the frequency components which have no interaction with atoms are eliminated, the quality of CPT signal is improved. When elliptically polarized light interacts with atoms, actually right and left circularly polarized lights simultaneously interact with atoms and will not produce spin-polarized trap state atoms. Furthermore, the FM-AM noises in PDs' outputs are from the same source, this common mode noise can be effectively reduced through subtraction. The experimental result reveals that the frequency stability can be improved by several times when comparing with the conventional scheme.

Author thanks National Natural Science Foundation of China for the supports.

References

[1] J. Vanier, Appl. Phys. B. **81**, 421 (2005).
[2] V. Gerginov et al., IEEE Trans. Instrum. Meas. **57**, 1357 (2008).
[3] B. Tan et al., Opt. lett. **40**, 3703 (2015).
[4] H. Lin et al., Europhys. Lett. **119**, 23001 (2017).

Compact CPT atomic clock based on a buffer-gas-filled Cs vapor cell

S.M. Ignatovich[1], M.N. Skvortsov[1], V.I. Vishnyakov[1,3], N.L. Kvashnin[1], V.A.Vasiliev[1], A.V. Taichenachev[1,2], S.N. Bagayev[1]

[1]*Institute of Laser Physics SB RAS, Novosibirsk, Russia*

[2]*Novosibirsk State University, Novosibirsk, Russia*

[3]*Novosibirsk State Technical University, Novosibirsk, Russia*

E-mail: vishnyakov@laser.nsc.ru

High-stability and compact clocks are in great demand for many applications, for example, such as global navigation satellite systems (GNSS), broadband communication networks and high-secret lines, smart electricity grids, geophysical measurements, etc. Many applications of the clocks require small size and weight ($V < 60$ cm^3, $m < 50$ g), low power consumption ($P << 1$ W) and high long-term frequency stability ($< 10^{-11}$ per a day). The most promising technology involves approach based on the coherent populations trapping (CPT) phenomenon [1,2], because it can combine all the features listed. Here we present the recent progress of development a version of CPT atomic clock, which involves a buffer-gas-filled glass-blown vapor cell. Buffer gas is usually used to achieve narrow dark resonances caused by the coherent population trapping. The resonances are required for obtaining the good error signals for feedback frequency stabilization loop in atomic clocks (e.g. see [3-5]). Our setup is based on a self-made glass-blown spherical Cs cell with 5-mm diameter and 100 Torr Ne buffer gas inside. The cell is placed inside the Helmholtz coils that are used to create a longitudinal magnetic field an order of 10 μT to eliminate the Zeeman energy levels' degeneracy and to separate a "clock" resonance. The cell is surrounded by a μ-metal shield. For the resonance observation we apply VCSEL laser at 894 nm corresponding to Cs D_1 absorption line. The VCSEL lasers are enabling technology for using in various miniature devices. They have proven to be almost ideal in such applications. Their minimal size and power consumption together with well-developed low-cost technology make them useful even in the chip-scale clock production [4]. We use the laser with thermoelectric cooler (TEC) inside, which is needed to control temperature of the laser and tune the wavelength. The VCSEL beam is divergent. In order to compensate this, lens are added to scheme to collimate the beam. The microwave current modulation can be supplied to the VCSEL for fast scanning the wavelength. To achieve high efficiency of microwave modulation and mixing, the bias tee is involved. The bichromatic scheme of cesium energy levels pumping has been realized by microwave modulation of the laser current at frequency 4.6 GHz. To achieve better resonance contrast the optical scheme composed of the circular polarized light waves has been chosen. Physical block with supplied electronic units has a volume of 57.5 cm^3. Resulting Allan deviation depicted on Figure 1. It is worth saying that our CPT clock has an stability better than 6×10^{-13} at 1000 seconds integration time.

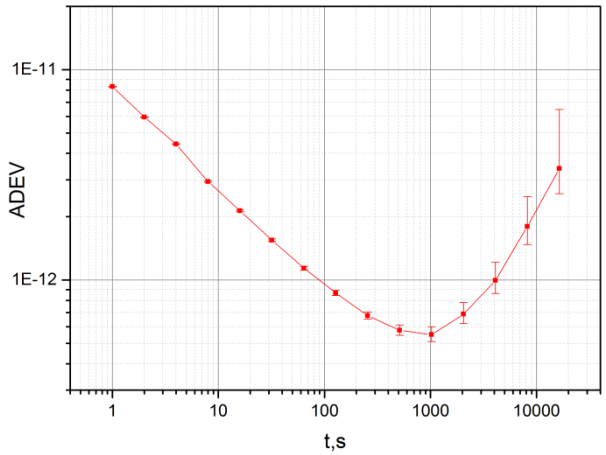

Fig. 1 Allan deviation of CPT clock at Cs D1 line.

References

[1] G. Alzetta, A. Gozzini, L. Moi, and G. Orriols, "An experimental method for the observation of r.f. transitions and laser beat resonances in oriented Na vapour", Nuovo Cimento B, vol. 36, pp. 5–20, 1976.
[2] E. Arimondo, "Coherent population trapping in laser spectroscopy", Progress in Optics, vol. 35, pp. 257-354, 1996.
[3] M. Merimaa, Th. Lindvall, I. Tittonen, and E. Ikonen, "All-optical atomic clock based on coherent population trapping in ^{85}Rb", J. Opt. Soc. Am. B, vol. 20, pp. 273-279, 2003.
[4] S. Knappe, P.D.D. Schwindt, V. Shah, L. Hollberg, J. Kitching, L. Liew, and J. Moreland, "A chip-scale atomic clock based on ^{87}Rb with improved frequency stability", Opt. Express, vol. 13, pp. 1249-1253, 2005.
[5] S.A. Zibrov, I. Novikova, D.F. Phillips, R.L. Walsworth, A.S. Zibrov, V.L. Velichansky, A.V. Taichenachev, and V.I. Yudin, "Coherent-population-trapping resonances with linearly polarized light for all-optical miniature atomic clocks", Phys. Rev. A, vol. 81, 013833, 2010.

Precision spectroscopy of Thulium in optical lattice

N. Kolachevsky[1,2], A. Golovisin[1,2], E. Kalganova[1,2], D. Tregubov[1], K. Khabarova[1,2], D. Sukachev[1], V. Sorokin[1]
[1]*P.N. Lebedev Physical Institute, Leninsky prospect 53, 119991, Moscow, Russia*
[2]*Russian Quantum Center, Novaya St. 100A, Skolkovo, 143025, Moscow, Russia*
E-mail: kolachevsky@lebedev.ru

Laser cooled hollow-shell lanthanides (Er, Dy, Tm, Ho) not only give new insights into physics of highly magnetic degenerate gases, but also can be considered as an interesting object for high precision spectroscopy and applications in optical frequency metrology [1]. We focus our studies on bosonic isotope Tm-169 possessing and inner-shell 4f-4f M1 transition at 1.14 micrometers. The transition is strongly shielded from external electric fields by outer closed $5s^2$ and $6s^2$ electronic shells which should provide low sensitivity to BBR shift and collisional perturbations. Previously, we demonstrated deep laser cooling and trapping of thulium in optical lattice [2], calculated polarizabilities of the clock levels and estimated the expected uncertainty budget for the clock transition frequency [3].

We load atoms in the vertical optical lattice formed by radiation of Ti:sapphire laser coupled to the enhancement cavity [4]. Spectroscopy of the clock transition (in collinear configuration) by linearly polarized radiation of ultrastable clock laser at λ=1.14 μm allows to determine differential polarizability between the upper and the lower lock levels at different lattice wavelengths (810-815 nm). Experimental results are demonstrated in Fig. 1 (left) in dots. One can see that the linear part of differential polarizability vanishes at around 813 nm. Accurate measurements of the magic wavelength done by analysis of the clock transition frequency shift *vs* lattice power gives 813.3185(8) nm (preliminary result). Experimental data show reasonable correspondence to the calculations done our method described in details in [3]. By extrapolation to the infrared region, we get very low differential polarizability of about 0.1 atomic units (modulus). It provides sensitivity to the BBR shift by three orders of magnitude lower than for the prominent clock transition in Sr at 698 nm [5].

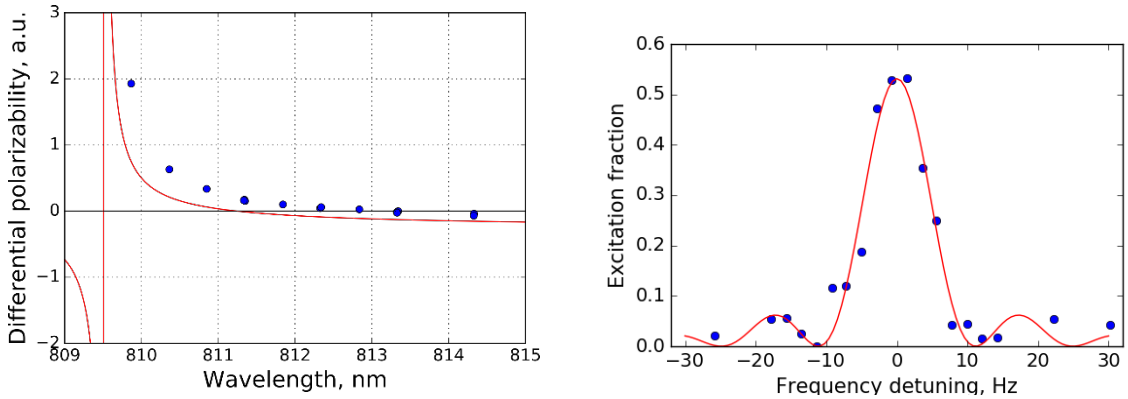

Fig. 1 Left: measured differential dynamic polarizability (in atomic units) between upper and lower clock levels in Tm (dots) and calculations (solid line). The magic wavelength corresponds to 813.3185(8) nm. Right: spectral line of the clock transition at λ=1.14 μm measured at the magic wavelength of the optical lattice (dots). The line width of 10 Hz is Fourier limited (corresponding fit is shown in solid line).

Fig.1 (right) shows the clock transition spectral line measured in the optical lattice at the magic wavelength (dots). Atoms were excited by the rectangular π-pulse of 80 ms duration. The spectral line width corresponds to 10 Hz (FWHM). The solid line shows the Fourier transform of the light pulse which shows that our line is Fourier limited. Typically, we have about 10^5 atoms in the lattice ready for spectroscopy which provides good signal-to-noise ratio.

Experimental and theoretical analysis of some major frequency shifts (quadratic Zeeman shift, hyperpolarizability and tensor polarizability shifts, BBR shifts) indicate that one can push the fractional frequency uncertainty for this transition to low 10^{-17} level.

References

[1] G. Vishnyakova et al., Phys. Usp. 59 168–173 (2016).
[2] E. Kalganova, Phys. Rev. A 96, 033418 (2017).
[3] D. Sukachev et al., Phys. Rev. A 94, 022512 (2016).
[4] Kalganova,E S et al. Quantum Electronics 48, 415 (2018).
[5] A. Kozlov et al., Phys Rev A 90, 042505 (2014).

Design and development of a surface-electrode ion trap for optical frequency metrology

C. Lacroûte, M. Delehaye, L. Groult, B. Achi, M. Souidi,
E. Bigler, J. Millo, P.-Y. Bourgeois, Y. Kersalé
FEMTO-ST Institute, univ. Bourgogne Franche-Comté, CNRS, ENSMM, 25030, Besançon, France
E-mail: clement.lacroute@femto-st.fr

We report on the ongoing realization of a compact optical $^{171}Yb^{+}$ clock on a chip. The targeted fractional frequency stability is $10^{-14}\tau^{-1/2}$ for a total volume of less than 500 L, including vacuum cell, optics and electronics. Such a compact clock would be part of the growing European optical clocks network that already triggers new applications in a large variety of domains, ranging from relativistic geodesy to fundamental science [1, 2].

Four lasers at 370, 398, 638 and 935 nm are needed for ionization, cooling and repumping, see Fig. 1. They are frequency controlled using a single wavelength meter with an accuracy of 60 MHz and a frequency drift of 20 MHz/day [3].

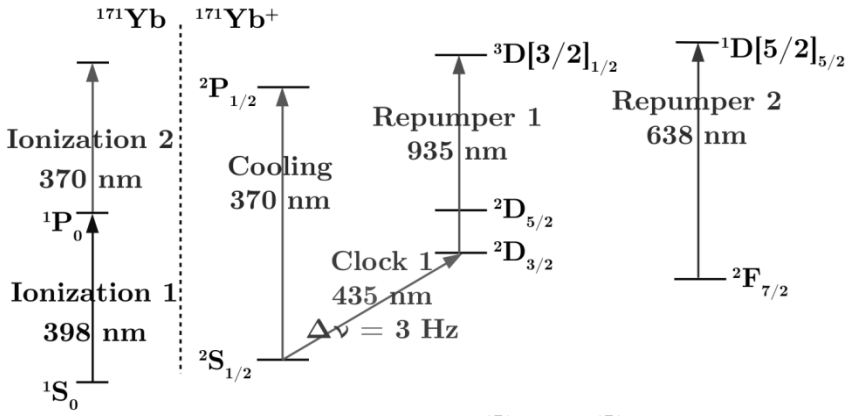

Fig. 1 Relevant atomic levels of ^{171}Yb and $^{171}Yb^{+}$.

The quadrupole clock transition of $^{171}Yb^{+}$ at 435.5 nm will be excited using a frequency-doubled laser diode at 871 nm. We have characterized the phase noise induced by the second harmonic generation modules with a Mach-Zehnder interferometer and observed a relative phase noise as low as -40 dBrad^2/Hz at 1 Hz, which makes them compatible with the best up-to-date optical clocks and ultra-stable cavities [4]. The compact reference cavity at 871 nm will be based on a 2.5 cm long Fabry-Perot resonator embedded in a compact setup [5].

The experiment control essentially relies on compact home-built digital electronics.

The ion trap is based on a surface-electrode linear Paul trap. It follows the "five wires" design and microfabrication techniques that have been primarily developed and used by the quantum information community [6]. It relies on two planar RF electrodes driven at 5.8 MHz and 190 V that generate a linear Paul trap of 300 meV depth and harmonic trapping frequencies of 360 kHz radially and 100 kHz axially. The ions are trapped 500 μm from the surface.

The current chip is 30×60 mm^2 large and has a mini-SD connector in order to allow fast plug-and-play replacements [7], see Fig. 2. This prototype trap is based on a PCB board, but the next version will take advantage of standard cleanroom microfabrication techniques.

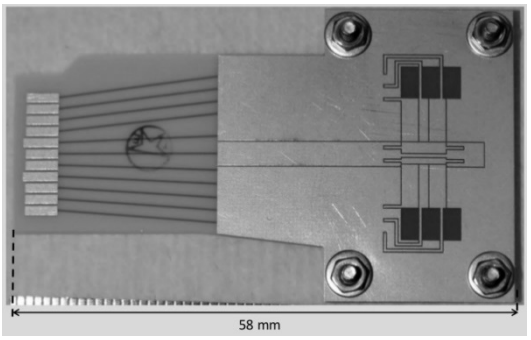

Fig. 2 Photograph of the trapping chip. It is driven at 5.8 MHz and 190 V to generate a linear Paul trap with 300 meV depth. The trapping electrodes are located on the right-hand side, while the micro-SD format on the left-hand side is used for electrical connection.

We recently demonstrated trapping of Yb^+ ions in this prototype trap (see Fig. 3), which will let us validate the proper operation of our optical setup, control electronics, and characterize our chamber base pressure. We will present the first characterization of our trap, including ion temperature, lifetime and heating rate measurements.

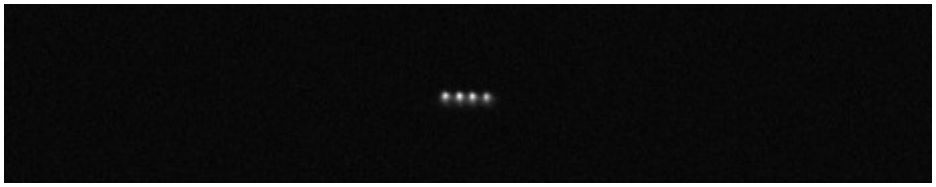

Fig. 3 Fluorescence image of a linear crystal of four $^{176}Yb^+$ ions in our prototype trap. The spacing between the ions is roughly 16 μm.

References

[1] C. Lisdat *et al.*, Nat. Comm. **7**, 12443 (2016).
[2] F. Riehle, Nat. Phot. **11**, 25 (2017).
[3] K. Saleh, J. Millo, A. Didier, Y. Kersalé, and C. Lacroûte, Appl. Opt. **54**, 9446 (2015).
[4] M. Delehaye *et al.*, IEEE Phot. Technol. Lett. **29**, 1639 (2017).
[5] A. Didier *et al.*, J. Phys. Conf. Ser. **723**, 012029 (2016).
[6] S. Seidelin *et al.*, Phys. Rev. Lett. **96**, 253003 (2006).
[7] C. Lacroûte *et al.*, J. Phys. Conf. Ser. **723**, 012025 (2016).

Precision spectroscopy on ion Coulomb crystals

T.E. Mehlstäubler, D. Kalincev, J. Keller, J. Kiethe, A. Didier, and A. Kulosa
Physikalisch-Technische Bundesanstalt, Bundesallee 100, 38116, Braunschweig, Germany
E-mail: Tanja.Mehlstaeubler@ptb.de

Optical atomic clocks based on trapped ions or neutral atoms, have both reached a relative inaccuracy of a few 10^{18} in laboratories today. While neutral lattice clocks have a superior short-time stability operating several 1000s of atoms and thus can work at extremly short integration times, ion clocks have a high potential to achieve lowest inaccuracies with well-controlled single atomic particles. In 2011, we proposed to build a multi-ion clock which can be a promising and combining path to profit best from both worlds [1].

Challenges are to control the complex dynamics of ion Coulomb crystal to a high degree. Based on our scalable trap design and a benchmarked prototype trap, we developed a high-precision ion trap at PTB, which has the capability to control ensembles of small trapped linear strings of ions in a one-dimensional array, so that about 100 ions can be interrogated simultaneously. We show the experimental characterization of our chip-based linear Paul trap and present an estimated error budget of an In+/Yb+ multi-ion clock based on trapped ions in the new chip trap [2, 3].

References

[1] D. J. Herschbach et al., Appl. Phys. B 107, 891 (2012)
[2] J. Keller et al. ArXiv: 1712.02335 (2017)
[3] J. Keller et al. ArXiv: 1803.08248 (2018)

Ramsey spectroscopy in vapour cells for compact high performance atomic clocks

C. Affolderbach, N. Almat, M. Gharavipour, F. Gruet, W. Moreno, M. Pellaton, and G. Mileti
Laboratoire Temps-Fréquence, Université de Neuchâtel, 2000, Neuchâtel, Switzerland
E-mail: gaetano.mileti@unine.ch

We will report our recent investigations on Ramsey spectroscopy in vapour cells and its application to atomic frequency standards [1]. First, we will briefly recall the physical principles of double-resonance (DR) Rubidium (Rb) atomic clocks that are used in fields of application such as secured telecommunications, network synchronization, seismic prospection and satellite navigation [2]. After having highlighted the impact of laser diodes on clock development and performance, we will focus on the specific topic of compact (< 5 L) high-performance (10^{-14} @ 1 day) vapour-cell atomic clocks.

The use of laser sources instead of plasma discharge lamps has greatly enhanced the resolution and scheme possibilities in atomic vapour-cell spectroscopy and clocks. After several decades of intense experimental and theoretical activities, this subject still constitutes a highly active field of scientific research, also thanks to the great number of potential applications. We will illustrate this interest with some examples of recent achievements in our group, in particular the demonstration of the new technique of optically-detected spin echo, ODSE, inspired by the classical NMR "spin echo" method, that allows the measurement of the intrinsic transverse relaxation time of the "clock-transition" in a Rb vapour cell, suppressing the effect of static magnetic field gradients [3].

In addition to these fundamental studies, laser sources have, on one side, allowed the improvement of the performances of several precision instruments and in particular atomic clocks. On the other side, laser diodes have introduced (or enhanced) sources of frequency instabilities as well as several other more practical concerns such as reliability, availability and price. In this respect, we will present two ongoing studies aiming to address these issues: long-term studies on spectral aging of laser diodes emitting at 780 nm, and the evaluation of alternative laser sources based on frequency doubling of telecom lasers emitting around 1.56 μm [4, 5]. In addition, we will report on an innovative technique to realize one of the key components of a Rubidium DR clock - the microwave cavity - by additive manufacturing, and the proof of concept of its suitability for high-performance atomic clocks [6, 7], see figure 1.

Approximately 20 years ago, a significant improvement in the short-term (averaging times between 1 and 100 seconds) frequency stability of Rb clocks using a laser source instead of a discharge lamp was first demonstrated [8]. Since then, similar or even better performances could be obtained using different atom species (in particular Cs) and clock schemes (such as Coherent Population Trapping) [9]. However, the lasers are also sources of frequency instability in the medium and long term (averaging times ranging from 1000 s to 1 day or more) and a number of studies have been realized in order to identify and suppress these instabilities. Thanks to the Ramsey scheme [10], it is possible to separate in time the atoms' interaction with the microwave field from the interaction with the optical field, which significantly reduces one of the main origins of clock frequency fluctuations: the AC Stark shift effect. Nevertheless, the laser intensity and wavelength variations do still affect slightly the detected reference atomic transition, as it will be discussed in our presentation.

We will conclude our presentation by showing how fluctuations of natural ambient pressure may become a significant source of clock frequency instabilities (see figure 2). This so-called "barometric" effect can cause tiny cell deformations, at the nanometer scale, that can still be responsible of non-negligible pressure changes inside the vapour cell which in turn impact the clock stability [11]. By suppressing this effect, a fractional clock frequency of $2 \cdot 10^{-14}$ for an averaging time of 100'000 s was achieved [12], see Figure 3.

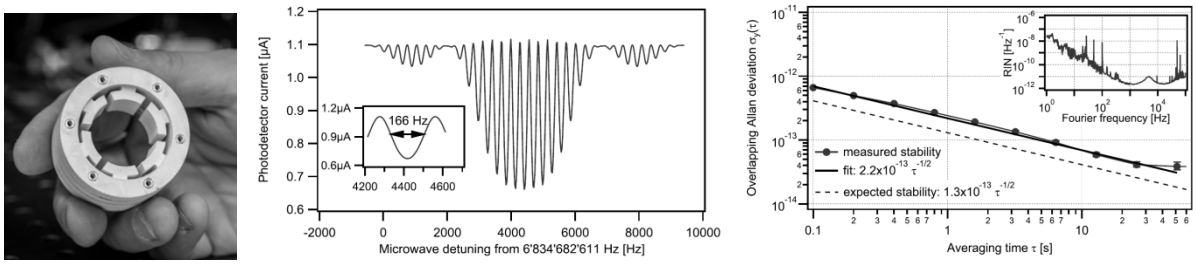

(a) (b) (c)

Fig. 1 (a) Photo of a 3D-printed microwave cavity for a high-performance Rubidium clock (from [6]). (b) Example of Ramsey fringes (from [7]). (c) Example of achieved short-term frequency stability (from [7]).

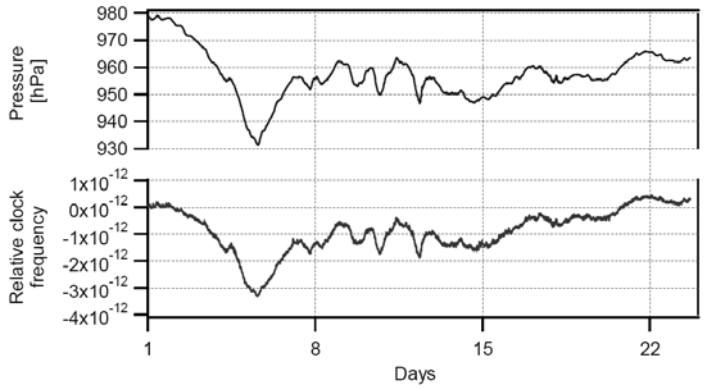

Fig. 2 Example of results obtained when measuring simultaneously the ambient pressure (top) and the clock frequency fluctuations (bottom) (from [11]).

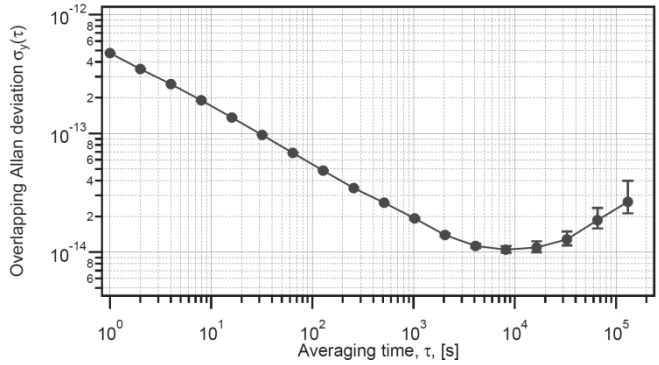

Fig. 3 Example of clock frequency stability measurement after suppressing the barometric effect (from [12]).

References

[1] M. Gharavipour, C. Affolderbach, S. Kang, T. Bandi, F. Gruet, M. Pellaton, G. Mileti, J. Phys. Conf. Ser. **723**, 012006 (2016)
[2] J. Camparo, Physics Today **60**, 33 (2007)
[3] M. Gharavipour, C. Affolderbach, F. Gruet, I. Radojičić, A. Krmpot, B. Jelenkovic, G. Mileti, New J. .Phys. **19**, 063027 (2017)
[4] N. Almat, M. Pellaton, W. Moreno, F. Gruet, C. Affolderbach, G. Mileti, Appl. Optics. **57**, 4707 (2018)
[5] N. Almat, W. Moreno, M. Pellaton, F. Gruet, C. Affolderbach, G. Mileti, IEEE TUFFC **65**, 919 (2018)
[6] M. Pellaton, C. Affolderbach, A. K. Skrivervik, A. E. Ivanov, T. Debogovic, E. de Rijk, G. Mileti, Electron. Lett. **54**, 691 (2018). See also the editorial "atomic clock microwave cavity", Electron. Lett. **54**, 671 (2018)
[7] C. Affolderbach, W. Moreno, A. E. Ivanov, T. Debogovic, M. Pellaton, A. K. Skrivervik, E. de Rijk, G. Mileti, Appl. Phys. Lett. **112**, 113502 (2018)
[8] G. Mileti, J. Q. Deng, D. A. Jennings, F. L. Walls, R. E. Drullinger, IEEE J. Quantum Electron. **34**, 233 (1998)
[9] M.A. Hafiz, G. Coget, M. Petersen, C. Rocher, S. Guérandel, T. Zanon-Willette, E. de Clercq, and R. Boudot, Phys. Rev. Appl. **9**, 064002 (2018)
[10] A. Godone, S. Micalizio, F. Levi, Phys. Rev. A **70**, 023409 (2004)
[11] W. Moreno, C. Affolderbach, M. Pellaton, G. Mileti, IEEE Trans. Ultrason., Ferroelectr., Freq. Control (2018) DOI: 10.1109/TUFFC.2018.2844020
[12] C. Affolderbach, N. Almat, M. Gharavipour, F. Gruet, W. Moreno, M. Pellaton, and G. Mileti, Proc. of the 2018 IFCS.

Laser spectroscopic characterization of the nuclear-clock isomer ^{229m}Th

M. Okhapkin[1], J. Thielking[1], P. Glowacki[1], D.-M. Meier[1], E. Peik[1], L. v.d. Wense[2], B. Seiferle[2], P. Thirolf[2], C. Düllmann[3-5]

[1]*Physikalisch-Technische Bundesanstalt, 38116, Braunschweig, Germany*
[2]*Ludwig-Maximilians-Universität München, 85748, Garching, Germany*
[3]*GSI Helmholtzzentrum für Schwerionenforschung GmbH, 64291, Darmstadt, Germany*
[4]*Helmholtz-Institut Mainz, 55099, Mainz, Germany*
[5]*Johannes Gutenberg Universität, 55099, Mainz, Germany*
E-mail: maksim.okhapkin@ptb.de

The isotope ^{229}Th is the only nucleus known to possess an excited state ^{229m}Th in the energy range of a few electron volts, a transition energy typical for electrons in the valence shell of atoms, but about four orders of magnitude lower than common nuclear excitation energies. The most promising application of this unique nuclear system is a highly precise nuclear clock that outperforms existing atomic timekeepers. We present the first laser spectroscopic investigation of the hyperfine structure of $^{229m}Th^{2+}$, yielding values of fundamental nuclear properties, namely the magnetic dipole and electric quadrupole moments as well as the nuclear charge radius, using precision hyperfine spectroscopy of Th^{2+} recoil ions, loaded from the α decay of ^{233}U [1]. The nuclear magnetic moment of the isomer is determined to be $\mu^m = -0.37(6)\mu_N$, which deviates significantly from the theoretical Nilsson model prediction of $-0.076\mu_N$ [2]. The intrinsic nuclear quadrupole moment of ^{229m}Th is determined as $Q^m = 8.7(3)e$b [3]. Within the experimental uncertainty it is identical to the intrinsic quadrupole moment of the nuclear ground state, and corresponds to theoretical predictions. From the amplitude of the hyperfine resonances, the 2% branching ratio into the isomer following the α decay of ^{233}U is verified experimentally for the first time. The change of the mean square charge radius is determined from the isomer shift in relation to the isotope shifts between ^{229}Th and ^{232}Th, and is given as $\langle r^2\rangle^{229m} - \langle r^2\rangle^{229} = 0.0105(13)$ fm^2 [4].

We can now apply this data to the known hyperfine structure of Th^+ and Th^{2+} [1,5] to achieve an efficient direct detection method for our experiment, which is searching for the optical excitation of the isomer in Th^+ and Th^{2+} ions via the electronic bridge or NEET process [6,7].

References

[1] J. Thielking et al., Nature **556**, 321-325 (2018).
[2] A.M. Dykhne, E.V. Tkalya, *JETP Lett.* **67**, 251–256 (1998).
[3] E.V. Tkalya, *Phys. Rev. Lett.* **106**, 162501 (2011).
[4] M. Safronova et al., to be published.
[5] M.V. Okhapkin et al., Phys. Rev. A **92**, 020503 (2015).
[6] S. G. Porsev et al., Phys. Rev. Lett. **105**, 185501 (2010).
[7] F.F. Karpeshin et al., Nucl. Phys. A **654**, 579 (1999).

Quantum logic spectroscopy of trapped ions

P.O. Schmidt[1,2]
[1]*Physikalisch-Technische Bundesanstalt, Bundesallee 100, Germany*
[2]*Leibniz Universität Hannover, Welfengarten 1, 30167, Hannover, Germany*
E-mail: Piet.Schmidt@quantummetrology.de

Precision spectroscopy is a driving force for the development of our physical understanding. In particular, laser cooling and manipulation has led to an advancement in precision spectroscopy. However, only few atomic and molecular species offer suitable transitions for laser cooling, limiting the variety of accessible species. This restriction can be overcome in trapped ions through quantum logic spectroscopy. Coherent laser manipulation originally developed in the context of quantum information processing with trapped ions allow the combination of the special spectroscopic properties of one ion species (spectroscopy ion) with the excellent control over another species (logic or cooling ion) [1].

We experimentally demonstrate how the internal state of a single $^{24}MgH^+$ molecular ion can be detected through coupling to a $^{25}Mg^+$ atomic ion (Fig. 1a). Starting from the ground state of motion of a joint motional mode, a molecular state-selective optical dipole force changes the motional state only if the molecule is in a specific rovibrational state. The change of the motional state is efficiently detected on the atomic ion. This way, we observe black body radiation-driven quantum jumps between rotational states in the molecule (Fig. 1b). The detuning-dependence of the coupling strength of the optical dipole force allows us to perform spectroscopy on a specific electronic transition in the molecule [2]. This non-destructive detection technique represents a first step towards extending the exquisite control achieved over selected atomic species to much more complex species, such as molecular ions. Possible applications are model-independent probes for a possible variation of the electron-to-proton mass ratio, tests of parity violation using chiral molecules, or measurements of the electric dipole moment of the electron.

Prospects for extending quantum logic spectroscopy to highly charged ions and first steps towards this goal will be discussed. Sympathetic cooling of Ar^{13+} has been demonstrated in a cloud of Be^+ ions [3]. In collaboration with the MPIK in Heidelberg, we have set up a compact electron beam ion trap (Fig. 1c) and cryogenic Paul trap (Fig. 1d) with high trapping frequencies that allows ground state cooling and quantum logic operations in an Ar^{13+}/Be^+ two-ion crystal. First steps towards precision spectroscopy of the $P_{1/2}$-$P_{3/2}$ fine-structure transition at 441 nm in Ar^{13+} will be presented. This will pave the way towards exploring highly charged ions as optical clock candidates with a high sensitivity to a change in the fine-structure constant and the electron-to-proton mass ratio [4].

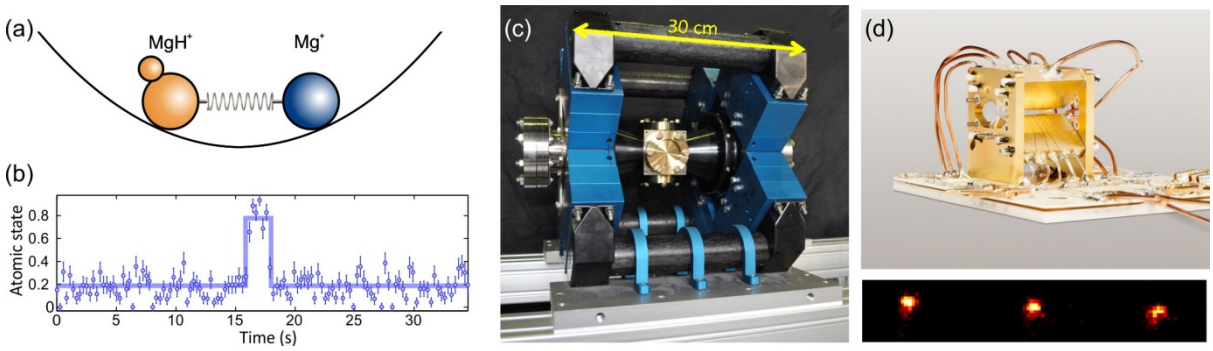

Fig. 1

References
[1] P. O. Schmidt et al., Science **309**, 749 (2005).
[2] F. Wolf et al., Nature **530**, 457 (2016).
[3] L. Schmöger, et al., Science **347**, 1233 (2015).
[4] M. G. Kozlov et al., arXiv:1803.06532 (2018).

Atomic clock based on magneto-dipole and two-photon transitions in highly charged ions

V.I. Yudin[1-3], A.V. Taichenachev[1,2], A. Derevianko[4], V.A. Dzuba[5]
[1]*Institute of Laser Physics, Novosibirsk, Russia*
[2]*Novosibirsk State University, Novosibirsk, Russia*
[3]*Novosibirsk State Technical University, Novosibirsk, Russia*
[4]*Department of Physics, University of Nevada, Reno, Nevada, USA*
[5]*University of New South Wales, Sydney, Australia*
E-mail: viyudin@mail.ru

A novel class of ultra-precise atomic clocks based on highly charged ions (HCI) was recently proposed [1]. In that paper, the authors studied highly-forbidden laser-accessible transitions within the $4f^{12}$ ground-state configurations of HCI. Their evaluation of systematic uncertainties demonstrated that such transitions may be used for building exceptionally accurate atomic clocks which may compete in accuracy with proposed nuclear clocks [2].

We evaluate the possibility of the use of magnetic dipole (M1) or two-photon optical transitions in HCI, which have two *p*-shell electrons. We focus on two classes of such laser-accessible M1 transitions in HCI. We identified clock transitions, which are insensitive to quadrupole shifts (see Fig.1, where quadrupole moment of clock states simply vanishes due to selection rules). In the case of two *p*-shell electrons we have found two possibilities: (i) odd isotopes with nuclear spin $I_n = 1/2$ and (ii) odd isotopes with nuclear spin $I_n = 3/2$. As to the fine-structure manifolds, we have found multiple HCIs with fine-structure M1 laser-accessible optical transitions. The constraint on Z_i (Z_i is the residual ion charge) depends on the balance between the total number of electrons and the nuclear charge. For example, for Al-like ions, $20 < Z_i < 30$.

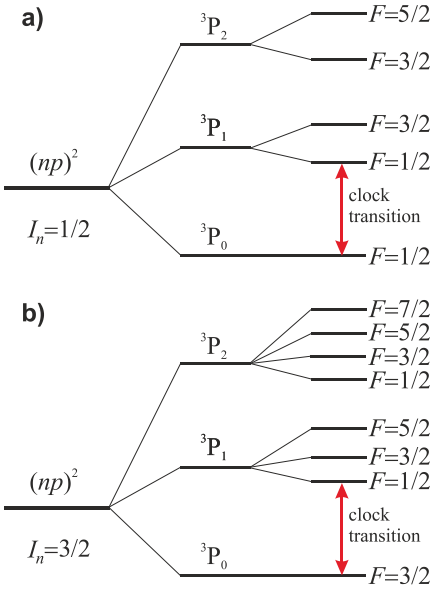

Fig. 1 Examples of M1 transitions with suppressed electric-quadrupole shift (due to selection rules) in the case of two *p*-shell electrons for odd isotopes: a) nuclear spin $I_n = 1/2$; b) nuclear spin $I_n = 3/2$.

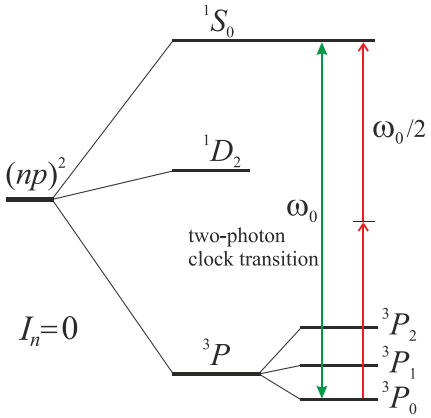

Fig. 2 Two-photon transition $^3P_0 \rightarrow {}^1S_0$ in the case of two *p*-shell electrons for even isotopes.

As an alternative, we have found the possibility to use a two-photon optical transition $^3P_0 \rightarrow {}^1S_0$ for ions with two *p*-shell electrons (see Fig.2). In contrast to previous variant based on M1 transition, here we use even isotopes (with zero nuclear spin, $I_n = 0$) and, therefore, we have not Zeeman substructure of energy levels for clock transition. Note that similar variant also exists in the case of four *p*-shell electrons. However, in this case the clock level $^3P_0$ will not be bottom level in the triplet ^3P.

Our analysis demonstrates that the atomic clocks based on the optical M1 or two-photon optical transitions in HCIs can have very small *inherent* uncertainties (at the fractional level below 10^{-19}) for the dominant systematic shifts (such as BBR, electric-quadrupole, Zeeman and AC-Stark shifts). Moreover, by contrast to the conventional atomic clock based on neutral atoms or singly charged ions such HCI clocks are exceptionally sensitive to hypothetical drifts of fundamental constants.

V.I. Yudin was supported by the Ministry of Education and Science of the Russian Federation (No. 3.1326.2017/4.6) and Russian Foundation for Basic Research (No. 17-02-00570). A.V. Taichenachev was supported by the Russian Science Foundation (No. 16-12-00052).

References

[1] A. Derevianko, V.A. Dzuba and V.V. Flambaum, Phys. Rev. Lett. **109**, 180801 (2012).
[2] E. Peik and Chr. Tamm, Europhys. Lett. **61**, 181 (2003); C. J. Campbell et al., Phys. Rev. Lett. **108**, 12080 (2012).

Atom femto trap

A.E. Afanasiev[1], A.Yu. Kalatskiy[1], A.A. Meysterson[1,2], P.N. Melentiev[1], V.I. Balykin[1]
[1]*Institute of Spectroscopy Russian Academy of Sciences, Fizicheskaya Str., 5, Moscow, Troitsk, 108840, Russia*
[2]*Moscow Institute of Physics and Technology, 9 Institutskiy per., Dolgoprudny, Moscow region, 141700, Russia*
E-mail: afanasiev.isan@gmail.com; balykin@isan.troitsk.ru

An atom "at rest" is an ideal physical object for many fundamental and applied investigations. A good approximation is an atom that is cooled by laser light and localized in one of the numerous traps that have been realized to date [1]. However, a potential localizing the atom provides an appreciable perturbing effect on both external and internal degrees of freedom of the atom. The best situation that may be expected is the cooling of the atom to a temperature corresponding to the energy of the atomic ground state, where the atom occupies the minimum phase space. Although the spatial motion of the atom is minimal in the ground state, this motion noticeably affects the internal degrees of freedom. Most fundamental and applied investigations are focused on the internal degrees of freedom.

It was proposed and analyzed approach to the minimization of the effect of the localizing field on the atom [2, 3]. Its essence is the use of the *short-term and time-periodic* action of the laser field on the spatial motion of a *very slow* atom. In such a scheme, the atom is free of the perturbing effect of the localizing field for a time interval $(1 - t_p / T)$, where t_p is the duration of the action and T is its repetition period. When femto second pulses are used, the relative time interval during which the atom is situated in the localizing field may be very short, i.e., 10^{-7}-10^{-6} of the total time interval during which the atom is confined in the trap.

We have shown theoretically that the approach under consideration may provide the situation wherein the atoms are subjected to the localizing field for only $(10^{-8}$-$10^{-9})$% of the total time interval of its localization; i.e., the atom is almost at rest. We have demonstreted in experiment the trapping of Rb atoms in time-periodic femtosecond laser field. The main problem of atom femto trap (photoassociation, impulse diffusion) have been investigated.

References

[1] R. Grimm, M. Weidemuller and Y. B. Ovchinnikov, "Optical dipole traps for neutral atoms", Adv. At. Mol. Opt. Phys., 42, 95 (2000).
[2] V. I. Balykin, "Motion of an Atom under the Effect of Femtosecond Laser Pulses: From Chaos to patial Localisation", JETP Letters, Vol. 81, 209, (2005).
[3] D.N. Yanyshev, V.I. Balykin, Y.V. Vladimirova, and V.N. Zadkov, "Dynamics of atoms in a femtosecond optical dipole trap", Phys. Rev. A, 87, 033411 (2013).

Spectroscopy of the electric quadrupole transition of the trapped ytterbium-171 ion

S.V. Chepurov[1], A.A. Lugovoy[1], O.N. Prudnikov[1,2], A.V. Taichenachev[1,2], V.I. Yudin[1,2], S.N. Bagayev[1]
[1]*Institute of Laser Physics SB RAS, Novosibirsk, Russia*
[2]*Novosibirsk State University, Novosibirsk, Russia*
E-mail: svc04@ngs.ru

Optical frequency standards based on single trapped laser-cooled ions are currently considered to be among the most stable ones. The key advantage of these systems is that an atomic ion having forbidden spectrally ultra narrow transitions used as an optical reference is stored in a well-controllable environment.

We report on the spectroscopic research of the electric quadrupole transition of the single trapped ion of ytterbium-171 in the course of development of a highly accurate optical frequency standard.

Miniature endcap trap is used for capturing and retaining the single ^{171}Yb ion in the Lamb-Dicke regime by means of a quadrupole radio frequency potential.

The quasicycling $^2S_{1/2}$ (F=1) → $^2P_{1/2}$ (F=0) electric dipole transition with natural linewidth of 23 MHz at 370 nm is used for Doppler cooling and detection of the ion [1, 2].

Narrow line probe laser at 871 nm is employed to excite the $^2S_{1/2}$ (F=0) → $^2D_{3/2}$ (F=2) electric quadrupole transition of the ion. The linewidth of the free-running laser is decreased to ~ 1 Hz by the Pound-Drever-Hall frequency stabilization to a high-finesse Fabry-Perot etalon made of ultralow expansion (ULE) glass.

The ion state is prepared and interrogated by a tailored laser pulse sequence. The probability of the $^2D_{3/2}$ (F=2, m_F=0) level exitation (quantum jumps) is registered as a function of the probe laser frequency. Detected excitation spectrum of the quadrupole transition consists of several resonances that contain information about the internal state of the trapped ion as well as about its motion and interaction with the environment. The carrier resonance is resolved with a linewidth of about 50 Hz.

The absolute frequency measurement and frequency shifts assessment of the quadrupole transition is under way.

References

[1] S.V. Chepurov, A.A. Lugovoy, S.N. Kuznetsov, Quantum Electronics **44** (6) 527–529 (2014).
[2] O.N. Prudnikov et al., Quantum Electronics **47** (9) 806 – 811 (2017).

Testing the parity symmetry in cold chiral molecules using vibrational spectroscopy

M. Pierens[1], L. Lecordier[1], D.B.A. Tran[1], M. Manceau[1], A. Cournol[1], R. Santagata[1,4], B. Argence[1,5], A. Shelkovnikov[1,6], A. Goncharov[1,7], O. Lopez[1], C. Daussy[1], C. Chardonnet[1], M. Abgrall[2], Y. Le Coq[2], R. Le Targat[2], H. Álvarez Martinez[2,8], W.K. Lee[2], D. Xu[2], P-E Pottie[2], R.J. Hendricks[3,9], T.E. Wall[3], J. Bieniewska[3], B.E. Sauer[3], M.R. Tarbutt[3], A. Amy-Klein[1], S.K. Tokunaga[1], and B. Darquié[1]

[1]*Laboratoire de Physique des Lasers, CNRS, Université Paris 13, Sorbonne Paris Cité, 93430, Villetaneuse, France*

[2]*LNE-SYRTE, Observatoire de Paris, PSL Research University, CNRS, Sorbonne Universités, UPMC Univ. Paris 06, 75014, Paris, France*

[3]*Centre for Cold Matter, Blackett Laboratory, Imperial College London, London, SW7 2AZ, United Kingdom*

[4]*present address: ONERA, The French Aerospace Lab., Centre de la Hunière, BP 80100, Palaiseau, 91123, France*

[5]*present address: Laboratoire Kastler Brossel, UPMC-Sorbonne Universités, CNRS, ENS-PSL Research University, Collège de France, F-75005, Paris, France*

[6]*permanent address: P.N. Lebedev Physics Institute, Russian Academy of Sciences, 119991, Moscow, Russia*

[7]*permanent address: Institute of Laser Physics of SB RAS, Pr. Lavrentyeva 13/3, Novosibirsk, 630090, Russia*

[8]*present address: Real Instituto y Observatorio de la Armada in San Fernando, Spain*

[9]*present address: National Physical Laboratory, NPL, Teddington, TW11 0LW, United Kingdom*

E-mail: benoit.darquie@univ-paris13.fr

Unlike other fundamental interactions, the weak interaction does not conserve the parity symmetry, *i.e.* the symmetry under spatial inversion. This was experimentally measured in nuclear, atomic and high energy physics. However, despite being theoretically predicted, parity violation (PV) has yet to be demonstrated in the molecular domain. The Standard Model predicts that parity violating electroweak interactions should lead to a tiny energy difference between enantiomers of chiral molecules (enantiomers are non-superimposable mirror images of a chiral molecule), and in turn to frequency differences in their rovibrational spectra potentially measurable using precise mid-infrared spectroscopic measurements. PV frequency shifts are however predicted to be extremely small, in the millihertz to hertz range for vibrational transitions at ~30 THz [1], depending on the species considered. A successful PV measurement will shed some light on the origins of biomolecular homochirality. It can also constitute a test of the Standard Model in the low-energy regime and a probe of physics beyond it, and serve as a stringent benchmark in relativistic quantum chemistry calculations.

Attempting a measurement of PV in chiral molecules starts with the choice of the molecular species to be probed. As the PV effects scale with the fifth power of the nuclear charge *Z*, large molecules with heavy atoms are considered [1]. Chiral species with a rhenium atom are currently under study [2]. The transitions of interest for measuring PV are vibrational transitions of modes involving the heavy atom, typically in the mid-infrared region of the electromagnetic spectrum (~10 μm). We are constructing a Ramsey interferometry experiment which comprises three parts: the preparation of molecules in cold, slow and intense beams, an interrogation zone using an ultra-stable and tuneable mid-infrared laser system and finally a detector of internal molecular state populations. Molecules will be prepared in high flux, low velocity buffer-gas-cooled beams, one of the latest molecular beam technologies. After exiting the cryogenic buffer-gas cell, the molecular beam will be probed in a Ramsey interferometer based on frequency stabilized quantum cascade lasers (QCLs) calibrated against primary standards. QCLs offer broad and continuous tuning and cover the entire mid-infrared window thus providing considerable flexibility on the chosen rovibrational transitions to be studied. After the mid-infrared Ramsey interrogation, the population needs to be measured. We are currently investigating new measurement procedures involving microwave fields driving rotational transitions to enhance the detection sensitivity compared to conventional direct mid-infrared absorption schemes and to enable enantiomer-specific measurements [3].

In this context, we will present our ongoing work towards producing buffer-gas beams of complex and heavy polyatomic species. We have demonstrated for the first time cryogenic buffer-gas cooling of gas-phase complex and heavy organometallic species methyltrioxorhenium (MTO, see Fig. 1) [4,5]. This molecule is closely related to chiral organometallic molecules where the parity-violating energy differences between enantiomers is measurable [2]. This extends buffer-gas cooling to a new

class of molecules, and we introduce them into the cell by laser ablation, previously used only for diatomic molecules. We have demonstrated the first precise spectroscopic measurements of buffer-gas-cooled molecules in the mid-infrared region around 10 µm, obtaining rotational and hyperfine-resolved absorption spectra allowing the determination of the nuclear quadrupole coupling of the excited vibrational state, which is unprecedented for such a complex molecule. We have also demonstrated cryogenic buffer-gas cooling of another 12 atoms polyatomic molecule, trioxane and have performed the first sub-Doppler spectroscopic measurements of buffer-gas-cooled molecules in the fingerprint region, recording saturated absorption spectra.

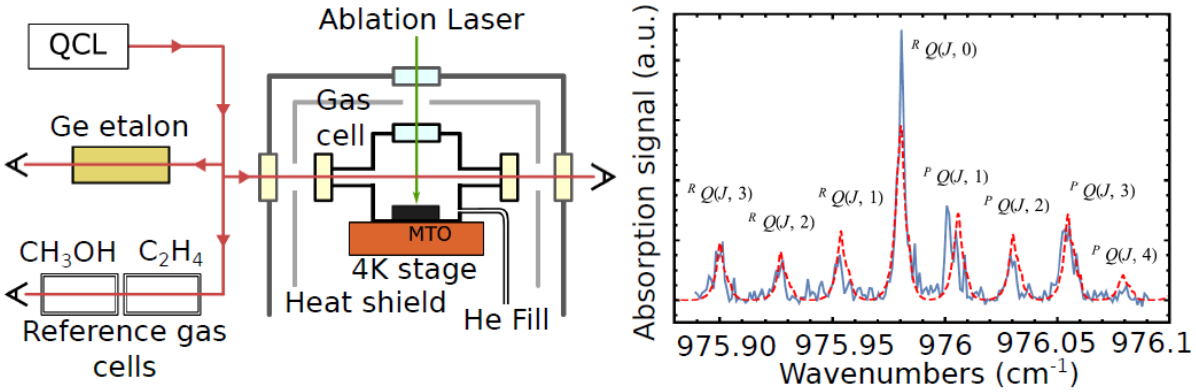

Fig. 1 Left: Setup, buffer-gas cooling and linear spectroscopy of MTO. Right: Linear absorption spectrum of the *Q* branch of the antisymmetric Re=O stretching mode of MTO.

We will also present our new widely tuneable spectrometer based on QCLs with direct traceability to primary frequency standards [6]. *Via* an optical frequency comb, a QCL is stabilized at the sub-Hz level on an ultra-stable near-infrared reference signal provided by the French metrology institute (SYRTE) to our laboratory and transferred through a 43-km long fiber cable. The stability of the reference is transferred to the QCL, which therefore exhibits a relative frequency stability lower than 2×10^{-15} between 1 and 100 s. Moreover, its absolute frequency is known with an uncertainty below 10^{-14} thanks to the traceability to the primary standards of SYRTE. The setup allows the QCL to be widely scanned over ~1 GHz while maintaining the highest stabilities and accuracies. We report saturated absorption spectroscopy investigations conducted around 10 µm on osmium tetroxide, methanol, ammonia and trioxane, allowing central frequencies to be determined with record uncertainties.

References

[1] S. K. Tokunaga, C. Stoeffler, F. Auguste et al., Mol. Phys. **111**, 2363 (2013).
[2] N. Saleh, R. Bast, N. Vanthuyne et al., Chirality **30**, 147 (2018).
[3] S. Eibenberger, J. Doyle, D. Patterson, Phys. Rev. Lett. **118**, 123002 (2017).
[4] S. K. Tokunaga, R. J. Hendricks, M. R. Tarbutt et al., New J. Phys. **19**, 053006 (2017).
[5] P. Asselin, Y. Berger, T. R. Huet et al., Phys. Chem. Chem. Phys. **19**, 4576 (2017).
[6] B. Argence, B. Chanteau, O. Lopez et al., Nature Photon. **9**, 456 (2015).

Non-linear spectroscopy of Mg and Ca atoms in optical frequency standards

V.D. Ovsiannikov[1], S.I. Marmo[1], S.N. Mokhnenko[1], and V.G. Palchikov[2,3]
[1]*Voronezh State University, Voronezh, 394006, Russia*
[2]*FGUP "VNIIFTRI", Mendeleevo, 141570, Moscow region, Russia*
[3]*National Research Nuclear University "MEPhI", Moscow, 115409, Russia*
E-mail: vitpal@mail.ru

The use of optical lattices for trapping ensembles of super-cooled atoms, practically non-interacting with one another allows for constructing high-efficient frequency standards of record precision. Magic frequencies of optical lattice enable elimination of the lowest-order dynamic Stark effect on the standard frequency. On the other side, the nonlinear, non-dipole and anharmonic-motion effects of higher-order atom-field interaction may introduce uncertainties constraining the standard precision. Elimination or/and high-precision account for the uncertainties require high-accuracy tuning parameters (intensity, frequency, polarization) of the lattice radiation introducing a concept of an "operational magic frequency" [1-3].

Mg and Ca atoms are the lightest of the alkaline-earth elements, therefore the most difficult for cooling and trapping in the field of optical lattice. Besides that, very low natural abundance of odd (fermion) isotopes of these elements (below 10% for Mg and below 0.15% for Ca) with non-zero nuclear angular momentum enabling magnetically induced mixing of a $^3P_1$-state to the metastable state $^3P_0$, impedes significantly observation of strongly forbidden line of the radiation transition from the metastable state. Nevertheless, a possibility for such observation exists with the use of the magnetic field mixing the states $^3P_0$ and $^3P_1$ [4-6]. The quality factor of the magnetically induced oscillations will depend on the magnitude of the magnetic field and on the energy of the spin-orbit splitting of the triplet state $^3P_{J=0,1,2}$.

In the present paper, the multipole, nonlinear and anharmonic effects on the optical-lattice-based clocks of Mg and Ca atoms are evaluated theoretically. Dipole polarizabilities, hyperpolarizabilities and multipolar polarizabilities for Mg and Ca atoms are calculated in the single-electron approximation with the use of analytical presentations for the Green's function in the modified model-potential approach.

Finally, the dependence on the intensity I of the magic-frequency optical lattice for the total shift of the standard frequency with account for the terms up to quadratic in I, may be presented, as follows for the Mg atom interaction with the field of the optical lattice radiation:

$$\Delta\nu_{cl}^{latt}(n,I,\delta)=\left(6.33\delta-8.25\right)\left(n+1/2\right)I^{1/2}-\left[0.42\delta+(0.397+0.021i)\left(n^2+n+1/2\right)\right]I$$
$$+0.(334+0.0177i)\left(n+1/2\right)I^{3/2}-(0.111+0.0059i)I^2 \quad \text{mHz},$$

where the intensity is measured in kW/cm^2. A similar equation for Ca atoms may be written as

$$\Delta\nu_{cl}^{latt}(n,I,\delta)=\left(0.0589\delta+0.432\right)\left(n+1/2\right)I^{1/2}-\left[0.273\delta+0.138\left(n^2+n+1/2\right)\right]I$$
$$+0.428\left(n+1/2\right)I^{3/2}-0.497I^2 \quad \text{mHz}.$$

From these equations an optimal value of the lattice frequency shift δ may be determined for minimizing uncertainties of the optical frequency standard.

References

[1] V. D. Ovsiannikov, V.G. Pal'chikov, A.V. Taichenachev, V.I. Yudin and H. Katori, Phys. Rev. A **88**, 013405 (2013).
[2] H. Katori, V.D. Ovsiannikov, S.I. Marmo and V.G. Pal'chikov, Phys. Rev. A **91**, 052503 (2015).
[3] V.D. Ovsiannikov, S.I. Marmo, V.G. Pal'chikov and H. Katori, Phys. Rev. A **93**, 043420 (2016).
[4] V.D. Ovsiannikov and E.V. Chaplygin, Opt. and Spectr. **90**, 149 (2001). [Opt. i Spektr. **90**, 185 (2001)].
[5] A.V. Taichenachev, V.I. Yudin, C.W. Oates et al., Phys. Rev. Lett. **96**, 083001 (2006).
[6] Barber Z.W., Hoyt C.W., Oates C.W. et al, Phys. Rev. Lett. **96**, 083002 (2006).

Superfluid dynamics in Bose gases

R. Dubessy, M. de Goër de Herve, A. Kumar, Y. Guo, T. Badr,
A. Perrin, L. Longchambon, and H. Perrin
Laboratoire de physique des lasers, CNRS UMR 7538 and Paris 13 University, Sorbonne Paris Cité
99 av. J.-B. Clément, 93430, Villetaneuse, France
E-mail: helene.perrin @ univ-paris13.fr

Ultra-cold gases, below the critical temperature of quantum degeneracy, exhibit superfluid properties when the interactions between atoms are weak and repulsive. This is the case, for example, of three-dimensional Bose-Einstein condensates. In dimension two, Bose-Einstein condensation is only present for a finite size system (trapped in particular). However, the gas is still superfluid below a critical temperature, through the Berezinskii-Kosterlitz-Thouless (BKT) vortex pairing mechanism.

Evidencing superfluidity in a quantum gas requires the use of experiments probing the gas dynamics. Indeed, superfluidity is characterized by different dynamical criteria:

- the existence of a critical speed for excitation, below which the superfluid remains at rest (Landau criterion); correlated with this is the resistance to the setting into rotation, with a vanishing moment of inertia; symmetrically, the persistence of the flow when the superfluid is set into rotation in an annular container (which can be an immaterial trap)

- the irrotational character of the flow and the quantization of the circulation of its velocity (its integral on a closed contour) in units of h/M, where M is the mass of the atom, which leads to the presence of quantized vortices when the gas is rotated fast enough.

At LPL we highlighted various signatures of the superfluid dynamics of a Bose gas: the existence of a scissor mode, whose local measurement of the frequency makes it possible to locate the boundary between the normal phase and the superfluid phase of an inhomogeneous 2D gas [1]; the multiplication of quantized vortices as the gas is rotated fast enough, with an analogy with the quantum Hall physics; and the presence of a persistent flow in a superfluid gas placed in annular geometry. The first experiment has been discussed at the previous MPLP conference in 2016. Here I will focus on the two last signatures.

Fast rotation of a Bose-Einstein condensate confined in an anharmonic trap: As a trapped Bose-Einstein condensate is set into rotation, vortices enter the cloud and arrange in an Abrikosov lattice, see Fig. 1, evidencing its superfluid character. Due to the centrifugal force, the trap opens are the rotation frequency is increases, and would vanish is the rotation exceeds the trapping frequency. We use however an anharmonic trap, where atoms are confined to the surface of an ellipsoid [2-4]. As the trapping frequency is exceeded, the atoms remain confined in this "bubble" trap and a hole forms in the center of the cloud. In the meantime, the vortex lattice melts. Our trapping geometry thus gives access to the extreme rotation regime, where interactions and finite temperature should govern the density and phase fluctuations.

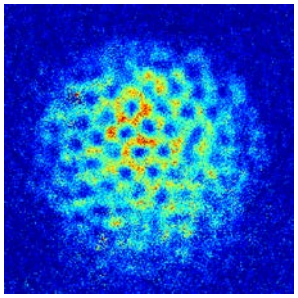

Fig. 1 Abrikosov vortex lattice resulting from a rotation of the condensate trapped at the bottom of the "bubble" trap (top view).

Circulation of an annular quantum gas: In another experiment, we placed the gas in an annular trap resulting from the former ellipsoid combined with a dipole trap which ensures a vertical confinement at the equator of the ellipsoid. The condensate is excited by imposing a weak anisotropy on the ring, which is rotated. This allows to prepare a persistent flow, with a non-zero circulation. A controlled circulation can also be prepared by phase imprinting [5]. The existence of a persistent flow is revealed after a time-of-flight expansion through the presence of a central hole in the density distribution, which size is determined by the circulation.

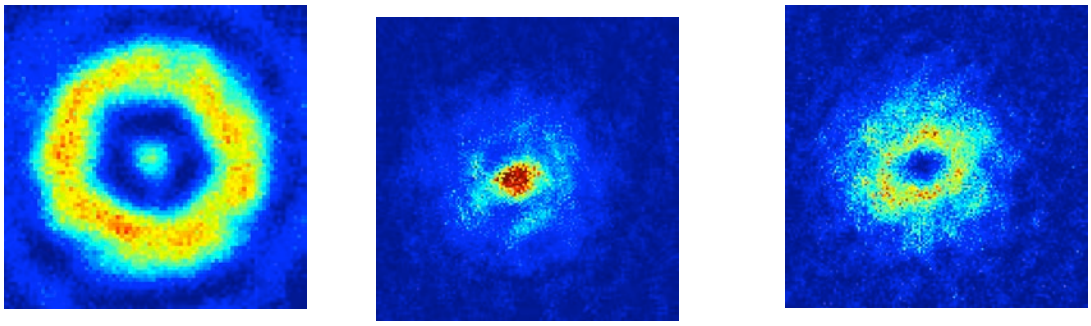

(a) (b) (c)

Fig. 2 In situ image of superfluid gas confined in an annular trap with a radius of 20 micrometers (the central point is the diffraction due to the resolution of the imaging optics). (b-c) Density distribution after time-of-flight. (b) The superfluid is at rest, the density is maximum at the center. (c) The superfluid has a non-zero circulation, which results in a hole in the center.

References

[1] C. De Rossi et al., New J. Phys. **18**, 062001 (2016).
[2] K. Merloti et al., New J. Phys. **15**, 033007 (2013).
[3] B. M. Garraway and H. Perrin, J. Phys. B **49**, 172001 (2016).
[4] H. Perrin and B. M. Garraway, Advances in Atomic, Molecular and Optical Physics **66**, Chapter 4, p. 181-262 (2017).
[5] A. Kumar et al., Phys. Rev. A **97**, 043615 (2018).

Laser cooling on narrow-line optical transitions

O.N. Prudnikov[1,2], R.Ya. Ilenkov[1,2], A.V. Taichenachev[1,2], V.I. Yudin[1-3]
[1]*Institute of Laser Physics SB RAS, 15B Lavrentiev ave., 630090, Novosibirsk, Russia*
[2]*Novosibirsk State University, 2 Pirogova str., 630090, Novosibirsk, Russia*
[3]*Novosibirsk State Technical University, 630073, Novosibirsk, Russia*
E-mail: oleg.nsu@gmail.com

Deep laser cooling of atoms nowadays has a lot of application for new quantum sensors like high sensitive atom interferometers [1] and modern atomic clocks. However, for atoms with single ground state ^{24}Mg, ^{40}Ca, ^{88}Sr, ^{174}Yb are of interest for developing optical time standard [2] the known techniques of sub-Doppler cooling cannot be applied. For example, for ^{24}Mg atoms with the ground state $^1S_0$ the limit of laser cooling temperature is Doppler cooling temperature ($k_BT_D \approx \hbar\gamma/2$) [3] on closed singlet transition $^1S_0 \rightarrow {}^1P_1$ (λ = 285.3 nm) is about 1.2 mK [4] that is relatively large for trapping the atoms in optical lattice for optical clock realization. The further sub-recoil cooling is required.

One way of reaching deeper cooling temperature for these atoms is to use a narrow-line optical transition (clock transition) with smaller natural linewidth γ. For these atoms one may expect the lower temperature. However, the basic semiclassical theory becomes no more valid due to violation of the main requirement that is called semiclassical limit $\omega_R << \gamma$ (with $\omega_R = \hbar k^2/2M$ is recoil frequency describes the energy obtained by atom at rest due to spontaneous emission or absorption of the light field photon with momentum $\hbar k$). For laser cooling study of atoms on narrow-line optical transition $\omega_R \geq \gamma$ the approach allowing to account the photon recoil accurately is required.

In the following, we build the theory of laser cooling of atoms in the regimes the quantum nature of laser-light interactions has significant recoil effect. We make analysis of time evolution and steady-state of laser cooling of atoms with use of narrow-line optical transition in standing wave and σ_+-σ_- light field.

We show that in the case $\omega_R \geq \gamma$ is far beyond the semiclassical theory of laser cooling the set of dimensionless parameters Ω_0/ω_R and δ/ω_R (i.e. Rabi frequency and detuning measured in recoil frequency units) uniquely describe the evolution of momentum distribution function for various atoms (Fig.1.). Moreover, the time evolution scales in γ^{-1} units apart from the semiclassical theory, where the cooling time scales in ω_R^{-1} units.

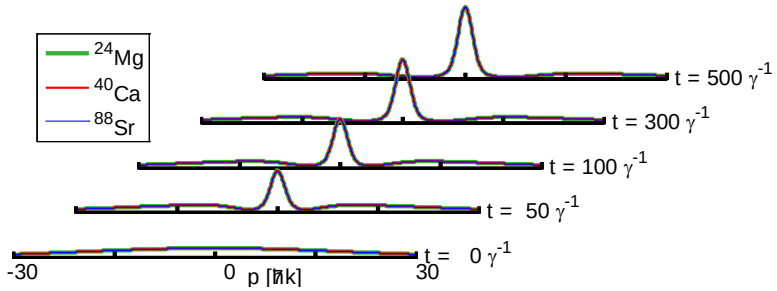

Fig. 1 Time evolution of momentum distribution of laser cooling different atoms for equivalent time in γ^{-1} units and light field parameters Rabi frequency per one wave $\Omega_0 = 5\ \omega_R$, detuning $\delta = -3\ \omega_R$. The initial momentum distribution is Gaussian function with $p_\sigma = 20\ \hbar k$.

The results can be used for analysis an optimal conditions of laser cooling of atoms with narrow lines like *Ca*, *Sr* and *Mg* are of interest for optical time standards.

The work was supported by Russian Science Foundation (project N 16-12-00054). O.N.P acknowledges the support of RFBR (18-42-540003).

References

[5] Jian Cheng Fang and Jie Qin, Sensors **12**, 6331-6346 (2012).
[6] Andrew D. Ludlow et al, Rev. of Mod. Phys **87**, 637 (2015).
[7] A. P. Kazantsev, G. I. Surdutovich, and V. P. Yakovlev, Mechanical Action of Light on Atoms (World Scientific, Singapore, 1990).
[8] F Y Loo, A Brusch et al., J. Opt. B: Quantum Semiclass. Opt. **6**, 81–85 (2004).

Coherent time/frequency links over fiber for relativistic geodesy, radioastronomy and seismology

C. Clivati[1], D. Calonico[1], A. Mura[1], A. Tampellini[1,2], and F. Levi[1]
[1]*Physics Metrology Division, Istituto Nazionale di Ricerca Metrologica, 10135, Turin, Italy*
[2]*Politecnico di Torino, 10134, Turin, Italy*
E-mail: c.clivati@inrim.it

Actively-stabilized optical fiber links allow the distribution of high-accuracy optical frequency signals through thousands of kilometers, outperforming satellite techniques by several orders of magnitudes for what concerns continental distances coverage. Recently, the first comparisons of frequency standards with optical fiber links have been performed [1-5]. At the same time, fiber-based frequency dissemination techniques are being adopted in other fields, such as spectroscopy [6-8], radioastronomy [9-11] and geodesy [5], where they provide improved measurement capabilities.

The Italian National Metrology Institute, INRIM, has developed a 1700 km coherent optical link for frequency and time dissemination to scientific users throughout the Country that are not involved in primary metrology. At the conference, we will describe our recent advances and the applications in fields such as radioastronomy, geodesy, and high-resolution spectroscopy.

A first 642-km-long phase-stabilized link, under operation since 2013, connects INRIM to the European Laboratory for Non Linear Spectroscopy (LENS). It provides a long-term-stable frequency reference that allowed quantum simulation experiments on a cold ^{173}Yb sample. Such kind of experiments relies on the cyclical, long-term interrogation of the ultranarrow $^1S_0$-$^3P_0$ ^{173}Yb transition, and cannot be performed with standard tools such as high-finesse optical cavities and GPS references alone [7]. At LENS, the fiber-disseminated signal was also used to provide absolute traceability for molecular spectroscopy in the mid-infrared [8].

A second 535-km link connects INRIM to the Radiotelescopes operated by the National Institute of Astrophysics in Medicina, central Italy. Here, it provides an ultrastable microwave reference for Very Long Baseline Interferometry, that successfully replaced the local hydrogen maser in several VLBI campaigns [9]. We are currently extending the network from the Medicina Radiotelescopes to the Space Geodesy Centre in Matera, 1700 km away from INRIM, to simultaneously disseminate the same frequency reference to multiple telescopes. With this combined infrastructure, we will investigate fundamental limitations of VLBI at an unprecedented resolution.

A third span connects INRIM to the Laboratorie Souterraine de Modane, in the French Alps (total length 150 km). This was realized as a part of an international collaboration in the framework of the EMPIR programme ("International Timescales on Optical Clocks" project) for a proof-of-principle relativistic geodesy experiment, in which optical clocks were used as probes for the geodetic potential [5]. This experiment paves the way for a new era in chronometric leveling, where transportable optical clocks, operated together with fiber links, could allow gravitational potential measurements with higher temporal resolution.

At the conference, we will describe the present fiber infrastructure and report on our recent results on the above-mentioned applications.

References

[1] J. Guéna, S. Weyers, M. Abgrall et al., Metrologia **54**, 348 (2017).
[2] Ch. Lisdat, G. Grosche, N. Quintin et al., Nat. Commun. **7**, 12443 (2016).
[3] P. Delva, J. Lodewyck, S. Bilicki et al., Phys. Rev. Lett. **118**, 221102 (2017).
[4] T. Takano, M. Takamoto, I. Ushijima et al., Nat. Photonics **10**, 662 (2016).
[5] J. Grotti, S. Koller, S. Vogt, et al., Nature Physics **14**,437 (2018).
[6] B. Argence, B. Chanteau, O. Lopez, et al., Nat. Photonics **9**, 456 (2015).
[7] C. Clivati, G. Cappellini, L. F. Livi, et al., Opt. Express **24**, 11865 (2016).
[8] G. Insero, S. Borri, D. Calonico, et al., Sci. Rep. **7**, 12780 (2017).
[9] C. Clivati, R. Ambrosini, T. Artz, et al., Sci. Rep. **7**, 40992 (2017).
[10] P. Krehlik, L. Buczek, J. Kolodziej, et al., Astron. Astrophys. **603**, A48 (2017).
[11] Y. He, K. G. H. Baldwin, B. J. Orr, et al., Optica **5**, 138 (2018).

Matter wave interferometers interacting with the external world: decoherence, gravity, complementarity and time irreversibility

R. Folman and the Atom Chip group / Ben-Gurion University of the Negev

Matter-wave interferometry provides an excellent tool for probing the environment and studying its coupling to isolated atoms. We will present several interferometry experiments done with a BEC on an atom chip [1] and in which different effects of the environment have been investigated. First, we will discuss fluctuations in the nearby environment probed by an interference of atoms trapped in a magnetic lattice very close (5μm) to a room temperature surface [2,3]. Here an order-of-magnitude improvement has been obtained over previous atom-surface distances for which spatial interference has been observed. Next, we will present a new interferometry of self-interfering clocks and show, in a proof-of-principle experiment, how it could probe the interplay of QM and GR [4]. We will also describe a rule for "clock complementarity", which we deduce theoretically and verify experimentally [5]. Finally, we will discuss Stern-Gerlach interferometry [6] and describe it in the context of time irreversibility [7]. To the best of our knowledge, this is the first time spatial Stern-Gerlach interferometry (as originally envisioned) has been realized, and we analyze our data in the context of previous theoretical work relating the difficulties in realizing Stern-Gerlach interferometry to time irreversibility.

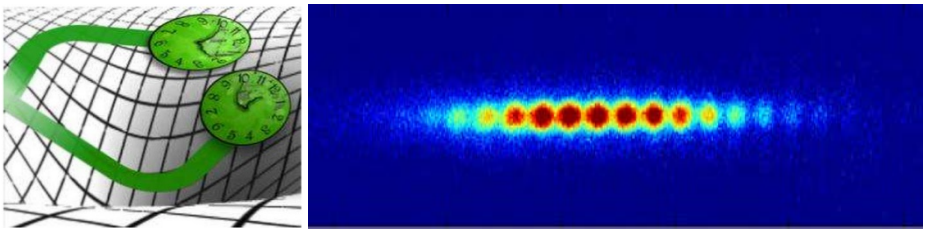

Fig. 1 Spatial clock interferometry [4].

References

[1] M. Keil et al., "Fifteen years of cold matter on the atom chip: Promise, realizations and prospects", Journal of Modern Optics **63**, 1840 (2016).
[2] S. Zhou et al., "Robust spatial coherence 5μm from a room temperature atom-chip", Phys. Rev. A **93**, 063615 (2016).
[3] Y. Japha et al., "Suppression and enhancement of decoherence in an atomic Josephson junction", New J. Phys. **18**, 055008 (2016).
[4] Y. Margalit et al., "A self-interfering clock as a 'which path' witness", Science **349**, 1205 (2015).
[5] Z. Zhou et al., "Clock complementarity in the context of general relativity", https://arxiv.org/abs/1802.09235 (2018).
[6] S. Machluf et al., "Coherent Stern-Gerlach momentum splitting on an atom chip", Nature Communications **4**, 2424 (2013).
[7] Y. Margalit et al., "Realization of a complete Stern-Gerlach interferometer", https://arxiv.org/abs/1801.02708 (2018).

Gravity, blackbody radiation and chameleons – Towards lattice atom interferometry

P. Haslinger[1], M. Jaffe[2], V. Xu[2], O. Schwartz[2,3], M. Sonnleitner[5], M. Ritsch-Marte[4], H. Ritsch[5], and H. Müller[2,3]

[1]*Vienna Center for Quantum Science and Technology, Atominstitut, TU Wien, Stadionallee 2, 1020, Vienna, Austria*
[2]*Department of Physics, 366 Le Conte Hall MS 7300, University of California–Berkeley, Berkeley, CA 94720, USA*
[3]*Molecular Biophysics and Integrated Bioimaging, Lawrence Berkeley National Laboratory, Berkeley, CA 94720, USA*
[4]*Division for Biomedical Physics, Medical University of Innsbruck, Muellerstrasse 44, A-6020, Innsbruck, Austria*
[5]*Institute for Theoretical Physics, University of Innsbruck, Innsbruck, Austria*
E-mail: philipp.haslinger@univie.ac.at

Within the last decades atom interferometry has proven its surprising versatility to sense with high precision tiniest forces. In this talk I will give an overview of our recent work using an optical cavity enhanced atom interferometer to sense with gravitational strength for fifths forces [1, 2] and for an on the first-place counterintuitive inertial property of blackbody radiation [3].

If dark energy, which drives the accelerated expansion of the universe, consists of a light scalar field it might be detectable as a "fifth force" between normal-matter objects. In order to be consistent with cosmological observations and laboratory experiments, some leading theories use a screening mechanism to suppress this interaction. However, atom-interferometry presents a tool to reduce this screening [4] on so-called chameleon models [5]. By sensing the gravitational acceleration of a 0.19 kg in vacuum source mass which is 10^{-9} times weaker than Earth´s gravity, we reached a natural bound for cosmological motivated scalar field theories and were able to place tight constraints [1, 2].

Blackbody (thermal) radiation is emitted by objects at finite temperature with an outward energy-momentum flow, which exerts an outward radiation pressure. At room temperature e. g. a cesium atom scatters on average less than one of these blackbody radiation photons every 10^8 years. Thus, it is generally assumed that any scattering force exerted on atoms by such radiation is negligible. However, particles also interact coherently with the thermal electromagnetic field [6] and this leads to a surprisingly strong force acting in the opposite direction of the radiation pressure [3].

References

[1] Hamilton, P., Jaffe, M., Haslinger, P. et al. *Science.* **349,** 849–851 (2015).
[2] Jaffe, M., Haslinger, P., Xu, V. et al. *Nat. Phys.* **13,** 938–942 (2017).
[3] Haslinger, P., Jaffe, M., Xu, et al. *Nat. Phys.* **14,** 257–260 (2018).
[4] Burrage, C., Copeland, E. J. & Hinds, E. A. *J. Cosmol. Astropart. Phys.* **2015,** 042–042 (2015).
[5] Elder, B., Khoury, J., Haslinger, P. et al. *Phys. Rev. D* **94,** 044051 (2016).
[6] Sonnleitner, M., Ritsch-Marte, M., Ritsch, H.. *Phys. Rev. Lett.* **111,** 023601 (2013).

BEC interferometry on ground and in space

E.M. Rasel for the QUANTUS/MAIUS cooperation
Institute of quantum optics and QUEST-LFS, Leibniz Universität Hannover
QUEST, Institut für Quantenoptik-Leibniz Universität, Hannover, Germany
E-mail: rasel@iqo.uni-hannover.de

Bose-Einstein condensation (BEC) was awarded with the Nobel prize only 17 years ago. At that time one only could "speculate on areas for the application of BEC. The new "control" of matter which this technology involves is going to bring revolutionary applications in such fields as precision measurement and nanotechnology".

I will motivate why BEC interferometry will become a cornerstone for applications of cold atoms on ground and in space and represents a new field in matter wave optics. These interferometers strive to increase the sensitivity by coherently spitting and separating wave packets over macroscopic spatial and temporal scales. Bose-Einstein condensates (BECs), representing a textbook example for a macroscopic wave packet, are the ideal source for performing this kind of interferometry in very long baseline interferometers stretching out over seconds on ground and during even longer interferometry times in space.

Indeed, BEC interferometry was exploited for the first time in the extended free fall with a chip-based atom laser for Rubidium ^{87}Rb in the QUANTUS collaboration. The design was successfully employed for a rocket based test of such an BEC interferometer, which paves the way for future experiments on sounding rockets, the ISS and on satellites: The explored methods are central to the next more complex sounding rocket missions, the NASA's cold atom laboratory (CAL), to be launched this year, and the envisioned DLR-NASA project of "BECCAL", a multi-user facility for experiments on quantum matter, quantum optics and BEC interferometry. Among others, they will demonstrate important techniques necessary for satellite based quantum tests of Einsteins principle of equivalence as pursued by the STE-QUEST mission, for satellite gravimetry and future gravitational wave detection based on ultracold atoms.

The QUANTUS cooperation comprises the group of C. Lämmerzahl (Univ. Bremen), A. Peters (Humboldt Univ. Berlin/Ferdinand Braun Institut), T. Hänsch/J.Reichel (MPQ/ENS), K. Sengstock/P. Windpassinger (Univ. Hamburg/Univ. Mainz), R. Walser (TU Darmstadt), and W.P. Schleich (Univ. Ulm).

This project is supported by the German Space Agency Deutsches Zentrum für Luft- und Raumfahrt (DLR) with funds provided by the Federal Ministry of Economics and Technology (BMWI) under grant number DLR 50 WM 0346. We thank the German Research Foundation for funding the Cluster of Excellence QUEST Centre for Quantum Engineering and Space-Time Research.

Atom interferometry and precision measurement

L. Zhou[1,2], B. Tang[1,2], J.Q. Zhong[1,2], X. Chen[1,2], Z.W. Yao[1,2], R.B. Li[1,2], J. Wang[1,2], and M.S. Zhan[1,2]
[1]*State Key Laboratory of Magnetic Resonance and Atomic and Molecular Physics, Wuhan Institute of Physics and Mathematics, Chinese Academy of Sciences, Wuhan, 430071, China*
[2]*Center for Cold Atom Physics, Chinese Academy of Sciences, Wuhan, 430071, China*
E-mail: wangjin@wipm.ac.cn

Atom interferometery has been widely applied in weak equivalence principle(WEP) test, rotation mensurement, gravity constant measuremnet, gravity and gravity-gradient menauremnet, and other precision measurments. Based on technology of cold atom interferometer(AI), we carried out gravity measurement and WEP test, developed key technologies and relevant theoretical research work.

We performed a precise measurement of local gravitational acceleration, observed tidal phenomena[1]. We developed a high precision gravimeter using ^{85}Rb atoms, and attend the International Comparison of Absolute Gravimeters 2017 which was held in the Changping Campus of National Institute of Metrology, China from 16th October to 11st November, 2017. The preliminary comparison shows that our atom gravimeter performs well.

In order to achieve longer free fall time, it is necessary to develop a large atom fountain which can provide enough space for atoms to undergo a free fall. In 2011, we designed and completed a long baseline AI for WEP test, and experimentally realized atom fountain with launch height of 6 m [2]. In 2015, we demonstrated a 10^{-8} level test of WEP using ^{85}Rb-^{87}Rb dual-AIs [3]. Recently, we demonstrate the experimental realization of a large atom fountain, the fountain height exceeds 12 m.

We demonstrated a hybrid wide-band, low-phase-noise scheme for Raman lasers in atom interferometry by integrating an acousto-optic modulator and a feedback loop [4]. We presented a new scheme for extracting the differential phase in dua latom interferometers by modulating magnetic fields, this scheme avoids the disadvantages of the ellipse fitting method for extracting the small differential phase, and it is useful for measuring the arbitrary differential phase of the dual AIs [5]. We proposed and realized a normalized detection by using the blow-away signal in cold atom interferometry, the detection system and procedure are simplified, both amplitude noise in atom source and short term phase noise of interference fringes are suppressed by more than a factor of 10 with normalized detection[6]. We investigated the location-dependent Raman transition in gravity-gradient measurements using dual atom interferometers, optimized the precision of the gravity-gradient measurements by adjusting the interaction location [7]. We theoretically analyzed the wave-front aberration phase noise (WAPN) in WEP tests using dual-species atom interferometers and proposed an expansion-rate-selection method to suppress the WAPN in both isotopic and non-isotopic atom interferometers [8].

We proposed and demonstrated a method for calibrating atomic trajectories in a large-area dual-atom interferometer gyroscope. The dual-atom-interferometer gyroscope is applied in the measurement of the Earth's rotation. The sensitivity is 1.2×10^{-6} rad s^{-1} $Hz^{-1/2}$, and the long-term stability is 6.2×10^{-8} rad/s @ 2000 s [9].

References

[1] L. Zhou, Z. Y. Xiong, W. Yang, et al., Chin. Phys. Lett. **28**, 013701(2011).
[2] L. Zhou, Z. Y. Xiong, W. Yang, et al., Gen. Relat. Gravit. 2011, **43**, 1931(2011).
[3] L. Zhou, S. T. Long, B. Tang, et al., Phys. Rev. Lett. 2015, **115**, 013003(2015).
[4] K. Wang, Z. W. Yao, R. B. Li, et al., Appl. Opt. **55**, 989, (2016).
[5] Y. P. Wang, J. Q. Zhong, X. Chen, Opt. Commun. **375**, 34(2016).
[6] H. W. Song, J. Q. Zhong, X. Chen, et al., Opt. Express **24**, 028392(2016).
[7] Y. P. Wang, J. Q. Zhong, H. W. Song, et al., Phys. Rev. A **95**, 053612(2017).
[8] J. G. Hu, X, Chen, J. Fang, et al., Phys. Rev. A **96**, 023618 (2017).
[9] Z. W. Yao, S. B. Lu, R. B. Li, et al., Phys. Rev. A **97**, 013620 (2018).

Heralded single-photon and two-photon sources based on nonlinear effects in ring microresonators

I.N. Chuprina[1,2], N.S. Perminov[2,3], and A.A. Kalachev[1,2]
[1]*Institute of Physics, Kazan Federal University, 420008, Kazan, Kremlevskaya str., 16*
[2]*Zavoisky Physical-Technical Institute, Kazan Scientific Center of RAS, 420029, Kazan, Sibirsky tract str., 10/7*
[3]*Kazan quantum center, Kazan National Research Technical University n.a. A.N.Tupolev, 420111, Kazan, K. Marx str., 10*
E-mail: a.a.kalachev@mail.ru

Developing integrated sources of single-photon and entangled two-photon states of light is an important problem of quantum optics and quantum informatics [1, 2]. One promising approach to designing such sources is to use nonlinear optical effects in CMOS-compatible materials, such as silicon nitride [3]. In particular, spontaneous four-wave mixing (SFWM) and third-order spontaneous parametric down-conversion (TOSPDC) in a ring microresonator allows one to combine a number of useful properties in one device. First of all, the rate of the nonlinear process can be substantially increased due to the small volume of modes and high finesse of the resonator, while an increase in the dispersion region in small resonators makes it possible to facilitate frequency demultiplexing and pump field filtering. Second, an increase in the rate of generation of photon pairs by means of a resonator simultaneously reduces their spectral width, making quantum states of light more suitable for recording in quantum memory devices. Third, the CMOS-compatible manufacturing process and high material stability allow one to embed sources into scalable photonic integrated circuits and to approach the deterministic emission of single photons via SFWM or photon pairs via TOSPDC using spatial multiplexing.

In this presentation, we would like to discuss some promising schemes of heralded sources of single photons and photon pairs based on SFWM and TOSPDC, respectively, in ring microresonators. In the first case, we present the optimal design for an integrated SFWM-based single-photon source, which consists of a system of coupled ring microresonators and provides the highest purity of generated photons [4]. In the second case, by considering silicon-nitride based microresonators, we show that the phase-matching condition for degenerate TOSPDC can be attained simultaneously with the zero group velocity dispersion for the triphoton field [5]. Under such conditions, nondegenerate TOSPDC is possible, thereby allowing to produce frequency entangled three-photon states and heralded frequency entangled two-photon states.

Author thanks Russian Science Foundation (Grant No. 16-12-00045) for their support.

References

[1] J.L. O'Brien et al., Nature Photon. **3**, 687 (2009).
[2] S. Tanzilli et al., Laser Photon. Rev. **6**, 115 (2012).
[3] D.J. Moss et al. Nature Photon. **7**, 597 (2013).
[4] I.N. Chuprina et al. (in preparation).
[5] M. Akbari, A.A. Kalachev, Laser Phys. Lett. **13**, 115204 (2016).

Dynamical control of the resonant interaction: Towards quantum x-ray optics and novel x-ray sources

T.R. Akhmedzhanov[1], V.A. Antonov[2], X. Zhang[1], K.C. Han[1], E. Kuznetsova[1], I.R. Khairulin[2], Y.V. Radeonychev[2], and O. Kocharovskaya[1]

[1]*Department of Physics and Astronomy, Texas A&M University, College Station, TX 77843, USA*

[2]*Institute of Applied Physics, Russian Academy of Sciences, Nizhny Novgorod, 603950, Russia*

E-mail: kochar@physics.tamu.edu

We discuss the possibilities to control the spectral/temporal characteristics of an x-ray radiation via variation in time/space of the parameters of its resonant interaction with a medium (atomic or nuclear transitions in gases, plasmas or solids) driven by a sufficiently strong low-frequency laser field. We consider several applications of such technique for (i) a production of the intense attosecond pulses in a soft x-ray range (including a "water window") promising for dynamical microscopy and imaging of material and biological nano-structures (including proteins in living cells), (ii) a spectral enhancement of XFELs radiation promising for ultrahigh resolution x-ray spectroscopy, development of the nuclear frequency standards and x-ray Raman spectroscopy, (iii) a control of the single x-ray photon waveform and a realization of quantum interfaces between single photons and nuclear ensembles.

Coherent intense sub-femtosecond (sub-fs) x-ray pulses would provide unique combination of the record high spatial and temporal resolution (ultimately determined by carrier wavelength and pulse duration accordingly). Modern table top x-ray plasma lasers produce high energy pulses (up to several mJ) but of rather long picosecond (ps) duration. The high-harmonic generation (HHG) technique allows to produce attosecond pulses extending to x-ray range, but of rather limited nJ energy. Following to our recent works [1,2], we suggest to combine the advantages of short pulse duration of HHG and high gain of x-ray plasma lasers via amplification of the high-harmonic radiation in an active resonant plasma medium modulated by the strong IR field of the same frequency as used for HHG.

The possibility to strongly amplify a train of attosecond pulses (produced via HHG) with a carrier wavelength 3.38nm (in a "water window" range) in inverted plasma of the resonant hydrogen-like C VI ions driven by an IR field with a wavelength $\lambda_{IR} = 2102.85nm$ and intensity $I_{IR} = 2.7 \times 10^{15} W/cm^2$ is illustrated in Fig.1. The C VI ion concentration and electron densities are chosen to be $N = 10^{19} cm^{-3}$, $N_{el} = 15N$ (corresponding to the maximum gain in x-ray plasma laser at 3.38nm based on C VI ion [3]).

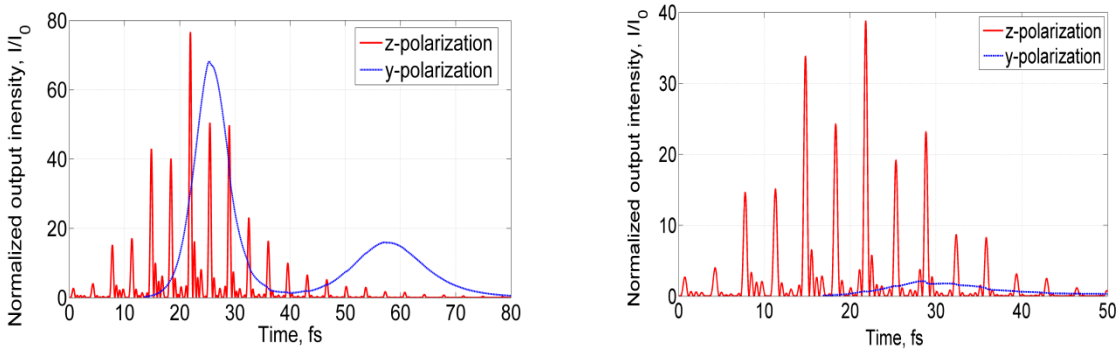

Fig. 1 Amplified z-polarized (red) and y-polarized (blue) X-ray pulses at the output of 1 mm of modulated inverted C VI plasma medium plotted for different peak pulse intensities of an incident z-polarized field: $I_0 = 10^{11} W/cm^2$ and $I_0 = 10^{12} W/cm^2$ accordingly.

Coherent forward scattering of synchrotron radiation is a well-established technique allowing to measure magnetic, structural and dynamic properties of materials. Its spectral resolution is currently limited by the width of the used nuclear transition, namely, 1.14 MHz linewidth at 14.4 keV transition in ^{57}Fe , the traditional "working house" of the Mössbauer spectroscopy.

Using of the longer lived nuclear transitions such as, for example, 12.4 keV transition from the 0.46 s life time isomeric state to the ground state in ^{45}Sc could greatly improve the spectral resolution. Moreover, such nuclear transitions could be potentially used for realization of the nuclear frequency standards of higher accuracy and stability than most advanced atomic optical frequency standards. However, modern x-ray emission sources, including the most advanced XFELs do not allow for observation of such narrow nuclear resonances due to the low spectral fluxes in the corresponding frequency range. We propose a technique for spectral enhancement of the XFELs radiation via spatial/temporal manipulation of its resonant interaction with a resonant nuclear absorber. The basic idea is illustrated by Fig.2. Our estimates show the possibility of about 100 spectral enhancement factor of XFEL's radiation in the vicinity of 12.4 keV transition in ^{45}Sc [4].

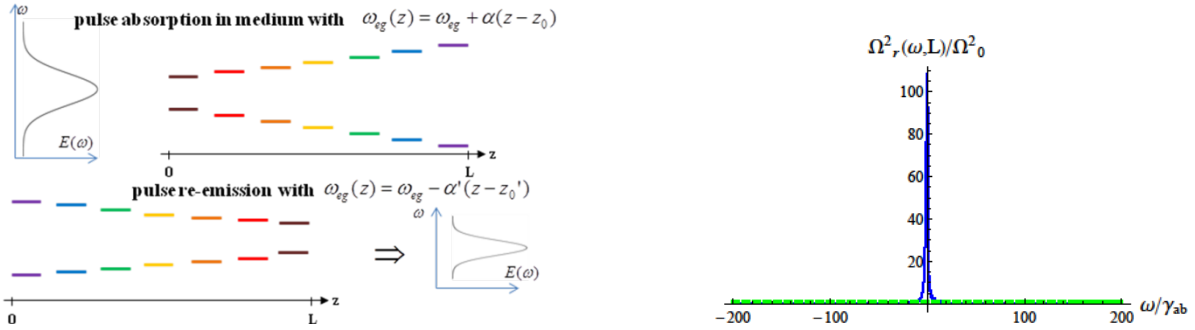

Fig. 2 Introducing the nuclear transition frequency gradient along the propagation direction of an x-ray pulse (matching the spectral width of an incident x-ray radiation) at the absorption stage of an x-ray pulse and switching it (matching the radiative line of the nuclear isomer) at the reemission stage allows to greatly amplify a spectral brightness of an XFEL radiation in the vicinity of the nuclear transition frequency.

We review an emerging field of quantum x-ray optics [5] and discuss advantages/disadvantages of the single hard x-ray photon – nuclear ensemble interfaces vs single optical photon – atomic ensemble interfaces. We demonstrate an efficient manipulation by the temporal waveforms of the single hard x-ray photon via modulation of the frequency nuclear transitions due to Doppler effect caused by an absorber vibrations and suggest a technique for implementation of the nuclear based x-rays quantum memories [6,7].

References

[1] T.R. Akhmedzhanov, M.Yu. Emelin, V.A. Antonov, Y.V. Radeonychev, M.Yu. Ryabikin, O. Kocharovskaya, Phys. Rev. A **95**, 023845 (2017).
[2] T.R. Akhmedzhanov, V.A. Antonov, A. Morozov, A. Goltsov, M. Scully, S. Suckewer, and O.Kocharovskaya, Phys. Rev. A **96**, 033825 (2017).
[3] Y. Avitzour and S. Suckewer, J. Opt. Soc. Am. B **24**, 819 (2007).
[4] E. Kuznetsova, X. Zhang, Yu. Shvyd'ko, M.O. Scully and O. Kocharovskaya, Spectral enhancement of XFEL radiation in a resonant medium via controllable inhomogeneous broadening, unpublished.
[5] E. Kuznetsova and O. Kocharovskaya, Nature Photonics **11**, 685 (2017).
[6] F. Vagizov, V.Antonov, Y.V. Radeonychev, R.N. Shakhmuratov, O. Kocharovskaya, Nature **508,** 80 (2014).
[7] X. Zhang, W.-T. Liao, A. Kalachev, R.N. Shakhmuratov, O. Kocharovskaya, Quantum memory and processing of gamma-photon in a nuclear ensemble, unpublished.

Self-sustained oscillator under a squeezing Hamiltonian

L.C. Kwek, S. Sonar, M. Hajdušek, M. Mukherjee, R. Fazio, V. Vedral, and S. Vinjanampathy
Center for Quantum Technologies, National University of Singapore
E-mail: cqtklc@nus.edu.sg

Self-sustained oscillators are oscillators that do not require external forces to develop oscillations. However, the emergence of synchronization in quantum systems is widely explored. In a recent study, we showed that strong entrainment is possible if a self-sustained oscillator is coupled to a squeezing Hamiltonian, even if the squeezing.

Optimizing the interaction of light with a single atom in free space

B. Srivathsan[1], M. Fischer[1,2], V.A. Averchenko[1], L. Alber[1,2], D.V. Strekalov[1,2], Ch. Marquardt[1,2], M. Sondermann[1,2], and G. Leuchs[1-4]

[1]*Max Planck Institute for the Science of Light, Erlangen, Germany*
[2]*Department of Physics, University Erlangen-Nürnberg, Germany*
[3]*Department of Physics, University of Ottawa, Canada*
[4]*Institute of Applied Physics, Russian Academy of Sciences, Nizhniy Novgorod, Russia*
E-mail: gerd.leuchs@mpl.mpg.de

The emission and absorption of light by a single atom is a most fundamental processes in quantum optics. For an atom in free space the experimental demonstration of optimized coupling is still pending. We distinguish two different scenarios:

1. A single atom should be able to efficiently shift the phase of narrow band coherent light by up to 180° if the light power is not too high.
2. One should be able to deterministically excite a single atom with a single photon.

The largest observed phase shift is of the order of 3° [1,2]. There is still ample room for improvement. Another question is how efficiently one can transfer an atom from the ground to the excited state. The reverse process, spontaneous emission of a photon by an atom, is 100% efficient and exactly one photon is emitted. Because of the unitary character of the evolution of the atom-field-system a single impinging photon should suffice to transfer the atom to the excited state with maximum efficiency [3]. We are trying to set-up a demonstration of this reversal of spontaneous emission by placing a single atom at the focus of a deep parabolic mirror. It is expected that such a 100% excitation requires sending in the time-reversed version of a spontaneously emitted photon, which would be emitted by the same atom if it were to decay. Regarding the spatial structure, focusing via the parabolic mirror generates the required ingoing spherical wave fronts. Concerning the temporal shape, the single photon wave packet should have an exponentially rising leading edge as opposed to the exponentially falling trailing edge of the wave packet created in a spontaneous emission process [4].

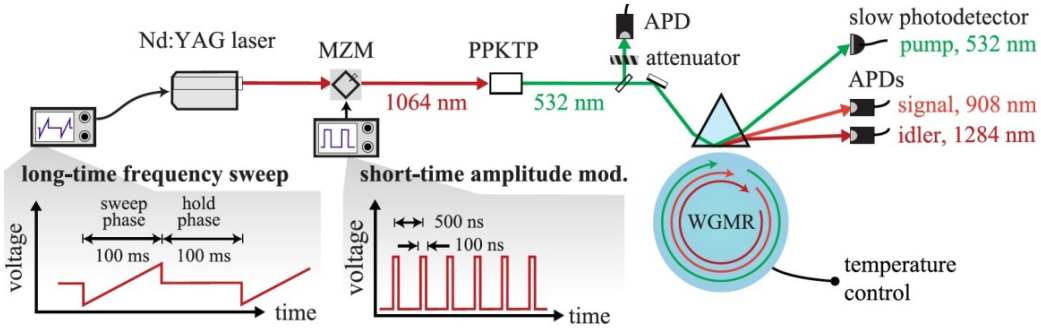

Fig. 1 Generation of temporally shaped single photon wave packets (from [5]).

We will generate the required temporally shaped single photon wave packet in a heralded way [5] from narrowband photon pairs produced in cavity-assisted spontaneous parametric down-conversion [6]. Time energy entangled photons with tailored spectro-temporal properties are particularly useful for efficiently interfacing light to a single atom

G.L. thanks the European Research Council for their supports (ERC-AG 'PACART').

References

[1] M Pototschnig, Y Chassagneux, J Hwang et al. , Phys. Rev. Lett. 107, 063001 (2011).
[2] M Fischer, B Srivathsan, L Alber et al., Appl. Phys. B 123, 48 (2017).
[3] S Quabis, R Dorn, M Eberler, , Opt. Commun. 179, 1 (2000).
[4] M Stobinska, G Alber, and G Leuchs, Euro Phys. Lett. 86, 14007 (2009).
[5] VA Averchenko, D Sych, G Schunk, U Vogl, Ch Marquardt, G Leuchs, Phys. Rev. A 96, 043822 (2017).
[6] G Schunk, U Vogl, DV Strekalov, M Förtsch, F Sedlmeir, HGL Schwefel, M Göbelt, S Christiansen, G Leuchs, Ch Marquardt, Optica 2, 773 (2015).

Spectroscopy of many-body interactions between cold Rydberg atoms

I.I. Ryabtsev[1,2], I.I. Beterov[1,2], D.B. Tretyakov[1,2], E.A. Yakshina[1,2], V.M. Entin[1,2], P. Cheinet[3], P. Pillet[3]
[1]*Rzhanov Institute of Semiconductor Physics SB RAS, 630090, Novosibirsk, Russia*
[2]*Novosibirsk State University, 630090, Novosibirsk, Russia*
[3]*Laboratoire Aime Cotton, CNRS, Univ. Paris-Sud, ENS Paris-Saclay, 91405, Orsay, France*
E-mail: ryabtsev@isp.nsc.ru

Strong long-range interactions between highly excited Rydberg atoms form the basis for quantum information processing with neutral trapped atoms [1]. Entangled states can be generated using a temporary excitation of ground-state atoms to a strongly interacting Rydberg state. In this report we will present our related experimental results on long-range many-body interactions between cold Rb Rydberg atoms in a magneto-optical trap, as well as our theoretical results on quantum information processing with many-body interactions of Rydberg atoms.

In the experiments with cold Rb atoms, we have observed for the first time a resonant dipole-dipole interaction (Stark-tuned Förster resonance) between two cold Rb Rydberg atoms confined to a small laser excitation volume [2]. We also observed radio-frequency-assisted Förster resonances in a few cold Rb Rydberg atoms which cannot be tuned by dc electric field [3,4]. They imply an efficient transition from van der Waals to resonant dipole-dipole interaction due to Floquet sidebands of Rydberg levels appearing in the rf-field. This method can be applied to enhance the interactions of almost arbitrary Rydberg atoms with large principal quantum numbers.

Some quantum gates and simulations demand to control the interactions of simultaneously three atoms. Three-body Förster resonances at long-range interactions of Rydberg atoms were first predicted and observed in Cs Rydberg atoms [5]. In these resonances, one of the atoms carries away an energy excess preventing the two-body resonance, leading thus to a Borromean type of Förster energy transfer. We have recently observed the three-body Förster resonances for a few Rb Rydberg atoms [6]. As the observed three-body resonances appear at the different dc electric field with respect to the two-body resonance, they represents an effective three-body operator, which can be used to directly control the three-body interactions in quantum simulations and three-qubit quantum gates with Rydberg atoms.

We proposed theoretically schemes of quantum gates based on the adiabatic passage of the Stark-tuned and radio-frequency-assisted Förster resonances [7-10]. We are also developing schemes to implement three-qubit quantum gates (e.g., Toffoli gate) based on coherent electrically-controlled three-body Förster resonances.

This work was supported by the RFBR Grants No. 16-02-00383 and 17-02-00987, the Russian Science Foundation Grants No. 16-12-00028 (for laser excitation of Rydberg states) and 18-12-00313 (for theoretical analysis), the Siberian Branch of RAS, the Novosibirsk State University, the public Grant CYRAQS from Labex PALM (ANR-10-LABX-0039) and the EU H2020 FET Proactive project RySQ (Grant No. 640378).

References

[1] I.I.Ryabtsev et al., Physics − Uspekhi **59**, 196 (2016).
[2] I.I.Ryabtsev et al., Phys. Rev. Lett., **104**, 073003 (2010).
[3] D.B.Tretyakov et al., Phys. Rev. A **90**, 041403(R) (2014).
[4] E.A.Yakshina et al., Phys. Rev. A **94**, 043417 (2016).
[5] R.Faoro et al., Nature Comm. **6**, 8173 (2015).
[6] D.B.Tretyakov et al., Phys. Rev. Lett. **119**, 173402 (2017).
[7] I.I.Beterov et al., Phys. Rev. A **94**, 062307 (2016).
[8] I.I.Beterov et al., Quantum Electronics **47** (5) 455 (2017)
[9] I.I.Beterov et al., Phys. Rev. A **97**, 032701 (2018).
[10] I.I.Beterov et al., Quantum Electronics **48** (5) 453 (2018).

Entangling two individual atoms of different isotopes via Rydberg blockade

Y. Zeng[1-3], P. Xu[1,2], X. He[1,2], Y. Liu[1-3], M. Liu[1,2], J. Wang[1,2], D.J. Papoular[4], G.V. Shlyapnikov[5], and M. Zhan[1,2,†]

[1]*State Key Laboratory of Magnetic Resonance and Atomic and Molecular Physics, Wuhan Institute of Physics and Mathematics, Chinese Academy of Sciences, Wuhan, 430071, China*

[2]*Center for Cold Atom Physics, Chinese Academy of Sciences, Wuhan, 430071, China*

[3]*School of Physical Sciences, University of Chinese Academy of Sciences, Beijing, 100049, China*

[4]*LPTM, UMR8089 of CNRS and Univ. Cergy–Pontoise, F–95302, Cergy–Pontoise, France*

[5]*LPTMS, UMR8626 of CNRS and Univ. Paris–Sud, F–91405, Orsay, France*

E-mail: xupeng@wipm.ac.cn; [†]mszhan@wipm.ac.cn

Among various platforms that have allowed the realization of quantum entanglement, trapped neutral atoms offer unique possibilities for quantum computing and simulations. This is because they allow for an excellent control of the interaction strength over 12 orders of magnitude [1], and for the creation of tunable multidimensional arrays of single atoms [2]. Although important experiments have been done towards realizing useful quantum information processing and quantum simulation with atomic systems, there are several primary challenges to be solved [3]. One of them is quantum non-demolition (QND) and low crosstalk qubit measurement with a few mm qubit spacing. The two-element neutral atom system shows an important advantage here, since substantially different resonant frequencies of the two species allow the spectral isolation and individual addressing of the qubits. Also, manipulating multi-element single atoms can provide extra degrees of freedom for quantum simulations. In realizing a Rydberg quantum simulator [4] another species atomic qubit can work as an auxiliary qubit to manipulate/mediate the many-body spin interaction in target qubits, or provide a dissipative element when being optically pumped.

Here, I will present the first realization of quantum entanglement of two individual neutral atoms of different isotopes [5]. We obtain an entangled state of 87Rb and 85Rb atoms confined in single–atom optical traps separated by 3:8mm. We first realize a C–NOT quantum gate with the raw fidelity of 0.73 ± 0.01 based on a strong heteronuclear Rydberg blockade. Then the entanglement of two different atoms is then deterministically generated with the raw fidelity 0.59 ± 0.03. We encode the control qubit in the ground hyperfine states $|F = 1, m_F = 0\rangle = |\downarrow\rangle$ and $|2, 0\rangle = |\downarrow\rangle$ of ^{87}Rb, whereas the target qubit is encoded inthe states $|2, 0\rangle = |\Downarrow\rangle$ and $|3, 0\rangle = |\Uparrow\rangle$ of ^{85}Rb. For both atoms, the Rydberg state is $|r\rangle = |79D_{5/2}, m_j = 5/2\rangle$. Unlike in the case of the same atoms, we exploit the difference in the resonant frequencies of the two atoms to individually address and manipulate them. In this way, we ensure a negligible crosstalk during state measurements and qubit operations at short interatomic separations. Our results pave a way towards quantum computing with heteronuclear systems and towards the realization of high fidelity state detection, which has recently been predicted not to have any fundamental limit even at room temperature. Our work will trigger the quest for new protocols and scheme to use the double species in quantum simulation and quantum computation.

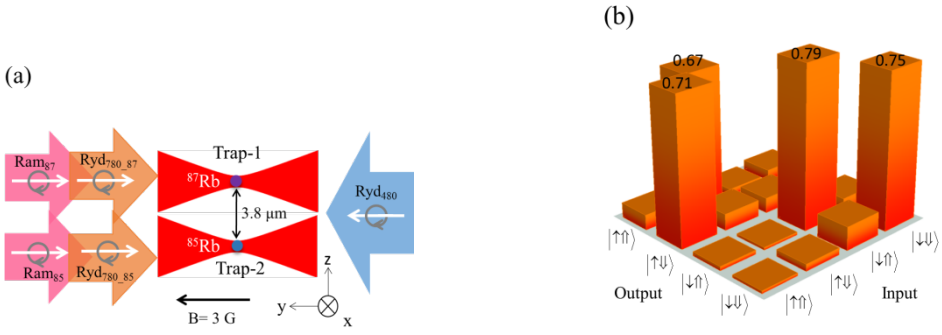

Fig. 1 (a) Experimental geometry. (b) Measured truth table for the CNOT gate which has the fidelity of 0.73 ± 0.01

References

[1] M. Saffman, T. G. Walker, and K. Mølmer, Quantum information with Rydberg atoms, Rev. Mod. Phys. **82**, 2313 (2010)
[2] H. Labuhn, D. Barredo, S. Ravets, S. de Leseleuc, T. Macri, T. Lahaye, and A. Browaeys, Tunable two-dimensional arrays of single Rydberg atoms for realizing quantum Ising models, Nature **534**, 667 (2016).
[3] M. Saffman, Quantum computing with atomic qubits and Rydberg interactions: progress and challenges, J. Phys. B **49**, 202001 (2016).
[4] H. Weimer, M. Muller, I. Lesanovsky, P. Zoller, and H. P. Buchler, A Rydberg quantum simulator, Nat. Phys. **6**, 382 (2010).
[5] Y. Zeng, P. Xu, X.D. He, Y.Y. Liu, M. Liu, J. Wang, D. J. Papoular, G. V. Shlyapnikov, and M.S. Zhan, Entangling Two Individual Atoms of Different Isotopes via Rydberg Blockade, Phys. Rev. Lett. **119**, 160502 (2017).

Ultrafast imaging of atoms and molecules with ultrafast intense laser pulses

X. Liu
Wuhan Institute of Physics and Mathematics, Chinese Academy of Sciences, Wuhan, China

Intense femtosecond laser provides a promising tool to explore the ultrafast electronic dynamics with unprecedented attosecond temporal and angstrom spatial resolution. We will report our recent progresses in ultrafast imaging of the structure and daynamics of atoms or molecules with intense femtosecond laser field.

Plasma physics and particle acceleration studies with high-intensity lasers

M. Starodubtsev, A. Soloviev, K. Burdonov, S.N. Chen, G. Revet, S. Pikuz, S. Ryazantsev, A. Stepanov, A. Murzanev, A. Korytin, A. Sladkov, A. Korzhimanov, V. Ginzburg, E. Khazanov, A. Kochetkov, A. Kuzmin, I. Shaykin, A. Shaykin, I. Yakovlev, J. Fuchs
Institute of Applied Physics RAS, Nizhny Novgorod, Russia
E-mail: mstar@ipfran.ru

A review of recent experimental activities on the PEARL laser system (IAP RAS, Nizhny Novgorod, Russia) in the field of laboratory astrophysics, high energy density physics and particle acceleration is presented.

Scalable femtosecond coherent beam combining

V.I. Trunov, S.N. Bagayev, S.A. Frolov, E.V. Pestryakov
Institute of Laser Physics SB RAS (ILP SB RAS), Novosibirsk, Russia
E-mail: trunov@laser.nsc.ru

The most promising way to create ultra-intense laser systems is to realize the high-efficiency coherent combining of femtosecond pulses amplified in multi-stage OPCPA systems [1]. In this case, it is necessary to use nonlinear-optical crystals in which there is no absorption in both the signal and idler spectrum range.

We review recent progress in coherent beam combining of laser and parametrically amplified femtosecond pulses with active relative jitter stabilization for achievement of ultrarelativistic intensities. Currently, analysis of the possible ways of implementing the coherent beam combining (CBC) for increasing peak intensities assume the use of multichannel systems up to multipetawatt peak power, based on laser and parametric amplification, operating both in single pulse mode (Extreme Light Infrastructure, Exawatt Center for Extreme Light Studies) and in the repetition mode [1]. As shown in our work [2], the efficiency of CBC of amplified pulses is determined by a large number of parameters, among which the most important are angular stability, temporal jitter, and phase distortions. Wherein only the requirements for the angular stability depend on the diameter of the combined beams and become stronger with its increase. Other important parameters of the amplified beams that may degrade with the increasing peak power are the phase distortion, spatial profile and their fluctuations from pulse to pulse. Unfortunately, there are no experimental statistical data on the fluctuations of the pulse parameters for petawatt and multipetawatt laser systems in the literature, only static data are given for some petawatt lasers. In case of using of thirty 0.85 PW beams with phase distortions presented in [3] is expected to achieve efficiency of CBC of about 89.4%.

At present dual-channel multiterawatt femtosecond laser system for investigation of features of CBC based on broadband parametric amplification of chirped Ti:Sa laser pulses in BBO and LBO crystals is designed and developed at ILP SB RAS [2]. The coherent combining efficiency of 95% is achieved with the use of original relative jitter two–loop stabilization setup with a slow loop based on amplified pulse error signal registration and a fast loop based on unamplified pulse error signal measurement, that allows to keep residual jitter as low as 40 as. The spatial distribution of the radiation under coherent combining using tight focusing (F/6.4 paraboloid) provides the total peak intensity of about $2 \cdot 10^{19}$ W/cm^2. Analysis of experimental data shows that reduction of F/D parameter and compensation of aberrations should allow potentially reaching a level of intensity of 10^{20}-10^{21} W/cm^2 in the created system. An analysis of the problem of creating aberration-free compressors for high-power lasers operating in the repetition mode for high efficient CBC and achieving intensities exceeding 10^{23} W/cm^2 is presented.

We also analyze possibility of employing parametric amplification cascades with multiple beam pump for reducing energy requirements for the pump laser and, consequently, to increase the pulse repetition rate in ultra-high-power laser systems [4]. We have performed analysis of BBO, LBO, DKDP and YCOB crystals for multiple beams pumping of optical parametric amplifiers. Also, we find that active angular stabilization of pump beams is important for good stability of amplified beams parameters and retaining high efficiency of their coherent combining.

Finally, the review on main problems in the implementation of the regime of high-efficiency CBC after bulk laser amplification stages is performed. Among them is temporal instability of phase distortions in a laser medium, determined by the combined action of the thermal and electronic mechanisms of their origin. This may be the main obstacle in the realization of the CBC regime.

References

[1] S.N. Bagayev, V. I. Trunov, E.V. Pestryakov et al., Laser Physics, **24,** 074016 (2014).
[2] V.E. Leshchenko, V.I. Trunov, S.A. Frolov, et al., Laser Phys. Lett., **11,** 095301 (2014).
[3] Z. Ren, X. Liang, L. Yu et al., Proc.SPIE, **7916**, 791611 (2011).
[4] S.A. Frolov, V.I. Trunov, Applied Optics, **56,** 6375 (2017).

Competition of high efficiency SHG and MID-IR OPO process in multigrating and fan-out PPMgO:LN pumped by pulsed Tm^{3+}:Lu_2O_3-ceramics laser

D. Kolker[3,5], O. Antipov[1,2], R. Kositsyin[1], D. Kal'yanov[2], S. Larin[4]
[1]*Institute of Applied Physics of Russian Academy of Science, Nizhniy Novgorod, Russia*
[2]*Nizhniy Novgorod State University, Nizhniy Novgorod, Russia*
[3]*Novosibirsk State University, Novosibirsk, Russia*
[4]*NTO «IRE-Polus», Fryazino, Moscow region, Russia*
[5]*Institute of Laser Physics SB RAS, Novosibirsk, Russia*
E-mail: dkolker@mail.ru

Periodically-poled MgO-doped lithium niobate (PPMgO:LN) crystals are well-known nonlinear elements for quasi-phase-matched (QPM) optical parametric oscillators (OPOs) typically pumped by 1-μm laser radiation [1-3]. At the same time, high multi-phonon absorption at wavelengths beyond 4 μm limits the use of PPMgO:LN elements in mid-IR OPO applications [4,5]. In addition to OPO manufacturing for the wavelengths below 4 μm, multigrating PPMgO:LN elements are also used for frequency doubling of the near-IR sources [6-8]. A distinct type of PPMgO:LN crystal, a fan-out PPMgO:LN structure, is suitable both for parametric laser frequency down-conversion from the near-IR to mid-IR region, and up-conversion from the near-IR to visible region by second-harmonic generation (SHG) [9-12]. The variation of a period for the same propagation direction in the structure provides flexible phase-matching conditions for nonlinear interactions [9,10]. Optimal QPM conditions for the fan-out PPMgO:LN structure can be chosen at a fixed temperature by changing the transverse position with respect to the pump beam direction or by changing the temperature at a fixed transverse position of a sample.

In our experiments, the periodical multigrating and fan-out domain structures were manufactured by "Labfer" Ltd. (Yekaterinburg, Russia) in MgO-doped congruent stoichiometric LiNbO3 single crystals. The 3-inch-diameter and 3-mm-thick single crystal wafers of MgO:LiNbO3 ("Yamaju Ceramics", Japan) were used. An 80-nm-thick Ta layer was deposited on both polar surfaces of the wafers by magnetron sputtering in Ar plasma. The periodical electrodes were created at Z+ polar surface by RIE etching of the Ta layer through the photolithographically defined photoresist mask. A negative photoresist "AZnl of 2020" ("AZ Microchemicals", Germany) was used. The periodical structures were produced at temperatures ranging from 423 K to 473 K by the multi-pulse poling technique. The multigrating domain structures had 20×3×10 mm spatial dimensions and were manufactured with 3 grating periods: 28.4 μm, 28.8 μm, and 29.7 μm (Fig. 1a). The fan-out domain structures had 3×20×50 mm spatial dimensions with the period varying from 27.42 μm to 32.5 μm along the Y crystallographic direction. The visualization of the periodical fan-out domain structure with duty cycle about 0.6 at Z+ polar surface was done by optical microscopy after selective chemical etching.

The input and output facets of the used crystals were coated by standard single-layer antireflective (AR) coating optimized at 1500 nm (Institute of Laser Physics SB RAS, Novosibirsk, Russia). A special temperature oven for manufacturing of the fan-out PPMgO:LN structures was constructed at ILP SB RAS, and a standard temperature controller "Thorlabs TC-200" was used in our experiments. A laser based on Tm3+:Lu2O3 ceramics pumped by CW Raman-shifted Er3+ fiber laser at 1670 nm (ELM-1670-50, produced by "IRE Polus", Fryazino, Moscow region) was used as a pumping source for PPMgO:LN crystals. The oscillation wavelength of the ceramic laser self-switched from 2067 nm at low output power (≤2 W) to 1966 nm at higher output power (≥5W) . The Q-switched radiation of the Tm3+:Lu2O3 laser had a linearly polarized single-transverse-mode Gaussian beam with an average power of up to 12 W at a repetition rate of 14-30 kHz. The pulse duration varied from ~35-40 ns at an output power of 8-10 W and a repetition rate of 14-20 kHz to 100-300 ns at the low power and repetition rate. An intracavity quartz etalon with 200-μm thickness, tilted at a Brewster angle, was used to decrease laser oscillation bandwidth and to stabilize the beam polarization.The Tm3+:Lu2O3-ceramic laser beam was focused into the PPMgO:LN element by lenses with the focal length of

70 mm or 100 mm. The efficient focal distances of the laser beam were ~100 mm or 140 mm, respectively. To optimize the SHG or OPO power, the focal point of a pumping beam was changed by shifting the PPMgO:LN sample along the Y-axis.

Our experiments demonstrated a competition of the optical parametric oscillations and SHG in the PPMgO:LN structures for 1966-nm laser pumping. The optical parametric oscillations in the mid-IR spectral region (at 3.7-4.1 μm) were achieved only in multigrating PPMgO:LN at temperatures of 405-425 K. Within this temperature range, SHG and OPO quasi-phase-matched conditions did not overlap. OPO based on the PPMgO:LN structure with a 29.7-μm period operated near degeneracy point (at wavelength of 3.7-4.2 μm).The parametric oscillations were not observed in a fan-out PPMgO:LN structure within the 390-440 K temperature range when the grating period was adjusted by shifting the nonlinear crystal. Instead, a high-efficient SHG of the laser beam at 1966 nm was registered. SHG at 983 nm with a power of up to 4.66 W was obtained in a fan-out PPMgO:LN structure with a conversion efficiency of up to 45%. The laser radiation at 983 nm can be used for specific near-IR applications: in medicine as a laser source for cancer diagnostics or LIDAR, or for the further frequency conversion to blue region. Combination of experimental results and discussion demonstrated that by tailoring the temperature and grating period parameters inside PPMgO:LN crystal placed in OPO cavity the SHG or OPO operation can be forced. If temperature and period conditions allowed parametric oscillations but were selected far from quasi-phase-matched levels for SHG, parametric oscillations were possible. If temperature and period conditions were dual-QPM, second harmonic generation prevailed.

References

[1]. L.E. Myers, R. C. Eckardt, M. M. Fejer, R. L. Byer, W. R. Bosenberg, and J. W. Pierce, JOSA B 12, 2102 – 2116 (1995).
[2]. L.E. Myers, R. C. Eckardt, M. M. Fejer, R. L. Byer, and W. R. Bosenberg Opt. Lett. **21**, 591-593 (1996).
[3]. L.E. Myers, and W.E. Bosenberg, IEEE J. of Quant. Electronics **33**, № 10, 1663-1672 (1997).
[4]. B. Wu, J. Kong, and Y. Shen, Opt. Lett. **35**, 1118–1120 (2010).
[5]. P.G. Schunemann, K. T. Zawilski, L.A. Pomeranz, D. J. Creeden, and P. A. Budni, JOSA B **33**, D36-D43 (2016).
[6]. M. M. Fejer, G. A. Magel, D.H. Jundt, and R.L. Byer, IEEE J. Quantum Electron. **28**, 2631–2654 (1992).
[7]. W. K. Burns, W. McElhanon, and L. Goldberg, IEEE Photon. Technol. Lett. 6 252–254 (1994).
[8]. N. Yu, J. Ro, M. Cha, S. Kurimura, T. Taira, Opt. Lett. **27**, 1046-1048 (2002).
[9]. P. E. Powers, T. J. Kulp, and S.E. Bisson, Opt. Lett. **23** , 159 – 161 (1998).
[10]. M. M. J. W. Van Herpen, S.L. Hekkert, S.E. Bisson, F.J.M. Harren, Opt. Lett. **27**, 640-643 (2002).
[11]. F. Adler, K. C. Cossel, M. J. Thorpe, I. Hart, M. E. Fermann, and Ye., J.Opt. Lett. **34**, 1330-1332 (2009).
[12]. B. Xiong, J.L. Ma, R. Chen, B.H. Wang, Q .J. Cui, L. Zhang, L. Guo, W. Hou, X.C. Xue-Chun Lin, J. M. Li, Opt. Comm. **284**, 1391-1394 (2011).

Dynamics in diode lasers: Effects of feedback and couplings

W. Barbosa, E. Rosero, J. Tredicce, A.Z. Khoury, and J.R. Rios Leite
Departamento de Fisica, Universidade Federal Pernambuco, Recife, Brazil
E-mail: rios@df.ufpe.br

Semiconductor lasers when subject to optical feedback show an enormous variety of dynamical behaviors including periodic, quasi-periodic and chaotic intensity pulsations. We shall describe features of this dynamics when two feedback signals are applied to one such laser.

Optical solitons in air

A.V. Mitrofanov[1,3,5,6], A.A. Voronin[1-4], D.A. Sidorov-Biryukov[1,3-5], A.B. Fedotov[1,3-5], A. Pugžlys[7], M.V. Rozhko[1,3], S.V. Ryabchuk, V. Shumakova[7], S. Ališauskas[7], A. Baltuška[7], and A.M. Zheltikov[1-5]

[1]*Physics Department, International Laser Center, M.V. Lomonosov Moscow State University, Moscow, 119992, Russia*
[2]*Department of Physics and Astronomy, Texas A&M University, College Station, TX 77843, USA*
[3]*Russian Quantum Center, ul. Novaya 100, Skolkovo, Moscow region, 143025, Russia*
[4] *Kazan Quantum Center, A.N. Tupolev Kazan National Research Technical University, Chetaev 18a, 420126, Kazan, Russia*
[5]*Kurchatov Institute National Research Center, Moscow, 123182, Russia*
[6]*Institute of Laser and Information Technologies, Russian Academy of Sciences, Shatura, Moscow region, 140700, Russia*
[7]*Photonics Institute, Vienna University of Technology, Gusshausstrasse 27-387, 1040, Vienna, Austria*
E-mail: zheltikov@physics.msu.ru

Atmospheric optics is one of the earliest fields among all the natural sciences. As a branch of knowledge dealing with an observation and explanation of the colors of the sky, rainbows, halos, and mirages, over hundreds of years it was exclusively concerned with the visible light and the visible spectral range, where atmospheric air is highly transparent. Systematic studies of radiation propagation in Earth's atmosphere, motivated by the needs of observational astrophysics and performed with an ever-increasing experimental accuracy over many centuries, helped achieve a detailed quantitative understanding of atmospheric transmission in the visible region. In the era of ultrafast laser technologies, enabling the generation of high-power ultrashort field waveforms within an ultrabroad spectral range from the visible to the mid-infrared, a deeper understanding of the group-velocity dispersion (GVD) of atmospheric air is needed. This call includes a quest for anomalous-GVD ranges as a top priority for long-distance signal transmission and remote sensing of the atmosphere.

Our experimental studies performed near the edge of the mid-infrared absorption band of atmospheric carbon dioxide reveal a remarkably broad and continuous dispersion anomaly stretching from approximately 3.5 to 4.2 μm, where atmospheric air is still highly transparent and where high-peak-power sources of ultrashort mid-infrared pulses are available. Within this range, anomalous dispersion acting jointly with optical nonlinearity of atmospheric air is shown to give rise to a unique three-dimensional field dynamics, enabling a highly efficient whole-beam self-compression of high-peak-power mid-infrared pulses to few-cycle pulse widths. Ultrashort high-peak-power 3.9-μm laser pulses are shown to exhibit such self-compression dynamics when exposed to the mid-infrared dispersion anomaly of air induced by the asymmetric-stretch rovibrational band of carbon dioxide. Even though the group-velocity dispersion cannot be even defined as a single constant for the entire bandwidth of mid-infrared laser pulses used in experiments, with all soliton transients shattered by high-order dispersion, 100–200-GW, 100-fs, 3.9-μm laser pulses can be compressed in this regime, as our experiments and simulations show, to sub-40-fs subterawatt field waveforms without any detectable energy loss.

This research has been supported by the Government of Russian Federation (project no. 14.Z50.31.0040, Feb. 17, 2017).

About real optical vortices in laser systems

J. Tredicce, P. Genevet, S. Barland, and M. Giudici
Institut des Sciences Exactes et Appliquées (ISEA), Nouméa, Nouvelle Calédonie
E-mail: jorge.tredicce@unc.nc

We studied an optical system consisting in a VCSEL coupled to a cavity containing a saturable absorber. The whole system has a large aspect ratio. We observe the appearance of optical vortices in a sufficiently large interval of the control parameter values.We discuss the relevance of the phase symmetry in the formation of such optical vortices.

Toward the themal-lens-free solid state lasers Heat Capacitive Active Mirror (HCAM) concept

K. Ueda[1-4]
[1]*Inst. Laser Science, UEC-Tokyho, Tokyo, Japan*
[2]*Inst. Laser Engineering, Osaka Univ., Osaka, Japan*
[3]*JST PRESTO, Tokyo, Japan*
[4]*Hamamatsu Photonics K.K., Hamamatsu, Japan*
E-mail: ueda@ils.uec.ac.jp

Why the major part of industrial laser market is occupied by fiber lasers? This is the most serious question for solid state laser technology. A fiber laser generates high power output by plane wave. The output of a high power solid state laser contains large number of higher order spatial mode due to the thermal lens effect. The cooling mechanism of solid state laser is the conduction cooling. High thermal gradient is the driving force of efficient cooling. This is a simple principle of this disk lasers. However thin disk keeps the thermal-lens-shift between excited and unexcited volume. I proposed several ideas to reduce the thermal lens in many conferences last 6 years. HCAM compensates the phase-shift difference by the simple technique of bottom cooling area control according to the thermal barrier effect.

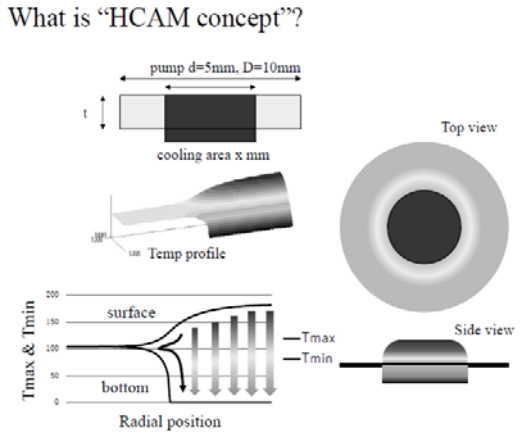

Fig. 1 HCAM cooling, temperature distribution and heat flow curve. Top and side view show the heat flow map.

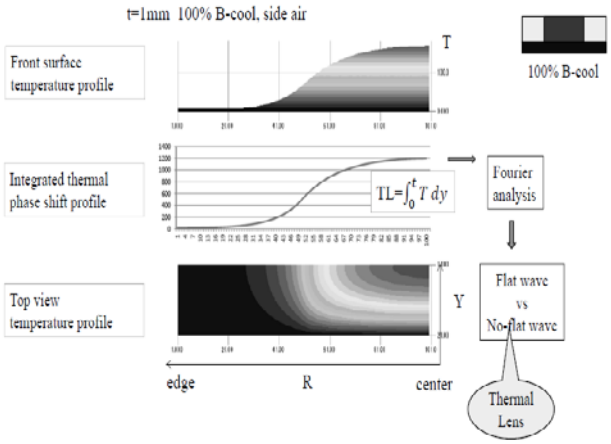

Fig. 2 Temperature profile of a 1mm thick active mirror @ 100% B-cool side view, top view and the phase shift curve by integrated T along the optical axis.

HCAM design is roughly described in Fig.1. The center part of active mirror (50% diameter) is pumped and the other volume is unexcited. This is the typical pump geometry of this disk lasers. The 50% bottom cooling scheme introduce the Heat Capacitive Volume in the unpumped area. The thermal induced phase shift over the full aperture has been calculated by Finite Element Method in cylindrical symmetry. The thermal lens effect is evaluated by the flat wave component of Fourier analysis of phase shift curve as a function of radial position as shown in Fig.2.

The phase shift curves at 50% B-cool for various disk thickness are shown in Fig.3. We found the phase shift curves in the heat capacitive volume are perfectly flat at the thermal equilibrium condition. The flatness of these curves were examined by the standard deviation along the calculation numbers. The standard deviation decreases exponentially. This is the heat capacitive volume effect. HCV is the result of thermal isolation. The net heat flow is zero because there is no heat generation and heat sink in HCV. As a result, the thermal lens effect decreases more than 50 times smaller than 100% B-cool case. Simple cooling area control demonstrated significant thermal lens reduction.

The thermal lens effect is drastically decrease at the optimum cooling area condition as shown in Fig.4. However, this technique is not so flexible. So, we try to introduce the fine tuning technique by addition small heater in the bottom isolated area, constant T and very thin ring heater. They are quite effective to tune the matching condition between the pump volume and HCV. They showed drastic

thermal reduction more than 3 order of magnitude, respectively. The thermal lens reduction curves are summarized in Fig.5.

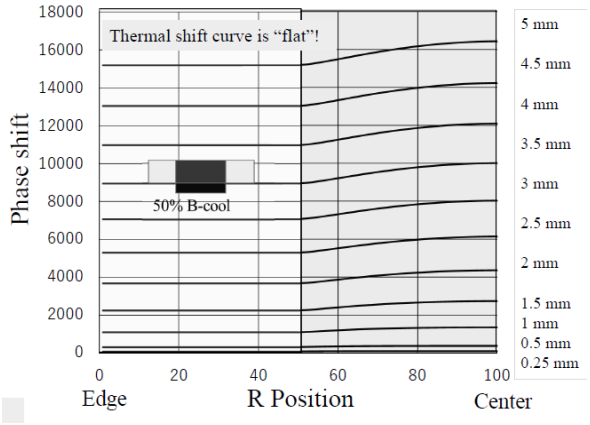

Fig. 3 Thermal-lens plateau was found in the heat capacitive volume @ 50% B-cool condition.

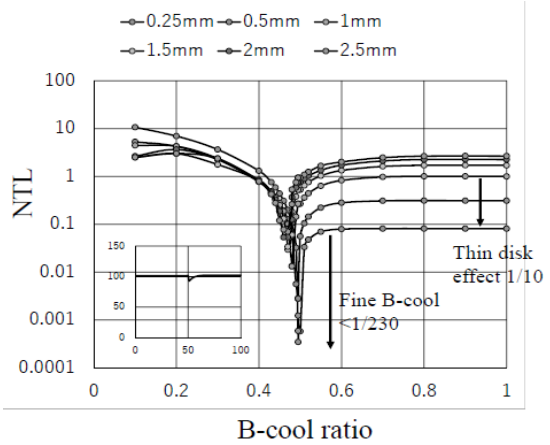

Fig. 4 Optimization of B-cool ratio.

HCAM effect is available for a top-capped thin disk laser. The backside volume in the top cap works as a heat reservoir. The top cap volume is effective to reduce the temperature max and thermal shock effect. But what is the effect of full aperture thermal lens reduction? When the active thickness is 0.25 mm (thin disk condition), the 50% B-cool HCAM reduces the thermal lens <1/50 as mentioned previously. In a typical case, tThe full aperture thermal lens decreases inversely proportional to the total thickness of active mirror. The critical cooling area to change the scaling is determined by the phase transition point where the phase shift of HCV is over the pumping volume. Such type of phase shift is the result of induced thermal barrier effect in the boundary area between pump volume and HCV. This is another kind of heat capacitive volume effect. The top cap volume behind the active volume is effective to reduce the thermal lens of HCAM laser. to the disk thickness including top cap volume over a wide range of active volume and top-cap thickness. We found the thermal lens effect has a phase change as a function of top cap thickness.

We propose a novel concept to develop thermal-lens-free solid state laser, HCAM, herein. The full area thermal induced phase shift becomes flat. HCAM concept should be the key for the paradigm shift of ultra-high power laser toward the unlimited power scaling.

This concept is quite universal. This work is partially supported by Mega Grant of the Russian Federation of (14.B25.31.0024) and the Institute of Applied Physics of the Russian Academy of Sciences.

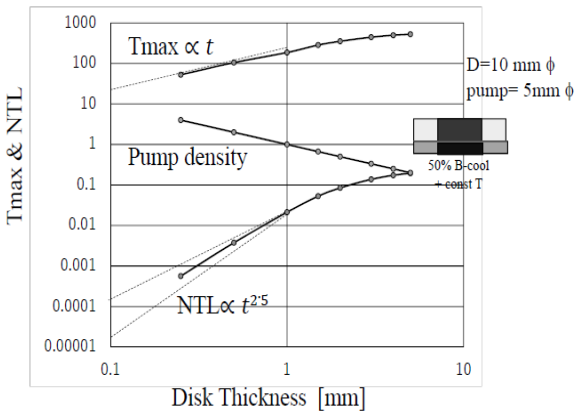

Fig. 5 The optimization of HCAM effect.

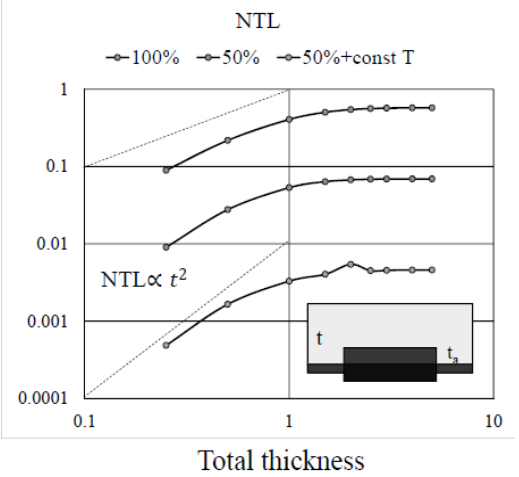

Fig. 6 Thermal lens reduction by top cap volume for a thin disk laser @ ta=0.25mm

MID-IR $BaGa_4Se_7$ optical parametric oscillator pumped by a Q-switched Nd:$YLiF_4$ laser

D.B. Kolker[2-4], N.Yu. Kostyukova[1,2], A.A. Boyko[1,2], V.V. Badikov[5], D.V. Badikov[5], A.G. Shadrintseva[1], N.N. Tretyakova[1], K.G. Zenov[1], A.A. Karapuzikov[1], and J.-J. Zondy[4]

[1]*Special technologies, Ltd., 1/3 Zeljonaja gorka str., 630060, Novosibirsk, Russia*

[2]*Research Laboratory of Quantum Optics Technology, Novosibirsk State University, 2 Pirogova Str., 630090, Novosibirsk, Russia*

[3]*Institute of Laser Physics SB RAS, 630090, Lavrentyev av. 13/3, Novosibirsk, Russia*

[4]*Novosibirsk State Technical University, 630073, K. Marx av. 20, Novosibirsk, Russia*

[5]*High Technologies Laboratory, Kuban State University, 149 Stavropolskaya Str., 350040, Krasnodar, Russia*

[6]*School of Science and Technology, Nazarbayev University, 53 Kabanbay Batyr Ave., 010000, Astana, Kazakhstan*

E-mail: dkolker@mail.ru

Widely tunable optical parametric oscillators are attractive laser sources for mid-infrared (MIR) nonlinear optics applications, because of the scarcity of direct-emitting conventional laser sources in this spectral region (2 – 20 μm). While oxide-based periodically-poled nonlinear compounds belonging to the ferroelectric crystal family (mainly $LiNbO_3$, $LiTaO_3$ and $KTiOPO_4$) are commercially available, their IR transparency does not exceed 5 microns and therefore they cannot be used for deeper MIR applications. Tunable coherent MIR laser sources are useful spectroscopic tools to probe rovibrational molecular fingerprints with various applications in trace gas sensing such as environmental monitoring, detection of hazardous species, life science or medical applications such as real-time breath analysis for early disease diagnosis [1-5].

Mid-infrared (MIR) idler wave tuning from 2.6 μm to 10.4 μm is demonstrated with an angle-tuned type-I (*o-ee*) *y*-cut sample, highlighting the superior performance of this novel large bandgap chalcogenide nonlinear crystal to generate tunable coherent radiation over its full MIR transparency range (0.47 – 18 μm). Damage threshold measurements yielded values as high as 2.04 J/cm^2 at 100 Hz pulse repetition rate at 1053 nm and 3.5 J/cm2 at 100 pulse repetition rate for 2070 nm one of the largest among existing MIR $\chi^{(2)}$ nonlinear materials. We have demonstrated a low threshold $BaGa_4Se_7$ nanosecond optical parametric oscillator pumped for the first time by a Q-witched Nd:$YLiF_4$ low power laser at 1.053 μm. The comparison of this experimental threshold with theory allowed us to estimate a nonlinear effective coefficient (for type-I (o-ee) downconversion in the *xz* plane) exceeding 12 pm/V. Such a large value seems to indicate that the relative sign of the d_{23} and d_{16} tensor elements of $BaGa_4Se_7$ should be the same. A maximum idler energy up to 45 μJ at 3.3 μm and 14 μJ at 8.1 μm has been achieved.

References

[1] Tittel F, Richter D and Fried A2003Mid-infrared laser applications in spectroscopy *Solid-State Mid-Infrared Laser Sources*Topics Appl. Phys.89, ed I. T. Sorokina and K. L. Vodopyanov (Berlin Heidelberg, Springer Verlag 2003) 445–516

[2] Sigrist M W2000Mid-infrared laser-spectroscopic sensing of chemical species *J.Adv.Res.***6** 529-33

[3] Emelin M Yu and Ryabikin M Yu 2013 On the potential of mid-IR lasers for generating high harmonics with subnanometer wavelengths in gases *Quantum Electron.***43** 211-16

[4] Le A T, Wei H, Jin C and Lin C D Strong-field approximation and its extension for high-order harmonic generation with mid-infrared lasers 2016 *J. Phys.* B*: At. Mol. Opt. Phys*. **49** 053001

[5] Le A T, Wei H, Jin C, Tuoc V N, Morishita T and Lin C D 2014 Universality of Returning Electron Wave Packet in High-Order Harmonic Generation with Midinfrared Laser Pulses *Phys. Rev. Lett*. **113** 033001

Laser-controlled cluster nanophysics: stability, dynamic quantum states, superconductivity opportunities…

V. Kavokin[1], S.M. Arakelian[2], A.O. Kucherik[2], S.V. Kutrovskaya[2], A.V. Osipov[2], A.V. Istratov[2]
[1]*School of Physics and Astronomy, University of Southampton, SO17 1NJ, Southampton, England, United Kingdom*
[2]*Department of Physics and Applied Mathematics, Vladimir State University, Gorky Str. 87, 600000, Vladimir, Russia*
E-mail: arak@vlsu.ru

1. We studied in both theory and experiment the laser-induced nanocluster structures of different types (in topology and element composition) with correlations in nanoparticle ensemble by quantum states. The problem of high temperature superconductivity due to topological surface structures with localized/delocalized couplied states is considered.

2. Experimental results for thin films composed of silver and/or gold are shown in Fig. 1. Measured current-voltage characteristics I(U) – CVCs – for the films with different heights display the jumps. The insert at the top of Fig. 1b shows in details the initial (left) part of the dependence of electrical resistance R on the size of the nanoparticles. Interestingly, this fragment of the curve can be represented as an analog of the Condo dependence for R on temperature T (i.e. R(T)) [1] but in our case this corresponds to dimensional dependence R(h) on the height h(see [2]).

The topology (the variation of parameters of the islands, including their overlap in some areas) of cluster structures leads to different mechanisms of charge carrier propagation and any of these can be observed in practice.

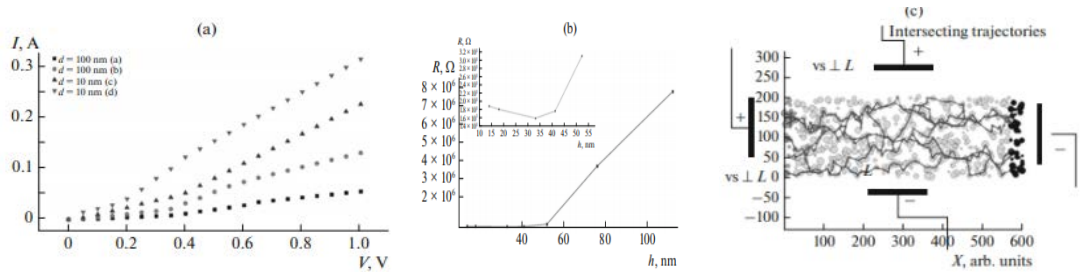

Fig. 1 (a) Experimental CVCs curves for deposited layers of cluster Au films with different heights h. (b) Dependence of electrical resistance R on h. The insert shows a more detailed image for the initial part of the dependence. (c) Scheme of the experimental setup for measuring the electrical conductivity of granular samples (two ways of applying the external electric voltage are shown).

For tunneling conductivity between different zones separated by a potential barrier it should be a delocalized/metallic conductivity on both sides of the barrier boundaries. The hopping conductivity between neighboring/close clusters, caused by charge transfer from one cluster to another (being the separated localized centers), is the effect of a quantum conductivity from corresponding discrete Hubbard levels with different hopping lengths.

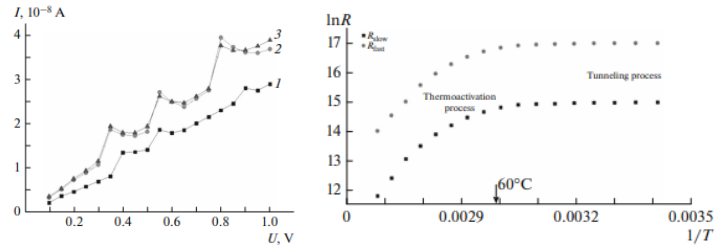

a) b)

Fig. 2 (a) Experimental CVCs for a deposited layer of bimetallic film with equivalent concentrations of Au and Ag (1/1): (1) size of the nanoparticles ~ 50nm, a single layer of closepacked particles; (2) size of the nanoparticles ~ 10nm, five layers; distance between particles 4nm;(3)size of the nanoparticles ~10nm, five layers; distance between particles 2 nm. (b)Temperature dependence of resistance R for the samples with bimetallic film (Au + Ag). Films with heights of ~50 nm were deposited in laser experiments at different scanning rates of the laser beam: slow (R_{slow} ~ 0.6 mms−1) and fast (R_{fast} ~ 1.5 mm s−1).

Such hopping conductivity σ in metallic structures is shown in Fig. 2a for certain experimental conditions. The behavior corresponds to the characteristic dependence for the Vannie–Stark effect observed in a superlattice [1]. The mechanism can be associated with cascade transition of charge carriers in a super-lattice ladder like it is happened in multiple quantum structure with discrete energetic levels. Obtained results demonstrate the absolutely reproducible negative slope (N-like differential electroresistance) due to concrete topology of the nanostructure resulting in transition from localized states of electrons to delocalized processes in whole.

At the same time, the effect of thermoactivation also affects the magnitude of the current in the resulting island structure. We obtained that the temperature effect in the 20 – 100°C range for the charge carrier propagation depends on different rates of laser deposition of the substance on the substrate (slow and fast scanning of the laser beam). for two samples with the same average thickness of 50 nm. As can be seen from the dependences in Fig. 2b the resistance of both samples is virtually constant at the initial stage of heating due to the prevalence of tunneling transitions of electrons in the gold and silver films. Starting at T = 60°C the resistance falls vs temperature. This is reasonably due to the thermoactivation of electrons. The activation energy determined from the slope of the Arrhenius-type curves ($\ln \sigma \sim 1/T$) is in the 0.98 – 1.1 eV range being a small value in comparison with much more magnitude for bulk samples (~4eV). The effect is due to surface conditions on the substrate (see e.g. [4]).

Another principal factor for the thermoactivation mechanism is the strength of the local field acting on the charge carriers in a potential well. If its strength is sufficient (which is determined by the specific topology of the sample's surface), the conductivity can increase dramatically due to the charge exiting from the potential well according to the energy parameters, regardless of the fixed value of temperature (cf. [3]). This effect of the amplification of the electrical conductivity (similar to the mechanism of SERS effect in spectroscopy) was also observed in our experiment.

3. Fig. 3 shows the variation of the R-value (in 4 orders of magnitude) on the dependence of the electrical resistivity R on the topology of a cluster structure deposited on a substrate. Fractal dimension D is a quantitative characteristic of topological features. Its value for different granular structures was estimated according to the procedure described in [2]. The measured (R_{meas}) and estimated (R_{calc}) values of the resistance are in good agreement. The latter value was estimated for the tunneling mechanism using standard percolation model.

By this result we may discuss the problem of high temperature superconductivity in topological nanostructures in the context of new principles of the state coupling occurring for systems with low dimensionality.

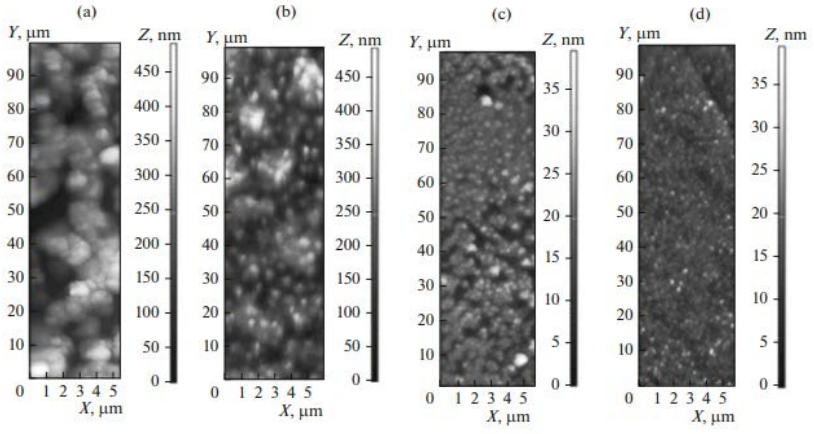

Fig. 3 Comparison of the both experimental and theoretical values of electrical resistance R for different topology of Au-nanostructures (AFM-images of surface structures are shown). The results for selected topological conditions: a) R_{meas}= 6.1 × 1011 Ω, D = 1.39, R_{calc} = 2.8 × 1011 Ω; b) R_{meas} = 8.3 × 1010 Ω, D = 1.57, R_{calc} = 1.9 × 1010 Ω; c) R_{meas} = 5.4 × 108 Ω , D = 1.84, R_{calc} = 9.3 × 108 Ω; d) R_{meas} = 3.6 × 107 Ω, D = 1.93, R_{calc} = 5.5 × 107 Ω, where R_{meas} and R_{calc} denote the measured and calculated values, respectively, D is the fractal dimension of the cluster structures. For samples a), b) the size of nanoparticles is a = 50 nm; for samples c), d) – a = 5 nm.

4. Achievements in this area should provide direction for possible applications of these phenomena in a new generation of femtonanophotonic devices. Hybrid schemes that combine the electrophysical and optical properties of such structures exhibiting macroscopic quantum states would seem to be most promising (cf. [5]).

The work has been carried out under of the state order №16.1123.2017/4.6 and with the support of the RFBR (grant No. 17-52-10003 KO_a).

References

[1] Landau, L.D. and Lifshitz, E.M., Electrodynamics of Continuous Media, Moscow: Nauka, 1982, 2nd ed.
[2] Arakelian, S.M., Kucherik, A.O., Prokoshev, V.G., et al., Introduction to Femtonanophotonics: Fundamentals and Laser Methods for Controlled Fabrication and Diagnostics of Nanostructured Materials, Arakelian, S.M., Ed., Moscow: Logos, 2015.
[3] Arakelian, S. M., Emel'yanov, V.I., Kutrovskaya, S.V., et al., Opt. Quantum Electron., 2016, vol. 48, no. 6, p. 342.
[4] Kavokin A. V., Kutrovskaya S. V., et. al. The crossover between tunnel and hopping conductivity in granulated films of noble metals. Superlattices and Microstructures V. 111, Nov. 2017, P. 335-339.
[5] Kutrovskaya S. V., Arakelian S. M., et. al. The Synthesis of Hybrid Gold- Silicon Nano Particles in a Liquid. Scientific Reports 7: 10284, 2017, 6 pp.

Advanced features of femtosecond pulse inscribed fiber Bragg gratings for fiber lasers

A.V. Dostovalov[1,2], A.A. Wolf[1,2], E.A. Zlobina[1], M.I. Skvortsov[1,2], S.I. Kablukov[1], S.A. Babin[1,2]
[1]*Institute of Automation and Electrometry of the SB RAS, Novosibirsk, Russia*
[2]*Novosibirsk State University, Novosibirsk, Russia*
E-mail: dostovalov@iae.nsk.su

Fiber Bragg grating (FBG) is a key element of fiber lasers. Advantages of femtosecond laser inscription technology – modification of non-photosensitive materials, high degree of localization of the induced refractive index change (down to ~1 μm^3), high-temperature and radiation resistance of femtosecond modifications – make the technology attractive for fiber devices and components with advanced technical characteristics. Direct writing techniques by femtosecond laser pulses allows one to write fiber gratings with any geometry without the use of additional optical components, such as phase mask and cylindrical lens. In this work the technology of point-by-point inscription is applied for the creation of FBG for applications in different schemes of fiber lasers, including distributed feedback (DFB) lasers, multimode and multicore Raman lasers. It is shown how the features of femtosecond pulse inscription can be used to improve output characteristics of such lasers.

DFB fiber lasers is of great importance in different research areas due to their unique characteristics – stable generation of single-frequency radiation with a narrow linewidth (~0.1–100 kHz), low noise level and power characteristics suitable for practical applications. The resonator of such a laser is formed by a special FBG containing π-phase-shift in the structure being inscribed in active fiber (Er, Yb, Tm). When phase-shifted FBGs are fabricated by conventional UV technology with a phase mask, the used phase mask fixes the resonant wavelength of FBG and the type of used fibers is limited by photosensitive ones.

In this work, long high-quality FBGs with π-phase shifts in the structure are inscribed directly in various single-mode fibers by femtosecond laser pulses [1]. Phase shifts are introduced in the grating structure during the inscription process with a piezoelectric actuator, which displaces the fiber along the direction of its movement. As a result, single- and double-π-phase-shifted FBGs with a length up to 34 mm and transmission bandwidth less than 1 pm are inscribed. It has been shown that distributed feedback fiber lasers can be created based on femtosecond point-by-point π-phase-shifted FBGs inscribed in both photosensitive and non-photosensitive Er-doped fibers [2].

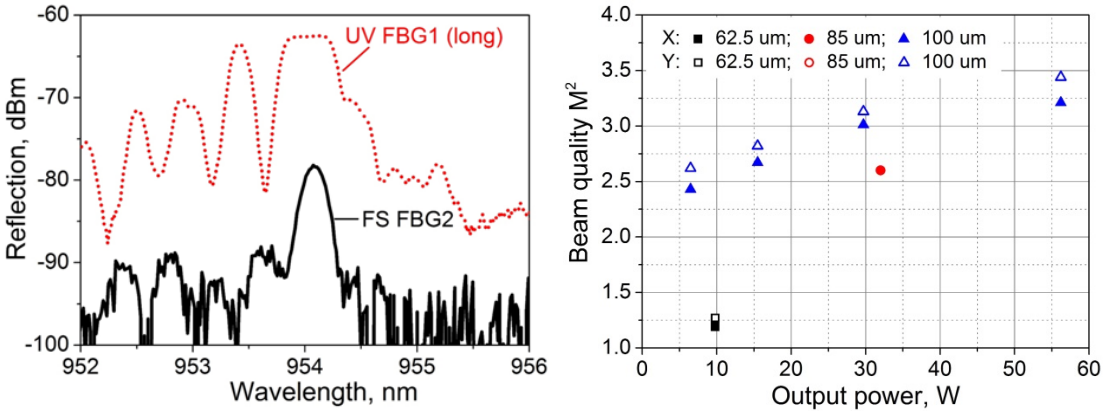

Fig. 1 Reflection spectra of long UV FBG1 (dotted line) and FS FBG2 (solid line) (a), Measured beam quality M2 as a function of output power for 62.5-μm (squares), 85-μm (circles) and 100-μm (triangles) GRIN fiber of optimal length (1.1, 1.5 and 1.1 km, respectively) (b).

The developed FBG inscription technique allows one to inscribe FBG in multimode (MM) fibers in a certain area of the core cross section (for example, in the central part of fiber core). It gives the opportunity for the transverse mode selection in an all-fiber CW Raman laser based on a multimode graded-index fiber. Selection properties of special fiber Bragg gratings inscribed by UV CW or IR

femtosecond radiation in the 100-μm core of graded-index fiber are experimentally compared (fig. 1a). It was found that the output power and slope efficiency of Raman lasers based on MM graded-index fibers increase sufficiently (from 47% to 84%) with the increase of fiber core diameter from 62.5 to 100 μm. At the same time of beam-quality parameter M^2 increases only slightly: from 1.3 to 3 (fig. 1b).

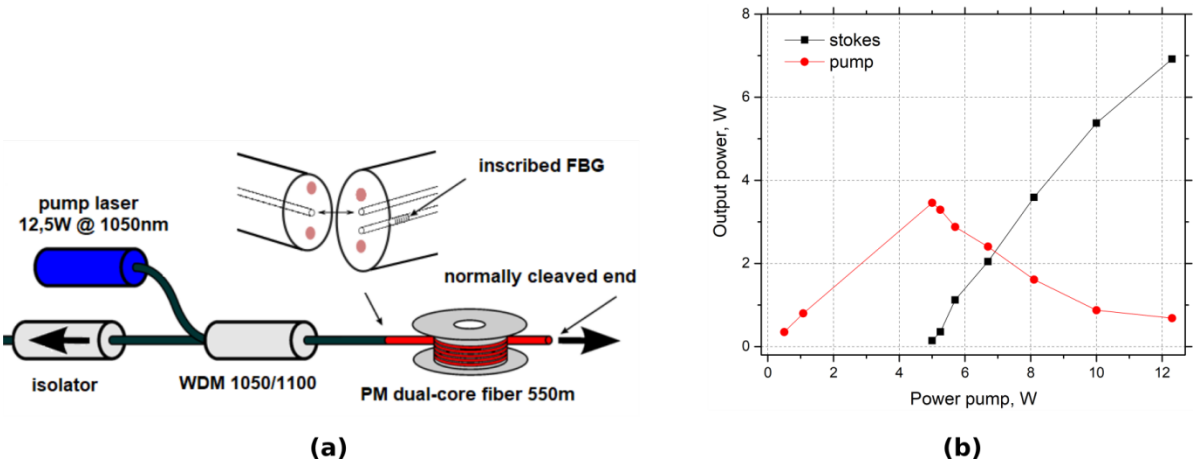

Fig. 2 Experimental setup of RFL based on dual-core fiber with the inscribed FBG (a), Output power of the RFL as a function of input pump power (b).

Point-by-point FBG writing technique also allows one to inscribe FBG selectively in one core of multicore fibers (MCF). So it is possible to create new schemes of fiber lasers based on FBG written in MCF, for example, Raman fiber lasers based on dual-core fiber with the FBGs inscribed selectively in one core, and both cores simultaneously. The proposed scheme of Raman fiber lasers is presented in fig. 2a. PM dual-core germanosilicate fiber with total length of 550 m was used as a medium for the Raman gain. The FBG was inscribed at the input of the cavity in one of the cores and the pump radiation is injected into the core without FBG. The central wavelength of highly reflective FBG was 1100 nm to reflect Raman lasing radiation. The normally cleaved end of fiber was used as the output mirror. The Fig. 2b shows transmitted pump power (circle) and Stokes emission (square) as a function of input pump power for this configuration. Lasing threshold amounts to ≈5W. The measured laser linewidth in the near-threshold regime was ≈ 45 pm. To create a scheme with random distributed feedback via Rayleigh backscattering, the output end of the dual-core fiber was cleaved at an angle more than 10° in order to avoid the Fresnel reflection. The threshold of lasing in this case was higher in agreement with [3], where a fiber loop mirror was used as a high reflective mirror. In the near-threshold mode, the spectral width was measured to be tens of pm. The reasons for narrowing linewidth of lasing include both the spectrally selective properties of the dual-core fiber and the weakening of nonlinear effects due to the power density reduction. The narrow linewith radiation of random laser may find applications in multicore fiber sensing for high sensitive shape measurement techniques.

The work on multi-core fiber is supported by Ministry of Education and Science of the Russian Federation (Minobrnauka) (14.Y26.31.0017) and the work on multimode fibers is supported by Russian Science Foundation (project No. 14-22-00118).

References

[1] A.V. Dostovalov, A.A. Wolf, A.V. Parygin et al., Opt. Express **24**, 16232 (2016).
[2] A. Wolf, A. Dostovalov, M. Skvortsov et al., Opt. Laser Technol. **101**, 202 (2018).
[3] A. E. Budarnykh, I. A. Lobach, E. A. Zlobina et al., Opt. Lett. **43**, 567 (2018).

Recent progress in the interaction of atomic vapors with material surfaces

M. Ducloy
Laboratoire de Physique des Lasers, Université Paris 13, France
E-mail: martial.ducloy@univ-paris13.fr

Hybrid clustered structures for photonic application

A. Kucherik, A. Antipov, S. Arakelian, S. Kutrovskaya, A. Osipov
Department of Physics and Applied Mathematics, Stoletov's Vladimir State University,
Gorky st. 87, Vladimir, 600000, Russia
Phone: +7(4922) 477796
Fax: +7(4922) 333369
E-mail: kucherik@vlsu.ru

The main goal of our work is the fabrication of nanostructured materials including the nano- and microclusters for control of electrical, optical and other properties of obtained structures.

Characteristic parameters of the problem with the dimension of length are, in the first place, «heat wave length» $\lambda_B = \sqrt{\frac{2\pi\hbar^2}{m\,k_B\,T}}$ (the de Broglie wavelength of a particle with mass m and the energy $k_БT$), and secondly, is the average distance between particles $\upsilon^{1/3} = \left(\frac{V}{N}\right)^{1/3}$. We will be interested in a case of occurrence of the correlations in the system, i.e. when $\lambda_B \sim \upsilon^{1/3} \gg R$, where R is the radius of influence of the interaction potential of the particles.

The principal question to the quantum behavior development is, the estimation for effective mass m for λ_B. E.g. for electrical transport properties of semiconductors the reduced coefficient form is not more than 0.1, and results in the value $\lambda_B \geq 25$nm. For quasi- particles with coupled states of different kind in collective phenomena the fact takes place, as well. So, nanoclusters can demonstrate the quantum behavior in some effects for room temperature. The fact is true for nonhomogenous structures with hollow structures under the tunnel effects development. For structures in figure we demonstrated the superconductivity tendency to increase the electrical conductivity (in several times for our case) at room temperature in comparison with homogenous sample.

The relative contribution of thermal and quantum fluctuations is determined by the fact that first appear in the range of energies $\Delta E \leq k_B \cdot T$, usually with large number of populations, and the second – when $\Delta E > k_BT$ with small number of populations. At low temperatures the role of quantum processes increases for this reason; increases the corresponding number of populations, as well.

We will be interested in the question, how quantum phase transitions still appear in the properties of macroscopic systems, located at finite temperature. The key parameter is the violation of coherence in the system of quantum particles, which occurs on the defasing length l_{df}, which has the meaning of the average size of quantum fluctuations.

Single plasmonic nanostructure: A playground for nonlinear and quantum optics

V.N. Zadkov[1,2], V.I. Balykin[1], P.N. Melentiev[1], Yu.V. Vladimirova[2], and F. Song[3]
[1]*Institute of Spectroscopy, Russian Academy of Sciences, Troitsk, Moscow, 108840, Russia*
[2]*Faculty of Physics, Lomonosov Moscow State Univ., Moscow, 119991, Russia*
[3]*Photonics Center, Nankai University, Tianjin, 300071, P.R. China*
E-mail: zadkov@isan.troitsk.ru

In this talk, we will explore quantum and nonlinear optical effects due to interaction of a single quantum emitter with a plasmonic nanostructure in an external electromagnetic field.

First, we will discuss our experimental results on nonlinear optical interaction of laser radiation with a single gold nanostructure in the split-hole resonator geometry, which shows several multipole plasmon resonances that will lead to SHG, THG, and light generation at the mixed frequencies. The THG nearfield amplitude reaches 0.6% of the fundamental frequency field amplitude, which enables creation of UV radiation sources with a record high intensity. The UV THG may then find many important applications including biomedical ones.

Second, we will overview the mechanisms of modification of the local field and radiative and nonradiative decay rates of a two-level quantum emitter located in close proximity to a plasmonic nanoparticle and will analyze the polarization distribution at the nanoscale around the nanoparticle. We will also analyze the photon-number statistics in resonance fluorescence of the quantum emitter near a metal nanosphere and the antibunching effect of photons from the resonance fluorescence.

The authors acknowledge financial support from the Russian Foundation for Basic Research (grants Nos. 16-02-00816, 18-52-53040).

Diode-pumped Raman fiber lasers

S.A. Babin[1,2]
[1]*Institute of Automation and Electrometry, SB RAS, Novosibirsk, 630090, Russia*
[2]*Novosibirsk State University, Novosibirsk, 630090, Russia*
E-mail: babin@iae.nsk.su

High-power fiber laser sources are usually utilize active rare-earth-doped fibers cladding-pumped by multimode laser diodes (LDs), but they operate in limited wavelength range defined by the dopant gain bandwidth (1-1.15, 1.5-1.65 and 1.9-2.1 μm for Yb, Er and Tm/Ho, accordingly [1]). Passive-fiber-based Raman fiber lasers (RFLs) are able to operate at almost any wavelength in the 1-2 μm range [2], but for their efficient pumping high-power singlemode rare-earth-doped fiber lasers are usually used that makes the RFL design rather complicated. One of interesting possibilities is to pump RFLs by cheap and reliable high-power multimode LDs directly into the core of graded-index (GRIN) multimode passive fibers. Using high-power LDs with operating wavelengths of 915-940 nm, it is possible to obtain high-power Raman lasing in wavelength range of 950-1000 nm, which is hardly possible to obtain with rare-earth-doped fiber lasers.

In the report, we review the latest results on the development of high-brightness fiber sources based on the directly diode-pumped multimode GRIN fibers.

The concept of LD-pumped GRIN-fiber based RFLs has been recently developed in two directions. First one explores high-power operation based on free-space pump coupling and external bulk mirror cavity [3-5], whereas second one aims at the high-quality beam generation using in-fiber Bragg gratings (FBGs) as cavity mirrors [6-8]. For detailed comparison of these techniques, see review paper [9]. In the first case, up to 154 W of output power is reported [6]. However, Raman output at ~1020 nm wavelength is not as interesting, because much higher power at this wavelength is available from Yb-doped fiber lasers [1]. In addition, in spite of significant improvement of the output beam quality in comparison with that for the pump beam (M^2 ~20) due to the clean-up effect in GRIN fibers, output beam parameter M^2 deteriorates from 4 to 8 with the increasing output power.

In the second case, nearly single-mode Raman lasing (M^2 ~1.3) with output power of 10 W at 954 nm was demonstrated due to the implementation of special FBG inscribed by a point-by-point femtosecond (FS) technique in the center of the 62.5-μm GRIN fiber core pumped by 915-nm LDs [8]. Such FBG plays a role of a selector for fundamental mode. As a next step, coupling of several LDs through the multimode fiber pump combiner allows us to increase the coupled pump power and to develop an all-fiber design of the multimode Raman laser [10]. This configuration has obvious advantages such as compactness, ease of operation, low cost, reliability, long-term stability and flexibility of output fiber. Output power at 954 nm wavelength was increased to 49 W at the expense of slight reduction of the beam quality (M^2 ~2.6) with fiber core enlargement to 85 μm. This results in a record value of brightness enhancement of ~20 (brightness of Raman laser related to that for LD pump) in RFLs based on GRIN fiber.

In the latest experiments, similar all-fiber configuration with 100-μm core GRIN fiber pumped by 915-nm multimode LDs with M^2~30 has been studied. With the core enlargement, the conversion efficiency increases to 84% while the output beam-quality parameter remains nearly the same. It has been also shown that it is strongly dependent on the exact wavelength near the Raman gain maximum: M^2 varies from 2 to 3 when the wavelength changes from 950 to 958 nm. At that the beam becomes unstable when operating at 958 nm, in a broad power range (being stabilized at the highest power levels). Operation at the long-wavelength tail of the Raman gain profile is characterized by higher gain coefficient for higher order modes thus leading to the observed mode instability. The highest power (62 W) defined by the second-order Stokes threshold has been obtained near the spectral maximum of Raman gain (954 nm). It is also observed that the beam quality (~2.6) and spectral width (~0.4 nm) are only weakly varying in the broad range of powers (10-62 W) thus indicating formation of stable group of coupled low-order modes.

In this configuration, experiments on random Raman lasing of the second Stokes component (978 and 996 nm), and second harmonic generation in blue spectral range (477 and 488 nm) are also

endeavored. The results of these experiments as well as the discussion on further scaling capabilities and potential applications of such laser source, will be presented at the conference.

The authors acknowledge financial support of the Russian Science Foundation (project No. 14-22-00118).

References

[1] D. J. Richardson, J. Nilsson, and W. A. Clarkson, JOSA B **27** (11), B63-B92 (2010).
[2] E. M. Dianov and A. M. Prokhorov, IEEE J. of Sel. Topics in Quant. Electronics **6**, 1022 (2000).
[3] T. Yao, A. V. Harish, J. K. Sahu, and J. Nilsson, Applied Sciences **5**, 1323-1336 (2015).
[4] Y. Glick, V. Fromzel, J. Zhang, A. Dahan, N. Ter-Gabrielyan, R. K. Pattnaik, and M. Dubinskii, Laser Phys. Lett. **13**, 065101 (2016).
[5] Y. Glick, V. Fromzel, J. Zhang, N. Ter-Gabrielyan, and M. Dubinskii, Applied Optics **56**, B97-B102 (2017).
[6] S. I Kablukov, E. I. Dontsova, E. A. Zlobina, I. N. Nemov, A. A. Vlasov, and S. A. Babin, Laser Phys. Lett. **10**, 085103 (2013).
[7] E. A. Zlobina, S. I. Kablukov, M. I. Skvortsov, I. N. Nemov, and S. A. Babin, Laser Phys. Lett. **13**, 035102 (2016).
[8] E. A. Zlobina, S. I. Kablukov, A. A. Wolf, A. V. Dostovalov, and S. A. Babin, Opt. Lett. **42**, 9-12 (2017).
[9] S. A. Babin, E. A. Zlobina and S. I. Kablukov, J. Sel. Top. Quantum Electron. **24**, 1-10 (2018).
[10] E. A. Zlobina, S. I. Kablukov, A. A. Wolf, I. N. Nemov, A. V. Dostovalov, V. A. Tyrtyshnyy, D. V. Myasnikov, S. A. Babin, Opt. Express **25**, 12581-12587 (2017).

Complex quantum state generation and coherent control based on on-chip frequency combs

P. Roztocki[1], C. Reimer[1,2], S. Sciara[1,3], L. Romero Cortés[1], Y. Zhang[1], B. Wetzel[1,4], M. Islam[1], A. Cino[3], S.T. Chu[5], B.E. Little[6], D.J. Moss[7], L. Caspani[8], J. Azaña[1], M. Kues[1,9], and R. Morandotti[1,10,11]

[1]*INRS-EMT, 1650, Boulevard Lionel-Boulet, Varennes, Québec, J3X 1S2, Canada*
[2]*John A. Paulson School of Engineering and Applied Sciences, Harvard University, Cambridge, 02138, USA*
[3]*Department of Energy, Information Engineering and Mathematical Models, University of Palermo, Palermo, Italy*
[4]*School of Mathematical and Physical Sciences, University of Sussex, Falmer, Brighton, BN1 9RH, UK*
[5]*Department of Physics and Material Science, City University of Hong Kong, Tat Chee Avenue, Hong Kong, China*
[6]*State Key Laboratory of Transient Optics and Photonics, Xi'an Institute of Optics and Precision Mechanics, Chinese Academy of Science, Xi'an, China*
[7]*Centre for Micro Photonics, Swinburne University of Technology, Hawthorn, Victoria, 3122, Australia*
[8]*Institute of Photonics, Department of Physics, University of Strathclyde, Glasgow, G1 1RD, UK*
[9]*School of Engineering, University of Glasgow, Rankine Building, Oakfield Avenue, Glasgow, G12 8LT, UK*
[10]*Institute of Fundamental and Frontier Sciences, University of Electronic Science and Technology of China, Chengdu, 610054, China*
[11]*ITMO University, St Petersburg, Russia*
E-mail: morandotti@emt.inrs.ca

Complex optical quantum states represent a key resource for fundamental science and applications such as quantum communications, information processing, and metrology. Entanglement is the prerequisite for several such uses. Concurrently, the state complexity can be increased by raising the number N of photons in the state and/or the photon dimensionality D (where the Hilbert space size scales as D^N). To reach the full potential of photons for quantum technologies demands the custom preparation and coherent manipulation of such systems. While the low-footprint and stability of integrated photonics has made it an attractive platform for quantum optics, complex state generation and control have however remained largely inaccessible or not scalable. Remarkably, a unique framework for the generation and control of states has been introduced by exploiting on-chip frequency combs.

Integrated frequency combs are monolithic light sources with a broad spectrum of evenly-spaced frequency modes, which are emitted from a nonlinear micro-cavity by optically-exciting one of its resonances [1]. When the micro-cavity is operated below the optical parametric oscillation threshold, two-photon states can be generated. In third-order nonlinear micro-resonators, spontaneous four-wave mixing (SFWM) can occur, where two excitation field photons are annihilated and two daughter photons, signal and idler, are generated [2,3]. The daughter photons can be created in a superposition of neighboring frequency comb mode states, and become spectrally-correlated due to the energy conservation of SFWM. Thanks to cavity field enhancement, quantum frequency comb (QFC) sources can deliver high quantum state generation rates at low excitation powers compared to plain-waveguide sources. However, to date, QFC generation has largely relied on micro-cavity excitation via lasers external to the sources, being neither versatile nor power-efficient (i.e. most of the laser bandwidth is not used to excite the narrow resonance –100's MHz– and is thus wasted). For this reason, some recent work has focused on developing efficient nonlinear-cavity excitation schemes based on nested configurations [4,5]. More importantly, the QFC concept provides a solution for state scalability and complexity by allowing several frequency modes (compatible with telecommunications wavelength-division multiplexing channels) to be accessible within a single waveguide spatial mode, as well as straightforward access to entanglement, superposition, and multi-partite states. Several QFC sources have already been demonstrated, among them combs of correlated photons [2], cross-polarized photon pairs [6], entangled photon pairs [7–9], multi-photon states [8], and frequency-bin entangled states [5,10,11].

Through a double-pulse excitation of an integrated micro-ring cavity resonance, we demonstrated the generation of time-bin entangled photon pairs over a broad frequency comb spectrum (where the daughter photon pair was produced in a superposition of two temporal modes, corresponding to the two coherent, separate pulsed excitations of the micro-ring). Stabilized interferometers, comprised of standard fiber telecommunications elements, were used to both prepare the pulse pair and project the time-bin entangled qubits for state processing. In the comb, signal-idler pairs may be generated on,

e.g. two separate resonance pairs simultaneously, the post-selection of these events enabling the generation of a four-photon time-bin entangled state. We confirmed the realization of these four-photon product states of maximally-entangled Bell states through four-photon quantum interference, showing a measured visibility of 89% without background correction [8]. The measured density matrix of these states also reached a fidelity of 64%, comparable in quality to other, non-integrated four-photon states.

To demonstrate an on-chip generation of high-dimensional entangled states, we spectrally filtered a mode-locked laser to excite a single resonance of an integrated micro-ring resonator. The produced photon pairs covered multiple resonances due to the broad phase-matching condition, and were intrinsically created as a high-dimensional superposition of resonance frequency modes, entangled via SFWM energy conservation. We then exploited a concatenation of standard telecommunications for the coherent manipulation of the state within a single spatial mode. Programmable filters were used to impose arbitrary phase and amplitude masks on the frequency components of the quantum state, while phase modulation deterministically shifted and mixed the different frequency components in a designed manner. The control scheme can then be used to implement arbitrary phase gates, as well as to perform deterministic high-dimensional projection measurements. We used this scheme to characterize the state dimensionality, concluding that it was formed by two entangled quDits with D=10. We then validated our platform by measuring violations of a high-dimensional Bell inequality and performing quantum state tomography. Specifically, we characterized the quantum interference for D = 2, 3, and 4, where we obtained visibilities of 83.7%, 86.6%, and 86.4%, respectively, all violating their respective high-dimensional Bell inequalities [12]. We then performed quantum state tomography to experimentally extract the density matrices of the states. The measured fidelities of 88.5%, 80.9%, and 76.6% for D = 2, 3, and 4, respectively [10] confirmed that the experimental quantum states were very close to the targeted maximally-entangled states.

Integrated quantum frequency combs thus provide a scalable and versatile approach to generate optical quantum states, and represent a practical potential platform for quantum information processing. Recent work demonstrates that microcavity-based complex states and their manipulation via standard telecommunications components can, especially if combined with gate implementations presently under development [13], open up new venues for reaching the state complexities and processing capabilities required for meaningful quantum information science.

References

[1] P. Del'Haye, A. Schliesser, O. Arcizet, T. Wilken, R. Holzwarth, and T. J. Kippenberg, Nature **450**, 1214–1217 (2007).
[2] C. Reimer, L. Caspani, M. Clerici, M. Ferrera, M. Kues, M. Peccianti, A. Pasquazi, L. Razzari, B. E. Little, S. T. Chu, D. J. Moss, and R. Morandotti, Opt. Express **22**, 6535 (2014).
[3] L. Caspani, C. Reimer, M. Kues, P. Roztocki, M. Clerici, B. Wetzel, Y. Jestin, M. Ferrera, M. Peccianti, A. Pasquazi, L. Razzari, B. E. Little, S. T. Chu, D. J. Moss, and R. Morandotti, Nanophotonics **5**, 351–362 (2016); L. Caspani et al., Light Sci. Appl. **6**, e17100 (2017).
[4] M. Kues, C. Reimer, B. Wetzel, P. Roztocki, B. E. Little, S. T. Chu, T. Hansson, E. A. Viktorov, D. J. Moss, and R. Morandotti, Nat. Photonics **11**, 159–162 (2017).
[5] P. Roztocki, M. Kues, C. Reimer, B. Wetzel, S. Sciara, Y. Zhang, A. Cino, B. E. Little, S. T. Chu, D. J. Moss, and R. Morandotti, Opt. Express **25**, 18940 (2017).
[6] C. Reimer, M. Kues, L. Caspani, B. Wetzel, P. Roztocki, M. Clerici, Y. Jestin, M. Ferrera, M. Peccianti, A. Pasquazi, B. E. Little, S. T. Chu, D. J. Moss, and R. Morandotti, Nat. Commun. **6**, 8236 (2015).
[7] D. Grassani, S. Azzini, M. Liscidini, M. Galli, M. J. Strain, M. Sorel, J. E. Sipe, and D. Bajoni, Optica **2**, 88 (2015).
[8] C. Reimer, M. Kues, P. Roztocki, B. Wetzel, F. Grazioso, B. E. Little, S. T. Chu, T. Johnston, Y. Bromberg, L. Caspani, D. J. Moss, and R. Morandotti, Science **351**, 1176–1180 (2016).
[9] F. Mazeas, M. Traetta, M. Bentivegna, F. Kaiser, D. Aktas, W. Zhang, C. A. Ramos, L. A. Ngah, T. Lunghi, É. Picholle, N. Belabas-Plougonven, X. Le Roux, É. Cassan, D. Marris-Morini, L. Vivien, G. Sauder, L. Labonté, and S. Tanzilli, Opt. Express **24**, 28731 (2016).
[10] M. Kues, C. Reimer, P. Roztocki, L. R. Cortés, S. Sciara, B. Wetzel, Y. Zhang, A. Cino, S. T. Chu, B. E. Little, D. J. Moss, L. Caspani, J. Azaña, and R. Morandotti, Nature **546**, 622–626 (2017).
[11] P. Imany, J. A. Jaramillo-Villegas, O. D. Odele, K. Han, D. E. Leaird, J. M. Lukens, P. Lougovski, M. Qi, and A. M. Weiner, Opt. Express **26**, 1825 (2018).
[12] D. Collins, N. Gisin, N. Linden, S. Massar, and S. Popescu, Phys. Rev. Lett. **88**, 040404 (2002).
[13] H.-H. Lu, J. M. Lukens, N. A. Peters, O. D. Odele, D. E. Leaird, A. M. Weiner, and P. Lougovski, Phys. Rev. Lett. **120**, 030502 (2018).

5kW monolithic continuous wave near diffraction-limited fiber laser directly pumped by laser diodes

W. Shi[1,2], Q. Fang[1,2], Y. Qin[2], J. Li[1,2], Z. Xie[1], Q. Shen[1], J. Yao[1]
[1]*College of Precision Instrument and Optoelectronics Engineering, Tianjin University, Tianjin, 300070, P.R. China*
[2]*Tianjin Institute of Modern Laser & Optics Technology, Tianjin, 300384, P.R. China*
E-mail: shiwei@tju.edu.cn

High power ytterbium-doped glass fiber lasers and amplifiers are emerging as the workhorse for providing multi-kilowatts and even tens of kilowatts high-brightness laser emission, benefiting from the development of high-brightness semiconductor laser diodes, novel fiber designs, new pumping schemes, and high-power fiber components over the past decade [1], [2]. Conventionally, high power glass fiber lasers and amplifiers are directly pumped by laser diodes. Several laser-diode-pumped multi-kilowatts fiber lasers with near diffraction-limited beam quality have been reported. Tandem pumping, in which fiber lasers operating at shorter wavelengths are utilized as high-brightness pumping sources for another fiber laser or fiber amplifier, are usually adopted to develop high power continuous wave (cw) fiber laser sources. In contrast to tandem pumped fiber lasers, laser-diode-pumped fiber lasers have higher wall-plug efficiency and can be packaged more compactly. With the increased brightness of pump laser diodes and the development of high-power fiber combiner, it is possible for the laser-diode-pumped fiber lasers to produce more laser power.

In this paper, we report a monolithic continuous wave (CW) fiber laser source at 1080 nm, producing > 5 kW average laser power. The laser consists of a CW fiber laser oscillator and one double cladding (DC) fiber amplifier in the master oscillator-power amplifier (MOPA) configuration. The oscillator is a linear cavity fiber laser with a pair of fiber Bragg gratings (FBG) centered at the wavelength of ~1080 nm. The active fiber utilized in the laser oscillator is ~ 20 meters 20/400 μm (diameter of the core/inner cladding) double cladding ytterbium-doped fiber. The numerical aperture (NA) is 0.06/0.46 (core/inner cladding). The oscillator can produce ~ 500 W laser power with ~ 700 w launched pump power, provided by fiber coupled laser diodes at ~976 nm. One fiber amplifier was built to boost the average power of the seed laser. A piece of double cladding ytterbium-doped fiber with 30μm core was utilized as the active medium in the fiber amplifier. The fiber amplifier was directly pumped by fiber coupled laser diodes at ~976 nm. >5kW laser power was achieved when ~5352 W pump power was launched into the amplifier. The optical-to-optical conversion efficiency of the fiber amplifier with respect to the launched pump power reach 86.5%. The beam quality factor was measured to be <1.6. This is the first demonstration of the >5 kW monolithic near diffraction-limited fiber laser directly pumped by laser diodes and no any tandem pumping technique was adopted.

References

[1] W. Shi, Q. Fang, X. Zhu, R. A. Norwood, and N. Peyghambarian, "Fiber lasers and their applications," Appl. Opt., vol. 53, no. 28, pp. 6554-6568, 2014.
[2] M. N. Zervas, and C. A. Codemard, "High power fiber lasers: a review," IEEE J. of Select. Topics in Quantum Electron., vol. 20, no. 5, pp. 1-23, 2014.

Nonlinear multimode fibers for high power fiber lasers

S. Wabnitz[1-3], K. Krupa[1], D. Modotto[1], G. Millot[4], D.S. Kharenko[3,5], V.A. Gonta[3], E.V. Podivilov[3,5], S. Babin[3,5], A. Tonello[6], A. Barthélémy[6], and V. Couderc[6]

[1]*Dipartimento di Ingegneria dell'Informazione, Università di Brescia, Via Branze 38, 25123, Brescia, Italy*
[2]*Istituto Nazionale di Ottica del Consiglio Nazionale delle Ricerche (INO-CNR), Via Branze 45, 25123, Brescia, Italy*
[3]*Novosibirsk State University, 1 Pirogova str., Novosibirsk, 630090, Russia*
[4]*Université de Bourgogne Franche-Comté, ICB, UMR CNRS, 6303, Dijon, France*
[5]*Institute of Automation and Electrometry, SB RAS, 1 ac. Koptyug ave., Novosibirsk, 630090, Russia*
[6]*Université de Limoges, XLIM, UMR CNRS, 7252, Limoges, France*
E-mail: stefan.wabnitz@unibs.it

Nonlinear multimode optical fibers have recently emerged as an easily accessible and versatile platform to control complex spatiotemporal optical beam and pulse reshaping phenomena [1]. In the anomalous dispersion regime of the fibers, multimode optical solitons have been observed in graded-index (GRIN) MMFs, resulting from the compensation of both chromatic and modal dispersion by Kerr nonlinearity [2]. On the other hand, light intensity oscillations owing to the self-imaging effect in graded-index GRIN MMFs lead, via the Kerr effect, to a dynamic long-period index grating, which may phase-match the generation of ultra-broadband sideband series. These can be generated by either spatiotemporally oscillating solitons in the anomalous dispersion regime [3], or quasi-CW pulses in the normal dispersion regime [4,5].

For relatively short GRIN fibers, beam self-cleaning activated by the Kerr effect was only recently observed, at a lower power threshold than that for the well-known Raman beam cleanup. The highly multimode speckled beam at the fiber output evolves, at high powers, into a high brightness, bell-shaped beam sitting on a low-power background of high-order modes [6]. A similar effect has been reported in the femtosecond pulse propagation regime, always with normal group velocity dispersion [7]. A remarkable property of beam self-cleaning is that it is frequency transferred to all parametric sidebands [4], and even to octave spanning supercontinua [8-9].

The brightness enhancement and spatial beam compression, accompanied by significant temporal compression [10], resulting from Kerr beam self-cleaning could be exploited as a building block of a new class of high power multimode fiber lasers. In fact, we have shown that self-cleaning is reinforced in active, Yb-doped MMF, thanks to the cooperation between the dispersive and the dissipative effects resulting from modal gain selection [11]. Intracavity self-cleaning in a composite cavity laser configuration involving an Yb-doped MMF has been reported, leading to mode-locking and parametric sideband generation within the laser [12].

In order to fully exploit laser beam dynamics in MMFs for applications to spatiotemporal laser beam mode-locking [13], it is necessary to accurately determine the conditions for the occurrence of the effect, by optimizing the spatial and temporal properties of the input laser pulses. We will describe a series of recent experiments that permit to unveil the physical mechanism of Kerr-beam self-cleaning, based on a complex cascade of parametric wave mixing processes.

This work was supported by the Ministry of Education and Science of the Russian Federation (Minobrnauka) (14.Y26.31.0017). K.K. has received funding from the European Union's Horizon 2020 research and innovation program under the Marie-Sklodowska-Curie action (No. 713694).

References

[9] L.G. Wright et al., Nature Photonics **9**, 306 (2015).
[10] W.H. Renninger, and F.W. Wise, Nature Communications **4**, 1719 (2013).
[11] L. G. Wright, et al., Phys. Rev. Lett. **115**, 223902 (2015).
[12] K. Krupa et al., Phys. Rev. Lett. **116**, 183901 (2016).
[13] L.G. Wright et al., Nat. Photonics **10**, 771 (2016).
[14] K. Krupa et al., Nat. Photonics **11**, 237 (2017).
[15] Z. Liu et al., Opt. Lett. **41**, 3675 (2016).
[16] G. Lopez-Galmiche et al., Opt. Lett. **41**, 2553 (2016).
[17] K. Krupa et al., Opt. Lett. **41**, 5785 (2016).
[18] K. Krupa et al., Physical Review A **97**, 043836 (2018)
[19] R. Guenard et al., Optics Express **25**, 4783 (2017).
[20] R. Guenard, et al., Opt. Express **25**, 22219 (2017).
[21] L.G. Wright et al., Science **358**, 94 (2017).

Breath study via mid-infrared spectroscopy: an individual`s island of stability (IOS)

K.S. Maiti[1], M. Lewton[1], E. Fill[2], and A. Apolonskiy[1-3]
[1]*Max-Planck-Institut fuer Quantenoptik, D-85748, Garching, Germany*
[2]*Department für Physik, Ludwig-Maximilians-Universität München, D-85748, Garching, Germany*
[3]*Novosibirsk State University, 630090, Novosibirsk, Russia*
E-mail: Alexander.Apolonskiy@physik.uni-muenchen.de

Background: How stable and unique are the individual's physiological data? The idea to define an individual's state on a long scale is known for 10 years (for example, an individual metabolic phenotype approach) but still a matter of debate. For breath, a stability of several moderate-size metabolites during 9 days was recently confirmed by using mass spectrometry.

Methods: We used a conventional mid-infrared FTIR spectrometer in the range 800-2500 cm^{-1} in conjunction with a water suppression system for breath samples (suppression factor: 2500). A healthy group of 15 volunteers were studied during a 5-month period. To present and analyze the data, principal component analysis (PCA) in combination with ANOVA, and visual inspection of absorption spectral ranges under study were used. The most reliable IOS representation is found in a multi-parameter space by using concentrations of volatile compounds as axes (CVC-space).

Results:1) There is strong evidence for an IOS identified in this preliminary study for healthy individuals. The IOS core stays stable at least for 5 months for the disease-free case in that period. For high and middle methane emitters as well as for smokers, the IOSs' (in CVC-space) are larger than that for low methane emitters and nonsmokers. 2) For every individual, there exist several ways to escape from his IOS e.g. by coffee and alcohol ingestion, physical exercise, mental activity, smoking, fasting (i.e. representing IOS core + "daily and weekly noise" noise). We analyzed these ways in terms of duration and relative strength by measuring CO_2, CO, acetone, methane, isoprene and ethanol concentrations in breath before and after the experiment. In addition, we found significant circadian variations.

Conclusions: 1) We demonstrate the feasibility of unambiguous characterization of individuals by means of their breath. Bearing in mind that only a limited set of volatile organic compounds was collected in the experiment because of a limited spectrometer detectivity (50 ppb), this is a promising result with a high potential. A wider set of accessible metabolites will extend the dimensionality of IOS thus allowing to increase the interpersonal distances and to make IOS "more individual". 2) A personal passport containing the multidimensional CVC-space IOS data averaged over some period could help in the strategy aiming at early detection of an abnormality in the body. Suppression of technical as well as "daily and weekly noise" leads to a smaller size of the IOS down to its core, helping thus to represent an individual and analyze the collective data (i.e. a cohort).

Next steps: 1) Further progress in laser-free and laser-based spectrometers is feasible. In combination with further water suppression, for the former one can expect detectivity on the 100 ppt level. 2) A pilot study of renal/urologic as well as mental diseases is on the way. In the study, comparison with a healthy cohort will be used based on the IOS concept.

Ring laser gyroscopes in the underground Gran Sasso Laboratories

N. Beverini
Dipartimento di Fisica, Università di Pisa and INFN, sezione di Pisa, I56127, Pisa, Italy
E-mail: nicolo.beverini@unipi.it

GINGER (Gyroscopes IN GEneral Relativity) is a proposed experiment with the aim of measuring in a ground laboratory the gravito-electric (known also as Lense-Thirrings effect) and gravito-magnetic effects (or De Sitter effect), foreseen by General Relativity through an array of ring laser gyroscopes.

GINGERINO is a square ring-laser prototype with a 3.6 m side (Fig. 1), which has been built to investigate the level of noise inside the Gran Sasso underground laboratories (LNGS) of INFN [1]. GINGERINO has already completed its task for GINGER, showing the advantage of the underground location. It cannot reach the sensitivity suitable for the fundamental physics measurements, but it can provide important data for geophysics and seismology. Its high sensitivity in the frequency band of fraction of Hz makes it suitable for seismology studies. It is located in a seismically active area, and it recorded part of the of central Italy earthquakes. During October–November 2016 it collected dozens of events of the Central Italy seismic sequence, spanning the 3.5–5.9 magnitude range and epicentral distances between 30 and 70 km [2]. This data set constitutes an unprecedented observation of the vertical rotational motions associated with an intense seismic sequence at local distance. Both local and far seismic events have been recorded (Fig. 1). Since May 2017 the acquisition of the data became continuously. The analysis of the first 90 days [3] shows a duty cycle is higher than 95%, with a quantum shot noise limit is of the order of 10^{-10} (rad/s)/√ Hz.

A new apparatus is now proposed to be built inside LNGS with the aim of achieving a sensitivity suitable for observing relativistic effects. It foresees an array of three square ring laser [4], one with the axis oriented along Earth rotation axis, one lying in the horizontal plane, while the orientation of third one will depend on the volume constrain in the final location in the laboratories. The long-term stability of the apparatus, which is of key relevance for our purpose, will be guaranteed by an active control of the geometry, applying the techniques that we are presently testing on a smaller apparatus in our laboratory in Pisa.

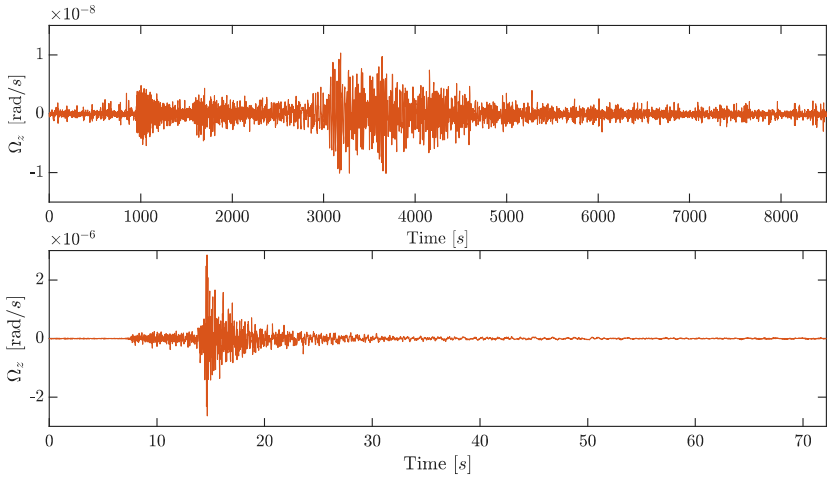

Fig. 1 Typical signal from a faraway strong Earthquake on July 18 2017, around 00 : 00 (UTC), Kamchatka, Russia, M 7.6 (TOP) and of a regional Earthquake, on October 16 2016 09:32:35 (UTC), Rieti, Italy Mw 4.0 (BOTTOM), Note the difference in the time scales. The Kamchatka signals is strongly expanded in time, as typical for teleseisms, reflecting the different velocity of the various kinds of seismic waves.

References

[1] J. Belfi, et al., Rev Sci Instrum **88,** 034502 (2017)
[2] A. Simonelli, et al, Geophys. J. Int. **214**, 705–715 (2018)
[3] J. Belfi, et al., Appl.Opt. (submitted)
[4] A. Di Virgilio, et al., Eur. Phys. J. Plus **132**: 157 (2017)

A glimpse on what high-power lasers can bring to astrophysics

J. Fuchs[1-3]
[1]*LULI–CNRS, CEA, École Polytechnique, Univ. Paris-Saclay, Sorbonne Univ., UPMC Univ. Paris 06, F-91128, Palaiseau cedex, France*
[2]*Institute of Applied Physics, 46 Ulyanov Street, 603950, Nizhny Novgorod, Russia*
[3]*ELI-NP, Magurele, Romania*
E-mail: Julien.fuchs @polytechnique.fr

Coupling high-power lasers and high-strength B-fields [1] helps gaining unique insight and understanding of a variety of phenomena of crucial importance for astrophysics. We have shown that such platform could be used to mimic the expansion of a young star isotropic disk wind threaded by a co-axial poloidal magnetic field [2,3]. In this case, our scaled laboratory experiments, representative of young stellar objects (YSOs) outflows, revealed that stable and narrow collimation of the entire flow can result from the presence of a poloidal magnetic field [4-6] whose strength is consistent with observations. The laboratory plasma becomes focused with an interior cavity. This gives rise to a standing conical shock from which the jet emerges. Following simulations of the process at the full astrophysical scale, we concluded that it can also explain recently discovered X-ray emission features observed in low-density regions at the base of protostellar jets, such as the well-studied jet HH 154.

The same platform could also be used to study (i) the issue of accretion dynamics in young star, in particular to shed light on the deficiency of x-ray emissivity in these systems [7], or (ii) the issue particle energization in astrophysical plasmas [8,9]. Regarding accretion, its dynamics in the forming of young stars is still object of debate because of limitations in observations and modelling. Through scaled laboratory experiments of collimated plasma accretion onto a solid in the presence of a magnetic field, we have opened a first window on this phenomenon by tracking, with spatial and temporal resolution, the dynamics of the system and simultaneously measuring multiband emissions. We observed in these experiments that matter, upon impact, is laterally ejected from the solid surface, then refocused by the magnetic field toward the incoming stream. Such ejected matter forms a plasma shell that envelops the shocked core, reducing escaped X-ray emission. This demonstrates one possible structure reconciling current discrepancies between mass accretion rates derived from X-ray and optical observations.

We will finally discuss perspectives offered by the upcoming new generation of lasers that will offer unprecedented levels of power (up to 10 PW), which will allow to generate very dense bunches of particles at high energy [10]. This could also have a positive impact on laboratory astrophysical studies, e.g. in the field of nucleosynthesis studies where extreme fluxes of neutrons are required in order to investigate double neutron capture, which is out of reach of existing, accelerator-based facilities, but which lasers might allow to tackle.

References

[1] B. Albertazzi, J. Béard, A.Ciardi, et al., Rev. Sci. Inst. **84**, 043505 (2013).
[2] A. Ciardi, T. Vinci, J. Fuchs, et al., Phys. Rev. Lett., **110**, 025002 (2013).
[3] B. Albertazzi A. Ciardi, M. Nakatsutsumi, et al., Science **346**, 325 (2014).
[4] D. P. Higginson, B. Khiar, G. Revet, et al., Phys. Rev. Lett. **119**, 255002 (2017).
[5] S. Ryazantsev, I. Skobelev, A. Faenov, et al., Physics of Plasmas **23**, 123301 (2016).
[6] D. P. Higginson, G. Revet, B. Khiar, et al., High Energy Dens. Physics **23**, 48-59 (2017).
[7] G. Revet, S.N. Chen, R. Bonito, et al., Science Advances **3**, e1700982 (2017).
[8] D. P. Higginson, Ph. Korneev, J. Béard, et al., High Energy Dens. Physics **17**, 190 (2015).
[9] P. Korneev, E. d'Humières, D. P. Higginson, et al., High Energy Dens. Physics **17**, 183 (2015).
[10] N. Nakatsutsumi, Y. Sentoku, S. N. Chen, et al., Nat. Comm. **9**, 280 (2018).

Tailored optics with a highly-discrete optical frequency comb; toward high resolution nonlinear spectroscopy in the vacuum ultraviolet wavelength region

C. Ohae[1,2], J. Zheng[3], K. Minoshima[1-3], and M. Katsuragawa[1-3]
[1]*Institute for Advanced Science, University of Electro-Communications, 1-5-1 Chofugaoka, Chofu, Tokyo, 182-8585, Japan*
[2]*JST, ERATO MINOSHIMA Intelligent Optical Synthesizer Project, 1-5-1 Chofugaoka, Chofu, Tokyo, 182-8585, Japan*
[3]*Department of Engineering Science, University of Electro-Communications,*
1-5-1 Chofugaoka, Chofu, Tokyo, 182-8585, Japan
E-mail: katsuragawa@uec.ac.jp

1. Introduction

This paper describes an attractive optical property of a highly-discrete optical frequency comb. The amplitude and phase distributions among such optical frequency comb are nearly arbitrarily manipulated simply by placing fundamental optical elements on the optical path and controlling their thicknesses precisely [1,2]. If we employ this optical property in linear optical processes, we can generate ultrafast optical pulses continuously with a repetition rate above 100 THz [1-5]. Furthermore, if we apply this optical property in nonlinear optical processes, we can design nonlinear optical phenomena in a variety of ways [6-8]. In this conference, we will discuss the point of the above idea, the current status of relevant experiments, and future prospects toward exploring high-resolution nonlinear spectroscopy in the vacuum ultraviolet wavelength region.

2. Simple optical device for arbitrarily manipulating amplitude and phase

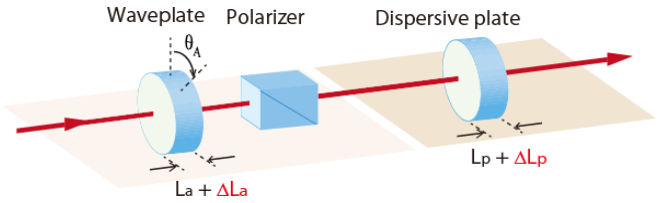

Fig. 1 Optical device for arbitrarily manipulating amplitude and phase

We place three fundamental optical elements, namely, a waveplate (a uniaxial birefringent plate), a polarizer, and a dispersive plate on an optical path, where the first two elements manipulate amplitudes and the last element manipulates phases. When the spectral discreteness of an incident radiation is very high (typically greater than 10 THz), the relative amplitude and phase distributions among the spectral modes are nearly arbitrarily manipulated by simply controlling the thicknesses of the waveplate and the dispersive plate, respectively [1,2].

3. Tailoring linear optical processes: generation of ultrafast optical pulses having a repetition rate above 100 THz

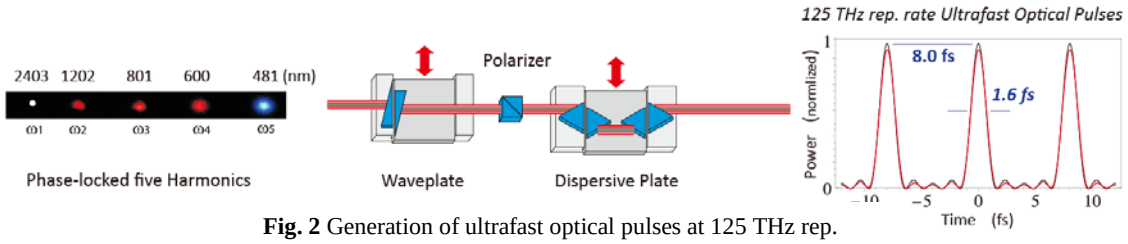

Fig. 2 Generation of ultrafast optical pulses at 125 THz rep.

We can generate ultrafast optical pulses with a repetition rate of above 100 THz in the time domain by employing the above optical device. Figure 2 shows a typical experimental result where we generated ultrafast optical pulses by applying such amplitude- and phase-manipulation technology to phase-locked five harmonics (a highly-discrete optical frequency comb with a 125-THz frequency spacing) [9] which were produced on the basis of the optical frequency divider technology. Stable ultrafast

optical pulses were produced over a long period of an hour or more with a pulse duration of 1.6 fs and a rep. rate of 125 THz [5].

4. Tailoring nonlinear optical processes: A single-frequency tunable laser having the potential to cover an entire wavelength region of 120 nm to 30 μm

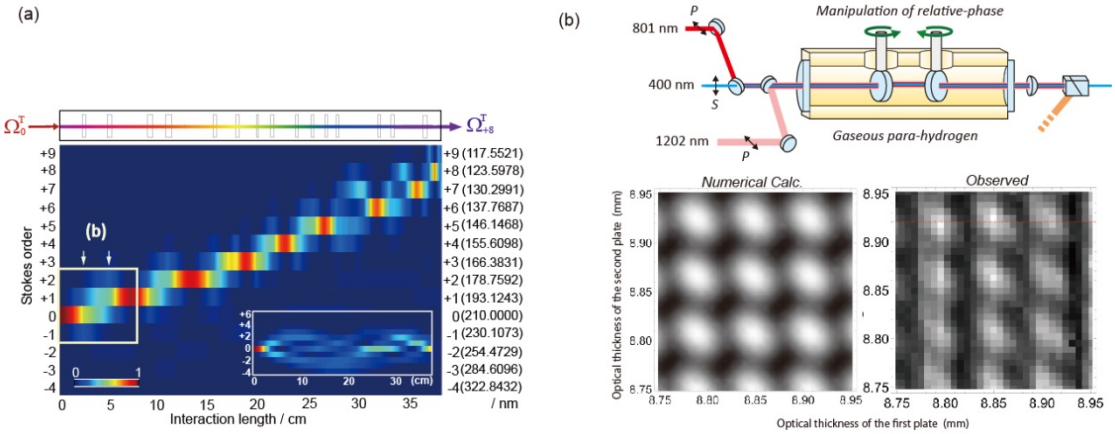

Fig. 3 Tailoring the Raman-resonant four-wave-mixing

If we apply this optical device in nonlinear optical processes, we can tailor the nonlinear optical phenomena in a variety of ways. The numerical simulation in Fig. 3a shows a typical result of how we could artificially manipulate the Raman-resonant four-wave-mixing by implementing the above phase-manipulation device in this nonlinear optical process [6]. When we did not apply any artificial phase-manipulation at all, the incident radiation was broadly converted to high-order Stokes and anti-Stokes radiations (inset in Fig. 3a). On the other hand, if at selected positions, we intentionally manipulated the relative phase relationships among the laser radiations relevant to this nonlinear optical process, incident energy was fully converted to an aimed specific Raman mode with near-unity quantum conversion efficiency as represented in Fig. 3a.

This conceptual idea itself is very general, and thereby we can apply it to a variety of nonlinear optical phenomena. In practice, we have also demonstrated a nonlinear interferometer in the frequency domain on the basis of this conceptual idea [8]. We examined the experiment corresponding to the first step of Fig. 3a, indicated by a white square (generation of 1st Stokes and/or 1st anti-Stokes radiations), and confirmed experimentally that we could tailor this nonlinear optical process according to the estimation by the numerical simulation as shown in Fig. 3b [7]. This confirmed the principle correctness of the fundamental concept.

Tailoring the Raman-resonant four-wave-mixing process shown in Fig. 3a has the potential to materialize a single-frequency tunable laser that can entirely cover an ultrabroad wavelength region of 120 nm to 30 μm [6]. We are now aiming to explore a new frontier: nonlinear high-resolution spectroscopy in the vacuum ultraviolet wavelength region [6].

References

[1] M. Katsuragawa and K. Yoshii, Phys. Rev. A, **95**, 033846 (2017).
[2] K. Yoshii, J. K. Anthon-y and M. Katsuragawa, Light: Sci. & Appl. **2,** e58 (2013).
[3] K. Yoshii, Y. Nakamura, K. Hagihara and M. Katsuragawa, CLEO/QELS 2014, OSA Technical Digest (online) (Optical Society of America, 2014), paper FTh1D.5.
[4] C. Zhang, D. Tregubov, K. Yoshii, C. Ohae, M. Suzuki, K. Minoshima, and M. Katsuragawa, The 24th Congress of the International Comission for Optics (ICO-24), paper Th1A-06.
[5] C. Ohae, N. S. Suhaimi, T. Gavara, K. Nakagawa, F. -L. Hong, K. Minoshima, and M. Katsuragawa, Nonlinear Optics 2017, paper NTh2B.1.
[6] J. Zheng and M. Katsuragawa, Scientific Reports, **5**, 8874-1-6 (2015). ; arXiv: 1406.3921 (2014).
[7] C. Ohae, J. Zheng, K. Ito, M. Suzuki, K. Minoshima, and M. Katsuragawa, Optics Express, **26**, 1452 (2018). ; arXiv: 1711.10772 (2017) ; Nonlinear Optics 2017, paper NM3B.1.
[8] J. Zheng, and M. Katsuragawa, Nonlinear Optics 2017, paper NM3B.3.
[9] N. S. Suhaimi, C. Ohae, T. Gavara, K. Nakagawa, F. -L. Hong, and M. Katsuragawa, Opt.Lett. **40**, 5802 (2015).

Temporal recompression of powerful laser pulses

S.Yu. Mironov[1], I.V. Yakovlev[1], V.N. Ginzburg[1], A.A. Shaykin[1], E.A. Khazanov[1], and G. Mourou[2]
[1]*Federal Research Center Institute of Applied Physics of the Russian Academy of Sciences, Russia*
[2]*IZEST, France*
E-mail: Sergey.Mironov@mail.ru

The last achievements in high –power laser system creation have made it possible to generate optical pulses with peak power exceeding 1 PW level. The focused radiation finds applications in different experiments on laser matter interaction, generation and acceleration electron, proton and more heavy ions bunches. But future experiments devoted to an investigation of nonlinearity of vacuum, generation electron positron pairs and others require significantly more peak power and peak intensity at focal plane. The further peak power increasing can be done by increasing energy level or implementation in experiments a pulse shortening technique [1], which is also called as Thin Film Compression technique. The idea of the pulse shortening method is rather simple and based on an implementation of self-phase modulation effect appearing at powerful pulse propagation through thin (less than 1 mm) plane parallel plate and spectral phase correction with help of chirped mirrors. The cubic nonlinearity of a material of the plate introduces spectral phase modulation and, as a result, it broadens spectral intensity of the powerful pulses. The chirped mirrors correct spectral phase and produce temporal compression. The plate and chirped mirrors should be placed inside vacuum chamber to exclude an influence of cubic nonlinearity of air. The technique can be applied several times (two, in particular), and it was shown in a theoretical work [1], that it is way to generate PW level laser pulses with a duration of single cycle of optical field oscillation. The plates can be done from fused silica, glasses or transparent polymers [1,2].

Previously the pulse shortening technique was successfully verified for femtosecond laser pulses with peak intensity ~TW/cm^2 and hundreds of mJ energy level [3]. Pulse compression from 33 fs down to 16 fs was demonstrated at laser system ALLS (Advanced Laser Light Source) placed in INRS, Canada. This method was also tested in IAP RAS at sub PW laser system PEARL. An output radiation of the system was used for experiments on pulse shortening. Laser beam with energy 5.5J, pulse duration T=57fs (FWHM), diameter 100 mm and central wavelength 920 nm passed through 0.5 mm polyethylene terephthalate plane parallel plate for spectrum broadening. Only small attenuated (approximately in 1000 times) portion of the beam was used for pulse shortening. Set of chirped mirrors with anomalous GVD (Group Velocity Dispersion) and system of diagnostic of laser pulse parameters were placed under air condition. It was demonstrated at the experiments the reduction of pulse duration down to 22 fs. An influence of spectral phase aberrations for spectrum broadening and pulse compression was investigated theoretically. It was shown, that the growth of peak power at the recompressed laser pulse linearly depends on the value of accumulated B-integral and do not sensitive to spectral phase aberrations of third and fourth order [4].

Full size experiments on pulse shortening with the following laser beam parameters: energy 18J, pulse duration T=60fs (FWHM) and beam size 175 mm are planned to be done with using laser system PEARL this year. A plane parallel fused silica plate with aperture 200 mm and 1 mm thickness will be used for spectral broadening. The plate and two chirped mirrors with clear aperture 200 mm and -100fs^2 GVD parameter will be placed inside vacuum chamber and should reduce the pulse duration down to 25-27fs. The peculiarities of the last and future experiments and results of 3D numerical modelling with experimental beam profile will be discussed thoroughly.

The work is supported by the Ministry of Education and Science of the Russian Federation (contract 14.Z50.31.0007).

References

[1] G. Mourou., S. Mironov, E. Khazanov, A. Sergeev, The European Physical Journal Special Topics **223**, 1181 (2014).
[2] S. Mironov, V. Ginzburg, E. Gacheva D. Silin, A. Kochetkov, Y. Mamaev, A. Shaykin, E. Khazanov, Laser Physics Letters **12**, 025301(2015).
[3] P. Lassonde, S. Mironov, S. Fourmaux, S. Payeur, E. Khazanov, A. Sergeev, J.C. Kieffer, G. Mourou G., Laser Physics Letters **13**, 075401 (2016).
[4] S. Mironov et al., Quantum electronics **47**, 614 (2017).

Terahertz non-destructive testing technologies for industrial applications

K.H. Park, E.S. Lee, K. Moon, I.-M. Lee, H.-S. Kim,
D.W. Park, J.-W. Park, J.-H. Shin, and D.-H. Choi
THz Creative Basic Research Section, ETRI, Daejeon, 34129, South Korea
E-mail: khp@etri.re.kr

Terahertz (THz) technologies have attracted great interest in their possibilities over a wide range of industrial applications such as wireless communications, spectroscopy, and imaging. Recently, as the manufacturing processes of the industry have been diversified, much attention has been focused on the novel non-destructive testing (NDT) technologies. Although there exist variety of well-established NDT technologies utilizing various technologies such as ultrasonic or visible, infrared or ultraviolet waves, considerable demands on novel NDT technology that can fill the lacks in the conventional technologies still keep growing in industries. In this aspect, THz NDT technologies have great potential for their advantageous characteristics: it can penetrate many materials that are absorptive to the lights with much higher spatial resolutions than those of conventional radio frequency waves, can be easily used as a stand-off NDT technology, and harmless to the human body.

Consequently, developing a THz system of smaller, inexpensive and easy to handle has long been the pursuit of the researchers in this field. For such an objective, THz technology based on continuous waves (CWs) has been regarded as the promising one, provided if the performance of CW THz systems, for example, power emission efficiency and detection sensitivity, can be enhanced.

In this view, we have developed several key components of CW THz systems based on photonics-based technology [1-4]. We have continuously improved the performances of the key components and have acquired the performances that are compatible to or better than those of the commercially-available ones in some devices. Recently, our photonics-based CW THz systems are about to see some outcomes as the industrial NDT applications in some manufacturing companies. Our proto-type for a CW THz system for inspecting a mass-production process of a car manufacturing company can be used as a stand-off NDT instrument to find human errors that may occur in the manufacturing process and hard to be found by other technologies (see, Fig. 1).

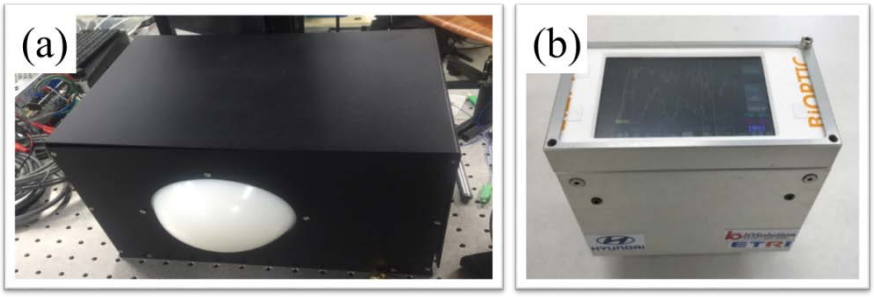

Fig. 1 Proto-types of our photonics-based CW THz NDE systems. (a) THz imaging system and (b) THz spectroscopic system. After some small modifications, these systems are expected to be applied as the mass-production NDE instruments in a globalized car manufacturing company.

Our recent progress in THz NDT technologies with some illustrative examples, their possibilities as industrial applications will be presented in the presentation [5]. In addition, our recent efforts in the basic researches for the CW THz systems will also be presented briefly [6, 7].

References

[1] N. Kim, J. Shin, E. Sim, et al., Opt. Express, vol. 17, no. 16, pp. 13851–13859 (2009).
[2] K. Moon, D. W. Park, I. -M. Lee, et al., Opt. Lett., vol. 38, no. 24, pp. 5466–5469 (2013).
[3] I.-M. Lee, N. Kim, E. S. Lee, et al., Optics Express, 23(2), pp. 846-858 (2015).
[4] S.-P. Han, H. Ko, N. Kim, et al., Optics Express, 22(23), pp. 28977-28983 (2014).
[5] E. S. Lee, K. Moon, I.-M. Lee, et al., J. Lightwave Tech. 36(2), pp. 274-283 (2018).
[6] J.-H. Shin, K. H. Park, and H.-C. Ryu, Nanotechnology, 27(19), 195202 (2018).
[7] K. Moon, E. S. Lee, I.-M. Lee, et al., Appl. Phys. Lett., 112(3), 031102 (2018).

THz QCL in a hybrid microdisk-dipole antenna resonator: a playground between optics and electronics

A. Pitanti
NEST Lab., CNR – Istituto Nanoscienze and Scuola Normale Superiore, piazza San Silvestro 12, 56127, Pisa (PI), Italy
E-mail: alessandro.pitanti@sns.it

Electromagnetic waves in the THz spectral range (0.5 – 10 THz) possess interesting properties which could be extremely beneficial in several fields, from medicine to security, quality control and astrophysics. THz waves and their applications have been scarcely investigated in the past, while their research was greatly boosted by the discovery/realization of THz quantum-cascade-lasers (QCL) in 2002 [1]. Being a high-purity, compact, electrically injected source of coherent light, THz-QCLs are an essential building block for THz based technologies. Although their many advantages of QCLs, few issues still need to be addressed to fully exploit THz waves in commercial applications
One particular issue relies in the challenging extraction of light from the cavity with high efficiency. In facts, double-metal ridge waveguides typically used to host the active, heterostructured material are deeply subwavelength in size, making the out beam at the laser facet strongly divergent. Few proposals exist for achieving a low-divergence emission; commonly they exploit interference in properly patterned grating/3rd order DFB [2, 3], yet a precise tuning of the features is required to achieve an overall good effect. Another intriguing route would be the vertical extraction of light from the devices; in this case, several solutions exist yet they either offer poor far field patterns or make use of macroscopic external elements such as mirror/lenses which prevent miniaturization and monolithically device integration (see ref. in [4]).

Interestingly, the spectral range of THz radiation lies in between the microwave and the optical domains; this permits the use and interchange of concepts which classically belongs to electronics or photonics, with the intriguing possibility of combining together antennas and LC oscillators with photonic crystals and resonant cavities. This hybrid approach enables novel functionalities and greatly increases the degrees of freedoms in devising new devices.

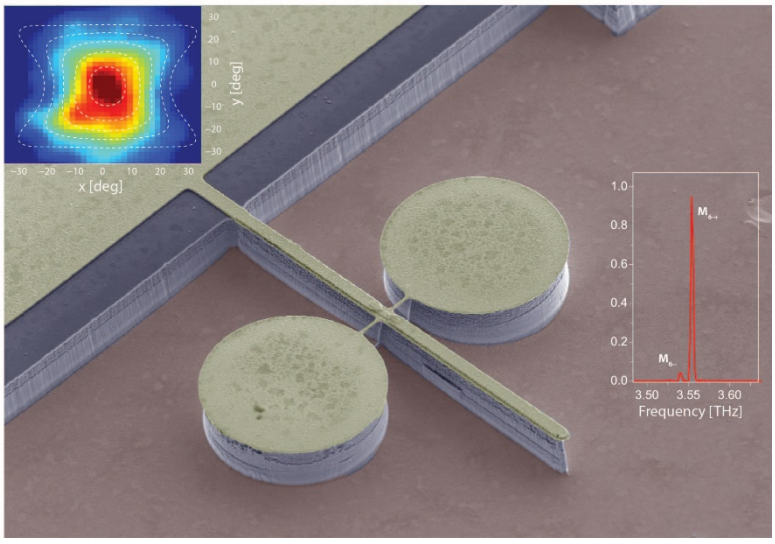

Fig. 1 False-color SEM image of the device. Laser spectrum at 7 K (right inset) and far-field emission map (top-left inset) are also reported. Simulated far-field emission is over imposed using white, dotted lines.

Starting from this concept, I will show a possible solution for achieving efficient low divergence emission from a subwavelength THz QCL. A proper device design, which combines a dipole antenna to resonant whispering gallery mode (WGM) cavities, let us achieve a 3.5 THz continuous-wave laser emission with a peak power if 250 μW at 7 K [4] and maximum operating temperature exceeding 50 K . A sketch of the final device is reported in Fig. 1, where the emission spectrum can be seen in the

rightmost inset. The antenna element (suspended bridge) reshapes the local electromagnetic field granting a highly desirable vertical emission with low divergence (±10° deg., see the top-left inset in Fig. 1) while, the high Q-factor of the WGMs gives low threshold and high slope efficiency. The tiny device footprint (10^{-2} λ^3) makes the device an ideal candidate for integration, large scale processing and, in general, for field applications. Furthermore, this particular geometry is compatible for observing optomechanical coupling between the laser and the antenna micro-vibrations, opening the route to THz optomechanics and novel functionalities for improved light control and modulation.

References

[1] R. Köhler, A. Tredicucci, F. Beltram, H. E. Beere, E. H. Linfield, A. G. Davies, D. A. Ritchie, R. C. Iotti and F. Rossi, Terahertz semiconductor-heterostructure laser, Nature **417**, 156 (2002).

[2] F. Castellano, S. Zanotto, L.H. Li, A. Pitanti, A. Tredicucci, E.H. Linfield, A.G. Davies and M.S. Vitiello, Distributed feedback terahertz frequency quantum cascade lasers with dual periodicity gratings, Appl. Phys. Lett. **106**, 011103 (2015).

[3] M. I. Amanti, G. Scalari, F. Castellano, M. Beck and J. Faist, Low divergence Terahertz photonic-wire laser, Opt. Expr. **18**, 6390 (2010).

[4] L. Masini, A. Pitanti, L. Baldacci, M. S Vitiello, R. Degl'Innocenti, H. E Beere, D. A Ritchie and A. Tredicucci, Continuous-wave laser operation of a dipole antenna terahertz microresonator, Light Sci. Appl. **6**, e17054 (2017).

Pulsed inductive discharge as a new method of pumping lasers

A.M. Razhev[1,2], S.N. Bagayev[1], D.S. Churkin[1,3]
[1]*Institute of laser physics SB RAS, Prosp. Ac. Lavrentyeva, 15B, Novosibirsk, Russian Federation*
[2]*Novosibirsk state technical university, Prosp. K. Marksa, 20, Novosibirsk, Russian Federation*
[3]*Novosibirsk state university, Pirogova st., 1, Novosibirsk, Russian Federation*
E-mail: razhev@laser.nsc.ru

In this work, a method for exciting gas laser active media by a pulsed inductive discharge is proposed and experimentally implemented in order to obtain lasing on electron transitions in atoms and molecules and vibrational-rotational transitions in molecules [1–5]. In contrast to conventional pulsed longitudinal and transverse discharges, a pulsed inductive discharge is formed due to the magnetic field induction produced by the pumping system without any electrodes in the active medium [6]. An appropriate choice of the tube material may ensure the purity of the active medium considerable endurance of lasers. The formation of such a discharge is not accompanied by the appearance of cathode spots on the surface of the electrodes, which are responsible for the instability and contraction of the discharge, deterioration of the homogeneity of the discharge, contamination of the gas mixture, quenching of lasing, and limitation of the pulse repetition rate. The application of the pulsed inductive discharge for excitation is a promising method for pumping not only gas lasers, but also metal vapor and solid state lasers. In addition, this method can be used to produce the plasma for obtaining radiation (including induced radiation) in any spectral range, especially that extending from 100 nm to THz, which is of considerable interest for microelectronics, photolithography and biomedicine.

In the work we used experimental systems based on Blumlein scheme, C-C transfer scheme [4, 8] and inductive RF pumping [5]. Pulsed inductive discharge of cylindrical type [1-5, 7] and transformer type [8] were used for excitation of various gas active media. In our experiments with inductive cylindrical discharge a ceramic tube with inner diameter of 42 mm and external diameter of 50 mm. In experiments with pulse inductive discharge of transformer type glass tubes consisted of capillary as working zone and a bypass channel to reduce the impedance of the discharge circuit are used. The tube was sealed by means of plane-parallel windows of CaF_2 oriented perpendicular to the tube axis. The optical resonator was formed by external plane dielectric mirrors. The rear dielectric mirror had the reflectance 99% in the selected spectral region. The reflectance of the output mirror was optimized during experiments to obtain the maximum output energy. Mirrors with reflectance from 8% to 93% were used. The inductor for cylindrical discharge consisted of separate sections representing solenoids made of a cable wire of cross section 1.5–6 mm^2. The solenoids were connected in parallel, and the total length (~ 68 cm) of the inductor was assumed the length of the active medium of the gas laser. In case of inductive discharge of transformer type the inductor of antenna type is used and the inductor is placed along the discharge tube. Gases or its mixtures were admitted from a gas system into the tube up to pressures 0.1 – 1000 Tor. Gases flowed longitudinally during experiments.

For the first time six pulsed inductive lasers on the different transitions of atoms and molecules have been created. The pulsed inductive UV nitrogen laser on self-limited electronic transitions at the $\boldsymbol{C}^3\Pi_u \rightarrow \boldsymbol{B}^3\Pi_g$ transition in molecular nitrogen at 337.1 nm and = 357.7 nm is created. The maximum generation energy 4.5 mJ of inductive N_2 lasers only at low pressures ~1 Tor is achieved. Pulsed peak power was 300 kW at pulse duration 15±1 ns. The divergence of the inductive nitrogen laser radiation is measured as 0.3 mrad.

Red laser on the electronic transitions of atomic fluorine (FI) pumped by a pulsed inductive cylindrical discharge is developed. Lasing at 8 wavelengths in the spectral area 624-755 nm is obtained by exciting He–F_2 (NF_3, SF_6) gas mixtures in a pressure range from 20 to 350 Torr. Energy of FI laser 2.6 mJ at pulse durations 80 ns is achieved. The divergence is 0.4 mrad.

Pulsed inductive discharge H_2 laser at the electronic transitions of hydrogen molecules in near IR laser has been developed. The laser action on four lines with 0.835 μm, 0.89 μm, 1.116 μm and 1.122 μm is obtained. Pulsed peak power 11 kW at duration 20 ns (FWHM) is achieved.

Lasing in near and mid IR region on electronic transitions of Xe atoms is achieved. Generation spectrum consisted of five lines with wavelengths λ_1 = 840.9 nm, λ_2 = 904.5 nm, λ_3 = 979.9 nm, λ_4 = 1733 nm, and λ_5 = 2026 nm. Pulse duration is measured for line 904.5 nm and it is 6±1 ns (FWHM). The divergence measured is 1±0.2 mrad. Lasing is obtained only for inductive discharge of transformer type.

Mid IR chemical HF laser with pulsed inductive discharge initiation, working in the range of 2.7 micron has been created. Gas mixtures $H_2 - F_2(NF_3$ or $SF6_6)$ and $He(Ne) - H_2 - F_2(NF_3$ or $SF_6)$ were used as active media. The FWHM pulse duration reached 0.42 μs. This value corresponded to a pulsed power of 45 kW. The emission spectrum of an inductive HF laser is investigated, which consisted of seven groups of bands with centers around the wavelengths of 2732, 2736, 2739, 2835, 2837, 2893 and 2913 nm. The amplitude instability of light pulses is no greater than 5% – 6%.

Far infrared on the vibrational-rotational transitions of CO_2 molecules in the ground electronic state with a wavelength of 10.6 μm has been created. It is demonstrated that the best results are achieved when using the excitation system based on RF power supply. This system allows form pulsed RF inductive discharge with respectively low-energy electrons. Thus major energy in this case is used to excite CO_2 molecules directly and low vibration levels of N_2 molecules. Laser operates with either only N_2-CO_2 mixture or multi component mixtures. The maximum energy of this inductive laser is about 500 mJ and maximum efficiency of 17% is obtained.

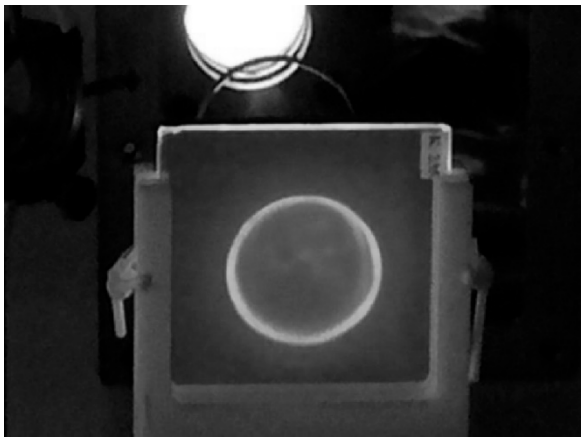

Fig. 1 Typical beam profile for laser pumped by a pulsed inductive cylindrical discharge

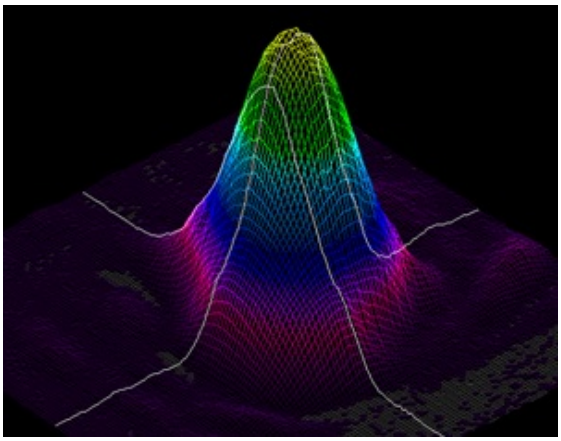

Fig. 2 Typical beam profile for laser pumped by a pulsed inductive discharge of transformer type (using semi confocal optical resonator)

Characteristic feature of the emission of lasers pumped by a pulsed inductive cylindrical discharge is ring-shaped laser beam (Fig. 1) with low divergence and pulse-to-pulse instability is within 1%. In the contrast, laser based on pulsed inductive discharge of transformer type allows using semi confocal resonator achieve laser shape close to Gaussian one (Fig. 2).

The work was supported by RFBR grant #16-02-00316.

References

[1] A. Razhev, V. Mkhitaryan, D. Churkin, JETP Lett., **82(5)**, 259 (2005).
[2] A. Razhev, D. Churkin, JETP Lett. **86(6)**, 420 (2007).
[3] A. Razhev, D. Churkin, A. Zavyalov, [J] Vestnik NSU, Seria Fizika **4(3)**, 12 (2009) (in Russian).
[4] A. Razhev, D. Churkin, Optics Communications **282(7)**, 1354 (2009).
[5] A. Razhev, D. Churkin, E. Kargapoltsev, Laser Physics **24**, 074004 (2014).
[6] E. Kral'kina, Uspekhi Fizicheskikh Nauk, **51(5)**, 519 (2008).
[7] A. Razhev, D. Churkin, A. Zhupikov, Quantum Electronics, **39(10)**, 901 (2008).
[8] A. Razhev, D. Churkin, R. Tkachenko, Optica Atosfery i Okeana **31(3)**, 182 (2018).

Broadband terahertz wave generation from "Liquid-like" media

A. Balakin, V. Makarov, N. Kuzechkin, I. Kotelnikov, P. Solyankin, and A. Shkurinov
Lomonosov Moscow State University, Moscow, Russia
E-mail: ashkurinov@physics.msu.ru

We present results of the research on generation of THz radiation in liquid like media under irradiating them with high-intensity femtosecond optical pulses: gas clusters and liquid nitrogen. We used a dual-frequency scheme when emissions of the main laser frequency and its second harmonic are mixed in the same medium.

Laser cleaning and its applications

F. Song, H. Wang, S. Man, H. Liu, L. Liu
Nankai University, Tianjin, China
E-mail: fsong@nankai.edu.cn

Laser cleaning is a promising technique to remove the unnecessary contaminants or coatings from the substances, for instances, the rust, oil, dust, and paint from various substrates. It is green and environment-friendly. We introduce the theory mechanics and the applications such as in the rust-removal, paint-cleaning.

Application of Raman spectroscopy for lipid research in biophysics

N.V. Surovtsev, **K.A. Okotrub**
Institute of Automation and Electrometry, Russian Academy of Sciences, Novosibirsk, 630090, Russia
E-mail: lab21@iae.nsk.su

Activity and life cycle of biological cells are tightly interrelated with lipid structures - spatial elements of cells, in which lipids are main structural components. In particular, the structure of cell membranes and lots of intracellular organelles is mainly determined by phospholipid layers, and the energy function of cells is largely realized through the energy of lipid droplets consisting of triglycerides. It is important to know how the lipid structures are arranged and work. Contribution of physics in solving these problems relates to the description of structure, composition and dynamics of lipid structures. In this way researchers study as real biological objects, also model systems, reducing the number of factors, which should be taking into account.

Present report reflects the experience of our group on the application of Raman spectroscopy for the characterization of synthetic phospholipid membranes and lipid granules of living cells. We found that the sensitivity of the Raman band of stretching vibrations of CC bonds to the conformational states of hydrocarbon tails can be used to describe the statistics of the conformational states of phospholipid molecules. This approach allowed us to propose a simple model of the conformational states of phospholipid chains and to describe their temperature dependences [1]. Raman spectrum of CH_2 groups is sensitive both to conformations of the hydrocarbon chain and to intermolecular interaction in phospholipid layer. Comparison of the behavior of CC and CH_2 lines provides information about the lateral phospholipid arrangement and/or interaction. For example, this method reveals the presence of defects in the bilayer structure of unsaturated phospholipids [2], which can be filled by cholesterol addition [3]. This experience in characterization of the conformational states of lipids was used in the application of Raman spectroscopy for the study of mammalian embryos during their cryopreservation. Raman spectra of lipid structures of mammalian early embryos reveal the lipid phase transition occurring in embryos during cryopreservation [4]. It is demonstrated that during cooling lipid droplets of different cell types can undergo the phase transition in different ways.

The phospholipid layer thickness is of about 3 nm, its eigen vibrations are in the range of 10-20 cm^{-1}. Recently, these modes have been found in Raman spectrum of frozen aqueous suspensions of multilayer phospholipid vesicles [5]. These lines are visible only when the water is in the ice state and the bilayer in the gel state. The frequency of eigen layer modes is determined by the ratio of the sound velocity and of the phospholipids layer thickness; the peak width reflects both homogeneous broadening and inhomogeneous broadening, while inhomogeneous broadening is caused by spatial inhomogeneities; Raman intensity of bilayer or monolayer modes depends on the interaction between the lipid layers. Therefore, the low-frequency Raman spectrum of phospholipid membranes contains a lot of useful information on its structure, but further studies are needed to correctly describe the spectrum and to clarify its nature.

This work was supported by RFBR Grant No. 16-03-00664.

References

[1] A.A. Dmitriev, N.V. Surovtsev // J. Physical Chemistry B 2015. V. 119 P.15613.
[2] N.V. Surovtsev, N.V. Ivanisenko, K.Y. Kirillov, S.A. Dzuba // J. Physical Chemistry B 2012. V. 116. P.8139.
[3] N.V. Surovtsev, S.A. Dzuba // J. Chemical Physics 2014. V.140. P.235103.
[4] K.A. Okotrub, S.Y. Amstislavsky, N.V. Surovtsev // Arch. Biochem. Biophys. 2017. V. 635. P.37.
[5] N.V. Surovtsev, A.A. Dmitriev, S.A. Dzuba // Physical Review E 2017. V.95.

1D and 2D imaging of magnetic nanoparticles by atomic magnetometry

A. Weis, S. Colombo, V. Dolgovskiy, Z.D. Grujić, S. Pengue, and V. Lebedev
University of Fribourg, Physics Department, Chemin du Musée 3, 1700, Fribourg, Switzerland
E-mail: antoine.weis@unifr.ch

Biomedical applications of magnetic nanoparticles (MNP) have witnessed a rapid development over the past decade, a main goal being cancer therapy by targeted drug delivery via functionalized MNPs. These applications call for fast, sensitive and reliable techniques for characterizing the size distribution and other physical MNP sample parameters as well as non-invasive methods allowing the quantitative localization of MNPs in biological tissues and fluids. In the past 4 years we have deployed atomic magnetometers (AM) for various MNP studies along those lines, viz.,

- the precision measurement of **blocked MNP** size distributions, their saturation magnetization, anisotropy constant, and iron content using magneto-relaxation (MRX) [1],
- the imaging of the magnetic field patterns from **blocked MNPs** by a *Magnetic Source Imaging Camera* [2], and more recently, source reconstruction from the field images,
- the recording of *M(H)* magnetization curves [3] and magnetic AC-suceptibilities $\chi_{AC} = dM(H)/dH$ [4] of **liquid-suspended MNPs**, and, based on this
- the demonstration of 1D and 2D MPI (Magnetic Particle Imaging) scanners following the proposal made in Ref. [5].

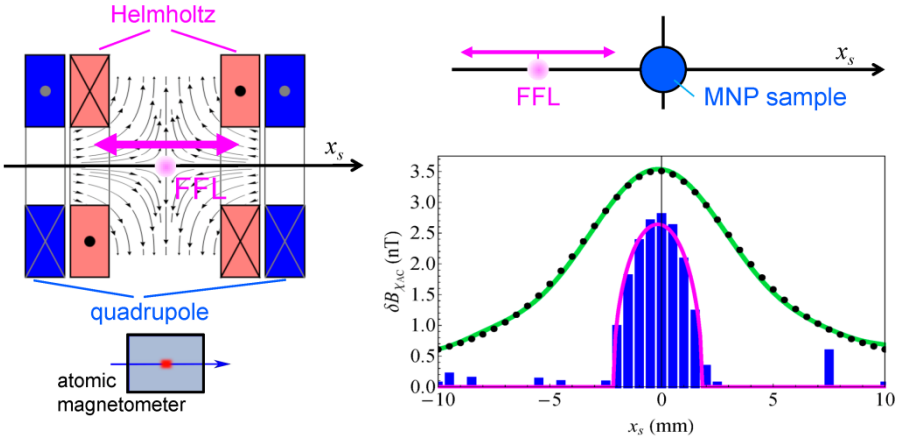

Fig. 1 Demonstration of AM-based 1D-MPI scanner. Left: A cylindrical quadrupole field with a field-free line (FFL) is produced by 4 straight conductors. A homogeneous field produced by a second set of straight conductors is superposed on the quadrupole field, permitting to displace the FFL along x_s. by scanning the homogeneous field magnitude. The AM detects the magnetic flux density from the MNPs. Right, top: An MNP sample (4 mm diameter capillary filled with ≈50 ml of Ferrotec© EMG707 ferrofluid oriented along the FFL) is located at the center of the coil system. Field modulation with lock-in demodulation detects signals only when the FFL is near the MNP sample. Right, bottom: Raw magnetometer data are shown as green line. Deconvolution of the raw data with the known system point-spread function allows inferring the MNP density distribution (blue histogram), which reproduces well the known density distribution (magenta line). The black dots represent the reconstruction of the experimental signal from the inferred density distribution.

References

[1] V. Dolgovskiy, V. Lebedev, S. Colombo et al., J. Magn. Magn. Mater. **379**, 137 (2015).
[2] V. Dolgovskiy, I. Fescenko, N. Sekiguchi et al., Appl. Phys. Lett. **109**, 023505 (2016).
[3] S. Colombo, V. Lebedev, Z. D. Grujić et al., Int. J. Mag. Part. Imag. **2**, 604001 (2016).
[4] S. Colombo, V. Lebedev, Z. D. Grujić et al., Int. J. Mag. Part. Imag. **2**, 606002, (2016).
[5] S. Colombo, V. Lebedev, A. Tonyushkin et al., Int. J. Mag. Part. Imag. **3**, 703006 (2017).

High-index frequency-modulation spectroscopy

C.C. Kwong[1,2], S.A. Adjunid[3], E.A. Chan[1,3], R. Shakhmuratov[4], and D. Wilkowski[1-3,5]
[1]*School of Physical and Mathematical Sciences, Nanyang Technological University, 637371, Singapore, Singapore*
[2]*MajuLab, CNRS-UCA-SU-NUS-NTU International Joint Research Unit, Singapore*
[3]*Centre for Disruptive Photonic Technologies, Nanyang Technological University, 637371, Singapore*
[4]*Kazan Physical-Technical Institute, Russian Academy of Sciences, Kazan, 420029, Russia*
[5]*Centre for Quantum Technologies, National University of Singapore, 117543, Singapore, Singapore*
E-mail: David.Wilkowski@ntu.edu.sg

Frequency modulation (FM) spectroscopy was proposed in 1980 by G. Bjorklund, as a new method for measuring weak absorptions and dispersions signal [1]. Here, the frequency carrier of the laser is scanned across the resonance under investigation. The subsequent amplitude and phase modification of the carrier are encoded in the beat note with the first sidebands in the weak modulation index limit. FM-spectroscopy was used in that regime and imposes itself as a key laser spectroscopic techniques.

We will discuss in the talk about a new regime, where the optical density (OD) of the medium is large [2]. We have in mind here an atomic or a molecular vapor, but the following argumentation can be generalized to other types of media as Dye solutions, Mie scatterers ensemble, point-defects in Diamond, or heavy doped glasses or crystals. With large OD, the carrier is almost fully absorbed and the usual FM-spectroscopy method is ineffective. Increasing the modulation index, such that the spectrum is dominated by the weakly absorbed first and second sideband, we show that we recover a FM-spectroscopic signal with similar sensitivity. Moreover, since we are probing the tails of the resonance, the signal mainly comes from the slow algebraic decay of the natural linewidth rather than the faster exponential decay of some frequency broadening mechanisms such as Doppler effect. Finally, the response time of the ensemble can be dramatically increased by the cooperative nature of interaction [3, 4].

We implement the high-index FM spectroscopy technique on an optically dense Cesium vapor, and observed the main expected features on the $6S_{1/2}$-$6P_{3/2}$ transition (See Fig. 1a). As an illustrative example, we show on Fig. 1b, two spectra taken at different optical density (OD) with a frequency deviation of Ω = 700 MHz and an index of modulation of β = 1.4. At low OD = 3, the spectrum shows a large contribution due to the Doppler broadening (Natural linewidth: 5.2 MHz, and Doppler broadening: 170 MHz). At OD = 100, a narrow dispersive-like occurs which is associated to the natural linewidth of the transition.

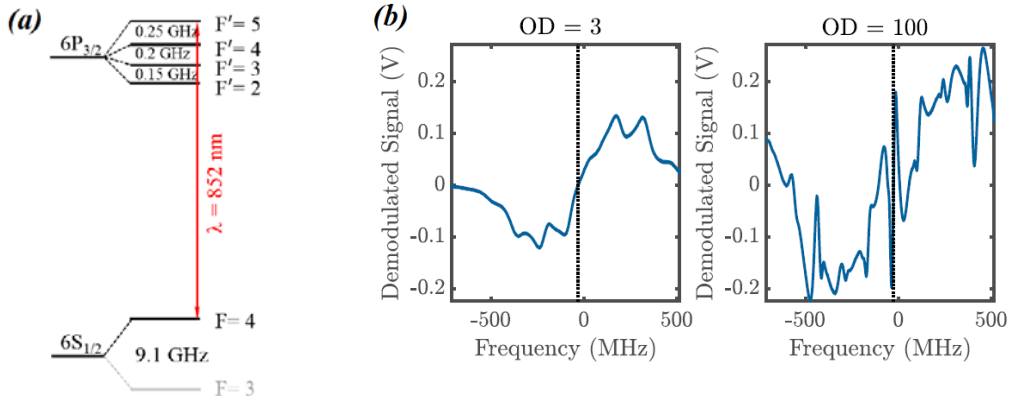

Fig. 1 (a) Energy spectrum of the Cesium D2 line. (b) Example of demodulated signal for Ω = 700 MHz and β = 1.4. The natural linewidth is 5.2 MHz and the Doppler broadening of 170 MHz.

References

[1] G. C. Bjorklund, Opt. Lett. **5**, 15 (1980).
[2] C. C. Kwong, E. A. Chan, S. A. Adjunid, R. Shakhmuratov, and D. Wilkowski, *in preparation*.
[3] C. C. Kwong, T. Yang, M. S. Pramod, K. Pandey, D. Delande, R. Pierrat, and D. Wilkowski, Phys. Rev. Lett. **113**, 223601 (2014).
[4] C. C. Kwong, T. Yang, D. Delande, R. Pierrat, and D. Wilkowski, Phys. Rev. Lett. **115**, 223601 (2015).

Composite laser-pulses in Ramsey interferometry

T. Zanon-Willette
Sorbonne Université, Observatoire de Paris, PSL Research University, CNRS, Laboratoire d'Etudes du Rayonnement et de la Matière en Astrophysique et Atmosphères, LERMA, F-75005, Paris, France
E-mail: Thomas.zanon@sorbonne-universite.fr

Probing an atomic resonance without disturbing effects is an ubiquitous issue in physics. This problem will be critical in laser spectroscopy for the next generation of atomic clocks based on completely forbidden transitions in bosonic systems, two-photon resonance or very weakly allowed transitions in some ions. Ultra-high resolution frequency metrology requires sophisticated interrogation schemes and robust protocols handling pulse length errors and residual frequency detuning offsets. I will review recent progress in such schemes, using sequences of composite laser-pulses tailored in pulse duration, frequency and phase in order to generate non-linear compensation of probe-induced frequency shifts. Various laser-pulses protocols will be discussed such as Hyper-Ramsey (HR), Modified Hyper-Ramsey (MHR), Generalized Hyper-Ramsey (GHR) and hybrid schemes as synthetic frequency-shift generation or auto-balanced Ramsey spectroscopy (ABRS). These techniques provide excellent protection against both probe induced light-shift perturbations and laser intensity variations. Some of them allow to reduce or completely eliminate imperfect correction of probe-induced frequency-shifts even in presence of decoherence due to the laser line-width. Finally, universal protocols based on $\pm\pi/4$ and $\pm 3\pi/4$ phase-modulated generalized Hyper-Ramsey resonances, which provide complete elimination of probe-induced frequency shifts in the general case where both decoherence and relaxation dissipation effects are active, will be presented. Merging Ramsey interferometry with sequences of composite pulses inspired by NMR and quantum information processing are offering new tools to finely tune coherent interaction between light and particles through very long-lived coherences.

References

[1] Thomas Zanon-Willette, Remi Lefevre, Remi Metzdor, Nicolas Sillitoe, Sylvain Almonacil, Marco Minissale, Emeric de Clercq, Alexey Taichevachev, Vareriy I Yudin and Ennio Arimondo, Composite laser-pulses spectroscopy for high-accuracy optical clocks: a review of recent progress and perspectives. Rep. Prog. Physics (2018). https://doi.org/10.1088/1361-6633/aac9e9

Dynamics of velocity selective optical pumping on the D_2 line hyperfine transitions in spatially restricted Cs vapor

C. Andreeva[1], T. Vartanyan[2], S. Gateva[1], A. Markovski[3], P. Todorov[1], S. Tsvetkov[1], S. Cartaleva[1]
[1]*Institute of Electronics, Bulgarian Academy of Sciences, 1784, Sofia, Bulgaria*
[2]*ITMO University, 49 Kronverkskiy Pr., 197101, St. Petersburg, Russian Federation*
[3]*Technical University of Sofia, 1756, Sofia, Bulgaria*
E-mail: c.andreeva@ie.bas.bg

For numerous applications, the reduction of the dimensions of photonic sensors is of great importance. It has been shown that the miniaturization of alkali metal vapor cells can induce changes in the well-known spectral profiles, as observed in conventional optical cells [1]. More specifically, the experimental study [2] and theoretical analysis [3] show that the one-dimensional miniaturization of the cell thickness down to the order of the resonant wavelength of the alkali atoms results in observation of sub-Doppler-width hyperfine spectra, as well as in significant difference between the absorption and fluorescence profiles, obtained by means of single-beam spectroscopy. Recently, using the pump-probe spectroscopy approach, narrow electromagnetically induced transparency [4] and velocity selective optical pumping [5] resonances in a micrometric cell with cesium were registered.

Here we report on the investigation of sub-Doppler-width resonances at the D_2 line of Cs atoms ($F_g = 4 \rightarrow F_e = 3, 4, 5$ hyperfine transitions), confined in two optical cells with thickness $L = 6\lambda$ ($\lambda = 852$ nm) and $L = 700$ μm. For comparison, the spectra obtained in a conventional $L = 2.5$ cm cell are also considered.

In the experiments, two narrow-band (2 MHz) diode lasers are used: (i) with frequency fixed on the $F_g = 4 \rightarrow F_e = 5$ transition or slightly detuned from resonance center, and (ii) a laser scanned over the $F_g = 4 \rightarrow F_e = 3, 4, 5$ transitions. Both laser beams are co-propagating and with mutually orthogonal linear polarizations. We register the absorption of the two lasers and the atomic fluorescence in dependence on the detuning of the scanned laser frequency. The comparison of the absorption spectra observed in the conventional (L=2.5 cm) optical cell and the $L = 6\lambda$ cell shows that in the thin cell, the light interaction with the fast atoms is essentially weakened, i.e. the spatial restriction of Cs vapor suppresses the interaction of the light with atoms whose velocity component in direction of the laser beam is significant.

We show that for zero frequency detuning of the fixed-frequency laser, its absorption spectrum in the thin cell consists of resonances with a spectral width of about 16 MHz and a good contrast with a very small Doppler background. This spectrum is highly sensitive to the frequency detuning of the fixed-frequency laser.

The observation of such narrow, high-contrast and controllable by a second beam spectral resonances is very attractive not only for the further study of hot spatially restricted atoms, but also for practical applications involving fast switching.

This work was funded by the National Scientific Fund of Bulgaria, Grants: DNTS/Russia 01/5/23.06.2017, "Nonlinear spectroscopy of spatially restricted alkali vapour: methodology and applications" and DO08-19/2016, "New coherent and cooperative effects in hot alkali vapour" and ST and SG acknowledge the Bulgarian Academy of Sciences for the funding within Grant DFNP-17-76/2017.

References

[1] D. Sarkisyan, D. Bloch, A. Papoyan, M. Ducloy, Opt. Commun. **200**, 201 (2001).
[2] S. Cartaleva, A. Krasteva, L. Moi, A. Sargsyan, D. Sarkisyan, D. Slavov, P. Todorov, K. Vaseva, Quantum Electronics **43**, 875 (2013).
[3] Г. Тодоров, В. Полищук, А. Крастева, А. Саргсян, С. Карталева, Т. Вартанян, Оптический журнал **83**, 17 (2016).
[4] A. Krasteva, B. Ray, D. Slavov, P. Todorov, P. Ghosh, S. Mitra, S. Cartaleva, J. Phys. B: At. Mol. Opt. Phys. **47**, 175004 (2014).
[5] S. Dey, B. Ray, P. Ghosh, S. Cartaleva, D. Slavov, Opt. Commun. **356**, 378 (2015).

About measuring the forbidden 1S-2S transition frequency of a hydrogen atom by stimulated Raman scattering

E. Baklanov[1,2], S. Kobtsev[2], and A.Taichenachev[1,2]
[1]*Institute of Laser Physics, Sberian Branch of RAS, 630090, Novosibirsk, Russia*
[2]*Novosibirsk State University, 630090, Novosibirsk, Russia*
E-mail: baklanov.ev@gmail.com

We demonstrate the possibility of measuring the forbidden 1S-2S transition frequency (121 nm) of hydrogen atom by the method of stimulated Raman scattering (SRS) when atom from 1S level moves to 2S level through intermediate 3P level. The frequency of the pumping field (103 nm) is close to the frequency of transition 3P-1S, and the frequency of the stimulated scattering (656 nm) - to the frequency of transition 3P-2S.

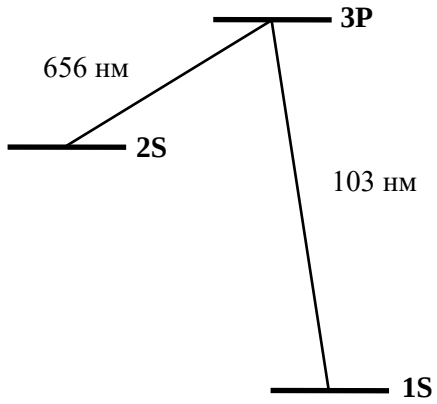

It is known that for lamda-schemes in the form of a line of stimulated scattering, there is a resonance with a homogeneous width of the transition line between the lower levels, which has been well studied theoretically and experimentally (see monograph [1]). Formally, this resonance is present in any problem with the lamda-scheme, but the greatest interest in it is associated with precision spectroscopy. Under the name of 'a coherent population trapping resonance' (CPT resonance), it is used as a reference in compact commercial atomic clocks. The analysis of SRS resonance is usually based on the use of standard equations for the density matrix. At a temperature of cooled atoms on the order of 1 mK, we can neglect the motion of atoms and solve these equations for a stationary atom. For the forbidden 1S-2S transition of hydrogen, we present a solution of these equations and a formula for the SRS resonance. The influence of Doppler broadening, the recoil effect, and the field shift is considered. It was shown there that by using the SRS method it is possible to measure the frequency of the 1S-2S transition in the hydrogen atom with an accuracy of ~1 kHz. We will note that the SRS method for transition 1S-2S in essence is an alternative to a method of two-photon absorption without Doppler broadening. The possibility of precision measurement has been considered by the last method in works [2], and experiments [3] are executed with a relative accuracy ~ 10^{-15}.

References

[1] V. Letokhov, V. Chebotayev, Ultrahigh-resolution nonlinear laser spectroscopy (Moscow, Nauka, 1990).
[2] E. Baklanov, V. Chebotayev, Optics Comms. **12**, 312 (1974);
[3] M. Niering, R. Holzwarth, J. Reichert et al., Phys. Rev. Letts. **84**, 5496 (2000).

Generalized autobalanced Ramsey spectroscopy

V.I. Yudin[1-3], A.V. Taichenachev[1,2], M.Yu. Basalaev[1-3], T. Zanon-Willette[4], J.W. Pollock[5], M. Shuker[5], E.A. Donley[5], and J. Kitching[5]

[1]*Novosibirsk State University, Novosibirsk, Russia*
[2]*Institute of Laser Physics SB RAS, Novosibirsk, Russia*
[3]*Novosibirsk State Technical University, Novosibirsk, Russia*
[4]*LERMA, Observatoire de Paris, PSL Research University, Paris, France*
[5]*National Institute of Standards and Technology, Boulder, Colorado, USA*
E-mail: viyudin@mail.ru, mbasalaev@gmail.com

Atomic clocks are based on high-precision spectroscopy of isolated quantum systems and are currently the most precise scientific instruments. Fractional frequency instabilities and accuracies at the level of 10^{-18} have already been achieved, with the goal of 10^{-19} on the horizon [1]. Frequency measurements at such a level could enable new tests of quantum electrodynamics and cosmological models, searches for drifts of fundamental constants, and new types of chronometric geodesy [2].

For some of the promising clock systems, a key limitation is the frequency shift of the clock transition due to the excitation pulses themselves (probe-field-induced shift). In particular, for ultranarrow transitions (e.g., electric octupole [3] and two-photon transitions [4, 5]), the off-resonant ac-Stark shift can be so large in some cases that high-accuracy clock performance is not possible. In the case of magnetically induced spectroscopy [6, 7], these shifts (quadratic Zeeman and ac-Stark shifts) could ultimately limit the achievable performance. A similar limitation exists for clocks based on direct frequency comb spectroscopy [8, 9] due to off-resonant ac-Stark shifts induced by large numbers of off-resonant laser modes. In addition to optical standards, probe-field-induced shifts can create significant instability for atomic clocks in the microwave range based on coherent population trapping (CPT) [10-12].

In this work, we present a method of generalized autobalanced Ramsey spectroscopy (GABRS) for the suppression of the probe-field-induced shifts in atomic clocks. Our method uses a two-loop approach to feedback on and stabilizes the clock frequency ω as well as a second (concomitant) parameter ξ, which is an adjustable property of the first and/or second Ramsey pulses τ_1 and τ_2. To determine the error signals, it is necessary to use Ramsey sequences (see Fig. 1) with two different dark times T_1 and T_2. The operation of GABRS consists of the correlated stabilization of both variable parameters ω and ξ. For stabilization of the frequency ω we need to form an error signal (differential signal). In our approach, we use phase jumps α_+ and α_- of the probe field before the second pulse τ_2 (see Fig. 1).

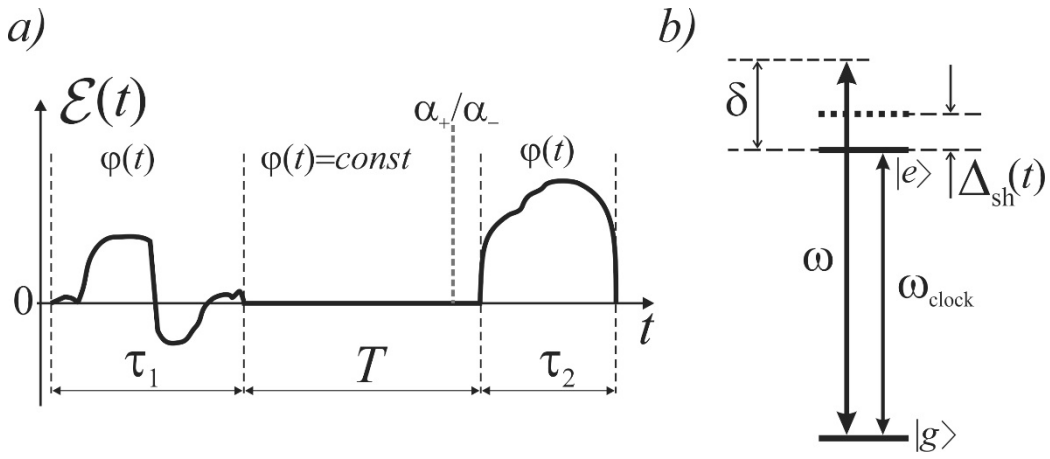

Fig. 1 *a)* Schematic illustration of a sequence of two arbitrary Ramsey pulses (with the real amplitude $\mathcal{E}(t)$ and durations $\tau_{1,2}$) which are separated by the dark time T. *b)* Scheme of the clock transition $|g\rangle \leftrightarrow |e\rangle$ (with unperturbed frequency ω_{clock}) interacting with the probe field at the frequency ω.

The main idea of GABRS is the following. First of all, apart from frequency ω for the frequency stabilization procedure we will use some additional (concomitant) variable parameter ξ, which is related to the first and/or second Ramsey pulses τ_1 and τ_2. For example, the parameter ξ can be equal to the phase ϕ_c of the second pulse as it was proposed in [14]. However, there are many other variants of the concomitant parameter ξ (e.g., frequency step, pulse duration and etc.) Thus, the error signal in should be considered as a function of two variable parameters: $S_T^{(\mathrm{err})}(\omega,\xi)$. Secondly, we will use the Ramsey interrogation of the clock transition for two different, fixed intervals of free evolution T_1 and T_2, i.e., we will use two error signals $S_{T_1}^{(\mathrm{err})}(\omega,\xi)$ and $S_{T_2}^{(\mathrm{err})}(\omega,\xi)$. For GABRS, the procedure for the frequency stabilization is organized as a series of the following cycles. For interrogation with dark time T_1, the parameter ξ is fixed, and we stabilize the variable frequency ω at the zero point of the error signal: $S_{T_1}^{(\mathrm{err})}(\omega,\xi_{fixed})=0$. After this procedure, we switch to interrogation with dark time T_2, where we fix the previously obtained frequency ω and stabilize the variable parameter ξ at the zero point of the second error signal: $S_{T_2}^{(\mathrm{err})}(\omega_{fixed},\xi)=0$. If we continue these cycles, then the final result (formally for $t\to\infty$) consists of the stabilization of both parameters, $\omega=\omega_0$ and $\xi=\xi_0$, which correspond to the solution of a system of two equations:

$$S_{T_1}^{(\mathrm{err})}(\omega,\xi)=0,\quad S_{T_2}^{(\mathrm{err})}(\omega,\xi)=0 \tag{1}$$

in relation to the two unknowns ω and ξ. It can be shown that (1) always contains the solution $\omega=\omega_{\mathrm{clock}}$ (where ω_{clock} is unperturbed clock frequency, see Fig. 1).

Note, in addition to the suppression of probe-field-induced shifts, the GABRS technique is protected against various processes of decoherence and also technical issues including time-dependent pulse area fluctuations (even more powerful than the common weak pulse area variation from previous schemes) and phase-jump modulation errors needed to generate the error signal.

This work was supported by the Russian Scientific Foundation (No. 16-12-10147). A.V. Taichenachev was supported by Russian Foundation for Basic Research (No. 18-02-00822). M.Yu. Basalaev was supported by the Ministry of Education and Science of the Russian Federation (No. 3.1326.2017/4.6), and Russian Foundation for Basic Research (No. 17-02-00570 and 16-32-60050 mol_a_dk).

References

[1] M. Schioppo, R.C. Brown, W.F. McGrew et al., Nature Photonics **11**, 48 (2017).
[2] A.D. Ludlow, M.M. Boyd, J. Ye, E. Peik, and P.O. Schmidt, Rev. Mod. Phys. **87**, 637 (2015)
[3] K. Hosaka, S.A. Webster, A. Stannard et al., Phys. Rev. A **79**, 033403 (2009).
[4] M. Fischer, N. Kolachevsky, M. Zimmermann et al., Phys. Rev. Lett. **92**, 230802 (2004).
[5] T. Badr, M.D. Plimmer, P. Juncar et al., Phys. Rev. A **74**, 062509 (2006).
[6] A.V. Taichenachev, V.I. Yudin, C.W. Oates et al., Phys. Rev. Lett. **96**, 083001 (2006).
[7] Z.W. Barber, C.W. Hoyt, C.W. Oates et al., Phys. Rev. Lett. **96**, 083002 (2006).
[8] T.M. Fortier, Y.Le Coq, J.E. Stalnaker et al., Phys. Rev. Lett. **97**, 163905 (2006).
[9] M.C. Stowe, M.J. Thorpe, A.Pe'er et al., Adv. At. Mol. Opt. Phys. **55**, 1 (2008).
[10] G.S. Pati, Z. Warren, N. Yu and M. S. Shahriar, J. Opt. Soc. Am. B **32**, 388 (2015).
[11] M.A. Hafiz, G. Coget, P. Yun et al., Appl. Phys. **121**, 104903 (2017).
[12] X. Liu, E. Ivanov, V.I. Yudin, J. Kitching, and E.A. Donley, Phys. Rev. Appl. **8**, 054001 (2017).
[13] A. Morinaga, F. Riehle, J. Ishikawa, and J. Helmcke, Appl. Phys. B **48**, 165 (1989).
[14] Ch. Sanner, N. Huntemann, R. Lange, Ch. Tamm, and E. Peik, Phys. Rev. Lett. **120**, 053602 (2018).

Silicon-based structural coloring

L.S. Basalaeva[1], Yu.V. Nastaushev[1], F.N. Dultsev[1], and N.V. Kryzhanovskaya[2]
[1]*A.V. Rzhanov Institute of Semiconductor Physics SB RAS, Lavrentieva 13, Novosibirsk, 630090, Russia*
[2]*St. Petersburg Academic University, Khlopina str. 8, St. Petersburg, 194021, Russia*
E-mail: basalaeva@isp.nsc.ru

Silicon-based structural color generation has aroused considerable interest with its promising applications in various fields (imaging sensors, optical filters, displays, data processing) [1-3]. The reflective properties of single nanopillars with characteristic heights and diameters on the order of a wavelength (or λ/2) are often described using the Mie theory [4]. However, when the lattice pitch and the light wavelength are comparable, one can observe diffraction and wave interference. The minimum geometric dimensions of Si NPs microarrays at which they demonstrate enhanced resonance light scattering are undetermined.

We investigate the tunable color generation from silicon nanopillars (Si NP) microarrays spatially arranged in a square lattice with pitches of 400, 500, 600, 800, and 1000 nm. Electron beam lithography and reactive ion etching are used for the formation of ordered Si NP arrays on the Si (100) wafer coated by thermal oxide of silicon (thickness is about 100 nm). We were among the first to develop the method of formation of ordered Si NP arrays by electron-beam lithography on a negative resist with subsequent reactive ion etching [4]. In this work we formed microarrays of Si NPs with diameters from 120 to 240 nm, a height of 350 nm. Fig.1 shows scanning electron microscopy (SEM) image of Si NPs array with 500 nm pitch. The reflection spectra from Si-NP microarrays were measured within the wavelength range from 400 to 1100 nm in linearly polarized light. Light was incident perpendicular to the substrate. The measured reflection spectra exhibited one or several minima. The reflection minimum position changes with changing Si-NP diameter. The minim position shifts to the red with increasing Si-NP diameter. Each nanopillar supports particular optical resonances, but the resonance wavelength shifts depending on the pitch of Si NPs in the array. It is experimentally shown that the reflection spectrum of the structures can be controlled changing the geometric parameters of Si NPs and their pitch in the square matrix. Previously, scientific studies were focused on nanopillars with geometric dimensions exceeding the incident-light wavelength. In the present work, we demonstrated enhanced resonance light scattering of nanopillars with heights and diameters that are smaller than the incident-light wavelength. The Si NPs with the medium aspect ratio (1.5÷3) are studied.

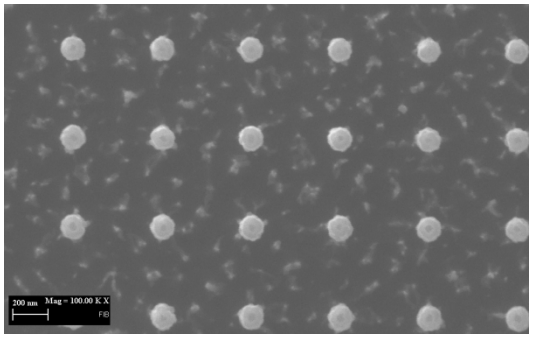

Fig. 1 SEM image of Si NPs array with 500 nm pitch (top view). Scale bar is 200 nm.

The reported study was funded by RFBR and Government of the Novosibirsk region according to the research project No. 17-42-543293.

References

[1] Y. Nagasaki, M. Suzuki, and J. Takahara, Nano Lett. **17**(12), 7500 (2017).
[2] T. Lee, J. Jang, H. Jeong, J. Rho, Nano Convergence **5**(1), 1 (2018).
[3] H. Park, Y. Dan, K. Seo et al., Nano Lett. **4**, 1804 (2014).
[4] L. S. Golobokova, Yu. V. Nastaushev, F. N. Dultsev et al., J. Phys.: Conf. Ser. **541**, 012074 (2014).

The strontium optical clock in the Russian National Time Scale

O. Berdasov[1,2], D. Sutyrin[1], A. Gribov[1,2], S. Strelkin[1,2], G. Belotelov[1], A. Kostin[1], R. Balaev[1], D. Fedorova[1,2], A. Malimon[1], and S. Slyusarev[1]

[1]*FSUE "VNIIFTRI", Mendeleevo, 141570, Moscow region, Solnechnogorskii district, Russian Federation*

[2]*National Nuclear Research University 'MEPhI', Kashirskoe sh. 31, 123182, Moscow, Russian Federation*

E-mail: berd_7@mail.ru

For more than fifty years since the SI second was defined by the ^{133}Cs hyperfine transition, microwave frequency standards realize all atomic time scales. Nowadays, advances in optical frequency standards (OFSs) during the last twenty years, results in improved frequency stability and accuracy over microwave frequency standards [1]. This situation has led the community of time and frequency standards to seriously consider the future redefinition of the SI second, where the SI second is realized by OFSs and the accuracy of the scale interval in International Atomic Time (TAI) is maintained by OFSs. Thereby it is an attractive option to integrate OFS into International Atomic Time (TAI) and to Coordinated Universal Time (UTC) [2]. As a step in this direction, developing of "optically steered" time scales in national metrology institutes is performing [3].

We develop a system to use ^{87}Sr OFS for the Russian National Time Scale UTC(SU) at FSUE "VNIIFTRI". In substance, there are two parts of work. The first part is focused on the increasing autonomic continues work operation of OFS [4], which is currently compatible with results of the other groups [5]. The second part, which we describe here, is a system for 1.5 km intra-object transferring the frequency of the VNIIFTRI strontium OFS to the primary time and frequency standard and the national time scale. It is necessary for long-term comparisons between OFS, rubidium and cesium fountains and an ensemble of clocks based on hydrogen masers. The developed system, on the one hand, allows to determine the absolute frequency of the OFS, and on the other - to determine the drift of the hydrogen timekeepers, which allows more accurately reproduce the size of the units of time and frequency and more accurately realize the national time scale.

The scheme of the system is shown in Fig. 1. The optical frequency comb is used to transfer characteristics of the OFS from the optical domain to the microwave. The HM 18 is a key element, which is placed in the same temperature stabilized room with the optical frequency comb. On one hand, HM 18 generates a 10 MHz reference signal for the OFS frequency counting system. On other hand, it is linked to the hydrogen masers ensemble referenced to the cesium and rubidium fountains, that form the microwave part of the UTC(SU). In this way, we build the link of the ^{87}Sr OFS with the fountains and national time scale, which is expanded up to THz domain. The system currently operates several weeks and after several months of work it will be reasonable to analyze the effect of OFS inclusion to the NTC.

In conclusion, we report on an accurate frequency comparison system between strontium optical lattice clock, group of hydrogen masers, rubidium frequency standards and cesium fountain. It is developed to enhance the National Time Scale and support redefinition of the SI second.

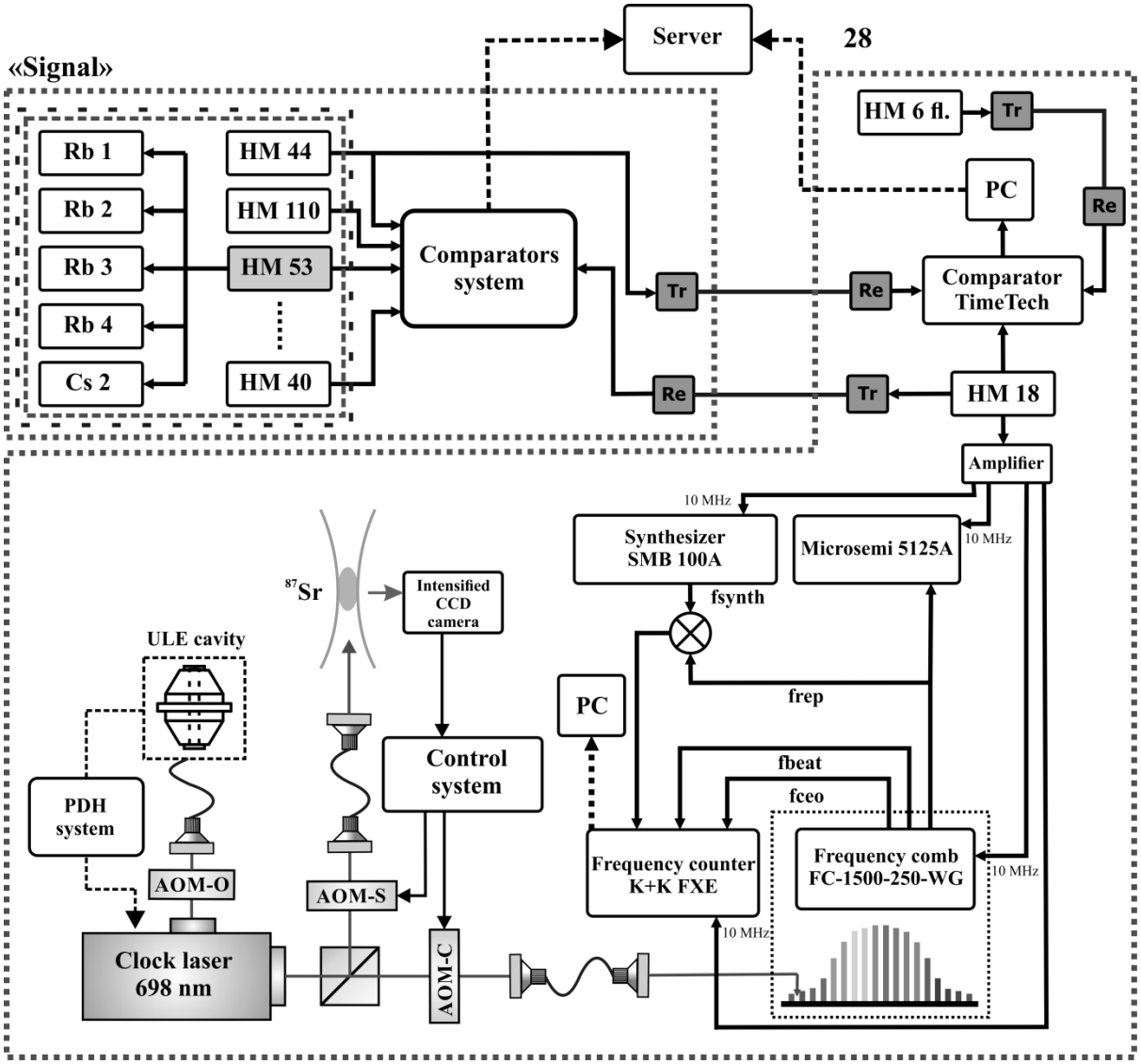

Fig. 1 Frequency comparison system: Tr – 10 MHz optical transmitter for the 10 MHz signal transfer; Re – optical receiver for the 10 MHz signal; 5125A Microsemi – phase-noise meter; PC – personal computer; AOM-П – AOM to tune clock laser frequency to atomic transition resonance during the atomic lock; AOM-C – AOM, to tune clock laser during the scanning stage; SMB 100A – microwave synthesizer.

References

[1] A. D. Ludlow, et al. Rev. Mod. Phys. 87, 637 (2015).
[2] P. Gill, Phil.Trans. Roy. Soc. London, vol. A369, p. 4109, (2011).
[3] H. Hachisu,. et al... Scientific reports, 8(1), 4243, (2018).
[4] O.I. Berdasov, et al., QUANTUM ELECTRON, 48 (5), 431–437 (2018)
[5] J. Lodewyck et al., Metrologia -T.53.-N.4.-C.1123. (2016)

Generation of Alfvén and magnetosonic waves produced by periodic laser plasma bunches in lower layers of the ionosphere

A.G. Berezutsky, V.N. Tishchenko, Yu.P. Zakharov, I.B. Miroshnichenko, M.A. Efimov, M.S. Rumenskikh, A.A. Chibranov, and I.F. Shaikhislamov
Institute of Laser Physics, SB RAS, Ac. Lavrentieva ave., 15b, Novosibirsk, Russia
E-mail: a.berezuckiy@yandex.ru

The mechanism of merging of waves (MMW), created by periodic laser plasma bunches of explosive nature is proved for gases, plasma with magnetic field and magnetic field in vacuum, which corresponds to the Earth's ionosphere-magnetosphere. In the interaction of the laser plasma source with the surrounding background, low-frequency waves are formed: in the air - infrasound, in a plasma with a magnetic field - torsion Alfvén (AW) and slow magnetosonic (MW) waves that carry the longitudinal and azimuth pulse in a narrow (~ R_d / 2) tube of the magnetic field [1,2,4]. In a magnetic field in a vacuum, the source creates a stream of rotating plasma, possessing the properties of AW and MW [3].

Resonance interaction of the source with the background observed under the following conditions:
1. $\omega \approx f R_d / C_A \approx 0.3$. f is frequency of repetition of clots, Rd their dynamic radius, C_A is velocity of the Alfven wave;
2. $R_L = r_L / R_d \sim 1$ is the Larmor radius normalized to Rd;
3. $\alpha = R_L / L_{pi}$ - L_{pi} - ion-inertial length (c / ω_{pi});
4. $M_A \sim V_0 / C_A \sim 0.5$ -1 - the Alfven-Mach number (the ratio of the initial velocity of the plasma expansion to the Alfven velocity in the background)
5. $\beta = 8\pi p / B^2 < 1$ is the ratio of the plasma background pressure to the magnetic field pressure.

When the criteria are fulfilled, intensive AW and MW propagate along the field and transfer of the longitudinal current, perturbations of electric and magnetic fields, and for $\alpha > 1$ and $R_L \sim 0.3 \div 1$, the intensity of the AW angular momentum is maximal.

In this paper, using of the numerical simulation, generation of AW and MW produced by laser plasma bunches in the ionosphere at low altitudes, when the ratio of the thermal pressure to the magnetic pressure is $\beta \sim 1$ was studied. To describe the interaction of plasma bunches with the surrounding background, a 3-fluid axisymmetric MHD model was used [2]. The parameters of calculation chosen from the conditions for the fulfillment of the MMW criteria (1-3).

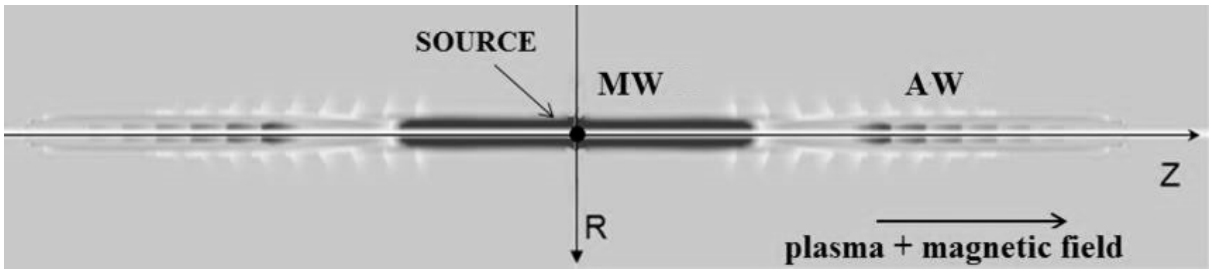

FIg.1 The source of the explosive plasma forms AW and MW propagating along the force lines of the magnetic field.

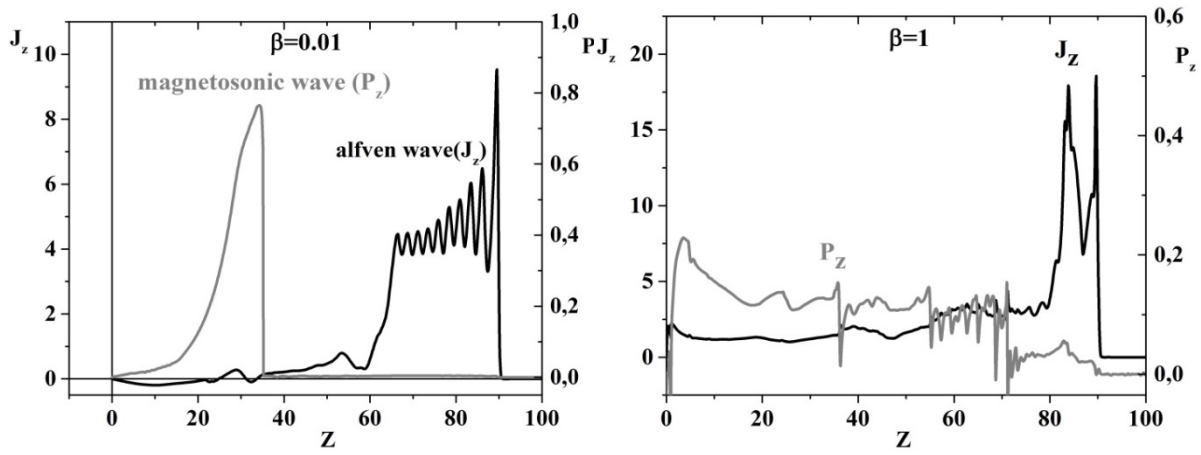

Fig. 2 Longitudinal pulse Pz and current Jz. Left is β = 0.01; right is β = 1. The source acts at the point of Z = 0. The dimensionless distance Z is normalized to Rd. Parameters of the simulations: ω = 0.4, L_{pi} = 0.3, M_a = 1, α = 7, m_s = 207 z_s = 2 - mass and charge of the source, m_b = 14,, z_b = 1 - mass and charge of the background.

Fig.2. (left) shows the propagation of AW and MW, produced by N = 10 plasma bunches. In the ionosphere, starting from ~ 300 km, AW propagates at a velocity greater than MW. AW is the torsional oscillations of the magnetic field produced by plasma bunches. AW transfers the angular momentum (plasma rotation), the longitudinal current and the azimuthal component of the magnetic field. MW is a packet of slow magnetosonic waves. This wave has a compression phase, which localized in a narrow channel on the propagation axis of magnetic force tube. The MW transfers the bulk of the source energy, the pulse, the compressed background plasma, the electric field and the inhomogeneity of the magnetic field. The advantage of generating AW and MW at altitudes above 300 km is due to the high intensity of the waves, which ensures a weak attenuation. Fig. 2 (right) shows the propagation of a longitudinal pulse and current at β = 1. It is seen from the distributions that the velocity of the MW is comparable with AW, which in turn delimits the transportation of the azimuthal pulse by AW. An analysis of the spectrum of perturbation shows the presence of high-frequency oscillations appearing in the lower layers of the ionosphere, which leads to a decrease in the intensity of the waves, which leads to their attenuation.

The reported research was funded by Russian Foundation for Basic Research and the government of the region of the Russian Federation, grant № 18-42-543019, № 18-32-00029, № 16-52-14006; Presidium of the Russian Academy of Sciences ("Basic Foundations of Dual-Use Technologies", Programme No. 31); SB RAS basic research project II.10 №0307-2017-0015 and RSF grant № 18-12-00080.

References

[1] V.N. Tishchenko, I.F. Shaykhislamov, Quantum Electronics **44**, No. 2, p.98, 2014.
[2] V.N. Tishchenko, I.F. Shaikhislamov, A.G. Berezutsky, "Supercomputer technologies in science, education and industry": M.: MSU, p. 65, 2014.
[3] V.N. Tishchenko, Yu.P. Zakharov, I.F. Shaikhislamov, A.G. Berezutsky et al., JETP Letters **104**, p.302, 2016.
[4] V.N. Tishchenko, A.G. Berezutsky, E.L. Boyarintsev et al., Quantum Electronics **47**, p.849, 2017.

Intracavity-contacted VCSELs with rhomboidal oxide current aperture for compact atomic clock

N.A. Maleev[1,2], S.A. Blokhin[1], M.A. Bobrov[1], A.G. Kuzmenkov[1,3], A.M. Ospennikov[4], and V.M. Ustinov[2,3]
[1]*Ioffe Institute, 194021, St Petersburg, Russia*
[2]*Saint Petersburg Electrotechnical University "LETI", 197367, St. Petersburg, Russia*
[3]*Research and Engineering Center for Submicron Heterostructures for Microelectronics, 194021, St. Petersburg, Russia*
[4]*Russian Institute of Radionavigation and Time, 192012, St. Petersburg, Russia*
E-mail: maleev@beam.ioffe.ru

Compact atomic sensors (miniature atomic clocks, magnetometers and nuclear resonance magnetic gyroscopes) are needed in single-mode polarization-stable vertical-cavity surface-emitting lasers (VCSELs). Specifically VCSELs for miniature atomic clocks should have low power consumption, high frequency modulation bandwidth, narrow spectrum linewidth (less than 100 MHz), stable linear polarization, precise emission wavelength exactly matched to the exploited atomic transition (usually D1 Rb87 line or D1 Cs133 line) and high temperature stability [1]. The key issue for single-mode polarization-stable VCSELs in atomic sensors is insufficient output power at elevated temperatures close to the operating temperature of the miniature gas cell (up to 85°C for Cs-based sensors). Conventional oxide-confined GaAs-based VCSELs with doped distributed Bragg reflectors (DBRs) and small round-shaped oxide aperture usually show stable fundamental transverse mode operation. However, they have strong current-induced self-heating due to high serial resistance and polarization instability caused by cylindrical symmetry. Currently the most of single-mode VCSELs with stable polarization are based on conventional VCSEL design combined with specific surface relief structures (usually sub-micron grating in output DBR) to provide polarization-dependent DBR reflectivity [2], but this approach has such drawbacks as additional diffraction losses and complicated sub-micron lithography on non-planar relief with precise alignment of the oxide aperture and surface relief.

Recently, we have developed an alternative approach for reliable polarization control based on advanced VCSEL design with inracavity-contacts and rhomboidal oxide current aperture (hereafter IC-VCSEL) [3-5]. In this paper, we discuss the potential of proposed VCSEL design for applications in compact atomic clocks.

IC-VCSEL structures were grown by molecular beam epitaxy. Active region based on InGaAs/InAlAs compressively-strained multi-quantum-well design and optimized to obtain emission close to D1 Cs line. The device fabrication process is similar to previously published [3]. According to the analysis of spontaneous electroluminescence at near-field regime as well as contrast difference of semiconductor-oxide interface under IR-illumination, the oxide current aperture of the developed VCSELs have rhomboidal shape. Light output power-current-voltage (L-I-V) characteristics, optical emission spectra, polarization behavior, small signal modulation response of the developed VCSELs were investigated at the operating temperature in the range from 20°C to 90°C. The output optical power was measured by a calibrated optical power meter PM100D (Thorlabs) with a sensor S130C. The emission spectrum was measured using an optical spectrum analyzer AQ-6315A (Ando). The laser linewidth was measured by a Fabry-Perot scanning interferometer SA200-5B (Thorlabs). Small signal modulation response was measured using a network analyzer E8364B (Agilent).

Figure 1 shows the L-I-V characteristics for 2.5 μm-aperture IC-VCSEL measured at three different temperatures and single-mode optical spectrum exactly tuned to D1 Cs line. At the working current of 2–4 mA the output power exceeds 0.5 mW and slope efficiency about 0.5 mW/mA for ambient temperatures up to 90°C. This values about two times better as compare with first commercial VCSEL for D1 Cs line [6]. The Cs D1 line wavelength is reached at current of 2.8 mA and a ambient temperature of 70°C, giving an output power of 1.2 mW and side-mode suppression ratio (SMSR) about 35 dB.

The curves in the Fig.2(a) show the orthogonal polarization suppression ration (OPSR) for 2.5 μm-aperture IC-VCSEL calculated from polarization-resolved L-I-V characteristic measured in

the two polarizations d at different current values and temperatures 20°C and 70°C. For working current of 2–4 mA the measured OPSR value exceed 17 dB. The lasing emission polarization of all single-mode IC-VCSELs is fixed along the minor diagonal of the rhomboidal oxide aperture, which is similar to previously studied 850 nm-range VCSELs [5].

In Cs-based miniature atomic clock, the VCSEL bias current need to be modulated at 4.596 GHz in order to create the first-order optical sidebands frequency split by 9.192 GHz. Figure 2(b) depicts the measured modulation response for 2.5 μm-aperture IC-VCSEL tuned to Cs D1 line. The maximum modulation bandwidth (or -3dB-frequncy) exceeds 8 GHz. According to the linewidth measurements, the IC-VCSEL emission spectrum width does not exceed 50 MHz at working current of 2–4 mA. Far-field emission patterns of 2.5 μm-aperture IC-VCSELs, taken without using a collimating lens, demonstrate Gaussian-like shape of output beam with angular divergence less than 12° (see insert in fig.2(b)).

In conclusion, proposed design of high-speed single-mode polarization-stable VCSELs with rhomboidal oxide current aperture and intracavity contacts is promising for applications in laser sources for compact atomic clocks.

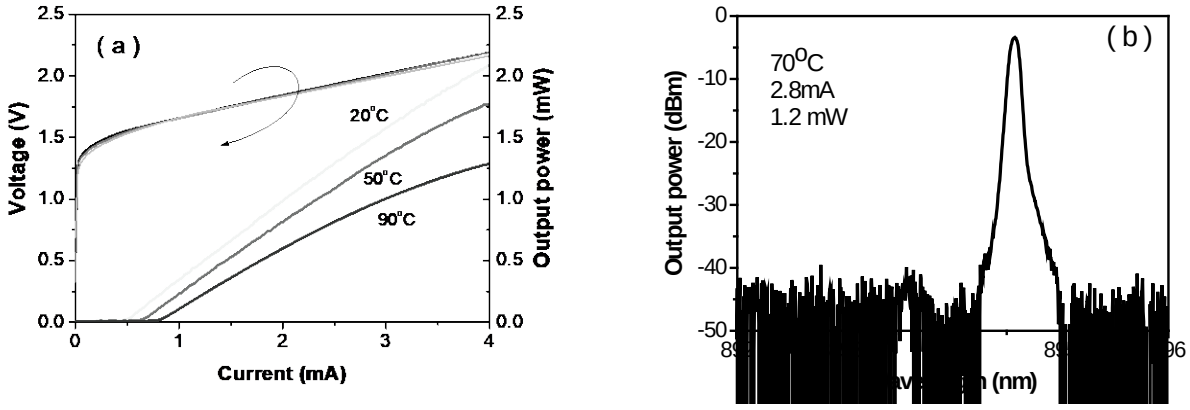

Fig. 1 2.5 μm-aperture IC-VCSEL: (a) L-I-V characteristics at different temperatures; (b) optical spectrum at 2.8 mA and 70°C

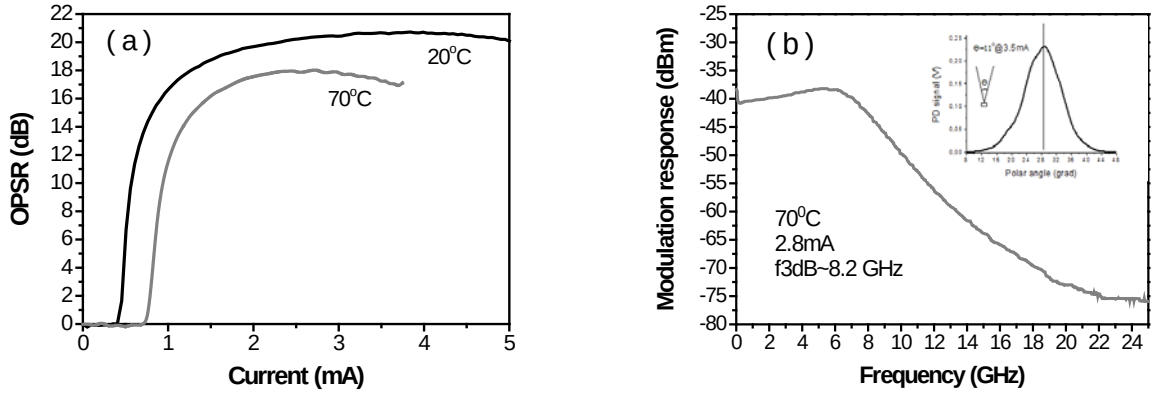

Fig. 2 2.5 μm-aperture IC-VCSEL: (a) OPSR at 20 and 90°C; (b) modulation response at 2.8 mA and 70°C

References

[1] D. K. Serkland et al. Proc. SPIE 6132, 613208 (2006).
[2] R. Michalzik, VCSELs, Fundamentals, Technology and applications of Vertical Cavity Surface- Emitting Lasers, Springer (2013).
[3] N.A. Maleev et al. Semiconductors, 47, 993 (2013).
[4] S.A. Blokhin, N.A. Maleev, A.G. Kuzmenkov, V.M. Ustinov, Patent RU 2 661 555 (2015).
[5] M.A. Bobrov et al. Journal of Physics: Conference Series 741, 012078 (2016).
[6] E. Kroemer et al. Applied Optics, 55, 8839 (2016).

Lithium niobate microdisk resonators on a chip

F. Bo, Z. Hao, L. Zhang, J. Wang, F. Gao, G. Zhang, and J. Xu
MOE Key Laboratory of Weak Light Nonlinear Photonics, TEDA Institute of Applied Physics and School of Physics, Nankai University, Tianjin, 300457, China
E-mail: bofang@nankai.edu.cn

Whispering gallery mode (WGM) resonators with high quality (Q) factors have the ability to store light for a long time in a small volume thereby enhancing nonlinear effects and improving the performance of sensors. WGM resonators made from lithium niobate (LN) crystal are naturally good candidate for active optical devices, such as optical modulators and wavelength convertors due to the excellent nonlinear optical, electro-optic, acousto-optic, and thermo-optic effects of LN crystal. However, the fabrication of LN WGM resonators on a chip is very difficult due to the extremely low and anisotropic chemical etching rate for LN crystal.

In this presentation, I will introduce our recent research progresses on the mass fabrication of LN microdisk resonators with high Q factors. Monocrystalline LN microdisk resonators with Q factors as high as 1.19×10^6 [1], polycrystalline LN silica hybrid microdisk resonators with $Q\sim1\times10^5$ [2], periodically poled LN microdisk resonator with Q approaching 1×10^6 were respectively fabricated in a batch with only micromachining technologies. The experimental and theoretical results associated with the all-optical [2], electrical [1,2], and thermal modulation [3] of light in the fabricated resonators will be presented. Nonlinear optical effects including second harmonic and sum-frequency generations will be demonstrated in these resonators as well [4].

References

[1] J. Wang, F. Bo, S. Wan, et al., Opt. Express **23** (18), 23072 (2015).
[2] F. Bo, J. Wang, J. Cui, et al., Adv. Mater., **27** (48), 8075 (2015).
[3] J. Wang, B. Zhu, Z. Hao, et al., Opt. Express **24** (19), 21869 (2016).
[4] Z. Hao, J. Wang, S. Ma, et al., Photon. Res. **5** (6), 623 (2017).

High-contrast saturated-absorption resonance observed in a MEMS vapor cell for development of a miniaturized optical-frequency-stabilized laser

M. Petersen[1], R. Boudot[1], G. Coget[1], N. Passilly[1], V. Maurice[1,2], C. Gorecki[1], and D.V. Brazhnikov[3,4]
[1]*FEMTO-ST, CNRS, UBFC, ENSMM, 26 rue de l'épitaphe, Besançon, 25000, France*
[2]*now at NIST, Time-Frequency Division, 325 Broadway, Boulder, 80305, Colorado, USA*
[3]*Institute of Laser Physics SB RAS, 15B Lavrentiev ave., 630090, Novosibirsk, Russia*
[4]*Novosibirsk State University, 2 Pirogova str., 630090, Novosibirsk, Russia*
E-mail: brazhnikov@laser.nsc.ru

Modern quantum technologies require the development of highly-sensitive, compact and even miniaturized, low-power consumption and high-performance devices, including atomic clocks, lasers or sensors. These instruments are to date often based on the use of chip-size diode lasers and microfabricated (MEMS) cells filled with alkali-atom vapors [1].

An interesting challenge concerns the development of miniaturized optical frequency references. Different approaches have been engaged in this direction. A recent example is the use of two-photon spectroscopy of rubidium atoms in a vapor microcell. Such an experiment, using a microfabricated cell and numerous chip-size components, has recently demonstrated a remarkable frequency stability level of $10^{-12}\ \tau^{-1/2}$ up to 1000 s [2]. The DBR laser and the conventional pump-probe saturated-absorption spectroscopy (SAR) [3] were implemented in [4] to demonstrate performance of a miniature optical-fiber integrated photonic spectrometer and to develop an optical frequency reference at 780 nm with a stability of 10^{-11} from 1 to 10^4 s. Besides these latest achievements, there are many other developments which demonstrate performance of compact laser systems stabilized by means of the regular saturated-absorption resonances in molecular gases. However, such the systems cannot be really chip-scale due to some reasons. For instance, the iodine-stabilized laser in [5] required using the 30-cm long cell. That resulted in total dimensions of the system equaled to about 55 × 25 cm.

In the present work, we consider an alternative approach based on the saturated-absorption resonance spectroscopy. It has been reported recently that the contrast of nonlinear SAR signals could be remarkably increased by using a dual-frequency regime of excitation, leading to demonstrate encouraging laser frequency stability results [6]. This approach was analyzed in detail theoretically and experimentally in [7] and was implemented with success to improve the short-term fractional frequency stability of a high-performance coherent population trapping Cs vapor cell clock [8]. In the latter studies, regular cm-size vapor cells were exploited for observation of the high-contrast SAR resonances.

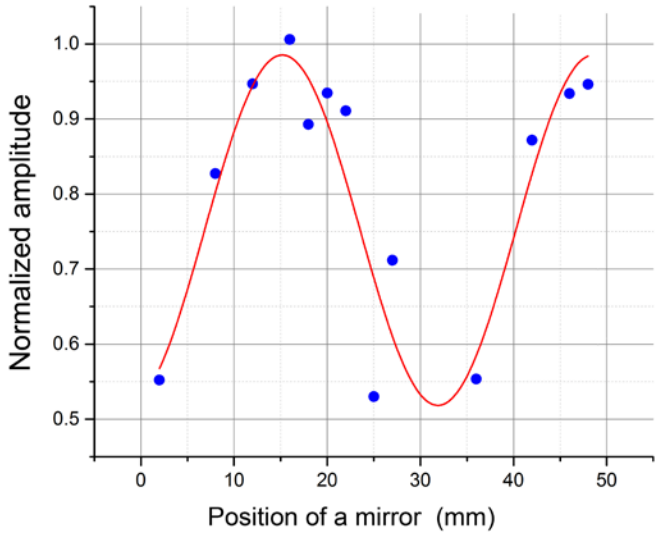

Fig. 1 Oscillations of saturated-absorption-resonance amplitude during changing position of the mirror.

In the present study, we report the investigation of dual-frequency saturated-absorption spectroscopy in a MEMS Cs vapor cell. The employed miniature cell technology is described in [9]. The cell diameter is 2 mm and its length is 1.4 mm. The used laser source is a narrow-linewidth external cavity diode laser tuned on the Cs D_1 line. We demonstrate the detection of high-amplitude Doppler-free resonances in a Cs microfabricated cell. We study the resonance amplitude, width and amplitude-to-width ratio of the detected resonance versus several experimental parameters (laser power, the cell temperature, etc.). The experimental setup is similar to that used in [7]. Results are compared with those obtained for a conventional single-frequency SAR scheme. In addition to this experimental study, we have developed a general theory of the high-contrast SAR effect beyond the qualitative theory developed previously in [7]. The latter qualitative model, presented in [7], allowed to reveal physical origins of the new effect but could not quantitatively predict any real values for the resonance amplitude and width.

Moreover, we also checked a theoretical prediction that the resonance amplitude may undergo oscillations during the reflecting mirror position changing. Figure 1 shows these oscillations. It is also seen from the figure that the SAR amplitude can be as high as magnitude of the wide Doppler background (the SAR amplitude in the figure is normalized to the Doppler-profile amplitude). The spatial oscillations effect has many in common with that described in [10] for the coherent-population-trapping resonances.

To conclude, we demonstrate the possibility for observation of the high-contrast saturated-absorption resonances in a MEMS vapor cell. The obtained results could be interesting for the development of a simple-architecture miniaturized frequency-stabilized laser. For instance, recent developments in the creation of narrow-linewidth vertical-cavity surface-emitting lasers (VCSEL) allow us to combine these lasers with our method of optical frequency stabilization. As it is expected, whole size of the devise can be pretty small.

D.V.B. thanks Russian Science Foundation (17-72-20089). Other authors thank LabeX FIRST-TF and Region de Franche-Comté for their support.

References

[1] J. Kitching et al., J. Phys. Conf. Ser. **723**, 012056 (2016).
[2] V. Maurice et al., Book of Abstracts of the 32nd EFTF Forum, Torino, Italy, April 10–12, 2018. Page 243.
[3] V. S. Letokhov, V. P. Chebotaev, "Nonlinear laser spectroscopy", Springer, Berlin, 1977.
[4] M.T. Hummon et al., Optica **5**, 443 (2018).
[5] T. Schuldt et al., Appl. Optics **56**, 1101 (2017).
[6] M. Abdel Hafiz et al., Opt. Lett. **41**, 2982 (2016).
[7] M. Abdel Hafiz et al., New J. Phys. **19**, 073028 (2017).
[8] M. Abdel Hafiz et al., J. Appl. Phys. **121**, 104903 (2017).
[9] M. Hasegawa et al., Sensors and Actuators A **167**, 594 (2011).
[10] S.V. Kargapoltsev et al., Laser Phys. Lett. **1**, 495 (2004).

Characteristics of a multipath optical monitoring system

A. Britvin, Yu. Kolomnikov, S. Konyaev, A. Povazhaev, B. Poller
Institute of Laser Physics SB RAS, 630090, Novosibirsk, Academician Lavrentiev Avenue, 15B
E-mail: lablis@mail.ru

The problems of acoustooptic interaction have a long history They are mostly associated with studies of light diffraction in the ultrasound and radiofrequency ranges. The questions of acoustooptic interaction in the region of infra-low frequencies remain practically unexplored. The article deals with the problem of recording by optical methods acoustic waves of the infrasonic range propagating in the atmosphere. Detection and registration of infrasound presents certain difficulties due to the fact that because of the low frequency of oscillations, the waves have a multi-meter length and are easily mixed with fluctuations of non-infrasound nature.

The acoustic wave front, characterized at the points of the medium by the values of the acoustic pressures, causes the occurrence of mechanical deformations in the medium. Therefore, each acoustic wave is accompanied by a variation of medium's refractive index, *n*. Taking this into account, for a plane monochromatic acoustic wave propagating along a given direction, the varying refractive index

For incident light, a medium with the refractive index (3) is a diffraction grating moving with a sound speed v. Passing through such a medium, the light is diffracted by inhomogeneities of the refractive index depending on the acoustic wave oscillation frequency. This can result in variations of the amplitude levels and propagation speeds of measurement waves, their phase-frequency transformations, which determine the possibilities of "beam reception" of acoustic oscillations [1].

Optical radiation passing through the atmosphere is subjected to refraction, absorption, and scattering. These interactions can be described depending on the refractive index and pressure.

The above relations determine the requirements to choosing conditions for recording of acoustic oscillations by a laser measuring line. In real conditions, the recording is affected by some disturbing factors, such as the atmosphere inhomogeneity, external noise, meteorological factors, etc. All external factors can be taken into account in natural experiments.

The choice of the length of the route can be determined by the following factors. When the optical channel is positioned coaxially with the propagation of an acoustic wave, the path length is equal to half the wavelength of the acoustic signal. The increase in the length of the optical channel will reduce the effect of the acoustic signal on the optical channel in comparison with the influence of other factors.

For an optical channel located perpendicular to the direction of propagation of the acoustic signal, the path length is independent of the wavelength of the acoustic signal.

To increase the possibility of separating the acoustic signal, several spaced optical channels can be used and correlational methods can be used.

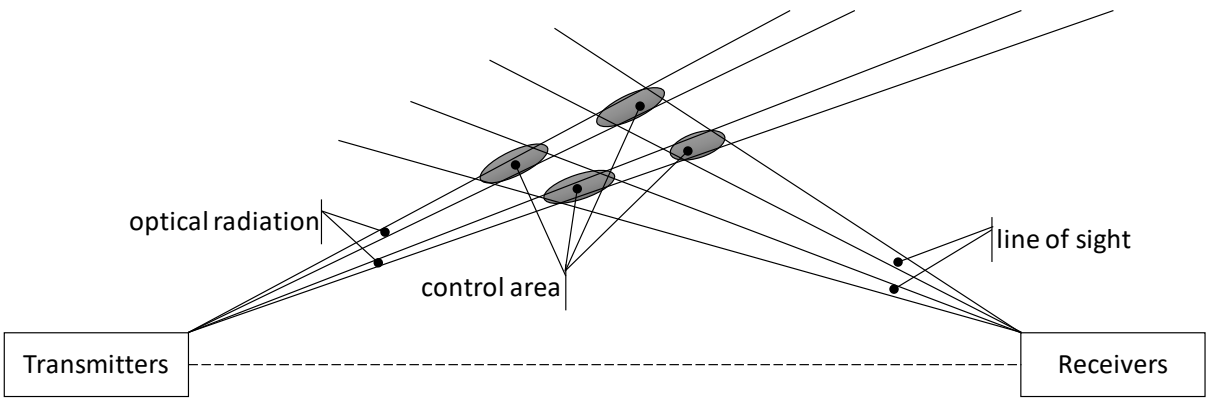

Fig. 1 Scheme of registration of acoustic oscillations by an optical channel non-line-of-sight.

Of greatest interest is the possibility of registering acoustic signals using a non-line-of-sight optical channel [2, 3]. In this channel, optical radiation scattered in the atmosphere is recorded at the receiver. In this optical channel, the modulation of the optical signal by an acoustic signal is much greater than in line-of-sight optical channel (Fig. 1).

The advantage of this recording system is the possibility of recording the scattered signal in a given region by changing the orientation angles of the receiver and the transmitter. In this case, the control zones can be operatively changed depending on the state of the atmosphere and the direction of propagation of the acoustic wave.

References

[1] M. Khairetdinov, G. Voskoboynikova, B. Poller, A. Britvin, G. Sedukhina. An Acoustooptic Interraction at Infralow Frequencies // Proceedings of International Multidisciplinary Scientific GeoConference Surveying Geology and Mining Ecology Management, SGEM 2017, Vol. 17, Issue 21, P. 775-782, DOI: 10.5593/sgem 2017/21/S08.099

[2] D.M. Reilly and C. Warde, "Temporal characteristics of single-scatter radiation," J. Opt. Soc. Am. 69(3), 464– 470 (1979).

[3] A.V. Britvin, Estimation of pulsed characteristics of the optical atmospheric ultravioletal channel with scattering, Bulletin of Novosibirsk State University. Series: Physics. 2010. T. 5. № 2. P. 5-7. (In Russian)

Building a bridge over lidar and radar

Z. Changming, Z. Zilong, Z. Haiyang, Y. Hongzi, and Z. Xingyuan
Beijing Institute of Technology, Beijing, 100081, China
E-mail: zhaochangming@bit.edu.cn

Both Lidar and Radar are using electromagnetic field as their detecting wave, and working on the same principle. Compared with radar，the most essential characteristics of lidar is its high spatial resolution, including transvers angular resolution and longitudinal distance resolution, originated from its shorter wavelength and high frequency. According to its detection method, lidar can be classified into two sorts, direct (incoherent) detection lidar & coherent detection lidar. Compared with radar, Lidar is suffered severely from atmospheric turbulence, especially in coherent detection.

We introduce here research works on a novel architecture-coherent dual frequency (CDF) lidar, which has both the high spatial resolution of lidar and, at the same time, has also the ability to resist atmospheric turbulence, and can be regarded as a bridge over lidar and radar.

CDF lidar based on the coherent dual frequency lasers, which is a lasers oscillating on two frequencies simultaneously. Besides, these two frequencies are coherent and optical beat is formed, and the beat frequency (frequency difference) is in the microwave domain. The beat frequency in CDF lidar is used for target detection. Therefore, the CDF lidar is basically a lidar, using laser beam as detection beam, with high spatial resolution of laser beam. Meanwhile, CDF lidar using the beat frequency as detection frequency, which is within microwave domain, in certain content, like radar. For this reason, CDF lidar can be regarded as a hybrid of, or a bridge over, lidar and radar.

Here, the word coherent has two meanings, the first one means the two frequencies of lasers are coherent, the second one means the detection method of CDF lidar is coherent. Instead of optical coherent, electrical coherent is used in CDF lidar. The optical beat formed electrical signal of photodetector is used as the local signal, interference with the receiving beam formed electrical signal of another photodetector.

Because frequency difference of the dual frequency lasers is small compared with laser frequency, the two frequencies undergo nearly the same phase distortion, when propagating through atmospheric turbulence. And the phase distortion can be compensated physically in CDF lidar, that is experimentally verified.

CDF lidar is developed for phase-shift range finder and Doppler velocimetry.

References

[1] Zheng Zheng,Zhao Changming, Zhang Haiyang, et al.,Optics & Laser Technology 80 (2016) 22-27.
[2] Zheng Zheng,Zhao Changming, Zhang Haiyang, et al.,Optics & Laser Technology 80 (2016) 169-175.
[3] Yang Hongzhi, Zhao Changming, Zhang Haiyang,et al., Acta Phys. Sin. 66 (2017) 184201.
[4] Hongzhi Yang, Marc Brunel, Haiyang Zhang,et al.,IEEE Photonics Journal 09 (2017) 7106609.
[5] Xingyuan Zheng, Changming Zhao, Haiyang Zhang,et al., Proceedings of SPIE 10619 (2017) 106190S1-12.
[6] Lijun Cheng, Suhui Yang, Changming Zhao,et al., IEEE Photonics Journal 10 (2017) 1500109.
[7] Hongzhi Yang, Changming Zhao, Haiyang Zhang,et al., IEEE Photonics Journal 10 (2018) 7100510.

On the mechanism of formation of the electromagnetically induced absorption resonances at closed transitions in spectroscopy of unidirectional waves

E. Saprykin[1], A. Chernenko[2]
[1]*Institute of Automation and Electrometry of SB RAS, Pr. Koptuga 1, Novosibirsk, 630090, Russia, tel. 330 68 69*
[2]*Insitute of Semiconductor Physics of SB RAS, Pr. Lavrentyeva 13, Novosibirsk, 630090, Russia, tel. 333 24 08*
E-mail: chernen@isp.nsc.ru

On the basis of numerical solutions of equations for the density matrix the physical processes forming the saturated absorption resonance spectra at the atomic transition with full level moments J_n=1- J_m= 2 under action of two linearly polarized unidirectional wave fields of arbitrary intensity are studied by changing directions of field polarizations. The contributions to the shape of nonlinear resonances of both incoherent population and coherent processes caused by the beating of the transition level populations, by effect of the magnetic level coherences induced by the strong field, including its transfer from the upper to the lower state levels, and also by the nonlinear polarization at the combination frequency $2\omega - \omega_\mu$ are considered.

It is established that the saturated absorption resonance manifests itself in the form of a traditional wide dip having an incoherent population nature and a narrow coherent structure near the line center. Parameters of the main dip are determined by the values of the level relaxation constants and intensity of the saturating field, but parameters of the narrow structures depend on the mutual direction of the light field polarizations and degree of the transition openness (the branching parameter of transition).

Moreover, the degree of transition openness determines a qualitative form of the narrow resonance structure: at the closed transition the structure manifests itself in the peak form (EIA resonance), and at the open transition - in the form of narrow dip (EIT resonance).

Investigation of contributions to the resonance line shape of transitions between separate magnetic sublevels of the upper and lower states has shown that the main contribution is made by transitions between sublevels with maximum magnetic numbers. These transitions also formate the EIA resonance in case of the closed transition.

It is shown that the physical reason for appearance of the narrow resonance structures is the specific relaxation of the transition level population beats in the bichromatic field of light waves [1]. The contribution to the resonance line shape of the transfer process of the level magnetic coherences from the upper state levels to the lower one is maximal at the closed transition and under conditions of calculations did not exceed ~ 10% of the amplitude of peak structure. The contribution of nonlinear polarization on combination frequency $2\omega - \omega_\mu$ is much smaller. This mechanism of formation of the narrow structures in the spectrum of saturated absorption of unidirectional waves is also valid for J_n- J_m= J_n +1 transitions.

The presented results show that the interpretation of mechanism of formation of the electromagnetically induced absorption (EIA) resonances in unidirectional waves [2, 3] as result of spontaneous transfer of the level magnetic coherence of the excited state to the ground atomic state [4, 5] is incorrect and needs to be refined.

References

[1] E.G. Saprykin, A.A. Chernenko and A.M. Shalagin, JETP **150**, 238 (2016).
[2] F.M. Akulshin, S. Barreiro and A. Lesama, Phys. Rev. A **57**, 2996 (1998).
[3] S. K. Kim, H. S. Moon, K. Kim et al., Phys. Rev. A **61**, 063813 (2003).
[4] A.V. Taichenachev, A.M. Tumaikin and V.I. Yudin, JETP Lett. **69**, 776 (1999).
[5] D.V. Lazebnyi, D.V. Brazhnikov, A.V. Taichenachev et al., JETP **148**, 1068 (2015).

Ion acceleration with ultra-intense laser pulses

S.N. Chen[1-3]
[1]*LULI–CNRS, CEA, École Polytechnique, Univ. Paris-Saclay, Sorbonne Univ., UPMC Univ. Paris 06, F-91128, Palaiseau cedex, France*
[2]*Institute of Applied Physics, 46 Ulyanov Street, 603950, Nizhny Novgorod, Russia*
[3]*ELI-NP, Magurele, Romania*
E-mail: sophia.chen@eli-np.ro

High-intensity lasers interacting with solid foils produce copious numbers of relativistic electrons, which in turn create strong sheath electric fields around the target. The proton beams accelerated in such fields have remarkable properties, enabling ultrafast radiography of plasma phenomena or isochoric heating of dense materials. In view of longer-term multi-disciplinary purposes (e.g., spallation neutron sources or cancer therapy), the current challenge is to achieve proton energies well in excess of 100 MeV [1], and to increase the repetition rate of the production of these sources, both of which is envisioned to be possible with the advent of upcoming multi-PW laser facilities (Apollon in France and ELI-NP in Romania) that will soon be available.

We will review how ultra-intense laser pulses offer unique possibilities in accelerating high-energy, extreme current ion bunches in a very short time as well as the mechanisms thereof, whether well assessed [1,2] or emerging [3,4]. We will also present the perspectives offered by the upcoming multi-PW lasers, and review some applications like ion stopping power in plasmas [5-7] which becomes with such beams uniquely possible.

Indeed, using high-flux proton beams accelerated by high intensity short pulse lasers, where there is a high number of particles in a picosecond pulse, is ideal for measurements of ion stopping power in quickly expanding plasmas. By reducing the energy bandwidth of the protons using a passive selector [8], we have made proton stopping measurements in partially ionized Argon and fully ionized Hydrogen plasmas with electron temperatures of hundreds of eV and densities in the range $10^{20} – 10^{21}$ cm^{-3}. In the first case, we have observed, consistently with previous reports, enhanced stopping of protons when compared to stopping power in non-ionized gas. In the second case, we have observed for the first time the regime of reduced stopping, which is theoretically predicted in such hot and fully ionized plasma. The versatility of these tunable short-pulse laser based ion sources, where the ion type and energy can be changed at will, could open up the possibility for a variety of ion stopping power measurements in plasmas so long as they are well characterized in terms of temperature and density. In turn, these measurements will allow tests of the validity of existing theoretical models.

References

[1] N. Nakatsutsumi, Y. Sentoku, S. N. Chen, et al., Nat. Comm. **9**, 280 (2018).
[2] A. Soloviev, K. Burdonov, S. N. Chen, et al., Sci. Rep. **7**, 12144 (2017).
[3] P. Antici, E. Boella, S.N. Chen, et al., Sci. Rep. **7**, 16463 (2017).
[4] S.N. Chen, M. Vranic, T. Gangolf, et al., Sci. Rep. **7**, 13505 (2017).
[5] S.N. Chen, S Atzeni, M. Gauthier, et al., Nuclear Instruments and Methods in Physics Research Section A: Accelerators, Spectrometers, Detectors and Associated Equipment **740**, 105 (2014).
[6] M. Gauthier, S. N. Chen, A. Levy, Phys. Rev. Lett. **110**, 135003 (2013).
[7] M. Gauthier, C. Blancard, S.N. Chen, et al., High Energy Dens. Physics **9**, 488 (2013).
[8] S. N. Chen, M. Gauthier, D. P. Higginson, et al., Rev. Sci. Instrum. **85**, 043504 (2014).

Particle trapping and manipulation using hollow beam with tunable size generated by thermal nonlinear optical effect

B. He, X. Cheng, H. Zhang, H. Chen, Q. Zhang, Z. Ren, S. Ding, J. Bai
Northwest University, Xi'an, China
E-mail: 15502928675@163.com

We generate the hollow beam of tunable size using thermal nonlinear optical effect, achieving particle manipulation by modulating the beam size rather than the power, which effectively prevents particle damage for intense laser is avoided.

Study of dielectric properties of DNA solutions by terahertz time-domain spectroscopy

N. Nikolaev[1,2], A. Mamrashev[2], D. Shpakov[1,3], E. Nemova[1], O. Cherkasova[1,4]
[1]*Institute of Laser Physics SB RAS, 15B, Academician Lavrentiev Ave., Novosibirsk, 630090, Russia*
[2]*Institute of Automation and Electrometry SB RAS, 1, Academician Koptyug Ave., Novosibirsk, 630090, Russia*
[3]*Novosibirsk National Research State University, Pirogova street 1, Novosibirsk, 630090, Russia*
[4]*Novosibirsk State Technical University, 630073, Russia*
E-mail: o.p.cherkasova@gmail.com

Terahertz (THz) spectroscopy becomes a promising method of biomolecule diagnostics. THz spectra depend on the molecule structure and flexibility [1, 2]. Frequencies of molecular oscillations that make big groups of atoms move together and frequencies of hydrogen bond breaking lay in the THz range. The hydrogen bonds keep a specific molecular structure, which is why many conformational transitions affect the hydrogen bonds and consequently the THz spectra [3].

DNA molecules normally assume the B-conformation in water and the A-conformation in water-ethanol solutions, unless the ethanol concentration is high enough to disrupt the hydrogen bonds between DNA strands [4]. The duplex period is equal to 10 b.p. for the B-conformation and 11 b.p. for the A-conformation. The planes of the nitrogenous bases are perpendicular to the molecular axis in the B-conformation and titled 20^0 with respect to the axis normal in the A-conformation [4]. These differences are expected to influence the dielectric properties of DNA solutions. The aim of the work was to study dielectric properties (frequency dependence of absorption, complex refractive index and dielectric permittivity) of water and water-ethanol DNA solutions measured by THz time-domain spectroscopy (THz-TDS).

The thymus calf DNA was purchased from Serva (USA) as a lyophilized substance and used without further purification. The DNA was weighed in a 1.5-ml Eppendorf tube, and water and/or 25% ethanol solution in water was added. The solution concentrations were 5 and 10 mg/ml. The studies were carried out using a conventional THz-TDS spectrometer based on frequency-doubled Er-fiber laser ($\lambda \approx 775$ nm, $\tau \approx 130$ fs, $f \approx 78$ MHz, $P \approx 100$ mW). We used an experimental setup and signal processing methods analogous to those described in [5].

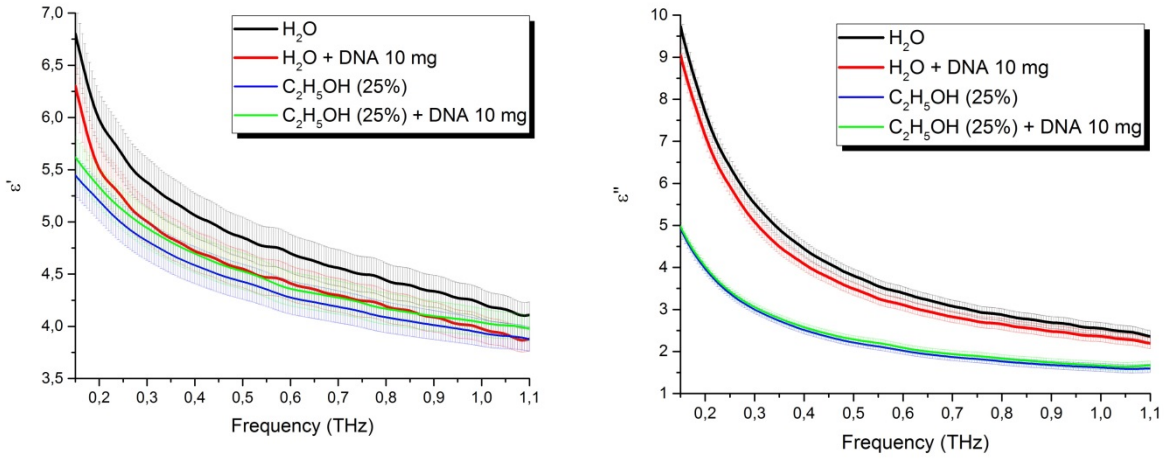

Fig. 1 (a) real and (b) imaginary part of the dielectric permittivity of water and ware-ethanol DNA solutions.

The real and imaginary parts of the dielectric permittivity of water and water-ethanol DNA solutions are demonstrated on fig 1. There is a sufficient difference between distillated water and all solutions (water-DNA, water-ethanol, and water-ethanol-DNA), while the difference in the dielectric properties of the water-ethanol mixture with and without DNA is below the experimental precision. The difference in the dielectric properties (absorption coefficient, index of refraction, and real and imaginary parts of permittivity) of pure water and water-DNA solution is almost independent on the

frequency. The features noticed can be explained by the fact that water absorption and dielectric permittivity are determined mainly by hydrogen bonds between water molecules. If the DNA-water and ethanol-water bonds interact with THz radiation weaker than the water-water bonds do, retracting hydrogen bonds from the water molecules by the DNA or ethanol ones leads to extra decreasing of absorption. It is worth noting that the percentage of changed bonds can exceed the concentration of DNA or ethanol molecules. For example, adding 22-27% of ethanol leads to complete rebuilding of the hydrogen bond structure [6]. Besides, ethanol-water hydrogen bonds may have higher dissociation energy and cannot change significantly if DNA molecules are added. In this case, there is almost no difference in the absorption spectra of water-ethanol solutions with and without DNA, as it was observed in the reported experiments.

The measurements were carried out in the Shared Equipment Center "Spectroscopy and Optics" of the Institute of Automation and Electrometry, SB RAS.

References

[1] X.-C. Zhang, Phys. Med. Biol. **47**, 3667 (2002).
[2] A. Markelz, S. Whitmirre, J. Hillebrecht, and R. Birge, Phys. Med. Biol**. 47**, 3797 (2002).
[3] I.N. Smirnova, D.A. Sapozhnikov, A.V. Kargovsky, V.A. Volodin, O.P. Cherkasova, R. Bocquet, and A.P. Shkurinov, Vib. Spectrosc. **62**, 238 (2012).
[4] M. Kulkarni and A Mukherjee, Prog. Biophys. Mol. Biol. **128**, 63 (2017).
[5] V.D. Antsygin, A.A. Mamrashev, N.A. Nikolaev, O.I. Potaturkin, T.B. Bekker, and V.P. Solntsev, Optics Communications, **309**, 333 (2013).
[6] T.A. Dolenko, S.A. Burikov, S.V. Patsaeva, and V.I. Yuzhakov, Quantum Electron. **41** (3), 267 (2011).

The effect of 0.14 THz radiation on human skin fibroblasts

M.A. Surovtseva[1,2], A.P. Lykov[1,2], O.V. Kazakov[1], A.V. Kabakov[1], O.V. Poveshchenko[1,2], A.F. Poveshchenko[1,2], D.S. Serdyukov[3,4], S. Kuznetsov[4,5], O.P. Cherkasova[3,6], A.Yu. Letyagin[1]

[1]*Researcher Institute of Clinical and Experimental Lymphology-branch of Institute of Cytology and Genetics SB RAS, Novosibirsk, 630060, Russia*

[2]*Institute of Circulation Pathology, Novosibirsk, 630055, Russia*

[3]*Institute of Laser Physics of SB RAS, Novosibirsk, 630090, Russia*

[4]*Novosibirsk State University, Pirogova street 1, Novosibirsk, 630090, Russia*

[5]*Rzhanov Institute of Semiconductor Physics SB RAS, Novosibirsk Branch "TDIAM", Novosibirsk, 630090, Russia*

[6]*Novosibirsk State Technical University, 630073, Russia*

E-mail: mfelde@ngs.ru

Motivation and Aim: THz (THz) radiation is already employed in certain industrial and medical applications, such as non-destructive evaluation and quality control of materials, imaging, diagnostics, therapy, and others. THz waves are a type of non-ionizing radiation in the electromagnetic spectrum lying between the infrared and microwave domains, at frequencies ranging from 0.1 THz to 10 THz (wavelengths 30 um – 3 mm). In biomedical research the THz band has aroused a noticeable interest due to much larger penetration depths of THz waves into optically opaque materials and some biological tissues versus IR rays and due to much smaller wavelengths relative to microwaves acceptable for imaging concealed targets with submillimeter spatial resolution. These factors make THz waves promising for medical imaging of internal structure of tissues inaccessible with conventional techniques. Suggested applications may include dermatological investigations for picking out cancerous lesions and wound assessment [1]. Meanwhile, the prospect of widely using THz radiation in medical diagnostics and therapy raises the issue of how the electromagnetic radiation in the 0.1–10-THz range affects biological objects. Since the skin is the main target for this radiation, most of the research studies employed skin fibroblasts as a cellular model [2]. The aim of our study was to evaluate the effect of THz irradiation on the proliferation, migration and NO production by the human skin fibroblasts (hFb).

Methods: Human fibroblasts were irradiated by coherent monochromatic 0.14 THz radiation from a solid-state IMPATT-diode-based source at different emission power (10, 30, 50, 70, and 100 mW) and exposure time of 20 minutes. A normal human fibroblast culture was established by an explant techniques using a normal skin tissue discarded during surgical procedures and cultured under standard conditions. The cell proliferation was measured by the MTT (3-(4,5-dimethylthiazol-2-yl)-2,5-diphenyl-2H- tetrazolium bromide) colorimetric assay 120 hours after the THz irradiation. The migration activity of hFb was investigated 48 hours after the irradiation using Axio Observer Z1 microscope by desquamation of the monolayer; the result shows the percentage of the area of the closure of desquamation. The NO inhibition assay was conducted using a Griess reagent kit for nitrite determination (Molecular Probes).

Results: It is established that irradiating the fibroblasts with 0.14 THz waves of examined power range (10–100 mW) does not influence on the cells'proliferation. We showed that after 120 hours of experiment the proliferative activity of irradiated cells did not differ from the non-irradiated control. The horizontal migration model revealed that after 48 hours from the experiment start, the area closing the wound surface of the irradiated fibroblasts was 50%, 72%, 42%, and 79% (at the THz emission power of 30, 50, 70, and 100 mW, respectively), that was comparable with the control (78%). The production level of nitric oxide by irradiated fibroblasts did not differ from the level NO of non-irradiated cells.

Conclusion: The present study demonstrated that the low-frequency THz radiation in our model does not affect the functional activity of human skin fibroblasts.

References

[1] C. Yu, S. Fan, Y. Sun, and E. Pickwell-Macpherson, Quantitative Imaging Med. Surg., **2** (1), 33 (2012).

[2] A.D. Amicisa, S.D. Sanctisa, S.D. Cristofaro et al., Mutation Research, **793,** 150 (2015).

Laser plasma dynamics in a magnetized background

A.A. Chibranov, A.G. Berezutsky, M.A. Rumenskikh,
M.A. Efimov, I.B. Miroshnichenko
Institute of Laser Physics SB RAS, Novosibirsk, Russia
E-mail: chibranov_25@mail.ru

Laboratory modeling makes it possible to study various space plasma and astrophysical processes and phenomena which is difficult to carry out in a natural environment [1]. The purpose of this work is to investigate the penetration flow of laser plasma cloud into a magnetized background [2], and also to confirm the theory of Larmor rotation of plasma ions moving relative to each other in a magnetic field.

To measure the characteristics of laser plasma, probe and spectral diagnostics were used. Spectral diagnostics is one of the most convenient methods to observe individual components of the laser plasma which is direct and contactless. However, due to optical limitations measurement is not localized and gives date integrared along the line of sight. Probe diagnostics, in its turn, allow register the signal in the local area, but cause some perturbations of the plasma, which can affect the quality of the recorded signal.

Data were obtained at the KI-1 facility [3] in the course of the MEGA experiment on simulation of explosive super-Alfvenic plasma expansion in ionospheric environment at Alphen-Mach numbers $M_A > 1$.

The experimental set up was following. The beam of CO2 laser pulse ($E_к$~200 J, 100 ns) was focused in a spot of 2 cm size on a flat polyethylene target inside a large (∅120 cm*5m), high-vacuum (10^{-6} Torr) chamber. As a result of ablation a Laser Plasma plume is generated expanding with velocity 150-100 km/s. LP expands into Helium background plasma, with density of $(2\text{-}3)\cdot10^{13}$ cm^{-3} previously created by theta-pinch, in a homogeneous magnetic field up to B_0=500 G. Relative to magnetic field cone of LP expansion is oriented perpendicular.

Results of laboratory modeling allowed making the following conclusions:

- The intensity of luminosity of the ion lines falls off with distance from the target as $\sim 1/R^2$, which corresponds to the inertial expansion of the laser plume (Figure 1).
- The speed of propagation of a laser plasma in a neutral gas of H_2 or magnetized background plasma is about 70 km/s, which is 1.5 times slower than the velocity of its propagation in vacuum (Figure 2).
- When the laser plasma propagates in a magnetized background, the Larmor rotation of laser ions is observed, which depends on the direction of the magnetic field.

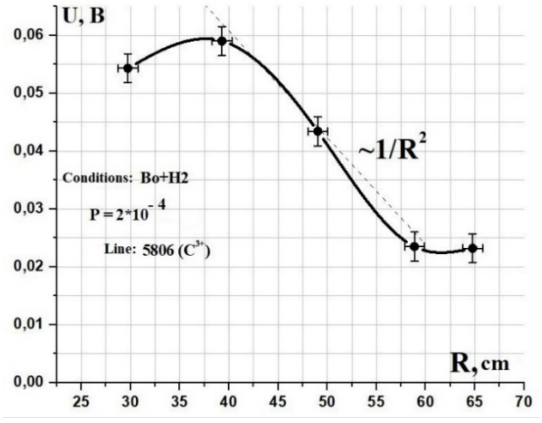

Fig. 1 Dependence of the emission intensity of the carbon C^{3+} line on the distance from the target. The dashed line shows the theoretical dependence of the intensity on the distance ($1/R^2$) related to inertial expansion and line-of-sight integration.

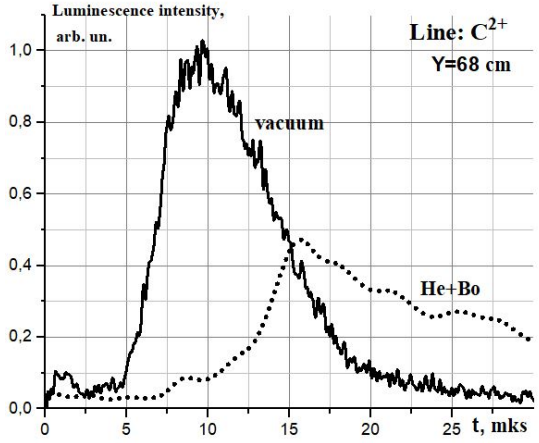

Fig.2. Dynamics of intensity of carbon C^{2+} line in a vacuum (solid) and in a magnetized background (dotted line). The distance from the target is R=68 cm.

The work was supported by RFBR grant № 18-32 00029, SB RAS basic research project II.10 №0307-2017-0015 and the RNF grant 18-12-00080.

References

[1] J. D. Huba, P. A. Bernhardt, J. G. Lyon. "Preliminary study of the CRRES magnitospheric barium releases." Journal of Geophysical Research: Space Physics, № A**1**, 11 (1992).

[2] Yu. P. Zakharov, V. A. Terekhin, A. G. Ponomarenko, I. F. Shaikhislamov, A. G. Berezutski, E. L. Boyarintsev, K. V. Vchivkov, A. V. Melekhov, V. G. Posukh, M. A. Rumenskikh, A. A. Chibranov. "Laboratory and numerical simulations of the generation of magnetized collisionless shocks by laser-plasma blobs with the ions of different mass (M/Z)." Khariton's scientific readings, 59 (2018).

[3] Yu. P. Zakharov, A. M. Orishich, A. G. Ponomarenko. "Laser plasma and modeling of nonstationary cosmophysical processes." SB AS USSR, edited by A. G. Preobrazhensky, Novosibirsk, 220 (1988).

Ramsey fringes in coherent population trapping resonance formed by counter-propagating σ^+ - σ^- polarized fields

D. Chuchelov[1,3], A. Taichenachev[4], E. Tsygankov[3], M. Vaskovskaya[1,3], V. Vassiliev[1,3], V. Velichansky[1-3], S. Zibrov[1,3], V. Yudin[4]

[1]*P.N. Lebedev Physical Institute, Russian Academy of Sciences, 119991, Moscow, Russia*
[2]*National Nuclear Research University, MEPhI, 115409, Moscow, Russia*
[3]*Atomiks Ltd., 125315, Moscow, Russia*
[4]*Institute of Laser Physics, Siberian Branch of RAS, 630090, Novosibirsk, Russia*
E-mail: Factorialzero@gmail.com

The sensitivity of quantum sensors based on the effect of coherent population trapping (CPT) [1, 2] is determined by the characteristics of the CPT resonance the most important of which are the width, the contrast and the signal-to-noise ratio. In the frequency standard at the metrological 0-0 transition the CPT resonance is detected by a circularly polarized laser field. In this case a significant part of the atoms falls on the extreme Zeeman (nonabsorbing light) sublevel, which reduces the contrast of the resonance. The work is devoted to the development of one of the methods [3-5] for eliminating this shortcoming.

CPT resonance is formed by two counter propagating waves of orthogonal circular polarizations. The method makes it possible to increase the resonance contrast by an order of magnitude [6], but this is accompanied by broadening of the resonance, negating its metrological value. Using the Ramsey spectroscopy (pulsed interrogation method), it is possible to achieve narrow linewidths with relatively high laser intensities. In this method the linewidth of Ramsey-CPT fringes is determined by the time T_R separating the two interaction pulses and power broadening is negligible compared to continuous wave (CW) mode.

In [7], CPT resonance was detected by counter propagating wave pulses, which allowed to increase the signal without line broadening and to reduce light shifts. However, the use of a cooled ensemble of atoms and, thus, of a small number of atoms limited the magnitude of the signal in this work. In this paper, we study the characteristics of the CPT resonance in a similar scheme, but without cooling the atoms. The experimental setup described in [6] was supplemented with an acousto-optic modulator and a pulsed synchronous detector for the Ramsey method. We use several self-made atomic vapor cells filled with ^{87}Rb and buffer gases (Ar, N_2) [8]. The efficiency of the method of counter propagating waves is manifested for cells with a longitudinal dimension much smaller than the wavelength of the microwave transition between the hyperfine sublevels of the ground state ($\approx$ 44 mm for ^{87}Rb). On the other hand, small dimensions of cells decrease the coherence lifetime. To find the optimal conditions we made cells of different lengths and gas pressures. Radiation with the necessary characteristics is obtained by using the injection locking system. The system consists of two diode lasers, one of which (master) imposes its spectral characteristics on the other laser (slave). An extended cavity diode laser is used as the master. Generation of resonance optical fields (side bands of the first order) was achieved by microwave modulation of the injection current of the driven laser. In CW mode the characteristics of the CPT resonance are studied versus several experimental parameters in order to get the maximum contrast/width ratio.

In the Ramsey mode the AM modulated radiation of the laser is a pulse train consisting of a pump pulse, a free evolution time, and a probing pulse. The characteristic pulse durations are 500 μs, 500 μs and 10 μs, respectively. In order to form a coherent superposition of states the radiation intensity during a pump pulse has to be relatively high. Detection time should be short enough so as not to disturb the atomic system. The properties of the CPT-Ramsey fringes are compared to those obtained using the CW interaction mode.

In CPT-Ramsey atomic clocks the central fringe serves as a reference, however distinguishing the central fringe among the side fringes is often a problem since they have nearly equal amplitudes. The "central" fringe is the one that corresponds to a zero-phase difference between the coherence oscillation and the RF field. We propose a simple method that allows to highlight the central Ramsey fringe. During the period between pulses the laser radiation is not completely switched off. In this

case due to the light induced relaxation all side fringes are suppressed while the central fringe is not owing to the coherence created by the residual low intensity radiation. In the case of uncompensated light shifts the central fringe may not correspond to the envelope center of the Ramsey oscillations (Fig.1), so this method can also be useful for obtaining a laser spectrum corresponding to compensated light shifts.

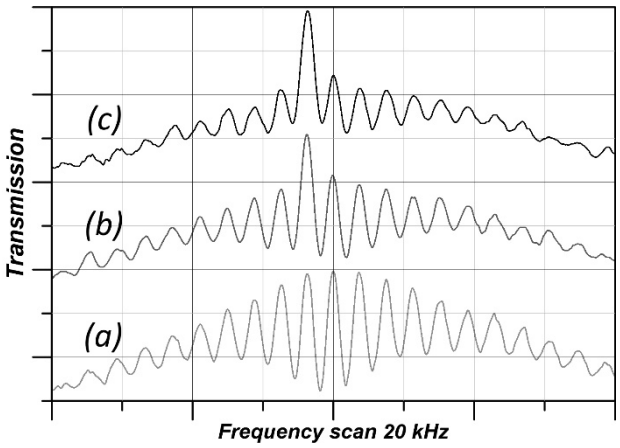

Fig. 1. CPT - Ramsey fringes for different values of radiation intensity I_R during the Ramsey period. (a) I_R = 0; (b) I_R = 0.8 mW/cm^2; (c) I_R = 1.6 mW/cm^2. In all three cases radiation intensity during the pump pulse Ip equals 25 mW/cm^2. The central fringe of the envelope does not coincide with the zero-phase fringe.

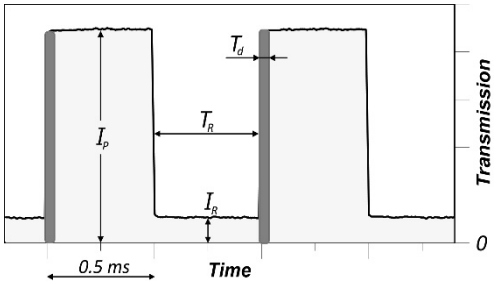

Fig. 2. Typical pulse train. T_R – Ramsey period; T_d – detection time; I_p - radiation intensity during pump pulse; I_R - radiation intensity during Ramsey period.

A significant increase in the contrast of the resonance while maintaining its width, as well as an essential suppression of the light shift, allow us to expect a significant improvement in the stability of the atomic clock of the proposed scheme.

References

[1] E. Arimondo, Prog. Opt. **35**, 257 (1996).
[2] S. Knappe. 'MEMS Atomic Clocks" Compr. Microsyst., **3**, 571 (2007).
[3] T. Zanon, S. Guerandel, E. de Clercq, D. Holleville, N. Dimarcq, and A. Clairon, Phys. Rev. Lett. **94**(19), 193002 (2005).
[4] A.V. Taichenachev, V.I. Yudin, V.L. Velichansky, and S.A. Zibrov, JETP Lett. **82**(7), 398 (2005).
[5] S.V. Kargapoltsev, J. Kitching, L. Hollberg, et al., Laser Physics Letters **1**(10), 4959 (2004).
[6] D.S. Chuchelov, S.A. Zibrov, V.V. Vasiliev, A.V. Taichenachev, V.I. Yudin, V.L. Velichansky, Bulletin of the Lebedev Physics Institute, **10**, 281, (2017).
[7] V.I. Yudin, A.V. Taichenachev, J. Kitching, Appl. Phys. Lett. **111**, 224102, (2017).
[8] D.I. Sevost'yanov, A.V. Sivak, S.S. Losev, Yu.V. Mas'yan, R.I. Fishman, V.V. Vasiliev, S.A. Zibrov, V.L. Velichansky, Electromagnetic Waves and Electronic Systems, **8**, 73, (2015).

IR inductive Xe laser pumped by a pulsed longitudinal inductive discharge of the transformer type

A.M. Razhev[1,2], D.S. Churkin[1,3], E.S. Kargapoltsev[1], R.A. Tkachenko[1,3], I.A. Trunov[2]
[1]*Institute of laser physics SB RAS, Prosp. Ac. Lavrentyeva, 15B, Novosibirsk, Russian Federation*
[2]*Novosibirsk state technical university, Prosp. K. Marksa, 20, Novosibirsk, Russian Federation*
[3]*Novosibirsk state university, Pirogova st., 1, Novosibirsk, Russian Federation*
E-mail: razhev@laser.nsc.ru

Lasers on inert gas transitions are currently one of the most popular sources of laser radiation in the near and middle IR regions. XeI lasers were widely used among such lasers. At present, Xe lasers are actively used with pumping by an electron beam and an RF discharge. In the first case, Ar-Xe or He/Ar-Xe mixtures are used as the active medium at a typical ratio of 100:1 and pressure up to several atmospheres. Laser radiation in such installations is most often at wavelengths of 1.73 μm, 2.03 μm, 2.63 μm, 2.65 μm, 3.37 μm. In beam Xe lasers, the energy of generation can reach 650 Joule [1], and the efficiency is up to several% (in electric-ionization lasers, almost 10% [2]). The duration of the generation pulses, as a rule, corresponds to the duration of the pump pulses and can reach from a value from several microseconds to several milliseconds [3]. In the second case, laser generation can be carried out in a continuous mode, while the power can reach 3.5 W [4]. The generation spectrum also, as a rule, consists of several (up to ten) lines in the region 1.7-7.7 μm [5].

In our experiments on the creation of gas lasers pumped by a pulsed induction discharge, we showed the possibility of pumping active gas laser media operating both in the transfer of excitation from atoms of the buffer gas [6] and in direct excitation of molecules (in this case nitrogen and hydrogen) by electron impact [7, 8]. In addition, the induction discharge is formed in the absence of any electrodes in the active medium, which, in combination with the inertness of the active medium itself, based on a mixture of noble gases Ar-Xe or He-Xe, makes it possible to create lasers with practically unlimited lifetime. Thus, a pulsed induction discharge can be proposed as an alternative method for pumping an infrared laser at transitions of neutral xenon atoms. Accordingly, the goal of this paper was to search for conditions for the formation of population inversion and to achieve a laser-generated regime on electronic transitions of neutral xenon atoms in a pulsed induction discharge.

To conduct the research, an experimental setup was developed, the electric circuit of which was carried out according to the Blumlein scheme [9]. As an induction laser emitter, a glass tube with a capillary and a bypass channel was used. Such a design allowed the current to flow in a closed loop, while the working area was formed by a 3 mm diameter capillary and 500 mm in length - to achieve a high current density - and the diameter of the bypass channel was much larger (20 mm) to reduce the impedance of the circuit. As an inductor, a set of frames made of copper insulated conductors of 2.5 mm2 cross section, installed along the discharge circuit, was used. In the literature, this type of a no-ferrite inductor is called an antenna.

For the first time, infrared radiation when xenon was pumped by a pulsed longitudinal inductive discharge of a transformer type was detected in our experiments in the range 900-1000 nm. It consisted of three lines with wavelengths $\lambda 1$ = 840.92 nm, $\lambda 2$ = 904.5 nm and $\lambda 3$ = 979.9 nm, respectively. Further experiments showed that in the region up to 5 μm there are two more lines in the lasing spectrum with wavelengths $\lambda 4$ = 1733 nm and $\lambda 5$ = 2026 nm. The intensity of these lines was approximately 100 times higher than that of the first three. The generation spectrum is shown in Fig. 1. The study of the spatial characteristics of the IR radiation of xenon was carried out using a diode line. It was found that in the cross section the beam profile has an intensity distribution close to Gaussian (Fig. 2).

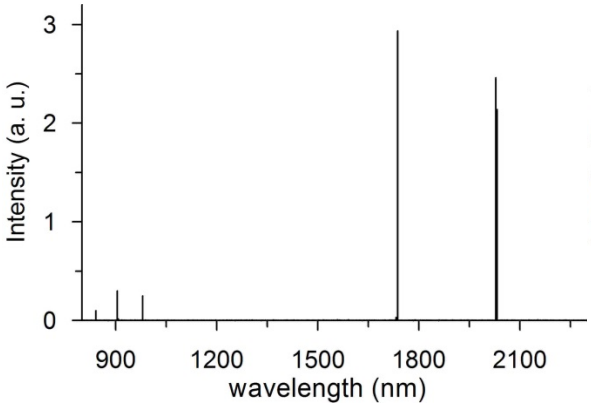

Fig. 1 Generation spectrum of the IR inductive XeI laser.

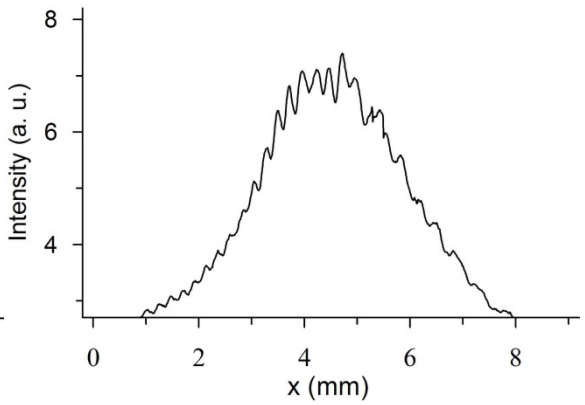

Fig. 2 Beam profile of the IR inductive XeI laser.

An estimate was made of the divergence by comparing the spot sizes at different distances from the output window of the laser (6-8 m). The divergence was determined as $\theta = \text{arctg}((sL - s0) / L)$ (where L is the distance from the output mirror, sL is the peak width at half-height for a given distance L, s0 is the peak width at half-height near the output mirror). The results of the measurements carried out in this way showed that the divergence is 1±0.2 mrad. In the first experiments, the generation energy did not exceed 0.1 mJ. Since under the given pumping conditions only the fact of detection of IR laser radiation on XeI atoms transitions in a pulsed induction discharge has been established, the purpose of our further investigations is a detailed study of the dependence of the energy, time, and spectral characteristics of the induction XeI laser on the pump conditions.

This work was supported by a grant from the Russian Foundation for Basic Research No. 16-02-00316.

References

[1] L. Littzenberger, D. Trainor, M. McGeoch, IEEE J. Quantum Electronics **QE-26(9)**, 1668 (1990).
[2] N. Basov, V. Baranov, A. Chugunov et. al., IEEE J. Quantum Electronics **QE-21(11)**, 1756 (1985).
[3] O. Sereda, V. Tarasenko, A. Fedenev et. al., Quantum Electronics, **23(6)**, 459 (1993).
[4] R. Morley, J. Wendland, H. Baker et. al., Opt. Comm. **142**, 244 (1997).
[5] J. Wang, J. Paranto, and C. Lovejoy, IEEE J. Quantum Electronics **QE-20(3)**, 276 (1984).
[6] A. Razhev, V. Mkhitaryan, D. Churkin, JETP Lett., **82(5)**, 259 (2005).
[7] A. Razhev, D. Churkin, JETP Lett. **86(6)**, 420 (2007).
[8] A. Razhev, D. Churkin, A. Zavyalov, [J] Vestnik NSU, Seria Fizika **4(3)**, 12 (2009) (in Russian).
[9] A. Razhev, D. Churkin, Optics Communications **282(7)**, 1354 (2009).

Periodic sequence of femtosecond pulses with preselected carrier envelope offset phase

N.N. Golovin[1], N.I. Dmitrieva[1], K.M. Sabakar[1], A.K. Dmitriev[1,2]
[1]*Novosibirsk State Technical University, 630073, Novosibirsk, Russia*
[2]*Institute of Laser Physics, Siberian Branch of Russian Academy of Science, 630090, Novosibirsk, Russia*
E-mail: alexander_dmitriev@ngs.ru

Implementation of the methods for expanding the emission spectrum of a femtosecond laser from above the octave made it possible to create f-2f interferometer, which allowed to measure the shift of the frequency comb and, therefore, to ensure the accuracy of measuring optical frequencies with an error not exceeding the parameters of the best modern frequency standards. When the pulse duration is of the same order as the wavelength, the phase shift between the envelope and the carrier significantly affects the frequency conversion efficiency in nonlinear optical processes and it is extremely important for production of attosecond pulses [1-3]. The use of a local oscillator laser makes it possible to eliminate the frequency offset of a femtosecond comb [4]. However, to implement such a scheme, it is necessary that the frequency of the local oscillator is located in the low-frequency region of the emission spectrum of femtosecond pulses, and its second harmonic belongs to the high-frequency part of the spectrum.

In the present paper we propose a method for the realization of femtosecond radiation without frequency comb shift with the possibility of selecting pulses with the required carrier envelope offset phase.

When repetition and offset frequencies are stabilized with radio frequency standard, the laser emission spectrum is a set of equidistant frequencies, the interval between which is equal to the pulse repetition frequency f with the offset of the laser frequency comb Δ

$$\nu_m = mf + \Delta \tag{1}$$

where the positive integer m is the mode number.

Fig. 1a shows the temporal sequence of femtosecond pulses with a frequency comb shift by $\Delta=f/3$. The pulse duration τ is limited by the spectral width of the femtosecond radiation ω and the number of optical oscillations in the pulse is determined by the ratio of the pulse duration τ to the period of the light oscillations $1/\nu_0$. In the spatial representation, the distance between pulses in vacuum and in the absence of diffraction divergence is equal to the optical length of the complete passage of the laser cavity L, from which another representation of the pulse repetition frequency arises: $f=c/L$, where c is the group velocity of light. In the general case, there is a phase shift φ between the envelope and the carrier. The slippage of the carrier envelope offset phase φ for the neighboring $(i+1)$-th and i-th pulses will be equal to

$$\Phi = \varphi_{i+1} - \varphi_i \tag{2}$$

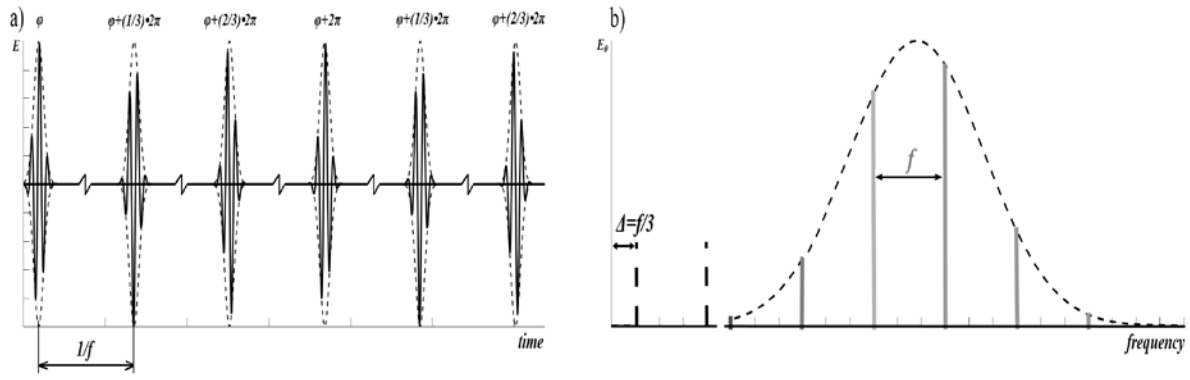

Fig. 1 The femtosecond pulse train (a) and their radia tion spectrum (b).

It can be shown that with the relation

$$k/q = f/\Delta, \tag{3}$$

where k and q are integers, when each k-th pulse is extracted from the femtosecond laser radiation a periodic sequence of identical pulses at the repetition frequency is obtained:

$$F = f/k. \tag{4}$$

In this case, the shift of the synthesized comb will be zero, so that the radiation spectrum represents a set of frequencies

$$\nu_p = jF \tag{5}$$

where j is a positive integer, and the number of components of the spectrum is k times larger than the same of radiation at the output of a femtosecond laser with the same width of the spectrum.

The minimum values of the time and spatial spacing between pulses in the synthesized sequence is realized for $k=3$, when $\delta=\pm 1/3$. Fig. 2a shows the propagation of such femtosecond pulses. In comparison with the radiation of a femtosecond laser (Fig. 1a), in the synthesized pulse train the interval between pulses increases three-fold, while the frequency interval between the spectral components becomes three times smaller, and the carrier envelope offset phase for each pulse becomes unchanged which leads to a situation where there is no shift in the frequency comb (Fig. 2b).

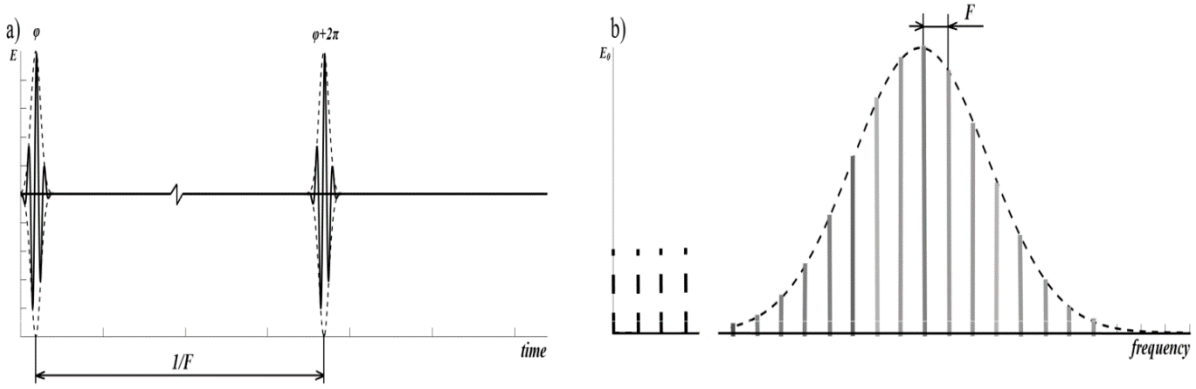

Fig. 2 Periodic sequence of synthesized femtosecond pulses (a) and their radiation spectrum (b).

Of all possible pulse sequences, the carrier envelope offset phase can be selected with a discreteness $2\pi/k$ from the minimum value $\varphi_{min} \leq 2\pi/k$ to 2π

The periodic sequence described above can be realized with a femtosecond laser. Frequencies f and F are set with the help of two synthesizers, the reference frequency for which is fed from the same standard. The signal at frequency F through the phase shifter came to a pulse generator that controlled the intensity modulator, at the output of which a sequence of identical femtosecond pulses with a repetition frequency F was synthesized. The phase shifter made it possible to extract a sequence of pulses with a predetermined phase difference between the carrier and the envelope.

The work was supported by the Ministry of Education and Science of the Russian Federation within the framework of a base part of the state task (the Project No. 3.6835.2017/8.9) and by Russian Foundation for Basic Researchers (Grant No. 18-02-00316).

References

[1] Bohan A.D., Antoine P., Milosevic D.B., Piraux B., Phys. Rev.Lett. **81**, 1837 (1998).
[2] Ivanov M., Corcum P.B., Zuo T., Bandrauk A., Phys. Rev. Lett. **74**, 2933 (1995).
[3] Christov I.P., Murnane M.M., Kapteyn H.C., Phys. Rev. Lett. **78**, 1251 (1997).
[4] Udem Th., Reichert J. Holzwarth R., Hänsch T.W. *Phys. Rev. Lett.,* **82**, 3568 (1999).

Diode laser with HF modulation of pump current for lasing of CPT resonances

A. Isakova[1], K. Savinov[1], N. Golovin[1], A. Dmitriev[1,2]
[1]*Novosibirsk State Technical University, 630073, Novosibirsk, Russia*
[2]*Institute of Laser Physics, Siberian Branch of Russian Academy of Science, 630090, Novosibirsk, Russia*
E-mail: alexander_dmitriev@ngs.ru

The use of semiconductor lasers with an external resonator for pumping a rubidium cell allows the creation of a combined frequency standard in both the optical and microwave ranges [1]. However, in this case, the amplitude of the high-frequency component was lower in the entire frequency range than the low-frequency component. This is results in a field shift.

It was suggested to use the multifrequency radiation of a femtosecond laser to reduce the field shifts of the resonances of coherent population trapping (CPT) [2]. However, there are no data on successful experiments. This is due to the fact that the emission spectrum of a femtosecond laser is many times greater than the width of the optical transitions used to pump the CIT of resonances, that leads to a low signal-to-noise ratio.

In this paper, we propose and implement a method for obtaining multifrequency optical radiation for pumping the CPT resonances with high-frequency modulation of the power supply current of a semiconductor laser with an external resonator.

The radiation spectrum was recorded on a scanned Fabry-Perot interferometer. A detailed description of the scheme of the installation is given in [1].

The emission spectrum for HF modulation was studied at different pump currents (from 45 mA up to 53 mA) and the power of the HF generator up to 10 dBm at frequencies of 34, 68, and 85 MHz. Figure 1 shows the recording of the emission spectra at different pump currents at an HF signal of 4 dBm and a frequency of 68 MHz.

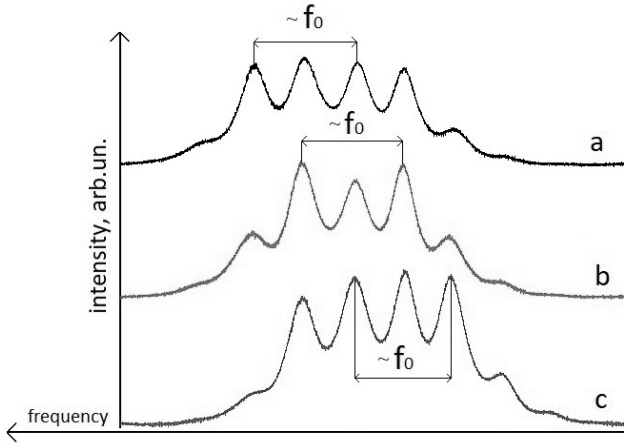

Fig. 1 The laser emission spectrum at pump currents: a – 45.8 mA, b – 47 mA, c – 49.4 mA.

The spectrum structure is given by laser intermode spacing, doubled value of which approximately equal to clock transition frequency. Equal intensity of spectrum components, divided by clock transition frequency, is observed on different pump current. At certain values of the pump current, it is also possible to achieve the equality of the amplitudes of the spectral components separated by the frequency of the clock transition (Fig. 2), which leads to a decrease in the field shift.

The difference in frequencies between these components of the spectrum is shown in Fig. 3. For certain parameters, the difference is equal to the frequency of the clock transition (6.8 GHz).

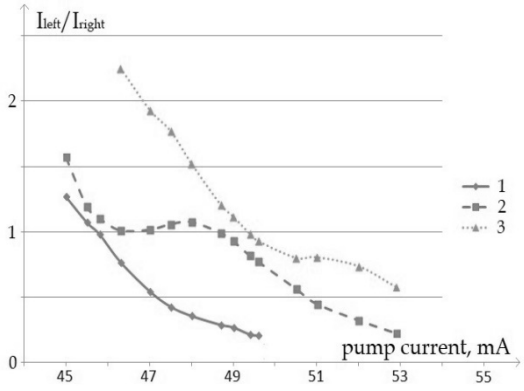

Fig. 2 The ratio of the amplitudes of the spectrum components spaced by the frequency of the clock transition as a function of the pump current (68 MHz, 4 dBm).

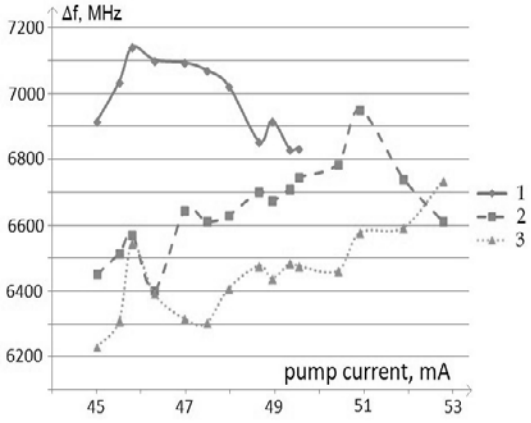

Fig. 3 The interval between the components of the spectrum spaced by the frequency of the clock transition (68 MHz, 4 dBm).

Similar studies were conducted with a change in the power and frequency of the HF generator. At each frequency, the amplitudes of the spectral components, spaced by the frequency of the clock transition, were equal (Fig. 4)

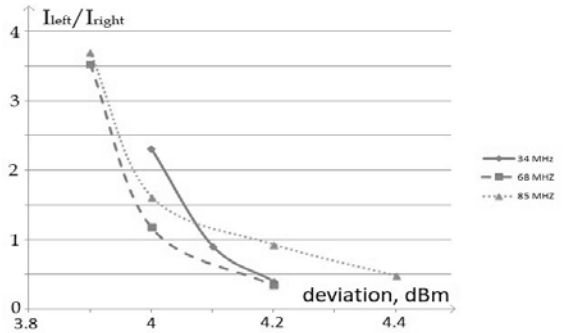

Fig. 4 The ratio of the amplitudes of the components of the spectrum, separated by the frequency of the clock transition, depending on the power of the RF generator, I = 65 mA.

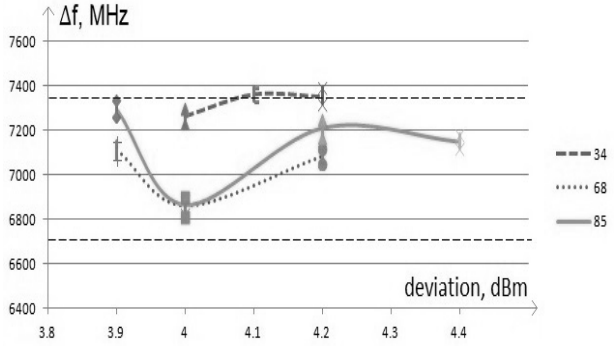

Fig. 5 The interval between the components of the spectrum spaced by the frequency of the clock transition, I = 65 mA.

The dependence of the frequency interval between these components on the frequency and modulation power is shown in Fig 5. For all HF frequencies, the envelopes of spectral components are separated by the laser intermode interval. The value of the interferometer bandwidth, equal to 1.1 GHz, didn't allow the "fine" laser emission spectrum components to be resolved, the interval between which is set by the frequency of the HF modulation.

Regimes for generating a diode laser in the case of HF modulation of the pump current with a radiation spectrum are obtained, the envelopes of the components of which are separated into intervals determined by the length of the external laser cavity. It has been experimentally demonstrated that under certain conditions an equal intensity of the optical frequencies can be achieved which can be used to pump CPT resonances, which allows eliminating their field shifts.

The work was supported by the Ministry of Education and Science of the Russian Federation within the framework of a base part of the state task (the Project No. 3.6835.2017/8.9) and by Russian Foundation for Basic Researchers (Grant No. 18-02-00316).

References

A. Isakova et al., Quantum Electronics **47(7)**, 610 (2017).
E. Baklanov, A. Dmitriev, Laser Physics **20 (1)**, 52 (2010).

Plasma parameters derived from spectrally resolved optical measurements

M.A. Efimov[1], M.S. Rumenskyh[1,3], A.A. Chibranov[1], A.G. Berezutsky[1], and I.B. Miroshnichenko[1,2]
[1]*Institute of Laser Physics SB RAS, Novosibirsk, Academician Lavrentiev st. 13/3, Russia*
[2]*Novosibirsk State Technical University, Novosibirsk, K. Marx st. 20, Russia*
[3]*Novosibirsk State University, Novosibirsk, Pirogova st. 2, Russia*
E-mail: mikle3496@gmail.com

The processes occurring in the Earth ionosphere-magnetosphere are difficult to modeling, and it is impossible to create physical models describing the interaction of cosmic plasma with external disturbances such as background plasma and a magnetic field, without experimental verification in the laboratory. Department of laser plasma of ILP SB RAS conducts experiments with laser plasma to simulate fast processes in the near-Earth space environment.

An important parameter is the velocity of various ionic components of the laser plasma. One of the methods for measuring the velocity is the Doppler broadening and the shift of the spectral lines [1]. In particular, this makes it possible to measure the transverse component of the velocity and the angle of propagation of the plasma flame relative to the normal of the target [2]. Applied (C_2H_4) target during ablation give hydrogen and carbon ions of different charges [3], which have a different expansion cone. Measurement of this effect is possible only by spectral methods with the use of a CCD ruler to register the profile of the spectral line.

At the KI-1 facility the processes of laser plasma propagation in a magnetic field of the order of B = 300 G and without was simulated. Plasma radiation was focused by a system of mirrors and lenses on the input slit of the monochromator. Spectrally resolved luminosity was focused on the CCD ruler, and the image sent to the computer. After analyzing a number of the registered spectral lines, we calculated the broadening of the individual spectral lines by the Doppler formula and found the propagation velocities of the ions from the target normal from the formula $\Delta\lambda/\lambda=\Delta V/c$.

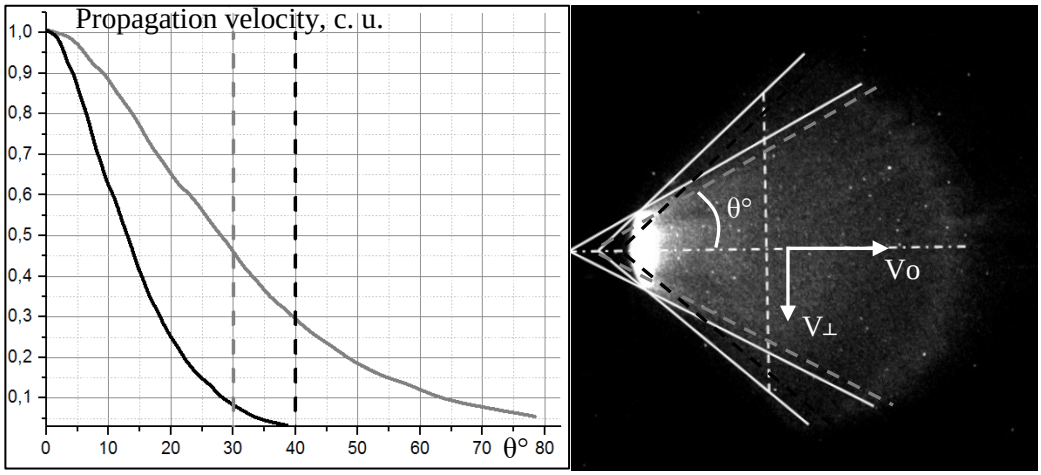

Fig. 1

Figure 1. Velocity profiles on the angle of propagation relative to the target normal derived from the line profile of Hα line of hydrogen (656.3 nm) The grey solid line shows the profile assuming simplest model $V_\perp$=const, while the black line - $V_\perp/V_o \sim \cos(\theta)$, where V_o is velocity along the target normal. The black vertical dashed line indicates the observed boundary of the plasma plume shown at the image, the grey dashed line – the boundary of more extended halo. Right panel shows picture of plasma plume obtained by gated imager.

We calculated the angular distribution of expansion cone of ions assuming different models of relations of transverse velocity to the normal expansion velocity, such as $V_\perp/V_o \sim\cos(\theta)$. These

distributions have been compared with plasma images. We also analyzed the spectral lines at various distances from the target and made conclusions on plasma interaction with magnetic field.

The work was supported by the RNF grant №18-12-00080, RFBR grant №18-32-00029 and SB RAS basic research project II.10 №0307-2017-0015.

References

[1] Shaikhislamov I. F., Antonov V. M., Zakharov Yu. P., Melekhov A. V., Posukh V. G., Stoyanovsky V. O. Application of the charge exchange process in the spectral diagnostics of the interaction of a laser plasma with a dipole magnetic field. PMTF, t.36, N4 (1995).

[2] I. F. Shaikhislamov. Kinetics of the process of charge exchange of dense flows. PMTF, t.41 (2000).

[3] Shaikhislamov, I. F., V. M. Antonov, Yu. P. Zakharov, E. L. Boyarintsev, A. V. Melekhov, V. G. Posukh, and A. G. Ponomarenko. "Laboratory simulation of field aligned currents in an experiment on laser-produced plasma interacting with a magnetic dipole." Plasma Physics and Controlled Fusion 51, No 10 (2009): 105005.

Exploring quantum thermodynamics on a single qubit

F. Zhou, L.L. Yan, T.P. Xiong, K. Rehen, and M. Feng
Wuhan Institute of Physics and Mathematics, Chinese Academy of Sciences, Wuhan, China
E-mail: mangfeng@wipm.ac.cn

Thermodynamics conventionally applies to macroscopic world, which concerns with heat and temperature as well as their relation to other forms of energy and work. Recently, much effort has been devoted to incorporating information into thermodynamics and assessing the entropic and energetic costs of manipulating information even at quantum level [1]. From the quantum perspective, the origin of fluctuations is no longer just thermal but also quantum, and most thermodynamic quantities should be retraced.

Here we report two of our recent experiments accomplished in an electro-magnetic trap, relevant to Jarzynski–related equalities in an non-equilibrium thermodynamic process and to the Landauer principle. Our operations are made on a single $^{40}Ca^{+}$ ion confined in a linear Paul trap, which has been cooled to be ultracold. We achieve precise manipulation of quantum states of the ion, including arbitrary quantum-state preparation, laser-controlled quantum-state time evolution, laser-phase modulation and arbitrary projection measurement. In the first experiment [2], we focus on a qubit encoded in two levels of the ion and show that the information-theoretic equalities, including the Jarzynski equality, could work nearly perfectly at the fundamental level of a single spin. In the second experiment [3], we consider a quantum Landauer principle by employing the two levels of the ion as the qubit and the vibrational degree of freedom of the ion as a finite-temperature quantized reservoir. Our experimental observation shows that the Landauer principle still holds even at quantum level after some modification by introducing quantum information quantities.

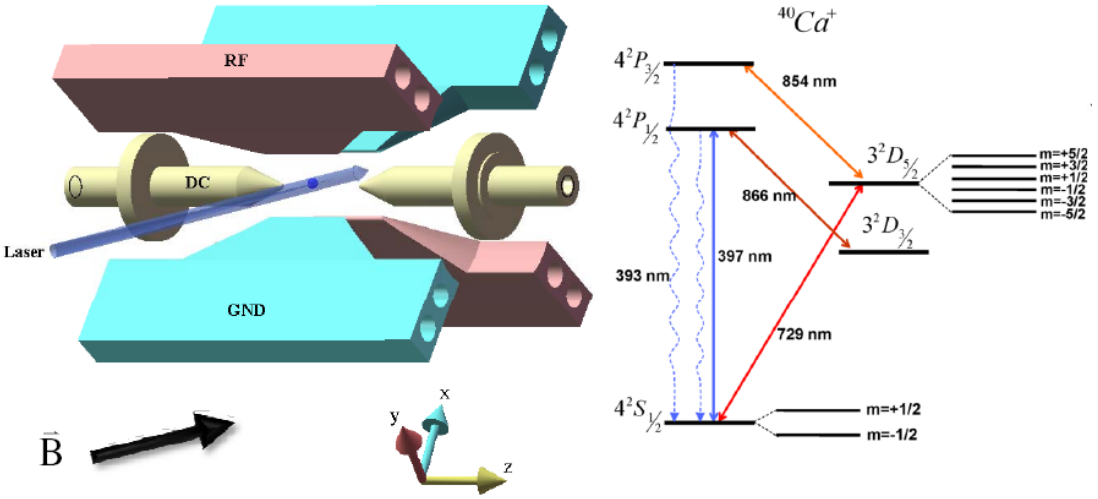

Fig. 1 (Left panel) Schematic of our device with a single ion confined under laser irradiation. (Right panel) Level scheme in our experiment.

Our experimental investigation substantiates an intimate link between information thermodynamics and quantum candidate systems for information processing, and helps for further understanding thermodynamic processes in quantum regime.

References

[1] J. M. R. Parrondo, J. M. Horowitz and T. Sagawa, "Thermodynamics of information", Nat. Phys. **11**, 131 (2015).
[2] T. P. Xiong, L. L. Yan, F. Zhou, K. Rehan, D. F. Liang, L. Chen, W. L. Yang, Z. H. Ma, M. Feng and V. Vedral, Phys. Rev. Lett. **120**, 010601 (2018).
[3] L. L. Yan, T. P. Xiong, K. Rehan, F. Zhou, D. F. Liang, L. Chen, J. Q. Zhang，W. L. Yang, Z. H. Ma, and M. Feng, Phys. Rev. Lett. **120**, 21060 (2018).

Reflection of light on a metal – dielectric boundary in FTIR

N.D. Goldina
Institute of Laser Physics SB RAS, Novosibirsk, 630090, Russia
E-mail: ngold@laser.nsc.ru

Consider an oblique incidence on the boundary quartz ($n_g = 1.46$) – air ($n_a = 1.0$). At angles of incidence greater than the critical angle ($\theta > \theta_{cr}$), total internal reflection (TIR) occurs [1, 2]. The field in the external medium exponentially decreases with increasing distance from the boundary. The angle of refraction θ_a is purely imaginary: $cos\theta_a = -i\sqrt{\left(\frac{n_g sin\theta_g}{n_a}\right)^2 - 1} = -iM$. Amplitude reflection coefficients for *p*- and *s*-polarizations are written in the form: $r = \frac{n_g - Y_a}{n_g + Y_a}$, where for the *p*-polarization: refractive index $n_{gp} = \frac{n_g}{cos\theta_g}$, admittance $Y_{ap} = \frac{n_a}{cos\theta_a} = \frac{in_a}{M}$ and for the *s*-polarization: $n_{gs} = n_g cos\theta_g$, $Y_{as} = n_a\, cos\theta_a = -in_a M$. The figures show the angular dependence of the real and imaginary parts of *Y* (Fig. 1) and *r* (Fig. 2) for *p*-polarization. At the incidence angles $\theta > \theta_{cr}$ admittances Y_{ap} и Y_{as} – are purely imaginary numbers ($Re\ Y_{ap} = Re\ Y_{as} = 0$).

The addition of thin metal film leads to the appearance of FTIR. To describe properties of metal we used the complex surface conductivity model, in which the metal layer is characterized by complex conductivity $\xi = \xi' + i\xi''$, where $\xi' = 2nk\gamma$, $\xi'' = (n^2 - k^2)\gamma$, $\gamma = 2\pi d/\lambda$ (*n-ik* – refractive index, *d* – film thickness).

For specific calculations is selected the aluminum film: $\xi = \xi' + i\xi'' = 1.8 + i6.7$ (*n*=0.8-i6.0, d= 16nm, λ= 532 nm). In the formula for the amplitude reflection coefficient, instead Y_a, will be sum $(Y_a + \xi)$: $r = \frac{(n_g - \xi' - ReY_a) - i(ImY_a + \xi'')}{(n_g + \xi' + ReY_a) + (ImY_a + \xi'')}$.

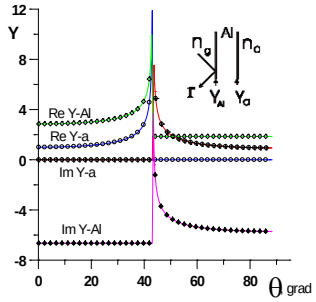

Fig. 1

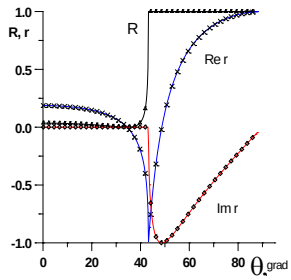

Fig. 2

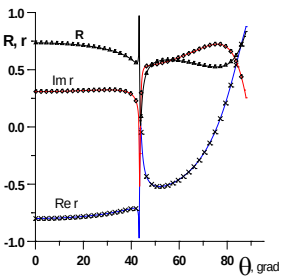

Fig. 3

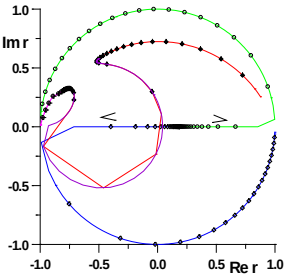

Fig. 4

Fig. 1 - the angular dependence of the real ReY_{ap} and imaginary ImY_{ap} parts for *p*-polarization. ImY_{ap} falls off as the angle increases ($ImY_{ap} > 0$). With the addition of a metal film (ξ''=-i6.7) the curve $Im\ Y_{Al}$ intersects the real axis at angle of $\vartheta = \theta_{min}$, when the condition $\xi'' + Im\, Y_{ap} = 0$ is fulfilled.

Fig. 2 and 3 - At a critical angle $ReY_{ap} = ImY_{ap} = 0$, and with a further increase in the angle an effect FTIR occurs: $R_p = (Re\ r_{ap})^2 + (Im\ r_{ap})^2 = 1$. Changes R_p in the addition of a metal film are shown in Fig. 3. In the region of the critical angle, sharp changes occur: the curve $Im\ Y_p$ intersects the real axis at an angle $\vartheta = \theta_{min}$, the minimum R_p tends to zero when the matching condition $n_{gp} = \xi'$ is satisfied.

Fig. 4 - The changes in the amplitude reflection coefficient for *p*- and *s*-polarization with increasing angle are more clearly visible on the complex plane *r*. From point $Re\ r_{ap}$ =0.18, the curves for r_{ap} and r_{as} diverge in opposite directions. At the critical angle the curves reach the unit circle, on which to make a half-turn for angle range $\theta = \theta_{cr}$-90°: r_{ap} - clockwise (blue curve), r_{as} – counter-clockwise (green) in increments of 0.22 degrees. Changes *r* with addition a metal film are shown red

curve (and with a small step 0.04 ° - lilac curve). For *s*-polarization, the change in the *r* is small (pink curve).

As shown in the fig .3, the reflection coefficient R_p reaches a sharp minimum in the area of a critical angle. The slope of the curve is proportional to the change of imaginary part ImY_{ap} for *p*-polarization at the boundary of the two dielectrics and to the magnitude of imaginary part ξ'' of the complex surface conductivity.

References

[1] N. D. Goldina, V.S. Terent'ev, V.A. Simonov. Opt. Spectrosc. **120**(5), 796 (2016).
[2] H. A. Macleod, Thin-Film Optical Filters (CRC, Taylor Francis, Boca Raton, FL, 2010).

Investigation of oxipane optical properties in THz frequency range

D. Gomon, P. Demchenko, and M. Khodzitsky
ITMO University, 49 Kronverksky Pr., St. Petersburg, 197101, Russia
E-mail: GomonDA89@ya.ru

THz radiation is widely used in such areas as telecommunications, radar and imaging systems, material spectroscopy, medical diagnosis and therapy. Compact tunable components for THz devices could make these technologies cheaper and more common for use in those areas [1]. Nowadays scientists over the world develop different solutions for production of tunable components by such materials as graphene, liquid crystals, vanadium oxide (VO_2), graphene oxide, carbon nanotubes [2].

Oxipane is an innovation high-temperature non-woven material from chopped polyacrylonitrile fiber. Oxipane could be used as a protective layer for such applications as heat protection [3, 4] and gas filters. It can be used as an efficient heat protection in the temperature regime below 300-450 °C. Upon the action of temperatures higher than 450 °C oxipane retains its physical and protection properties, doesn't burn, doesn't melt, doesn't flow, doesn't maintain combustion. In the heat insulation regime, oxipane works in the temperature range from 300 to 450 °C, and it sustains open fire for 10–15 min at 700 °C. Manufacturing of gas filters: oxipane filters vapors and aerosols of acids, alkalis, and solvents, including those heated to 450 °C. That why oxipane is perspective candidate for sewing of working clothes: an oxipane lining possess a low heat conductance and, as a consequence, possesses a decrease in the thermal effect on the human organism.

Material oxipane may present effective absorbance in THz frequency range. That means that oxipane could be used for THz radiation screening.

In this paper we investigate the oxipane optical properties (such absorbance, permittivity, refractive index) in THz frequency range using THz time domain spectroscopy [5]. We studied two oxipane samples with different density: (95 and 110 g/m^2). Their absorbance, permittivity and refractive index spectra are shown in Fig. 1.

It is clearly seen from Fig 1 (a, b) that absorbance increases while increasing radiation frequency and it reaches maximal values of 9 cm^{-1} (a) and 11 cm^{-1} (b) at the frequency of 1 THz. Therefore absorbance increases with an increase in oxipane density. In this way oxipane layer with high density could be used for THz screening. Oxipane permittivity and refractive index values close to air properties, so oxipane layer doesn't make a phase delay, only absorb part of radiation.

So an oxipane material shows necessary optical properties to construct compact THz devices.

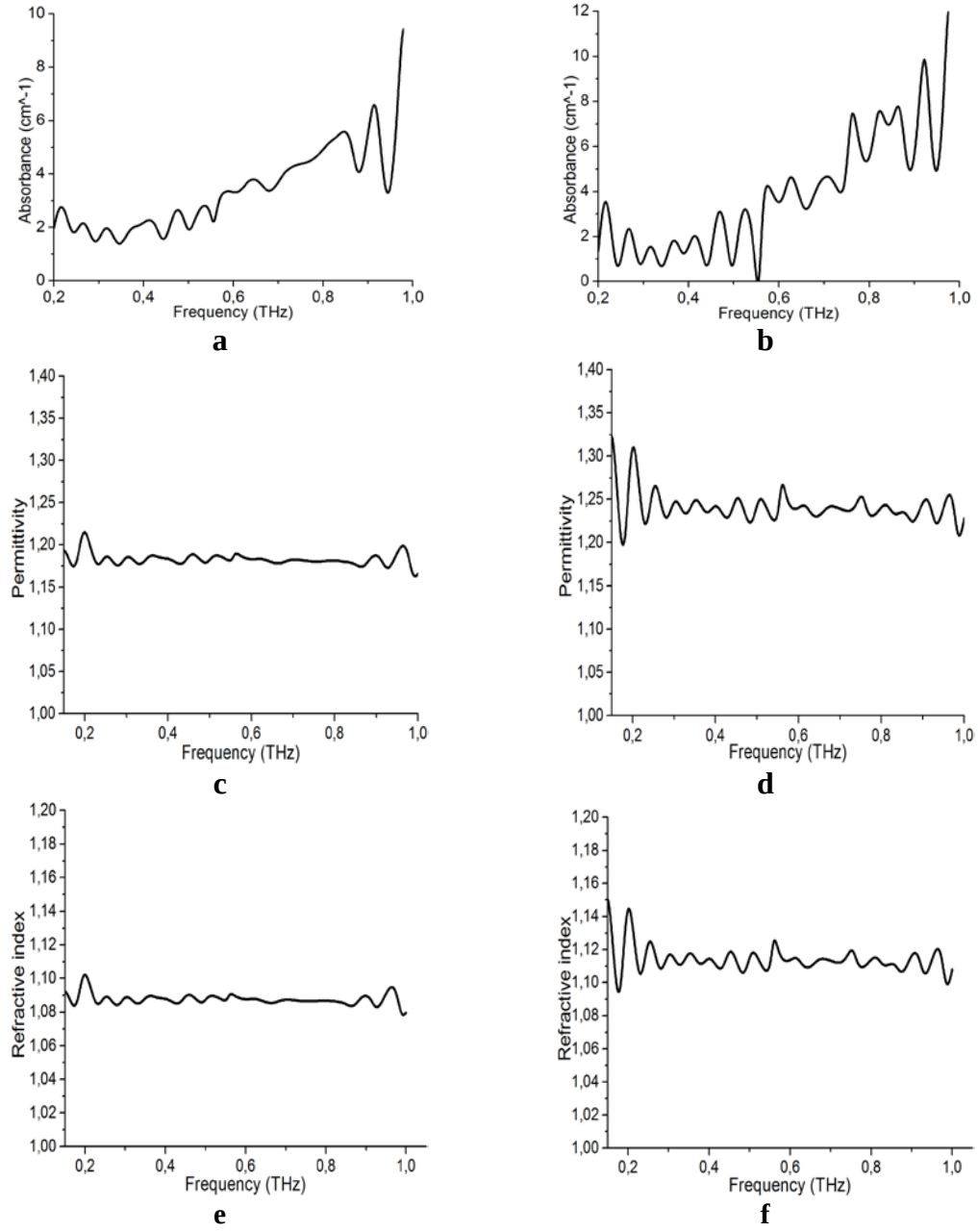

Fig. 1 Absorbance, permittivity and refractive index spectra of experimental samples with different density: 95 (a, c, e).and 110 (b, d, f) g/m^2.

References

[1] Gomon, Daniel, et al. "Influence of the geometric parameters of the electrical ring resonator metasurface on the performance of metamaterial absorbers for terahertz applications." *Chinese Optics*11.1 (2018): 47-59.]

[2] Smirnov, S., Anoshkin, I. V., Demchenko, P. S., Gomon, D., Lioubtchenko, D., Khodzitsky, M. K., & Oberhammer, J. "Optically Controlled Dielectric Properties of Single-Walled Carbon Nanotubes for Terahertz Wave Applications." *Nanoscale* (2018).

[3] Kang, Tae Jin, et al. "Effect of punching density on the mechanical and thermal properties of needle-punched nonwoven carbon/phenolic composites." *Polymers & polymer composites* 10.7 (2002)

[4] Lee, Jae Yeol, and Tae Jin Kang. "Thermal conductivity of needle punched preforms made of carbon and OxiPAN fibres." *Polymers and Polymer Composites* 13.1 (2005): 83-92.

[5] Zaitsev, K. I., et al. "Terahertz spectroscopy of pigmentary skin nevi in vivo." *Optics and Spectroscopy* 119.3 (2015): 404-410.

Glucose level sensor based on metasurface in THz frequency range

S. Gusev, V. Soboleva, and M. Khodzitsky
ITMO University, St.Petersburg, Kadetskaya line VO, 3b, Russia
E-mail: mail@gusev-spb.ru

There is still lack of non-invasive technique of glucose level measuring [1]. In our previous works there were shown correlation of glucose concentration and optical properties *in vitro* measurements in THz frequency range [2,3], which is widely used in biomedical diagnostics [4,5]. In addition, in order of non-invasive technology establishing we made numerical simulation of non-invasive experiment [6]. This article represents using other approach to detect correlation between optical properties and glucose concentration. Represented work is focused on investigation of correlation between blood glucose concentration and resonance frequency shift of layered sample structure, which includes metasurface and whole human blood.

Metasurface used in this work meant as metal thin film with carved off cross-shaped holes. Size of these holes is comparable with radiation wavelength. Such resonators can be described by three parameters: period (P), length (L) and width (W) are shown in Fig. 1.

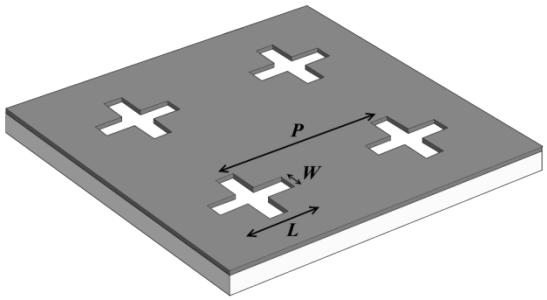

Fig. 1 Scheme of band-pass metasurface.

Metasurface filters with flexible substrate are the most suitable for biosensing tasks. Due to this fact, our filter was composed from polymethylmethacrylate (PMMA) flexible substrate with a thickness of 68 μm, and aluminum metasurface with a thickness of 0.5 μm.

The general spectral parameters of filter are: transmission resonant frequency f_r (frequency of maximal transmission), Q-factor (which is equal to the ratio of the resonant frequency f_r to the bandwidth Δf). The main influencing factor on the resonant frequency f_r (and as a result on the Q-factor) is the metasurface resonators period *P*. Numerical simulation using COMSOL Multiphysics showed that increasing of resonators period *P* entails decreasing of bandwidth Δf and non-linear growth of Q-factor.

The results of the simulation are shown in Fig. 2 and represent following correlation: increasing of blood permittivity (and increasing glucose level) corresponds to increasing shift of resonance frequency to lower values.

Results of simulation show, how resonance frequency shift has linear dependence on refractive index (Fig. 3a). There is different sensitivity of biosensors with different spectral characteristics: the highest sensitivity level detected for filter with resonance frequency f_r of 0.5 THz. Changing of glucose concentration at 1 mmol/l corresponds to 103 GHz.

This work represents possibility of using band-pass filter based on cross-shaped resonators as high-sensitivity sensor for blood glucose concentration estimation. Dispersions of permittivity for samples with different glucose concentration had been used to create numerical model of experiment with whole blood and THz filters. Numerical simulation in COMSOL Multiphysics brought transmission spectra of filters (PMMA + Al) and reflection spectra of layered structures (PMMA + Al + whole blood).

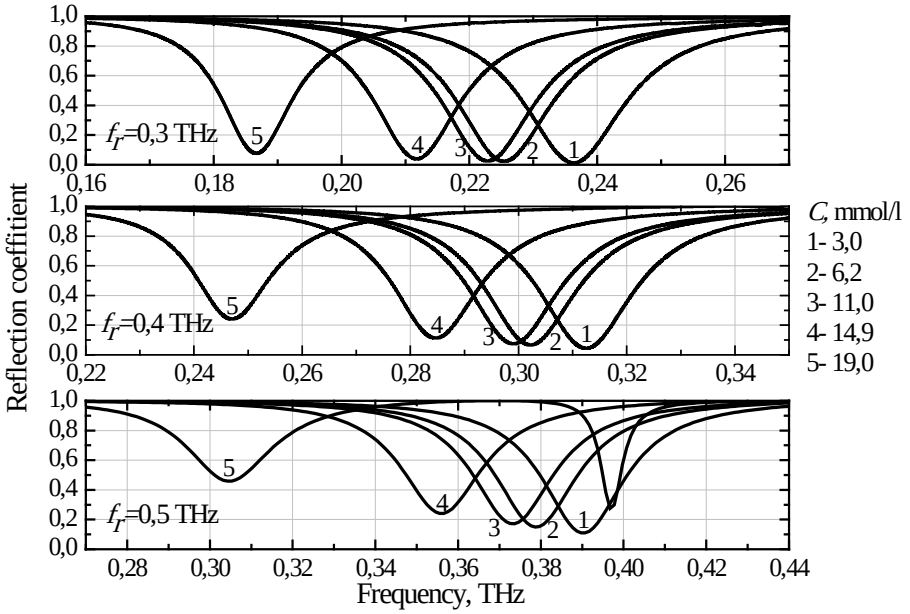

Fig. 2 Resonance frequency shift of biosensors after contact with blood samples with different glucose concentration.

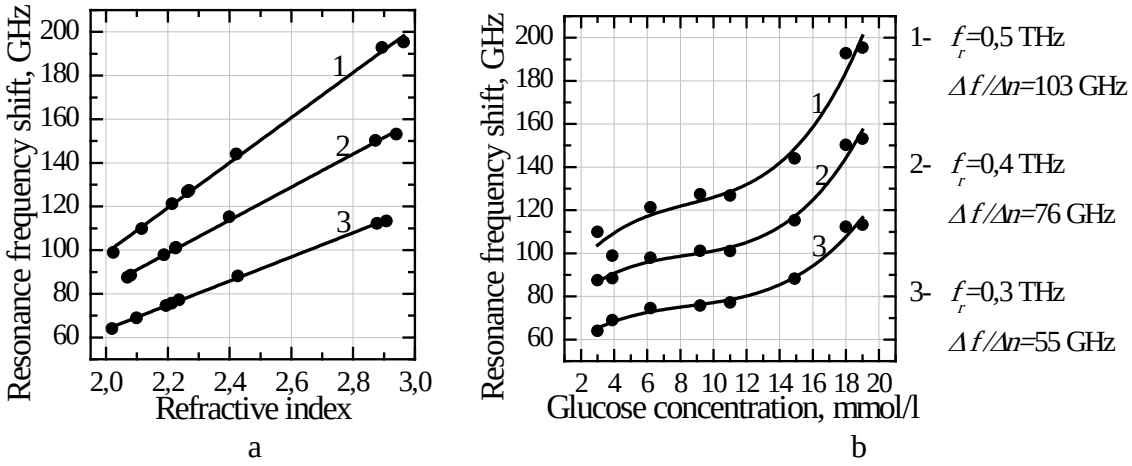

Fig. 3 Dependence of biosensor resonance frequency shift on blood refractive index (a); on blood glucose concentration (b).

The highest sensitivity level had been observed for filter with resonance frequency of 0.5 THz: sensitivity of 2.0 mmol/l for concentration range of 8-12 mmol/l and sensitivity of 0.5 mmol/l for concentration range of 12-19 mmol/l. This numerical experiment uses time domain THz spectroscopy approach, which maximal resolution is about 5 GHz. Using continuous-wave spectrometer could improve resolution up to 1 kHz. Other approach to increase sensitivity is using filters with higher resonance frequency.

References

[1] J. L. Smith The pursuit of noninvasive glucose: Hunting the deceitful turkey (2015).
[2] S. I. Gusev, M. A. Borovkova, M. A. Strepitov et al., Proc. of SPIE-OSA **9537**, 95372A (2015).
[3] S. I. Gusev, P. S. Demchenko, O. P. Cherkasova et al., Chinese Optics **11**(2), 182 (2018).
[4] M. Borovkova, M. Serebriakova, V. Fedorov et al., Biomedical optics express **8**(1), 273 (2017).
[5] M. Borovkova, M. Borovkova, M. Khodzitsky et al., Biomedical optics express **9**(5), 2266 (2018).
[6] S. I. Gusev, P. S. Demchenko, E. A. Litvinov et al., Nanosystems: Physics, Chemistry, Mathematics **9**(3), 1 (2018).

Optimization of deep laser cooling of atoms on narrow-line optical transitions in standing wave

R. Ilenkov[1,2], O.N. Prudnikov[1,2], A.V. Taichenachev[1,2], and V.I. Yudin[1-3]
[1]*Institute of Laser Physics SB RAS, 630090, Novosibirsk, Ave. Ac. Lavrentieva 15B, Russia*
[2]*Novosibirsk State University, 630090, Novosibirsk, Str. Pirogova 2, Russia*
[3]*Novosibirsk Technical State University, 630073, Novosibirsk, Karl Marx Avenue 20, Russia*
E-mail: ilenkov.roman@gmail.com

The theoretical description of the kinetics of neutral atoms in the polarized light fields with all the atomic levels, the coherence, the recoil effect is both important and challenging problem. The first step toward understanding mechanisms of interaction between atoms and light was called quasi-classical approach. [1,2] It lies in the fact that the equations for the density matrix can be reduced to the Fokker-Planck equation for the Wigner function in the phase space. But the semiclassical approximation is inapplicable for investigating the cooling of atoms at clock transitions, because the quasiclassical parameter (the recoil frequency) is not small (in comparison with the natural line width). Later quantum methods were developed [3], for example, the secular approach which describes cooling and localization of atoms in the optical potential. Secular approximation fails high vibrational levels and for atoms in high vibrational states.

We have developed an own quantum method [4] to obtaining the stationary distribution of two-level atoms in a standing wave of arbitrary intensity, allowing full account the recoil effects. The quasiclassical regimes of laser cooling of atoms have been studied in sufficient detail, but the attention given to quantum regimes is not enough. Hundreds of calculations for Ca, Sr, Mg have been carried out which have made it possible to reveal some interesting and completely new regularities that open up new prospects for laser cooling of atoms on weak optical transitions. If in the semiclassical regime the Rabi frequency (Ω_0), detuning (δ) and recoil frequency (w_r) is conveniently expressed in units of spontaneous relaxation (γ), then in the quantum ($w_r \sim \gamma$) and ultraquantum ($w_r >> \gamma$) it changes radically. If we express these parameters in units of recoil frequency, then we obtain the absolute universality of stationary distributions of ^{24}Mg ($w_r = 1100\gamma$), ^{40}Ca ($w_r = 32.3\gamma$), ^{88}Sr ($w_r = 0.635\gamma$) atoms cooled on optical transitions (Fig.1). Narrow peaks in the momentum distribution are the manifestation of a selective coherent population trapping rate (VSCPT) at points corresponding to the momentum of one photon, observed in a weak light field.

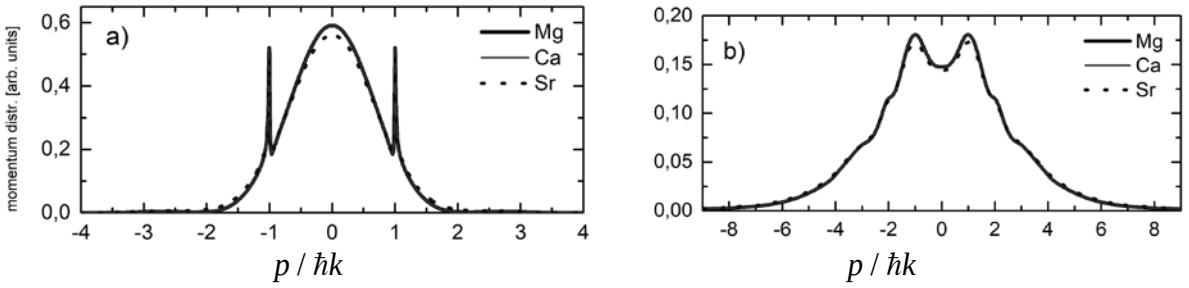

Fig. 1 The steady-state state momentum distribution of different atoms (^{24}Mg, ^{40}Ca, ^{88}Sr). Light field detuning: $\delta = -3w_r$. Rabi frequency of one wave: a) $\Omega_0 = 0.64w_r$ b) $\Omega_0 = 6.4w_r$.

A minimum temperature of laser cooling in a weak light field was searched (Fig.2). Fig. 2a shows the impulse distributions for various detunings. In case of small detuning, extremely strong manifestations of VSCPT can be observed at points corresponding to the momentum of one photon. The minimum temperature of the impulse distribution is reached when the detuning is equal, in absolute value, to three units of the recoil frequency.

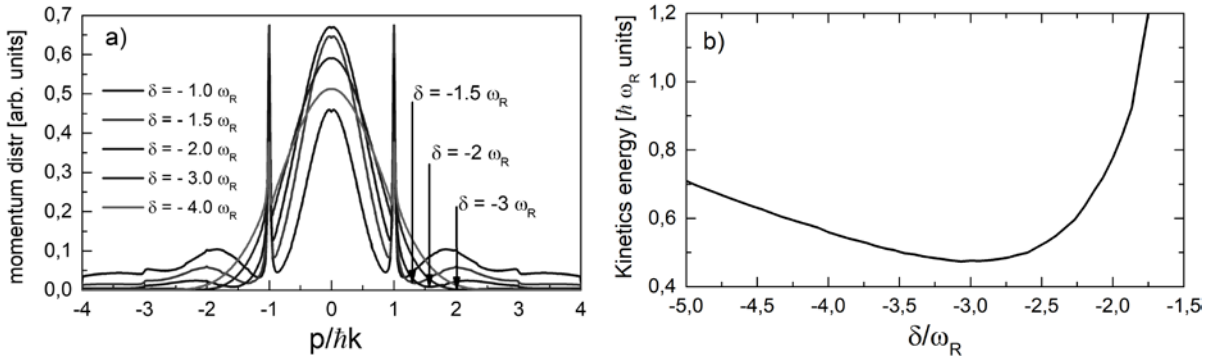

Fig. 2 a) The steady-state state momentum distribution for different light field detuning b) dependence of kinetic energy of atoms on the detuning of the light field. Rabi frequency of one wave: $\Omega_0 = 0.64 w_r$.

The time and kinetic energy of atoms as a function of the intensity of the light field is shown in Fig 3. The cooling time is determinated by the slowest processes of evolution of atomic density matrix. In semiclassical limit it is scaled by w_r^{-1} units. In quantum regime of laser cooling the cooling time can be expressed in universal form for different atoms and scaled in by γ^{-1} units. The cooling time depends on the width of the initial momentum distribution of the atoms. Initial momentum distribution for magnesium atoms is of the order of 1 mK. For a larger initial temperature, the time increases linearly.

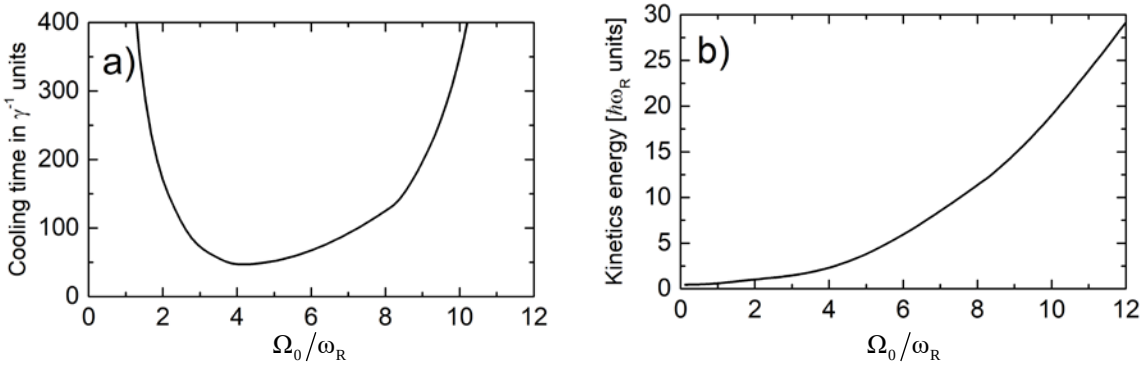

Fig. 3 Dependences of a) time of laser cooling of atoms b) kinetic energy of atoms on the intensity of light field for optimal light field detuning: $\delta = -3 w_r$.

Investigation show that there is a narrow region of intensity of the light field, which allows dramatically reduce the time of laser cooling and achieve ultra-low temperatures, on the order of 3 - 15 μK. The most significant result of the research is the complete equivalence of time, temperature, and stationary impulse and spatial distributions of various atoms cooled on clock optical transitions, with the correct choice of the frequency of the detuning of the light field $\delta = -3 w_r$. Which in turn, enables the cooling of magnesium atoms by a standing light wave that had previously been considered impossible.

The work was personally supported by Russian Science Foundation (project № 17-72-10139).

References

[1] V.G. Minogin, V.S. Letokhov, Laser Light Pressure on Atoms, Gordon and Breach, New York, (1987).
[2] A. P. Kazantsev, G. I. Surdutovich, and V. P. Yakovlev, Mechanical Action of Light on At-oms, World Scientific, Singapore, (1990).
[3] A. Aspect, E. Arimondo, R. Kaiser, N. Vansteenkiste, and C. Cohen-Tannoudji, Phys. Rev. Lett. **61**, pp.826 (1988).
[4] O. N. Prudnikov, R. Ya. Il'enkov, A. V. Taichenachev, A. M. Tumaikin, V. I. Yudin, JETP **112**, pp.939-945 (2011).

Laser structuring of submillimeter metal targets in an ethanol-aqueous solution of various concentrations

D. Kamynina[1,2], V. Kazakevich[1], P. Kazakevich[1], and P. Yaresko[1]
[1]*Samara branch of P.N. Lebedev Physical Institute of the Russian Academy of Sciences, Novo-Sadovaya 221, Samara, 443011, Russia*
[2]*Samara University, Moskovskoe shosse 34, Samara, 443011, Russia*
E-mail: kamyninada@gmail.com

Laser treatment of titanium in water-containing solutions is a promising direction. By this technique both nanoparticles of titanium dioxide and developed surfaces covered with a layer of TiO_2 can be produced. Titanium dioxide exhibit photocatalytic activity, which finds application in the decomposition of organic pollutants [1]. Besides the synthesis of micro / nanostructured surfaces coated with a TiO_2 layer, is proposed to create flow-through filters by laser ablation metod in combination with the electrochemical deposition of films. These filters are structured micron-thickness films with through holes with diameter from hundreds of nanometers up to 1 micron. The implementation of the technique was carried out on nickel, the application of which had already been worked out. Nickel also differs in catalytic activity [2].

To obtain perforated microstructured metal films, the following procedure was used:
1) electrochemical deposition of a nickel layer 6 μm thick on a polished metal substrate. Electrolyte composition: $NiSO_4$+ $7H_2O$ (140-200 g/l), $NiCl_2$+$6H_2O$ (30-40 g/l), H_3BO_3 (25-40 g/l), Na_2SO_4 (60-80 g/l); electrolysis current: 0.5 - 2 A / dm^2; electrolyte temperature range: 20-55 ° C; electrolysis time – 30 minutes;
2) transfer of the formed nickel film to the slide using an acetone-soluble adhesive; transfer to the glass is performed to exclude the sintering of the nickel film from the metal film during subsequent laser processing;
3) laser processing of a nickel film on a slide was performed at dynamically mode in a C_2H_5OH medium (95% and 55%). The speed of the sample moving relative to the laser radiation focusing spot is 30 μm / s, the shift step in the other coordinate is 1.6 μm. The radiation source is the Nd: YAG laser (λ = 1064 nm, τ = 250 ps, ν = 20 Hz, Q = 0.3 mJ, Q_S = 0.4 J / cm^2). The thickness of the liquid layer above the sample is 5 mm;
4) after laser processing the sample was placed in a bath with acetone, as a result of which the structured nickel film was peeled off from the glass substrate;
5) analysis of the structured nickel film was carried out using a scanning electron microscope Carl Zeiss Evo 50, equipped with a nitrogen-free energy-dispersive detector X-Max 80 (EDX).

Figure 1 shows the SEM images of a nickel film obtained and structured according to the technique described above. The irradiated film surface is covered with a developed system of dumbbell structures, characteristic of the laser ablation technique (Fig. 1a). Diameter of structures is from 0.5 to 1 μm, and the height is 5 μm. Investigation of the back side of the film revealed the presence of perforations with a density of 1 perforation at 20 μm^2. The diameter of the holes was from 0.5 to 1 μm (λ / 2, λ).

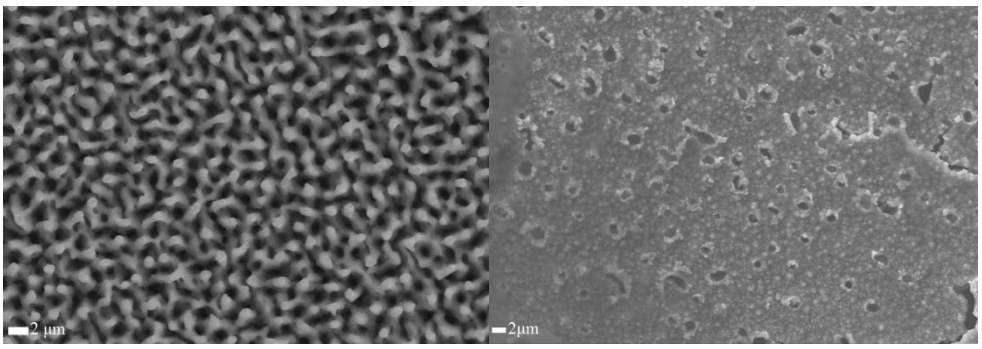

Fig. 1 SEM-image of the structured in C_2H_5OH Ni film (a) the irradiated surface; (b) the back side surface.

The results of the experiment showed the principal possibility of thin perforated metal films synthesis. Irradiation of metals in a water-containing ethanol environment can lead to the formation of developed structures covered with an oxide layer on their surface [3]. Therefore, a further step in the research will be the application of the described technique to titanium samples and the subsequent study of their photocatalytic and filtering properties.

References

[1] K. Nakata, A. Fujishima, J. of Photochemistry and Photobiology C: Photochemistry Reviews **13**, Issue 3, 169 (2012).
[2] S. Pasynkiewicz, E. Oledzka, A. Pietrzykowski, J. Mol. Catalysis. A. **224**, 117 (2004).
[3] V.S. Kazakevich et.al., IOP Science J. of physics **741**, 012188 (2016).

New visible pulse gas-discharge pumped atomic Ne I-laser

A.M. Razhev[1,2], E.S. Kargapol'tsev[1], D.N. Kapusta[1,2], D.S. Churkin[1,3]
[1]*Institute of laser physics SB RAS, Prosp. Ac. Lavrentyeva, 15B, Novosibirsk, Russian Federation*
[2]*Novosibirsk state technical university, Prosp. K. Marksa, 20, Novosibirsk, Russian Federation*
[3]*Novosibirsk state university, Pirogova st., 1, Novosibirsk, Russian Federation*
E-mail: razhev@laser.nsc.ru

The results of an experimental investigation of spectral, energy and temporal characteristics of pulsed gas-discharge high-pressure Ne I-laser are presented. Laser performance with HV excitation system in order to obtain a powerful generation of noble Ne gas electronic transition of gaseous active media without the buffer gas was designed. Laser action on the electronic Ne atoms transition $3p[1/2]_1 - 3s[1/2]_0$ (λ=743.889 nm) with pulse duration (FWHM) 12 ns was obtained and reported for the first time. The laser spectrum is presented by one sharp laser line. Also, the output laser radiation divergence was estimated. The laser action was realized by transverse high-voltage excitation with UV preionization of a high-pressure high purity Ne gas without helium gas.

Gas discharge lasers are most common class of gas lasers, in which for the active media inversion electrical discharges in gases are used initiated by simple compact and electrical excitation circuits. But, despite that in the last decade, this method of pumping paid less attention of researchers. High-pressure lasers on electronic transitions of neutral noble atoms are convenient, multi-purpose high-power laser radiation sources in visible, near and mid-infrared range. The main advantages of these lasers are low lasing threshold; long life of the gas mixture; absence of toxic gas components; the ability to work on a set of wavelengths; high beam quality because of high active media homogeneity; high frequency stability; high output power in a CW mode.

It should be noted a possibility and necessity for effective application of the considered lasers in medicine and in scientific research.

This report will be considered the pulse self-sustained transverse electric discharge with automatic preionization by UV radiation from the sparks of the gas high-pressure laser media on electronic transitions of neutral atoms of noble gases such as neon (Ne).

For excitation of the laser active volume ~ 75 cm^3 the high-voltage electric drive circuit, developed and described by us in earlier publication [1] was used. The laser radiation energy was estimated by the PE50-BB (Ophir Optronics) pulse energy meter. Pulse shape of radiation was recorded using FK-15 photodiode and a digital four-channel oscilloscope Tektronix TDS 2014B. For spectral studies monochromators SpectraPro -500 and Solar laser System S-150 with a set of spectral filters 0.2-1.15 mm were used.

Laser action visible atoms transition laser line at Ne I $3p[1/2]_1 - 3s[1/2]_0$ (λ=743.889 nm) are obtained and reported for the first time (See laser spectrum on the fig.1).

At this moment of the experimental investigation Ne I-laser output pulse energy is too small - about 100 μJ. Total working gas pressure was up to 6.0 atm. The pulse duration Ne I-laser was close to 12 ns (FWHM).

Output laser radiation divergence was estimated and is about 0,3 mrad.

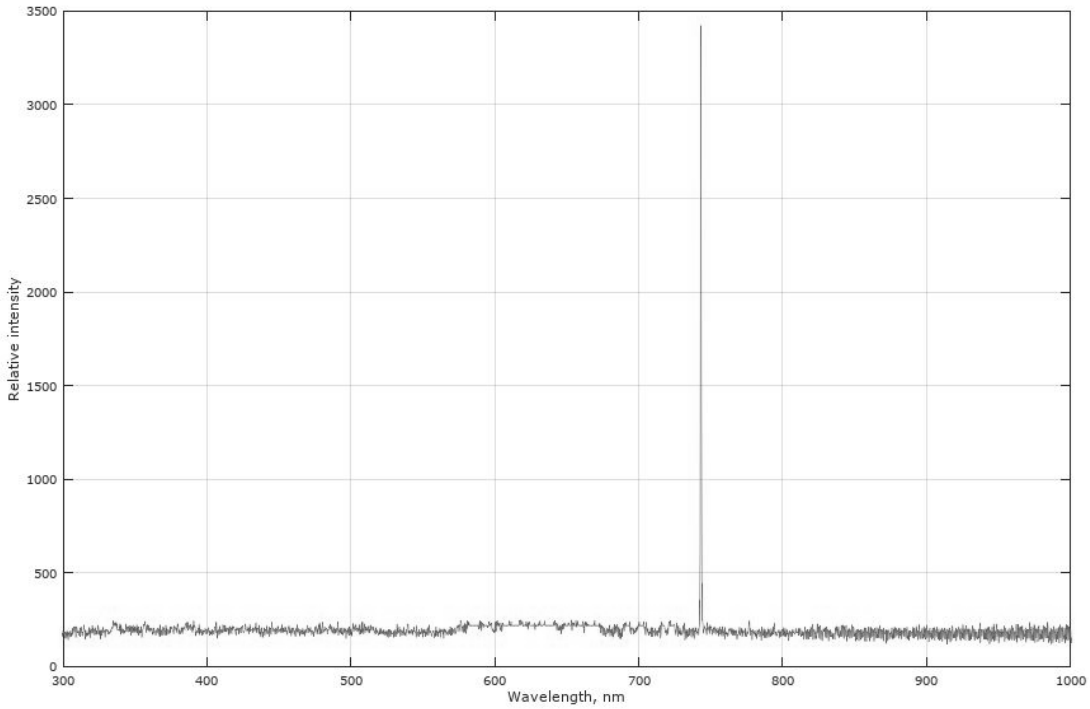

Fig. 1 The Laser spectrum of atomic Ne I high-pressure gas-discharge pumped visible laser.

References

[1] Razhev A.M. and all. Journal of Quantum Electronics. **34**, 901 (2004).

Laser-plasma surface modification of steels and Fe-based alloys

M. Khomyakov, P. Pinaev, P. Statsenko, G. Grachev
Institute of Laser Physics SB RAS, Lavrentyev Ave., 15B, 630090, Novosibirsk, Russia
E-mail: mnkhomy@laser.nsc.ru

The work is devoted to a new high-efficiency laser-plasma (LP) method of metal's surface modification. It was developed at the Institute of Laser Physics of the SB RAS. The method is based on the use of optical-pulsed discharge plasma. The discharge is ignited with CO_2-laser pulses repeated with a high frequency (tens of kHz), focused on the surface being processed, in the flow of the doping gas. The flow of plasma-forming gas (nitrogen, carbon dioxide, air) is created in the processing head coaxially with laser radiation [1].

The thermo-chemical action of the breakdown plasma was demonstrated for the first time in a series of works [2] with neodymium lasers generating pulses of millisecond duration [3]. Similar technology using different types of lasers (XeCl, KrF, Nd: YAG) with low repetition rate (≤100 Hz) is described in [4, 5]. The use of a pulse-periodic CO_2-laser proves to be preferable because of the low threshold of gas breakdown and the possibility to provide high processing efficiency due to the high pulse repetition rate (up to 120 kHz).

To carry out the laser-plasma modification, a laser-plasma process installation was created in the institute. The installation includes:
1) CO_2-laser generator-amplifier system (GAS) with an average power of up to 2 kW and a pulsed hundred kW on the basis of a LOK-3 laser operating in a pulse-periodic mode with a repetition rate of 20-120 kHz. GAS is the basis of the installation, which determines its technological capabilities. The original optical scheme of the GAS makes it possible to form a beam with a plane front, a smooth intensity distribution and a quality close to the diffraction limit, and also to eliminate the self-excitation effects of the «laser-metal near the focus» system, which lead to distortion of the pulse shape (decrease in the pulsed power) and, as a result, instability of laser-plasma treatment [6].
2) coordinate table with movable optics;
3) a two-mirror scanner and a focusing head with a slotted nozzle mounted on a movable carriage of a coordinate table. The scanner provides a scanning frequency in the range of 50-300 Hz with amplitude of 3-10 mm. The principle of scanning is based on a multiple run of the laser spot across the sample movement. In this case, the surface temperature fluctuates in the range from the quenching temperature to the melting point or evaporation of the metal. As a result, the time of metal holding in the heated state, the depth of penetration of the heat wave into the metal and, correspondingly, the depth of the hardened layer in comparison with the usual "one-pass" technique is increased.
4) cooler of the sample to be processed;
5) a system for monitoring the parameters of radiation and the technological process.

The installation makes it possible to vary the conditions of LP processing in wide ranges: according to the intensity of the beam (up to 2-3 GW/cm^2), the gas pressure in the processing head (up to 5 atm.) And the flow velocity at the output from the processing head (up to 300 m/s).
The periodic action of laser plasma on a metal surface in an alloying atmosphere simultaneously forms:
- high-hardness nanostructured coating of metal compounds with alloying elements (nitrides, carbides);
- a diffusion wave, the formation of a doped layer or solid solution;
- thermal wave and structural-phase transformations;
- hyper-intense (amplitude up to 10-15 MPa) ultrasound, which helps compact the microstructure in the hot zone.

Thus, as a result of the laser-plasma modification of the metal surface, a unique composite structure is formed, consisting of a high-hardness nanostructured surface layer and an intermediate doped or hardened sublayer up to 1 mm thick. Besides that, the productivity of laser-plasma treatment is 7-10 times higher than that of traditional laser hardening. This is explained by high efficiency of

energy exchange between laser plasma and metal (4-5 times higher than direct absorption of laser radiation) and the action of hyperintense ultrasound. The effective energy absorption coefficient of laser radiation by a steel sample (surface roughness Ra = 0.32 μm) in the regime with a near-surface laser plasma was determined experimentally by calorimetric method. It is established that it reaches 40%.

The paper presents the results of experimental studies on LP modification of the following steels: 40H, 65G, 60S2, 30HGSA, SHX-15, 38H2MUA, 40H13, 10G2S1, Y10 and wheel steel grade "2" in accordance with GOST 398-2010 for the production of railway wheels, as well as $Fe_{71.75}C_{4.81}Cr_{3.33}Si_{3.54}B_{14.10}Mn_{1.74}V_{0.73}$ and $Fe_{66.8}Mn_{2.84}C_{2.85}Si_{5.3}B_{11.42}Cr_{10.79}$ alloys. It is shown that for steels the microhardness of the hardened layer reaches values of 10-14 GPa, the thickness of the layer is 0.3-1 mm. In the alloys the LP treatment results in disintegration of microstructure and forming a highly dispersed structure (up to amorphous) surface layer 5-20 μm in thickness.

Samples of steel grade "2" with surface hardening were tested for wear resistance in comparison with standard samples without hardening. It is shown that the wear resistance of hardened samples exceeds the wear resistance of comparative ones by 8-12 times, depending on the treatment regime, and the actual wear of hardened specimens is significantly less both at the initial stage and for the entire test time.

Thus, the experimental studies carried out have shown the promise of the laser-plasma modification method, which leads to hardening of the surface layer of steels with 2-4 times increase in microhardness at a depth of up to 1 mm. The results of the wear tests showed that the LP modification technology of hardening the surface layer of a locomotive bandages is promising in terms of increasing the resistance of the bandage to defects.

The reported study was funded by RFBR according to the research project №17-20-03197 as well as RFBR and Government of the Novosibirsk region according to the research project № 17-48-543315.

References

[1] Bagayev S.N., Grachev G.N., Smirnov A.L., Smirnov P.Y. Method of modification of metal surfaces and device // Patent № RU 2 425 907 C2. Published: 10.08.2011 Bull. № 22.

[2] Rikalin N.N., Uglov A.A. Laser-plasma treatment of metals at high gas pressures // Quantum Electronics. 1981. v. 8. n 6. pp. 1193-1201.

[3] Prokhorov A.M., Konov V.I., Ursu I., Mikhailesky I.N. Interaction of laser radiation with metals. Moscow: publishing house «Nauka», 1988 г.

[4] Schaaf P. «Laser nitriding pf metals» //Progress in Materials Science. 2002. v. 47. P. 1-161.

[5] D.Hoche, H.Schikora, H.Zutz, R.Queitsch, A.Emmel, P.Schaaf Microstructure of TiN coatings synthesized by direct pulsed Nd^YAG laser nitriding of titanium: Development of grain size, microstrain, and grain orientation //Appl.Phys.A. 2008. v. 91. P. 305-314.

[6] Statsenko P.A., Grachev G.N., Smirnov A.L., Myakushina A.A. // abstracts of the 22nd Int. Conf. "Lasers. Measurements. Information - 2012 ». St. Petersburg, 2012. v. 2. pp. 168-176.

Polychromatic stimulated Raman scattering at low-frequency transitions

V. Kochanov
Laboratory of Theoretical Spectroscopy, V.E. Zuev Institute of Atmospheric Optics, Siberian Branch, Russian Academy of Sciences, 1, Academician Zuev square, 634021, Tomsk, Russia
E-mail: koch@iao.ru

The theory of stimulated Raman scattering of light (SRS) is developed with the generation of a large number of Stokes and anti-Stokes scattering components. Raman-active low-frequency rotational transitions of molecules are modeled by a quantum lambda-system. The influence of various factors on the efficiency of generation of a large number of components and the qualitative features of the scattering spectrum is considered. Namely, the spatial oscillations of the components, the degree of inelasticity of SRS (the ratio of the frequency of the Raman transition to the frequency of the pump radiation), the effect of phase asynchronism caused by the linear and nonlinear dispersion of the medium and the phase difference of the dichromatic pump waves at the entrance to the medium are analyzed.

In the simplest case of synchronous SRS and the low frequency of the Raman transition, the equations for the amplitudes of the components have a simple form:

$$\frac{dE_n}{d\zeta} = E_{n+1} - E_{n-1}.$$

An algebraic solution of these equations was obtained. The oscillations with changing the optical thickness of the medium ζ and the number of the scattering component ($n < 0$ corresponds to the Stokes branch) are shown in Fig. 1. The effect of the degree of inelasticity of SRS and the linear wave detuning related to the gain (η) on the generation of components is shown in Fig. 2 and 3, respectively.

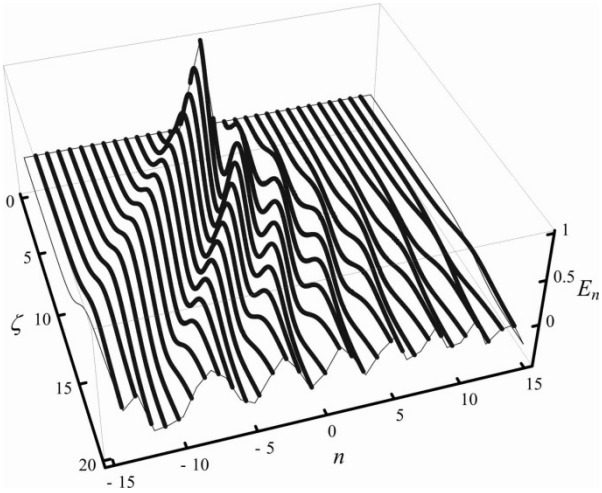

Fig. 1 Broadband generation of scattering components in the simplest case described by the upper equation. Here and below, the ratio of the amplitude of the Stokes pump component to the main component is 0.5.

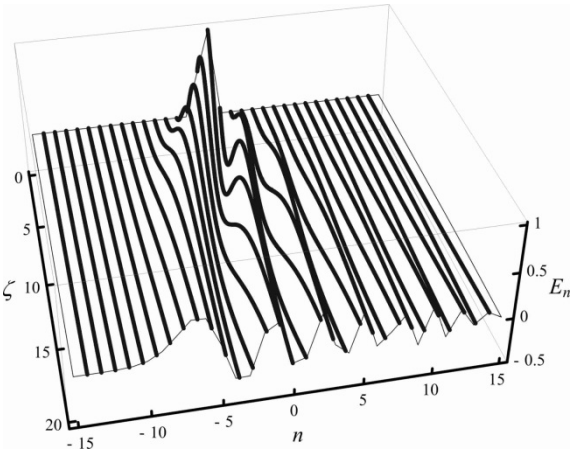

Fig. 2 The influence of the ratio $\omega_{21}/\omega_0 = 0.03$, where ω_{21} and ω_0 are the frequencies of the Raman transition and the pump, respectively. The Stokes branch is suppressed. $\eta = 0$.

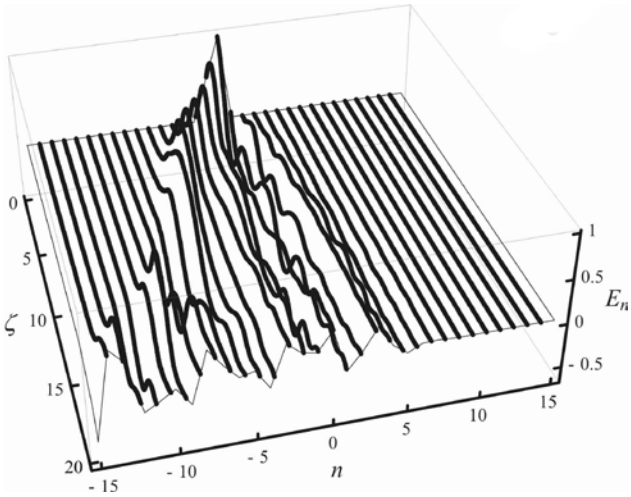

Fig. 3 The influence on SRS of the wave detuning $\eta = 0.2$ at $\omega_{21}/\omega_0 = 0$. The anti-Stokes branch is suppressed.

A detailed exposition of the problems discussed and the method used to solve the multi-wave SRS problem are presented in [1] in connection with the three-wave Raman scattering.

References

[1] V. Kochanov, Quantum Electronics **40**, 1131 (2010).

Retrieval of small- and large-angle scattering collision frequencies from H_2O line profiles near 0.8 μm

V. Kochanov[1], L. Sinitsa[2,3]
[1]*Laboratory of Theoretical Spectroscopy, V.E. Zuev Institute of Atmospheric Optics, Siberian Branch, Russian Academy of Sciences, 1, Academician Zuev square, 634021, Tomsk, Russia*
[2]*Laboratory of Molecular Spectroscopy, V.E. Zuev Institute of Atmospheric Optics, Siberian Branch, Russian Academy of Sciences, 1, Academician Zuev square, 634021, Tomsk, Russia*
[3]*Department of Physics, Tomsk State University, 36, Lenin ave., 634050, Tomsk, Russia*
E-mail: koch@iao.ru

A new method of retrieving quantitative information on the hard, soft, and diffraction collision's frequencies from inhomogeneously pressure broadened line profiles was proposed and tested. The essence of the method lies in the processing of recorded profiles using various profiles' models containing these frequencies treated as adjustable parameters in different manners. Three self-broadened H_2O absorption lines free of an instrumental function were processed with the use of four model line profiles. Retrieved set of pressure line broadening and narrowing constants allows finding out the sought frequencies. The estimation of the total scattering cross-section, ~ 630 Å^2, in pure water vapor was made.

Involvement of various physical mechanisms of forming the line shape increases the number of the profile's adjustable parameters. Certain parameters may have a direct physical meaning and thus they can serve as a source of valuable additional information extracted from a line shape. Such are the frequencies of soft and hard velocity-changing collisions. The structure of the collision integral implies division of its kernel onto three parts related to hard, soft, and diffraction scattering collisions [1−5]. These three types of collisions function to a great extent additively due to considerable difference in widths of the corresponding differential scattering cross-sections. Consequently, the total output frequency of the collision integral ν_t can be represented as a sum [1−5]

$$\nu_t = \gamma + \nu_h + \nu_s + \nu_d, \tag{1}$$

where ν_h, ν_s, and ν_d are the input collision integral frequencies of the elastic hard, soft, and diffraction scattering collisions, respectively, and the Lorentzian collision half-width at half-height γ contains the contributions of elastic and inelastic collisions. If the above frequencies enter into a model collision integral explicitly, then the line profile derived from the respective muster equation for a density matrix will contain these frequencies as adjustable parameters [3, 4]. This opens a possibility to retrieve the newly introduced parameters from processing experimental line profiles. Four profiles profile derived in [2−5] were used for this purpose. The main difference of them consists in different determination of the narrowing parameters:

$$\alpha = \nu_h/\gamma, \quad \alpha_{tot} = \left(\nu_h + \nu_s + \nu_d\right)/\gamma. \tag{2}$$

Also it was important to use the ratio $r = \nu_s/\nu_h$, which either can be calculated or determined from fitting the profiles to the experimental ones. So, the knowledge of the parameters γ, α, α_{tot}, and r obtained from the data processing allowed us to retrieve all the frequencies

$$\nu_t = \left(1+\alpha_{tot}\right)\gamma, \quad \nu_h = \alpha\gamma, \quad \nu_s = r\alpha\gamma, \quad \nu_d = \left[\alpha_{tot} - \left(1+r\right)\alpha\right]\gamma. \tag{3}$$

The high-resolution spectra of H_2O were recorded with the use of the photo-acoustic spectrometer based on a single-mode Ti-Sapphire laser pumped by an Ar-ion laser [6, 7]. Three H_2O lines centered

at ν_0 = 12415.204, 12413.977, and 12411.404 cm^{-1} (≈ 805 nm) were used to perform the estimations outlined above. The self-broadening of these lines in a pure water vapor was registered within the pressure range 1 Torr ≤ p ≤ 20 Torr. The instrumental function of the spectrometer was small compared with the widths of the recorded spectral lines.

The obtained values of the sought frequencies (1) are presented in the Table:

ν_0, cm^{-1}	ν_d/γ	ν_s/γ	ν_h/γ	ν_t/γ
12415.19306	8.6±3.0	0.23±0.14	0.17±0.04	10.0±3.2
12413.96286	8.1±1.4	0.24±0.18	0.14±0.04	9.5±1.7
12411.39004	4.8±0.7	0.4±0.4	0.16±0.10	6.3±1.2

The theory [8] allows expressing the frequency ν_t through the total scattering cross-section σ_{tot}. In particular, in the case of dipole-dipole intermolecular interaction the following relation takes place:

$$\nu_t = 1.457\, N_b \bar{V} \sigma_{tot}, \tag{4}$$

where N_b is the density of molecules. From here and the Table we obtained the estimation σ_{tot} ~ 630 ± 150 $Å^2$. For comparison, the typical values of gas-kinetic cross-sections of many molecules are of the order 50 – 70 $Å^2$. Relatively large errors (95% confidence intervals) in σ_{tot} may be caused by insufficiently accurate experiment as well as by a rough net used in numerical integrating over velocities in vicinity of a character point determining diffraction scattering [3]. The above estimation of σ_{tot} for H_2O molecule is close to total cross-sections of other molecules obtained by direct measurements of ν_t with the aid of nonlinear spectroscopy methods. Namely, in pure gas of CH_4 σ_{tot} ≈ 380 [9], 350 [10], and 370 $Å^2$ [11]; in CO_2 σ_{tot} ≈ 500 $Å^2$ [12].

One of the authors (L. Sinitsa) expresses his gratitude to cowokers from University of Science and Technology (Hefei, China) for the possibility to use Ti-sapphire laser.

This work is partly supported by RFBR (Grants № 16-43-700492).

References

[1] S. Rautian, G. Smirnov, A. Shalagin, Nonlinear resonances in spectra of atoms and molecules, Nauka SB, Novosibirsk (1979).
[2] V. Kochanov, JETP **118,** 335 (2014); Zh. eksp. teor. fiz. **145**, 387 (2014).
[3] V. Kochanov, J. Quant. Spectrosc. Radiat. Transf. **159,** 32 (2015)
[4] V. Kochanov, J. Quant. Spectrosc. Radiat. Transf. **177,** 261 (2016).
[5] V. Kochanov, Opt. Spectrosc. **89,** 684 (2000); Opt. Spektrosk., **89**, 743 (2000).
[6] V. Lazarev, Yu.Ponomarev, L. Sinitsa, Han Jia-Xian, Hao Lu-Yuan, Zhu Qing-Shi, SPIE Proceedings **3090**, 245 (1997).
[7] V. Serdyukov, L. Sinitsa, A. Dudaryonok, N. Lavrentieva, A. Shcherbakov, Russian Physical Journal **58**, 1 (2016).
[8] V. Kochanov, J. Quant. Spectrosc. Radiat. Transf. **112,** 1931 (2011).
[9] R. Barger, J. Hall, Phys. Rev. Lett. 22, 4 (1969).
[10] S. Bagayev, E. Baklanov, V. Chebotayev, ZhETF Pis. Red. **16,** 15 (1972).
[11] W. Radloff, V. Stert, Sov. J. Quant. Electronics **6,** 817 (1976); Kvantovaya elektronika **3,** 1509(1976).
[12] V. Chebotayev, V. Kochanov, L. Vasilenko, Optics Communications **20,** 409 (1977).

Frequency down-conversion of solid-state laser sources in barium chalcogenide nonlinear crystals

N. Kostyukova[1-3], A. Boyko[1-3], E. Erushin[4], D. Malakhov[2], D. Kolker[1,2,4]
[1]*Research Laboratory of Quantum Optics Technology, Novosibirsk State University, 2 Pirogova Str., 630090, Novosibirsk, Russia*
[2]*Institute of Laser Physics SB RAS, 15b pr. Akademika Lavrent'eva, 630090, Novosibirsk, Russia*
[3]*Special Technologies, Ltd., 1/3 Zeljonaja gorka Str., 630060, Novosibirsk, Russia*
[4]*Novosibirsk State Technical University, 20 pr. K. Marksa, 630073, Novosibirsk, Russia*
E-mail: n.duhovnikova@gmail.com

The development of coherent radiation sources widely tuned in the mid-IR range is actual task in the recent years. Interest to such sources is caused by the fact that this spectral covers the windows of atmospheric transparency. In addition, there are characteristic absorption lines of various compounds, such as CO_2, CH_4, NH_3, SF_6, in the mid-IR range. These compounds can be used as gasses-indicators for industrial monitoring or so-called "biomarkers" for medical diagnostics. Frequency down-conversion of solid-state laser is an effective way to expand generation range of existing lasers. An important advantage of frequency down-conversion devices is the ability to provide continuous wavelength tuning in a wide spectral range.

At the present time the search for new highly efficient non-oxide nonlinear crystals suitable for light generation in the mid-IR part of the spectrum is very important. Samples of new and perspective crystal – barium selenogallate $BaGa_4Se_7$ (BGSe) of optical quality were grown very recently [1,2]. This crystal has very wide transparency range of 0.5–18 μm at 0-level. BGSe has approximately four times more effective nonlinearity coefficient than its sulfur analog $BaGa_4S_7$ (BGS). We have been demonstrated BGSe OPO pumped at 1.064 μm for the first time in 2016 year [3]. Both type-I and II phase matching was investigated in this work [3]. Extremely wide wavelength tuning from 2.7 to 17 μm could be achieved with a BGSe oriented for type-I. The maximum idler energy was 3.7 mJ at 7.2 μm. The type-II phase matching shows a significantly narrower wavelength tuning, from 3.6 to 9.6 μm, and 4.7 mJ of idler energy at 5.3 μm. However, it is worth noting that BGSe is biaxial monoclinic crystal and characterization of it becomes more complicated.

Recently, in 2012 year, new class of potential nonlinear crystal namely a quaternary barium chalcogenide $BaGa_2GeS_6$ (BGGS) и $BaGa_2GeSe_6$ (BGGSe) was presented and first sample of these crystals with optical quality were grown in 2016 [4]. Both crystals are uniaxial. BGGS has transparency range from 0.41 μm to 11.8 μm at 0-level. BGGSe crystal is transparent over a broader range from 0.52 μm (for o-wave) to 18 μm, like a BGSe crystal.

This work is devoted to comparison of two barium chalcogenide crystals: BGSe and BGGSe. The Fig. 1 shown calculated with Sellmeier expressions from [4,5] tuning curve of OPO pumped by Nd:YAG laser with wavelength of 1.064 μm. There are the type-I phase matching in BGSe (solid line) and in BGGSe (dash line) on Fig. 1a and type-II phase matching in BGSe (solid line) and in BGGSe (dash line) on Fig. 1b.

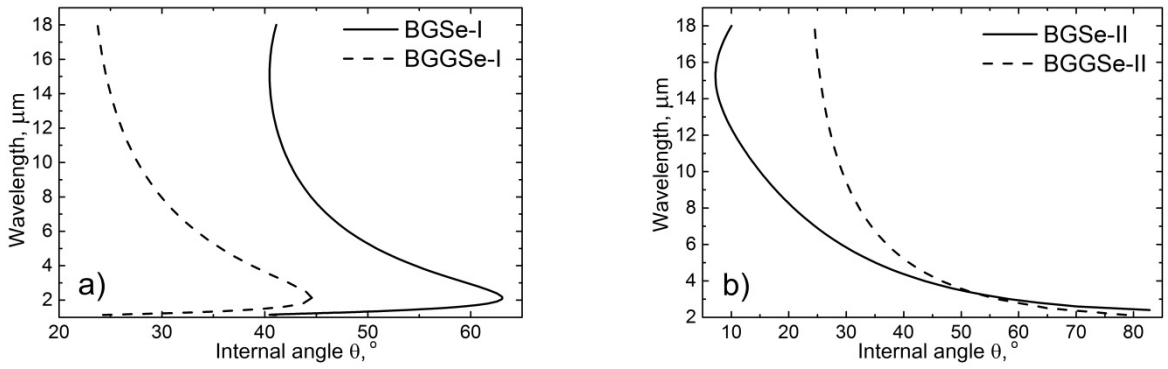

Fig. 1 Calculated angle tuning of the OPO pumped by 1.064 μm: a) type-I phase matching in BGSe (solid line) and in BGGSe (dash line); b) type-II phase matching in BGSe (dot line) and in BGGSe (dash line).

To ensure the wavelength tuning of OPO in the spectral range from 2.5 μm to 17.0 μm, it is necessary to rotate the crystal by an internal angle of at least 20°, this corresponds to an external rotation of 50.0°, at realization of type-I phase matching in both crystals as it shown on Fig.1a. The wavelength tunability is smoother in the case of type-II phase matching (Fig. 1b) and to ensure the wavelength tuning in the same spectral range from internal rotating angle must be 80.0° (corresponds to external angle of 200.0°) for BGSe and 50.0° (external angle is 125.0°) for BGGSe. This circumstance essentially extends the resonator of the OPO and thus significantly increases the generation threshold. The use of several crystals oriented for type-II phase matching, but with different angles θ, it will allow to get around this inconvenience.

The largest component of the quadratic nonlinearity tensor of BGSe is d_{23}, equal to 14.2 ± 0.8 pm/V [123], while the value of the maximum component of the quadratic nonlinearity tensor of the BGGSe d_{11} is approximately 5 times more and equal to 66±15 pm/V [4]. The BGGSe crystal having such a high nonlinearity and such a wide transparency range (up to 18 μm) in frequency down-conversion devices will allow to create a radiation source tunable in the same wide spectral range as in [3], but with a higher conversion efficiency. Therefore, the development and research of frequency down-conversion devices based on BGGSe seems to be a very promising task. In the near future, we plan to study the BGGSe damage threshold and demonstrate the OPO in this new crystal.

The reported study was funded by Russian Foundation for Basic Research according to the research project № 18 32 00105.

References

[1] J. Yao, D. Mei, L. Bai et al., Inorg. Chem. **49**, 9212 (2010).
[2] V. Badikov, D. Badikov, G. Shevyrdyaeva et al., Phys. Status Solidi **5**, 31 (2011).
[3] N. Kostyukova, A. Boyko, V. Badikov et al., Opt. Lett. **41,** 3667 (2016).
[4] V. Badikov, D. Badikov, V. Laptev et al. Opt. Mater. Express **6**, 2933 (2016).
[5] K. Kato, K. Miyata, V. Petrov, Appl. Opt. **56**, 2978 (2017).
[6] E. Boursier, P. Segonds, J. Debray et al. Opt. Express **40**, 4591 (2015).

Ultra-stable laser systems based on Fabry-Perot cavities

D.S. Kryuchkov[1], N.O. Zhadnov[1], K.S. Kudeyarov[1], I.A. Semerikov[1], K.Yu. Khabarova[1], N.N. Kolachevskiy[1,2]
[1]*P.N. Lebedev Physical Institute of the RAS, 119991, Moscow, Russia*
[2]*Russian Quantum Center, 143025, Skolkovo, Moscow, Russia*
E-mail: denis.kryuchkov@phystech.edu

Nowadays lasers with spectral linewidth less than 1 Hz are primary instruments in most of high-precision spectroscopy experiments. Masterpiece systems now provide fractional frequency instability of 4×10^{-17} on 1-100 seconds averaging time [1]. Such sub-Hz systems are key instruments in most accurate frequency standards: they provide spectroscopy of ultranarrow clock transitions in modern optical clocks. Moreover, "clock" laser define stability of optical clock on short averaging times (less than ensemble preparation time) and limits stability on longer times due to Dick effect, that is determined by the level of laser noise as well. Accordingly, laser systems with a very low fractional frequency instability are more and more in demand, and our main goal is to improve their efficiency, and, as a result, to provide laser systems with fractional frequency instability about 10^{-16} on 1 second averaging time.

Basic technique to obtain ultra-low fractional instability is locking laser frequency to the mode of a passive monolith ultra-stable high-finesse Fabry-Perot cavity. It has to be vibro-isolated and thermostabilized, is usually kept in ultra-high vacuum. Under those conditions fractional instability is fundamentally limited by thermal noise of cavity's mirrors (i. e. instability of length).

Allan variance of thermal noise—σ_y—can be used to predict best achievable fractional instability of cavity's eigenmode. In dependency on major parameters it is given as:

$$\sigma_y \propto \frac{\sqrt{T \times \phi_{coat}}}{L^{5/4} \times \lambda^{1/2} \times E^{1/2}}$$

Here, T—temperature, ϕ_{coat}—loss angle of mirror coating, L—cavity length, λ—laser wavelength, E—Young's modulus of mirror's substrate. Hence, main ideas of performing more stable laser systems are: using high-Q materials, low temperatures and enlarging base of reference cavity.

In present work we consider four ultra-stable systems. The idea of lowering temperature with stabilization at the point of zero extension is presented by two cryogenic single-crystal silicon cavities - one with dielectric SiO_2/Ta_2O_5 mirrors (1) and one with crystalline GaAs/AlGaAs mirrors (2). Silicon is a very promising material for upcoming ultra-stable cavities because it has a temperature of zero extension at 124K and has a very low mechanical loss angle. It is also transparent for 1.5 μm wavelength, which is covered by convenient erbium fiber lasers. The idea of enlarging cavity's base is realized by two large vertical and horizontal (3,4) cavities made of Ultra-low Expansion glass, operating on 698 nm wavelength.

Accurate calculations, proceeded for our systems, resulted in following fundamental fractional instability limits: 3×10^{-16} and 6×10^{-17} for cavities with dielectric (1) and crystalline mirrors (2) respectively, and 7×10^{-17} for large-base (480 mm) cavities (3,4) [2]. We have systems (1,2) assembled at this moment. (1) has finesse about 580'000, measured by ring-down method; (3)—about 250'000. Both silica cavities are mounted in UHV cryogenic chambers and stabilized at 124K with precision better than 3 mK. Fractional instability characterization via frequency correlation for two silica cavities will be performed in future. Also, vertical and horizontal cavities were numerically analyzed with finite element method to find out proper shape and optimal vibration-immune suspension configuration. Was found out that biconical is the best shape for (3): it affords least vibration susceptibility. For system (4) vibration-immune suspension system was developed, where bearings are located at the Airy points. Deformations under the action of horizontal and vertical accelerations were simulated for (3,4) as well.

Presented systems (3,4) will be used as clock lasers in Sr optical lattice clock in VNIIFTRI [3], systems (1,2)— as optical frequency synthesizer stabilizers and for stabilizing long fiber-optic communication lines.

References

[1] D. Matei et al. Phys. Rev. Lett. 118, 263202 (2017).
[2] N. Zhadnov et al. Quantum Electronics, 48 (5), 425–430 (2018).
[3] O. Berdasov et al. Quantum Electronics, 47 (5), 400 (2017).

Indirect measurements of the temperature inside active elements of high power laser amplifier

G.V. Kuptsov[1,2], V.V. Petrov[1-3], A.I. Nozdrina[1,3], V.A. Petrov[1,3], A.V. Laptev[1], A.V. Kirpichnikov[1], and E.V. Pestryakov[1]

[1]*Institute of Laser Physics SB RAS, 15b Ave. Ac. Lavrentyeva, Novosibirsk, 630090, Russia*
[2]*Novosibirsk State National Research University, 2 St. Pirogova, Novosibirsk, 630090, Russia*
[3]*Novosibirsk State Technical University, 20 Ave. K. Marksa, Novosibirsk, 630073, Russia*
E-mail: kuptsov.gleb@gmail.com

Recently, progress in laser systems that generate at the same time high average and high peak power radiation enables to access a fundamentally new physical domain of laboratory astrophysics and laser nuclear physics, as well as the design of the sources of pumping of optical parametric amplifier for high harmonic generation [1]. This makes researches aimed to development of high average-high peak power laser systems very actual.

A high power diode pumped multidisk closed-loop cryogenically cooled Yb:YAG laser amplifier is an important part of the all diode-pumped all solid state laser system that is being developed. The system aims to produce sub-Joule level pulses at pulse rate of 1 kHz. The amplifier consists of eight diffusion-bonded YAG-Yb:YAG disks with 10 at.% of dopant concentration. The diameter of the disk is 25 mm, and its total thickness is 5.75 mm, with 2 mm of undoped medium. The multidisk laser amplifier is expected to amplify pulses energy from 10 mJ to 300 mJ pulses with 1 kHz repetition rate.

It is not possible to measure the temperature in the pumped volume of the active element directly, since one is not able to install a thermal sensor inside. Usually, one has to relate to the data obtained from a thermal sensor installed in vicinity, however, it can be shown that the actual temperature in the pumped volume is significantly higher than surrounding media [6]. To estimate the average temperature of the active element in the pumped volume, an indirect measuring method based on the dependency of the absorption coefficient on temperature is proposed. The procedure of the method goes as follows: the absorption coefficient dependency on the temperature at the amplification wavelength is being fitted with an appropriate function. In case of Yb:YAG, we used the Boltzmann formula to fit the curves, based on the data published previously concerning Yb:YAG dependency of absorption coefficient at 1030 nm on temperature. Then, it is possible to obtain dependency of the temperature on transmitted probe laser power using Beer–Lambert–Bouguer law. The experimental setup is robust: one need to carry out regular amplification experiment,

An indirect measuring method of the temperature inside the pumped volume of a cryogenically cooled active element of a high-power laser amplifier is proposed and experimentally implemented. Based on the results of the temperature measurements, the optimal spot size of pump and seed beams is calculated and experimentally verified. All the data obtained are used for further augmentation and development of the all diode-pumped cryogenically cooled all solid state laser system operating with 1 kHz repetition rate.

This work is supported in parts by RAS Presidium Program №6 "Extreme light fields and their interaction with matter" and Government program (SB RAS).

References

[1] M. Puppin, Y. Deng, O.Prochnow et al. // Optics Express, 23, 2 (2015).
[2] V.V. Petrov, A.V. Laptev, G.V. Kuptsov et al. // Proc. of SPIE 10614, 106140U (2018).
[3] A.V. Kirpichnikov, V.V. Petrov, G.V. Kuptsov et al. // Proc. of SPIE 10614, 106149 (2018).
[4] G.V. Kuptsov, V.V. Petrov, V.A. Petrov et al. // IOP Conf. Series: JPCS 999, 012008 (2018).
[5] V.V. Petrov, G.V. Kuptsov, V.A. Petrov et al. // Quantum Electronics 48, 358 (2018).
[6] V.A. Petrov, G.V. Kuptsov, V.V. Petrov et al. // AIP Conf. Proc. 1893, 030121 (2017).

Cooperative effects in an ensemble of impurity atoms located in a charged Fabry-Perot cavity or near a single charged conductive plate

A. Kuraptsev and I. Sokolov
Peter the Great St. Petersburg Polytechnic University, St. Petersburg, Polytechnicheskaya, 29, Russia
E-mail: aleksej-kurapcev@yandex.ru

Since the seminal work of Purcell [1] light interaction with atoms localized inside a cavity or waveguide as well as near its surface has attracted a considerable attention. Now it is understood that a cavity modifies the spatial structure of modes of electromagnetic field. This leads to modification in radiative properties of atoms, in particular, to the enhancement and inhibition of the spontaneous decay rate [2]. Therefore one has an exciting tool to control over the atomic radiative properties by choosing the cavity parameters appropriately. Light matter interaction in the presence of nanophotonic structures, such as nanofibers, photonic crystal cavities and waveguides propose future applications for quantum metrology, scalable quantum networks and quantum information science.

Modification of the spatial structure of field modes causes changes not only in the spontaneous decay rate but also in the nature of photon exchange between different atoms. In its turn it leads to alteration in dipole-dipole interatomic interaction [3,4] as well as associated cooperative effects [5,6]. Dipole-dipole interaction plays an important role in the case of dense atomic ensembles, in which the interatomic distance is comparable with the wavelength of resonant radiation. Cooperative effects cause density-dependent shifts of atomic transition as well as distortion of spectral line shape. It influences both on the properties of atoms as well as on scattered radiation characteristics.

In fact, not only cavity can modify the modes of electromagnetic field, but also any conductive device has this property, in particular, metallic conductive surface. For this reason optical properties of atomic ensemble located near a single mirror differ from ones in the case of the same ensemble in free space.

We have developed a consistent quantum microscopic approach to describe cooperative polyatomic effects in dense ensembles of pointlike impurity atoms located in a Fabry-Perot cavity or near a single mirror [7,8]. This approach is based on the solution of the non-steady-state Schrodinger equation for the wave function of the joint system consisting of all atoms and a weak electromagnetic field including the vacuum reservoir. On the basis of the general theory we study the excitation dynamics of an ensemble of motionless point atoms located in a Fabry-Perot cavity with perfectly conducting mirrors as well as near a single mirror.

Fig. 1 shows the time dependence of the total excited state population and the cooperative decay rate both for the ensemble in free space and in the Fabry-Perot cavity with the distance between the mirrors $d = 3$. We consider the inversed wave number of radiation resonant to the atomic transition, k_0^{-1} as a unit of length. We see that cooperative decay dynamics is described by multiexponential law, and the cooperative decay rate depends on time. Furthermore, we observe, that all the curves differ from each other. The total excited state population in the case of a cavity decreases slower than one in the case of free space. Besides that, the decay rate of Zeeman sublevels $m = \pm 1$ in a cavity is less than one of the sublevel $m = 0$. It is connected with mentioned features of the field modes structure in the cavity.

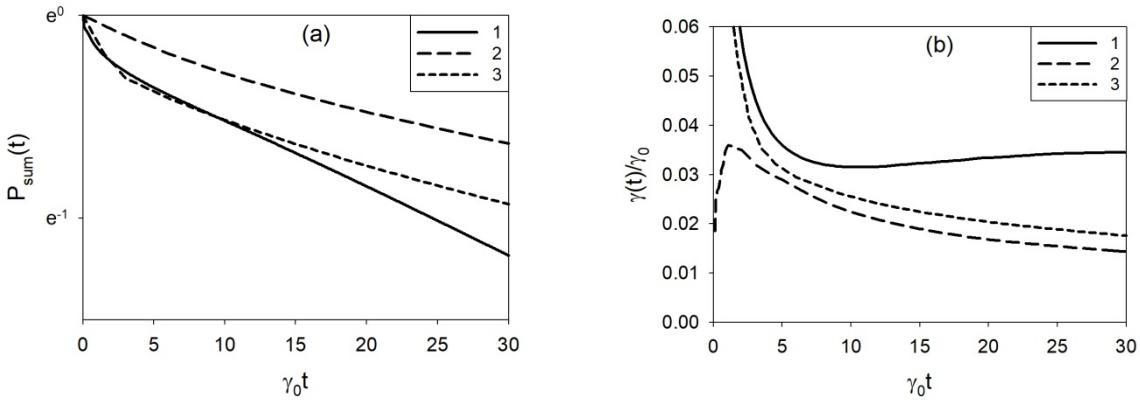

Fig. 1 (a) - Time dependence of the total excited state population. (b) - Cooperative decay rate. Atomic density $n = 0.1$, the radius a sample $R = 14$. 1 - free space; 2 - cavity, $d = 3$, $m = \pm 1$; 3 - cavity, $d = 3$, $m = 0$.

In the case when the mirrors of a cavity are charged, an electrostatic field causes Stark shifts of atomic energy levels, which leads to additional modification in the dipole-dipole interaction. The same takes place in atomic ensemble located near a single charged conductive plate. On the basis of the general approach we also analyze the influence of an electrostatic field on the cooperative properties of an atomic ensemble.

References

[1] E.M. Purcell, Proceedings of the American Physical Society **69**, 681 (1946).
[2] G.S. Agarwal, Phys. Rev. A **12**, 1475 (1975).
[3] T. Kobayashi, Q. Zheng, T. Sekiguchi, Phys. Rev. A **52**, 2835 (1995).
[4] G.S. Agarwal, S.D. Gupta, Phys. Rev. A **57**, 667 (1998).
[5] R. Rohlsberger, K. Schlage, B. Sahoo et. al., Science **328**, 1248 (2010).
[6] M.D. Lee, S.D. Jenkins, Y. Bronstein et. al., Phys. Rev. A **96**, 023855 (2017).
[7] A.S. Kuraptsev, I.M. Sokolov, JETP **123**, 237 (2016).
[8] A.S. Kuraptsev, I.M. Sokolov, Phys. Rev. A **94**, 022511 (2016).

Industrial quantum key distribution

A. Duplinskiy[1,2], E. Kiktenko[1,3,4], N. Pozhar[1,3], M. Anufriev[1,3], R. Ermakov[1], A. Kotov[5], R. Yunusov[1], V. Kurochkin[1,6], K. Fedorov, and Y. Kurochkin[1,6]

[1]*Russian Quantum Center, Skolkovo, Moscow, 143025, Russia*
[2]*Moscow Institute of Physics and Technology, Institutskii 9, Dolgoprudny, Moscow region, 141700, Russia*
[3]*QApp, Skolkovo, Moscow, 143025, Russia*
[4]*Steklov Mathematical Institute of the RAS, Moscow, 119991, Russia*
[5]*AMICON Co., Ltd., Moscow, 117587, Russia*
[6]*QRate, Skolkovo, Moscow, 143025, Russia*
E-mail: v.kurochkin@rqc.ru

Quantum key distribution (QKD) provides theoretic information security in communication based on the laws of quantum physics. If we create quantum networks [1] when number of devices are growing the price of the network should be affordable. Due to significant losses in the urban fiber-optics communication lines, we use recently suggested one-way scheme of key distribution with fast polarization encoding [2]. The setup is based on $LiNbO_3$ phase modulators, single-laser source for states generation, and two single-photon detectors. This optical scheme easily stabilized and allow to work with high pulse repetition rate.

We implemented this optical scheme in an industrial device and used it for quantum-secure data transmission in standard communication lines in Moscow. Communication line is realized on the basis of the already deployed urban fibre-optic communication channels with significant losses. Line attenuation is 14 dB with 25 km length. We realize the decoy-state BB84 QKD protocol. QKD is driven by Virtex-7 processor. Pulse repetition rate is currently 300 MHz which is limited by the gated single photon detectors design. Laser pulse duration is 100 ps while the detector gate duration is 500 ps. The phase modulator pulse duration is 400-800 ps. Decoy states are 0,17, 0,08 and 0,01 photon/pulse and the result quantum bit error rate is 5%. Monitoring detector controls average power to stabilize intensity modulator drift. The good feature is that both phase modulators drift can be compensated with the polarization controller together with the line drift. The laser source emits polarized optical pulses at 1,550 nm. Transmitting unit to encode bits of the secret key in polarization states with the help of the $LiNbO_3$ modulator. To weaken the pulse a variable optical attenuator is used. After the quantum channel, the piezo-driven polarization controller compensates the state of polarization, drifts, and rotates it so that the polarization components along the lithium niobate crystal axes switch places, compensating the birefringence of $LiNbO_3$. The receiving unit performs measurements in one of the bases for the implementation of protocol BB84.

The communication line between two server rooms consists of eight segments (six segments outside the buildings and two inside the buildings). Few connections give us ≈4% of reflection. To prevent detector blinding, we separate clock synchronization signal and quantum signal not only in wavelength but also on time. The resulting raw key generation rate in our experiments is ≈2 kbit/s. After performing the QKD session, we realize the standard sifting procedure, which is needed for dropping the positions with inconsistent bases from the raw quantum keys, using the authenticated communication channel. The resulting keys are called sifted keys. The decoy state statistics is announced at this stage as well. The error correction is made with LDPC codes [3]. The final secure key rate after privacy amplification is 0,1 kbit/s. Generated keys are then used for continuous key renewal in the hardware devices for establishing a quantum-secured Virtual Private Network Tunnel. Such a hybrid approach offers possibilities for long-term protection of the transmitted data, and it is promising for integrating in the already existing information security.

The work was supported by the Russian Science Foundation (Grant No. 17-71-20146).

References

[1] Frohlich, D. et al. Nature **501**, 69-72 (2013).
[2] A. Duplinskiy, V. Ustimchik, A. Kanapin and Y. Kurochkin, Opt. Express, **25**, Is. 23, pp. 28886, (2017).
[3] E. Kiktenko, A Trushechkin, Y. Kurochkin and A. Fedorov, J. Phys. Conf. Ser. **741**, 012081, (2016).

Metal-carbyne materials: New possibility of laser synthesis and applications

S. Kutrovskaya[1,2], A. Kucherik[1], A. Povolotckii[3], V. Samyshkin[1], S. Arakelian[1], and A. Kavokin[2-5]
[1]*Vladimir State University, 87, Gor'kii st., Vladimir, Russia*
[2]*International Center for Quantum Optics & Quantum Technologies Limited Liability Company, Business Center «Ural», 100, Novaya st., Skolkovo, Russia*
[3]*St. Petersburg State University, St. Petersburg, 199034, Russia*
[4]*CNR-SPIN, Viale del Politecnico 1, I-00133, Rome, Italy*
[5]*School of Physics and Astronomy, University of Southampton, Southampton, United Kingdom*
E-mail: 11stella@mail.ru

The development of methods for the materials synthesis has opened up new possibilities for carbon line form – a carbyne. One of the problems of studying the properties of linear carbon structures is the difficulties of their practical production, due to their high chemical reactivity and mechanical instability, which leads to their transformation from structures with sp-hybridization to other allotropic forms of carbon. The stabilization of carbynes may be achieved due to the effect of the environment in a colloidal solution and due to the stabilization by silver and gold nanoparticles attached to the ends of the chains. We observe the signatures of linear carbyne chains in the photoluminescence and Raman spectra of the solutions. Depositing the stabilized chains on a substrate we obtain a hybrid metal-carbon metamaterial that exhibits interesting optical properties and may be used for biosensing and plasmonic devices.

Linear carbon structures are suitable candidates for demonstrating high-temperature superconductivity (experimental confirmations of the phase transition at 15 K are known [1]). In our case, linear carbon chains (with polyyn or cummulene bonds) will be trapped between metallic nanoparticles - anchors. Such approach will allow to stabilize the one-dimensional structure of the carbyne [2] and observe electrophysical effects in a one-dimensional medium due to the bias apply through microcontacts of metal nanoparticles attached to the ends of the chain.

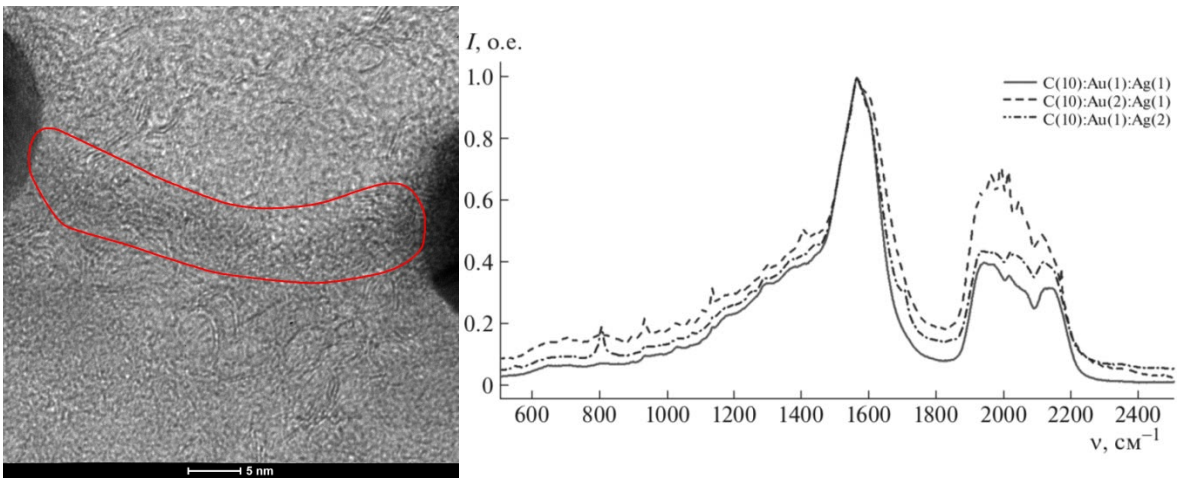

Fig. 1 Image made by transmission electronic microscopy of metal-carbyne system on the left and its Raman spectra in liquid on the right.

References

[1] Z. K. Tangetal., Science **292**, 2462 (2001).
[2] Shi, L. et al. Nat. Mater. **15**, 634 (2016).

Extension of PEARL Nd:glass pump laser to subkilojoule level

A.A. Kuzmin, A.A. Shaykin, I.A. Shaykin, E.A. Khazanov
Institute of Applied Physics of the Russian Academy of Sciences, Nizhny Novgorod, Russia
E-mail: alexeyhsgap@yandex.ru

The output energy of the existing Nd:glass laser which radiation is used for pumping PEARL OPSPA facility has been increased from 300 to 600 J by means of splitting the input nanosecond pulse into two orthogonally polarized sub-pulses. The number of amplifying stages, the total small signal gain and the optical load on the elements of the laser has not been changed.

The energy ratio of the two replicas was changed by rotating the half-wave plate installed before the splitting polarizer. The delay between the pulses was 1.9 ns. This time exceeds the pulse duration and allows one to expect that the 300 J limit of the maximum energy will be imposed separately on each pulse.

The multistage laser amplifier consisted of nine Nd:glass rod amplifiers with diameters of 10, 20, 45, 45, 60, 85, 100, 100 and 100 mm. Vacuum spatial filters were placed between them to transfer images from one amplifier to another. After the first 100 mm in diameter amplifier pulses divided by a polarizer into two beam lines and then amplified separately in two additional 100 mm in diameter rods. Finally we obtained two output pulses 300 J of energy each. We constructed special Faraday isolators allowing us transmit radiation of any polarization in one direction and avoid backward propagation.

Fig. 1 shows the near-field intensity distributions and the oscillogram of the output pulses. Note that the second pulse freely passes through all the spatial filters even at the maximum energy, i.e., the plasma formation time in their apertures exceeds 5 ns.

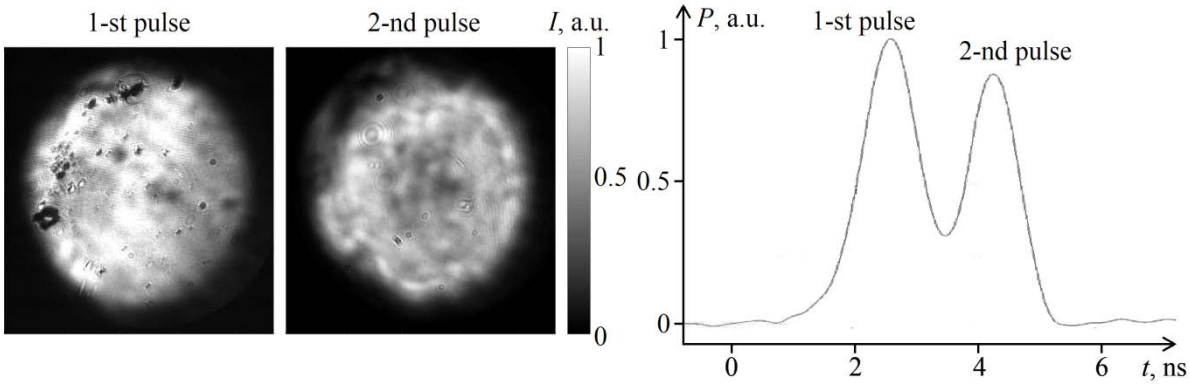

Fig. 1 Output intensity distributions (a) in the near-field zone and (b) in time domain. The beam diameter is 100 mm. Pulses are orthogonally polarized.

After frequency doubling the energy of pulses is about 180 J. Both of them can be used for pumping two parametric amplifiers of a petawatt laser: the first pulse pumps the first amplifier (as before), and the second pulse will pump an additional amplifier, which will lead to a considerable increase in the power of the output femtosecond pulse of PEARL facility.

Acknowledgements. The work was supported by the grant program of the President of the Russian Federation for young scientists and postgraduate students engaged in advanced research and development in priority areas of modernization of the Russian economy (Grant No SP-703.2016.2).

High power solid state laser and its applications

X. Lin, D. Li, P. Zhao, and Z. Zhang
Institute of Semiconductors, Chinese Academy of Sciences
E-mail: xclin@semi.ac.cn

High-power all-solid-state laser has the significant advantages of small size, light weight, high efficiency, good beam quality, high reliability, and so on. It was widely used in scientific research, industrial processing, military and other fields. Laser processing with high precision, small deformation, high speed has become one of the most advanced processing technologies.

All-solid-state light source laboratory focuses on the research of high-power all-solid-state lasers and their applications. A series of key technologies of high efficient pumping, depolarization compensation, cascade amplification, high beam quality control, and fiber coupling were broken through. In 2012, we successfully achieved 7.13kW laser with electro-optical efficiency of 18.4% and beam quality of 50.3mm • mrad through master oscillator power amplifier. Using orthogonal dual acousto-optic Q-switching, average output power of 1023W quasi-continuous laser with 82ns pulse width, 20kHz repetition rate was generated. The high-power all-solid-state lasers were successfully used in laser welding, cladding, quench, cleaning and other fields. Cooperation with domestic brand Chery Automobile, laser welding in critical components of CVT automatic transmission has been successfully used in the new Chery Tiggo SUV. The processing effect is good. Cooperation with the world's third-largest oil supplier Weatherford, the laser cladding of the drilling unit was carried out. The quality of laser cladding is very good. This is the first time that this kind of components developed and produced by China instead of Europe and America.

Compensation of the light shifts of the resonance of the coherent population trapping under the Ramsey response scheme in an optically dense medium

G.V. Voloshin, K.A. Barantsev, E.N. Popov, A.N. Litvinov
St. Petersburg Polytechnic University of Peter the Great, 195251, St. Petersburg, Russia
E-mail: kostmann@yandex.ru, andrey.litvinov@mail.ru

The phenomenon of CPT has been studied for more than 40 years. During this time, a wide range of questions has been studied both on the various conditions for observing the CPT effect, and on the influence of various factors on the shape of the CPN resonance. To improve the characteristics of metrological devices, it is important to increase the contrast of the reference resonance, that is, to increase the ratio of the amplitude of the resonance to its width, and to reduce the light shifts. One of the main directions in the study of the CPT effect is the search for ways to reduce the width of the resonance line. A significant narrowing of the CPT resonance line can be achieved if the so-called Ramsey's scheme of restriction [1].

The theory of the resonance of the coherent population trapping, which is detected by the Ramsey method, is developed in the work under conditions of finite optical thickness and the presence of collective effects in a rarefied medium. The scheme of energy levels of atoms is described by a four-level model, in which two excited levels and two main generators of the forbidden transition are considered. Bichromatic radiation, which is a sequence of two pulses and implements the Ramsey detection scheme, falls on the medium. The carrier frequencies of the field are quasiresonant to the optical transitions of the atoms. The mathematical model consists of a dynamic equation for the atomic density matrix, solved together with the wave equation of electromagnetic field transfer, taking into account the collective effects associated with the superposition of the fields created by atoms in the wave zone.

It is found that the Ramsey "comb" is modified as the field passes through the medium, namely, the amplitudes of the peaks change and their shifts appear. In this case, there is also a light shift of the CPT resonance. Conditions under which it is possible to achieve shift compensation for the fluorescence signal are determined.

The work was done under financial support of Ministry of Education and Science of the Russian Federation in terms of FTP ‘‘Research and development on priority trends of Russian scientific-technological complex evolvement in 2014–2020 years (Agreement # 14.578.21.0211, Agreement unique identifier RFMEFI57816X0211)’’.

References

[1] N.F. Ramsey // Phys. Rev. 100, 1191

Narrow linewidth laser for the spectroscopy of the quadrupole transition of single Yb ion

A. Lugovoy, N. Kvashnin, S. Chepurov, and S. Bagayev
Institute of Laser Physics SB RAS, 13/3 Lavrentiev av., Novosibirsk, Russia
E-mail: lugovoy@laser.nsc.ru

The past few years have seen the advent of a number of stationary optical clocks with a frequency uncertainty below 10^{-17} [1]. The three main parts of any modern frequency standard are a short-term-stable local oscillator, which is itself disciplined in the longer term by an absolute frequency reference, and frequency counting mechanism, which is capable of relating the frequency of the standard to other standards or applications. The one of the simply realized candidates for using as a quantum discriminator is a quadrupole transition at 435.5 nm in a single Yb ion trapped in RF Paul trap [2]. The natural linewidth of this transition is 3.1 Hz. The easiest way to achieve this wavelength is using frequency doubled commercially produced external-cavity diode lasers at 871 nm. The linewidth of the free-running laser at the level of several MHz is decreased by the Pound-Drever-Hall frequency stabilization to a commercial high-finesse Fabry-Perot etalon made of ultralow expansion (ULE) glass spacer and optically contacted quartz mirror substrates with low-loss high-reflective dielectric coatings. The ULE cavity finesse was measured to be $\sim 3\times10^5$. The transmission of the cavity is more than 70%.

If a laser system has a well-designed locking electronics, the fractional frequency stability of the laser is given by the fractional stability of the optical length of the cavity. To prove the performance of self made automatic frequency control (AFC) system used we analyzed the residual signal inside the loop and found that it does not limit the laser frequency stability at the level of 1 Hz. The achieved bandwidth of AFC is estimated at the level of 1 MHz and seems to be limited by the measured laser diode frequency response versus current modulation.

The cavities' length stability is fundamentally limited by statistical Brownian noise of the mirror coatings, substrates, and spacer. Before achievement of such performance the influence of several technical limiting factors should be minimized. To suppress fluctuations of the cavity length caused by low-frequency mechanical and acoustic perturbations the horizontally oriented laser cavity suspended inside a vacuum chamber at specially defined points [3]. In addition a vacuum chamber with a vacuum at the level of 10^{-8} Torr were mounted on a passive vibration isolation platform. The long-term variation of stabilized laser frequency determined by thermal expansion and aging of cavity spacer. ULE is a titania-doped silicate glass that has a zero thermal expansion coefficient (CTE) at some temperature in the range 0-30°C. To find this point we perform the cavity mode frequency measurements against Yb:YAG/I_2 laser frequency standard at 1030 nm [4]. The frequency gap between lasers was filled with the help of the femtosecond comb produced by MenloSystems. The method of frequency comparison used allows direct observation of the beat between optical frequencies separated by 54 THz. The precision of the measurement within 1-100s interval was limited by the short-term stability of the reference Yb:YAG laser standard. Longer measurements were limited by the constant drift of reference cavity frequency due to the aging of the spacer at the level of 0.05 Hz/s. The temperature at which CTE is nearly zero was found to be 26.09°C. The frequency measurement during one and half years showed that the frequency drift slope slightly decreased with time.

The precise control of the difference frequency between the laser and resonance in high-finesse cavity and stabilization of laser intensity coupled to the TEM_{00} cavity's mode were

realized with double-passed acousto-optic modulator (AOM) driven by low-noise RF generator. The computer-controlled sweeping of RF frequency allows making spectroscopy of the ytterbium ion's resonances with a resolution defined by the linewidth of the probe laser. Two additional AOMs were used to stabilize the second harmonic radiation power at 435 nm and to precisely form the temporal intensity modulation that is necessary to detect transition by the electron shelving techniques.

References

[1] F. Riehle, Nature Photonics **11**, 25 (2017).
[2] S. Chepurov et.al., IOP Conf. Series: Journal of Physics: Conf. Series **793,** 012004 (2017).
[3] T. Nazarova et.al., Appl. Phys. B **83,** 531 (2006).
[4] S. Ignatovich et.al, IOP Conf. Series: Journal of Physics: Conf. Series **793,** 012010 (2017).

Nonlinear applications of beta-barium borate in the terahertz regime

A. Mamrashev, N.A. Nikolaev, T.B. Bekker, K.A. Kokh, G.V. Lanskii, Yu.M. Andreev
Institute of Automation and Electrometry SB RAS, Novosibirsk, Russia
E-mail: mamrashev@iae.nsk.su

Optical properties of beta-BBO crystals were studied by THz-TDS in the range of 0.2-2.0 THz at the temperatures of 293 K and 81 K. The measured o- and e-wave refractive indices were formulated in the form of Sellmeier equations. Phase-matching conditions for the IR-THz and THz-THz frequency conversion were calculated.

Influence of rf channel power transmission on the laser pulses stability of waveguide CO_2 lasers

A. Karapuzikov, A. Markelov
Institute of Laser Physics SB RAS, Novosibirsk, ave. acad. laurentian 15B, Russia
E-mail: ir@laser.nsc.ru, markellexa@mail.ru

Waveguide CO_2 lasers with radio-frequency (rf) excitation are widely used in technology, instrumentation and medicine. Investigations of such lasers are devoted to a number of works [1 - 4], which deal with the laser output power, excitation of rf discharge in long waveguides, and the features of operation in various lasing regimes. Laser with periodic pulse operation is used to create compact devices with autonomous power supply. One of the most important radiation parameters of the laser is the stability of laser pulses. The output laser pulses stability is influenced by a number of factors, including the rf generator power, the loss in the elements of the matching circuit and the resonance circuit of the laser, etc.

We developed theoretical model of rf channel power transmission (rf cpt) of the waveguide laser, considering properties of an optical waveguide as transmission line, influence of the laser design and the matching circuit. Results of calculations were compared to impedance measurements of rf cpt for the laser without discharge in waveguide cannel with waveguides and housings from various materials. For each case comparative measurements of instability of average output power were spent.

The rf cpt is designed to effectively transmit the power of the rf generator to the active laser medium and includes the transmission cable, the matching circuit, the vacuum rf feed-through and the electrode assembly. The rf generator operates at frequency of 144 MHz and is able to generate pulses with power up to 1 kW. The electrode assembly is a parallel resonant circuit consisting of copper inductors and a capacitor formed by a "hot" and "ground" electrodes, between which is a dielectric or metal-dielectric optical waveguide. Because of the large length of the capacitor relative to the rf field wavelength, it is considered as a transmission line with distributed losses. For this type of laser the rf cpt affects on laser excitation efficiency, stability ignition of the discharge and therefore the stability of the energy laser pulses.

The scheme of the rf cpt used in the simulation is shown in Fig. 1. The electrode assembly consists of the optical waveguide between electrodes that excite a transverse rf discharge in the gas mixture inside the hollow waveguide. On the other hand, the electrode assembly is a transmission line with losses due to the conductivity of the plasma and losses in the passive elements forming the electrode assembly, for example in the material of dielectric waveguide or in the material of housing.

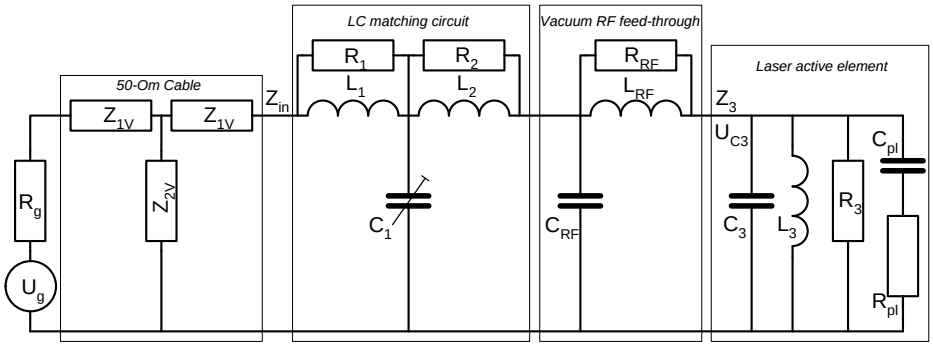

Fig. 1 The electrical diagram of the waveguide CO_2 laser rf channel of power transmission.

In the theoretical model, for convenience of calculation, taking into account the features of the circuit, the transmission line was replaced by two artificial transmission lines consisting of n elementary units located symmetrically relatively the center of the waveguide where the rf feed-through is located. The coil of inductance L_3 was assumed to consist of several inductances, symmetrically located relatively to the center of the line. The total inductance of these inductances was considered in the first approximation equal to L_3. The discharge plasma resistance R_{pl} was

assumed to be 400 kOhm, which corresponds to the absence of a discharge in the waveguide channel, since in this mode the parameters of the rf cpt of the laser electrode assembly could be calculated and measured experimentally.

In the calculation, the input impedance of the transmission line was first determined. Then, the impedances were calculated in sequence, taking into account the rf feed-through, the matching circuit, the 50 Ohm coaxial cable and parameters of the rf generator. Then the calculation was carried out in the reverse order to determine the currents, voltages and power losses in all elements of the rf cpt, as well as VSWR.

Experiments to measure the characteristics of real rf cpt of compact waveguide CO_2 lasers were carried out using a CABAN R140 vector reflect meter. With the use of this device, a method for determining the characteristic impedance of the transmission line, which is necessary for calculations in the theoretical model, was developed. Various materials of dielectric hollow waveguide were used in the experiments, such as the C52-1 glass and BeO ceramics, as well as various materials of the laser housing - stainless steel and aluminum alloy. Figure 2 shows the recording power of laser radiation when the power of each pulse was measured for lasers with different materials of waveguides and housing.

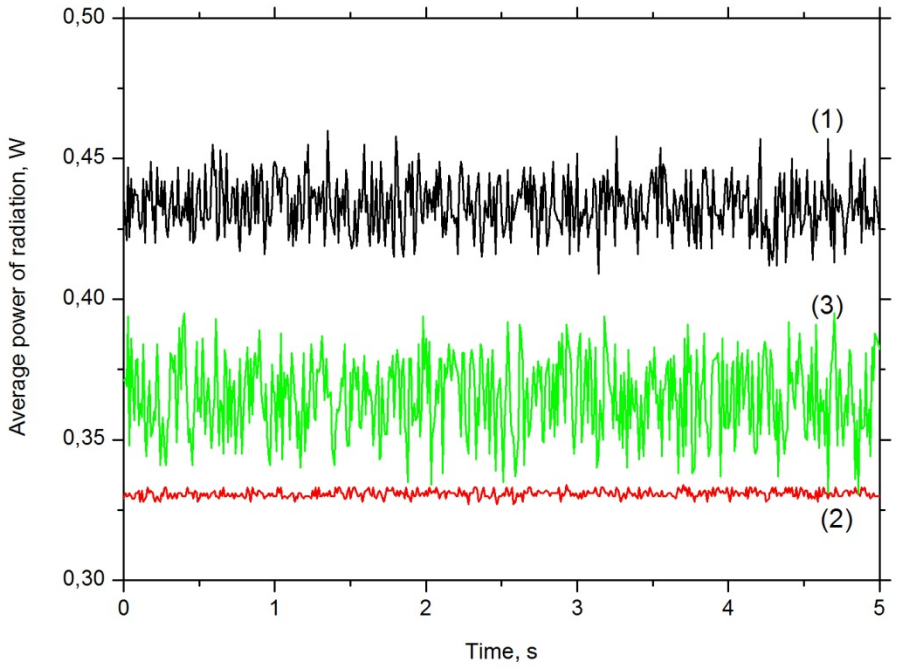

Fig. 2 Time dependences of the radiation power for a glass waveguide laser in a stainless steel (1) and aluminum alloy (2) housing, and the same for BeO waveguide laser with stainless steel housing (3).

The results of the simulation are consistent with the experimental data obtained with the using of the vector reflect meter, which indicates the primacy of the theoretical model. It is shown that the quality factor of the internal laser circuit directly affects on the stability of the generation pulse parameters, and when a certain value is reached, the jitter or instability of the appearance of laser radiation pulses is substantially reduced. This is clearly seen from Fig. 2 for a laser with an aluminum-based housing.

References

[1] D. Hea and D. R. Hall, Appl. Phys. Lett. 43, №8,726-727 (1983).
[2] D. Hea and D. R. Hall, IEEE JQE, 20, № 5, 509-514 (1984).
[3] B. Heeman-llieva, Yu. B. Udalov, et al, Appl. Phys,. 74, №7,4786-4788 (1993).
[4] F. Villarreal, P. R. Murray, H. J. Baker and D. R. Hall, Appl. Phys. Lett., 78, №16, 2276-2278 (2001).

Photodynamic fractional laser photothermolysis by transcutaneous photosensitization

A. Mayorov[1], S. Nikonov[3], S. Strutz[1], O. Kazakov[2], D. Bredikhin[3]
[1]*Institute of Laser Physics SB RAS, Novosibirsk, Russia*
[2]*Research Institute of clinical and experimental lymphology SB RAS, Novosibirsk, Russia*
[3]*Novosibirsk state university, Novosibirsk, Russia*
E-mail: mayorov@laser.nsc.ru

Development of transdermal medical products transport methods using fractional laser photothermolysis and photodynamic therapy (PFLF) for problem and aging skin. For the first time, the method of PFLF has been tested, which proved safety, low invasiveness, efficiency and availability for use in dermatocosmetology.

Laser making of elements of heart prosthetic from biological tissue

A. Mayorov[1], A. Goncharenko[1], D. Bordzilovskiy[1], I. Zhuravleva[2], E. Kuznetsova[2]
[1]*Institute of Laser Physics SB RAS, Novosibirsk, Russia*
[2]*National Medical Research Center named after academician E. N. Meshalkin, Novosibirsk, Russia*
E-mail: mayorov@laser.nsc.ru

This paper describes the laser conditioning (removal of crispness, smoothing) is presented to a fibrous surface of elements cardiovascular bioprostheses at their cutting from a pericardial tissue. The description of results of experiments of the influence on a pericardial tissue by laser radiance with various wave length and the description of the program operating of moving of a portal, at performance of surface conditioning. The sequence of technological operations of manufacturing of elements cardiovascular bioprostheses on the laser installation "Melaz-Kardio" developed at Institute of the laser physics of the Siberian Branch of the Russian Academy of Science is shown.

The object of the study is the pericardium of cattle, preserved with ethylene glycol diglycidyl ether. This biological material (pericardial tissue) is used for the manufacture of a large number of products for transplantation in cardiac surgery, including for the manufacture of artificial heart valves. The serous side of the pericardial tissue is smooth, and the fibrous side is fleecy (Fig. 1). In the artificial heart valve, the valve leaflet, cut from pericardial tissue, is kontachat with blood on both sides.

After implantation of an artificial valve to the patient, endothelium is formed on the biological tissue, however, on a loose fibrous surface, endothelium is formed badly, which can lead, in case of violation of the drug regimen and diet, to calcination of the fibrous surface of the artificial valve folds (Fig. 2).

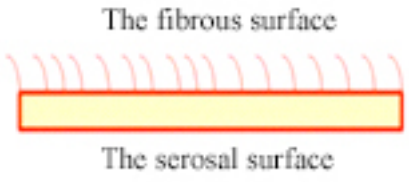

Fig. 1 Schematic representation of the pericardium in the section.

Fig. 2 Massive blood clots localized on the fibrous surface of xenopericardial heart valve valves.

The technology of laser conditioning is based on the laser action on the fibrous surface of the pericardial tissue and evaporation from the surface of the fleecy part of the tissue. Laser sources, the radiation of which is well absorbed by the pericardial tissue and water contained in it, were chosen to implement the technology of smoothing the fibrous surface of the xenopericardial. Such sources are: solid-state pulsed Er: YAG laser with absorption coefficient in water ~10000cm-1 and gas CO2 laser with absorption coefficient in water ~1000cm-1 .

The first series of experiments was carried out using the radiation of a tube-pumped solid-state Er:YAG laser. The emission of this laser has the largest absorption coefficient in water. Since the wet tissue (preservative or saline, the main component of which is water) is treated, it is possible to evaporate a wet layer of pericardial tissue with a thickness of several microns. For the experiments we used a laser with the following characteristics: wavelength laser of 2.94 microns, pulse duration of laser radiation of 450±20 μs, pulse energy (max) of 0.8 J, the repetition rate of laser pulses from 1 to 25 Hz, the average power of laser radiation - 10 W.

The size of the spot on the surface of the pericardial tissue was regulated by a lens from 1mm to 4mm in diameter. Studies have shown that the best results of conditioning using a pulsed Er: YAG laser are obtained with the following radiation parameters: laser pulse energy-200mJ, pulse duration of 400 microseconds at a spot size of 2mm in diameter. Each subsequent pulse was directed to the

pericardial tissue with the overlap of the previous spot by 50% (Fig. 3). With such characteristics of radiation, without damage to deep-lying tissue structures (Fig. 5.), a layer of pericardial tissue with a thickness of 20-30micron was removed in one pass.

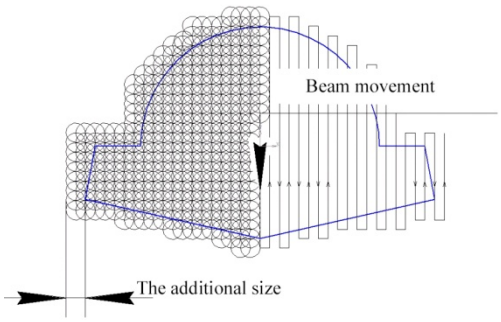

Fig. 3 The trajectory of the laser beam from pulse to pulse (conditioning of the Heart valve fold).

In the next series of experiments, a continuous CO2 laser with a wavelength λ=10.6 μm and an average power of 40 W was used; the maximum speed of the portal movement is 6000 mm/min. The Experimental setup allowed to change the following parameters: radiation power, spot size on the tissue, current to modulate radiation and to regulate the velocity of the portal coordinate table. The optimal air conditioning mode, when using a CO2 laser was observed at the following parameters: laser power 20W, spot 0.8 mm, air conditioning step 0.5 mm, portal speed 3000 mm / min, break - 2 seconds after each pass to reduce the temperature of the treated layer (Fig. 4).

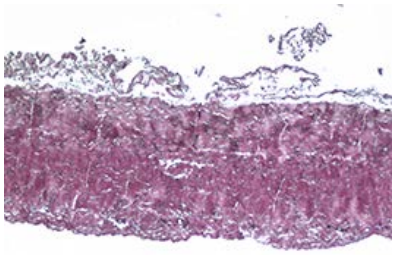

Fig. 4. Sample of bovine pericardium (without laser treatment).

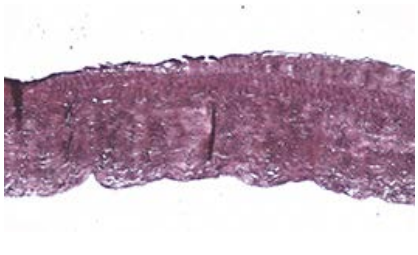

Fig. 5. Sample of bovine pericardium, after conditioning by Er: YAG laser.

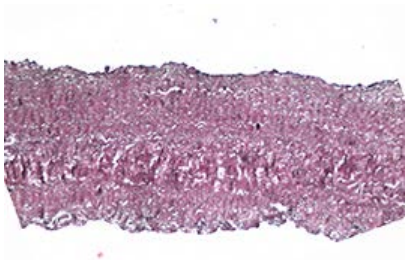

Fig. 6. A sample of bovine pericardium, after conditioning with CO2 laser.

Experiments to remove the hairiness from the fibrous surface of xenopericardial band was accompanied by histological studies, which assessed the degree of smoothness and destructive changes in the depth of the pericardial tissue. All pericardial tissue samples were preserved in 5% diglycidyl ethylene glycol ether, stained with hematoxylin-eosin and exhibited with an increase in X40.

The method of conditioning the fibrous surface of pericardial tissue used for the manufacture of elements of biological cardio-vascular prostheses. The efficiency of surface fibers removal with full preservation of deep-lying collagen structures was verified histologically.

Technology of the tissue conditioning is integrated into the hardware of the laser complex "Melas-Cardio", created on the basis of the CO_2 laser in ILP SB RAS and is intended for processing pericardial tissue and the cutting elements of the artificial valve of heart.

Plasma polarization in scientific, technical and technological applications

A. Medvedev and P. Pinaev
Institute of Laser Physics SB RAS, Prospect Lavrentyev, 15B, 630090, Novosibirsk, Russia
E-mail: arey100x@gmail.com

The main property of the plasma, which makes it possible to use it in a number of applications, is the possibility of amplifying electric fields to values substantially exceeding the external field. The high-frequency branch of the polarization characteristic of plasma has been intensively studied since the middle of the last century and is now widely used in a number of scientific and technical applications. The most well-known is the acceleration of electrons in the wakefields of a lasers pulse. However, low-frequency polarization also leads to an amplification of the electric field at the boundaries of the plasma bulk.

Figures 1, 2 show the simulation results of a plasmatron for the laser-plasma technologies, where the effect of field amplification at the boundaries of a spherical plasma bulk is clearly seen due to the polarization and screening of the field in the plasma itself. Screening of the external field by plasma makes it necessary to concentrate the electric field at its boundaries, where ionization takes place and the production of charged particles for entry into the volume. Despite the fact that simulation at a frequency of 2.45 GHz is presented, this situation is typical for below the plasma frequency, down to a constant current, when one speaks of the cathode and anode layers of a glow discharge.

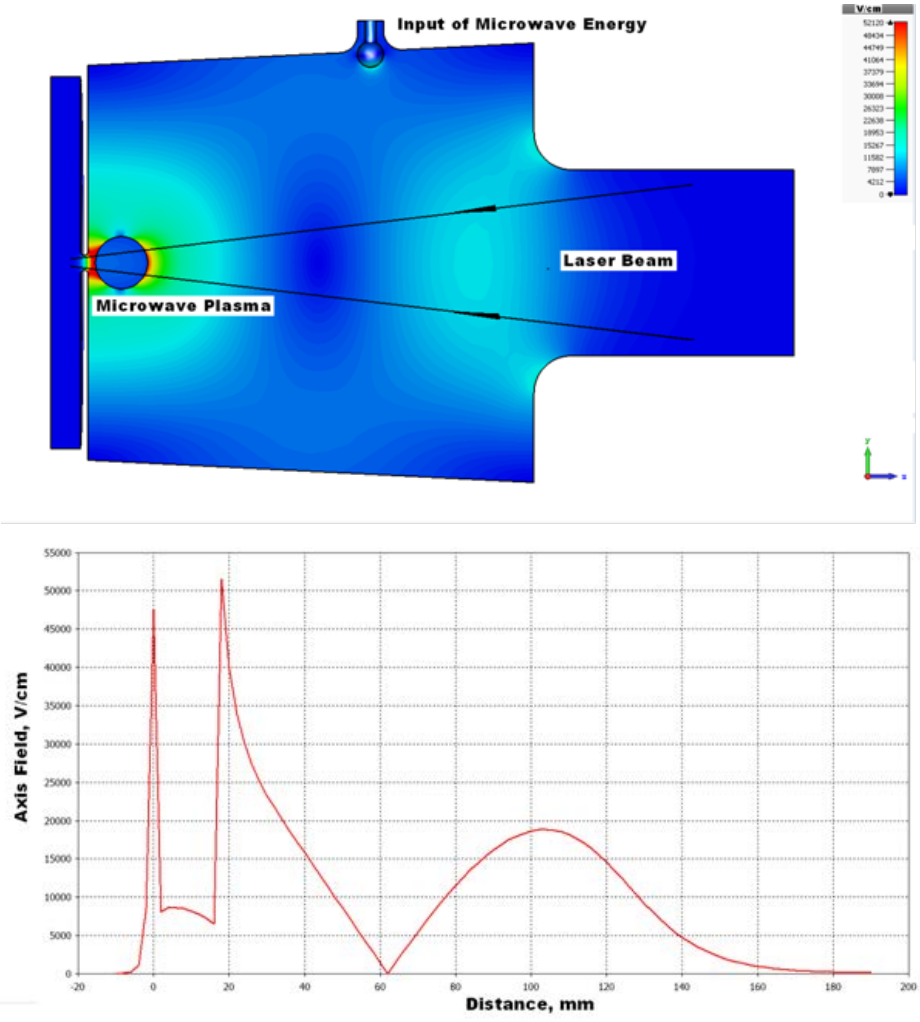

Fig. 1, 2 The distribution of the electric field TE_{011} mode in a quasi-cylindrical resonator with a laser beam passing through the microwave plasma.

In plasma, especially at moderate and high pressures, we can often take the charge separation layers of the plasma components become very thin and the collisional relaxation times are sufficiently short, so that in the overwhelming majority of cases each component can be represented as a continuous medium with an unchanged distribution function. Considering the electric forces, the forces of the gas kinetic pressure and the momentum exchange between the plasma components in collisions, for the selected component of the medium we have a change in momentum per particle with mass *m*:

$$m\left(\partial \mathbf{v}/\partial t + \left(\mathbf{v}\cdot\nabla\mathbf{v}\right)\right) = e\left(\mathbf{E} + \mathbf{v}\times\mathbf{B}\right) - \nabla\cdot\mathbf{p}/n - m\nu\left(\mathbf{v}-\mathbf{v}_0\right) \qquad (1)$$

Assuming that the plasma is nonrelativistic (v << c) and isothermal ($\nabla p = kT\nabla n$), the pattern of motion of the particles is stationary, and the velocity of the interesting us particles (**v**) of significantly larger slow particles of the medium ($\mathbf{v}_0$), and large enough to neglect the convective terms, for the velocity and density of the particle flux ($\mathbf{j}$) of the chosen plasma component we will receive:

$$\mathbf{v} = \frac{e\mathbf{E}}{m\nu} - \frac{kT}{m\nu}\frac{\nabla n}{n},\ \mathbf{j} = \mu n\mathbf{E} - D\nabla n, \qquad (2)$$

where $\mu = e/m\nu$, $D = kT/m\nu$ is the mobility and diffusion coefficients, ν is frequency of collisions the particles of the selected component with the other particles. Using expressions for the fluxes (2) and the equation of continuity of particles: $\partial n/\partial t + \nabla n\mathbf{v} = \dot{n}$ ($\dot{n}$ is the velocity of the bulk processes of generation and loss of charged particles), as in the derivation of the diffusion equation, we try to eliminate the electric field, but we will not neglect terms with the spatial charge density and the dependence of the electron mobility on the field. Then, using the Einstein relation $D = \mu T$ (T is expressed in units of electric potential) and the condition for the electric current $\mathbf{div}\,\mathbf{j} = 0$ we obtain the plasma transport equation (**PTE**): $\partial n/\partial t - \dot{n} = -\mathbf{div}\left(\mu_a\mathbf{f}\right)$, with the acting on the plasma elementary volume force vector: $\mathbf{f} = -\mathbf{grad}\left(w_T + w_E\right) + \mathbf{j}/\mu_e$, where n is the plasma particle densities, $\mu_a = \mu_i\mu_e/\left(\mu_e + \mu_i\right)$ is the plasma ambipolar mobility coefficients, μ_i, μ_e are the mobility coefficients of ions and electrons respectively, $w_T = T_e n_e + T_i n_i$ is the thermal energy of the plasma, $w_E = (n_i - n_e)\varphi$ is the energy of the electric interaction of particles or the plasma electric field energy, T_i, T_e are the parameters characterizing the average energy of the components, called the temperature of positive ions and electrons, n_i and n_e are the densities of ions and electrons, φ is the electric field potential, and $\mathbf{j}$ is the reduced to the electron charge electric current density vector.

From the obtained **PTE**, completely describing the discharge structure at moderate and high pressures [1], [2], the polarization effect with low fields in the volume and high at the boundaries is follows. As follows from (1) in a collisionless plasma, the polarization of the plasma, due to the inertia of the motion of the electrons, leads to an increase in the field in the plasma $\mathbf{E}$ over the external field $\mathbf{D} = \varepsilon\mathbf{E}$, which determines $0 < \varepsilon < 1$. Oscillate of electron in antiphase with the applied field at low frequencies ($\omega < \omega_p$) would lead to a practically zero field, however, the effect is not manifested due to the growing role of collisions: $\varepsilon = 1 - 4\pi e^2 n_e \nu_m / m\left(\omega^2 + \nu_m^2\right)$ and the vanishingly small polarization current with decreasing field frequency. At a low field frequency, the electrons oscillate in the drift mode. Then the screening of the field in the bulk takes place and due to this the field intensification at the boundaries.

Thus, for high-frequency polarization, the field amplification occurs due to the build-up of electrons in the antiphase with the external field, then for low-frequency polarization, due to screening and displacement of the field to the plasma boundaries.

References

[1] A. Medvedev EPJ D **70**, 37 (2016).
[2] A. Medvedev Proc. of SPIE **106141**, 106141W-1 (2018).

Harmonic generation in an inhomogeneous plasma in the relativistic plasma field regime

I. Metelskii[1,2], V. Kovalev[1-3], and V. Bychenkov[1,2]
[1]*Dukhov All-Russia Research Institute of Automatics, ROSATOM, Moscow, 127055, Russia*
[2]*P.N. Lebedev Physical Institute, RAS, Moscow, 119991, Russia*
[3]*Keldysh Institute of Applied Mathematics, RAS, Moscow, 125047, Russia*
E-mail: metelski@lebedev.ru

It is common knowledge that a nonlinear transformation of an electromagnetic wave excited by a laser in an inhomogeneous plasma leads to a resonant enhancenment of a potential electric field in the vicinity of a plasma critical density and the harmonic radiation in vacuum. The harmonic generation process of a low-intensity radiation propagating in an inhomogeneous plasma was investigated in [1] using perturbation theory. In that framework an exponential decrease in the harmonic amplitude with increase in the harmonic number was obtained. The authors of [2] went beyond the perturbation theory by taking into account the nonlinearity of electron motion, but neglecting the relativistic effects. By applying the renormalization group transformation approach, they calculated the amplitudes of harmonics of the electromagnetic wave incident on a nonuniform plasma. They also found that the intensity of harmonics decreases much more slowly with increasing harmonic number than it was predicted by the weakly nonlinear theory. An adequate generalization of the nonlinear theory of the harmonic generation at high laser intensities, when relativistic effects near the plasma resonance becomes essential, is still lacking.

In this study we present the harmonic generation theory by the relativistic plasma resonance mechanism in an inhomogeneous laser plasma. A stationary analytical solution of the nonlinear equations governing the spatiotemporal structure of the electromagnetic field and electron dynamics in the vicinity of the plasma resonance are calculated [3] via the renormgroup symmetries method. Application the formalism of renormalization group transformations to construct the solution allows us to take into account the nonlinearity of electron motion, including the relativistic effects. A nonlinear current, which is the source of the harmonic generation in vacuum and harmonic amplitudes, are found. Relativistic nonlinearity of the plasma wave leads to the phase modulation of the electron oscillations, which determines the power-law decrease in the harmonics amplitudes of the radiation field. Dependences of the harmonic generation efficiency on the laser radiation incidence angle and on the plasma inhomogeneity scale are presented. It is shown that with fixed pump field intensity the efficiency of the higher harmonic generation increases with increasing the plasma inhomogeneity scale. The applicability limits of the obtained theory, which are determined by the conditions of plasma wave breaking near the resonance, are established and analyzed in detail for typical laser and plasma parameters. Comparison with non-relativistic theory shows that the conclusions obtained in the weakly nonlinear [1] and nonlinear nonrelativistic [2] theories of the harmonic generation should be partially reviewed and corrected.

References

[1] N. S. Erochin, S. S. Moiseev, and V. V. Mukhin, Nucl. Fusion **14**, 333 (1974).
[2] V. F. Kovalev and V. V. Pustovalov, Teor. Mat. Fiz. **81**, 69 (1989).
[3] I.I. Metelskii, V.F. Kovalev, V.Yu. Bychenkov, Plasma Phys **43**, 175 (2017).

Electro-optic waveguide modulators based on poled chromophore-doped polymers

S.L. Mikerin[1,2], A.E. Simanchuk[1,2], A.V. Yakimansky[3], N.A. Valisheva[4]
[1]*Institute of Automation and Electrometry, SB RAS, Novosibirsk, 630090, Russian Federation*
[2]*N.N. Vorozhtsov Novosibirsk Institute of Organic Chemistry, SB RAS, Novosibirsk, 630090, Russian Federation*
[3]*Institute of Macromolecular Compounds RAS, St. Petersburg, 199034, Russian Federation*
[4]*Institute of Semiconductor Physics SB RAS, Novosibirsk, 630090, Russian Federation*
E-mail: mikerinsl@iae.sbras.ru

Chromophore-doped polymers have a huge potential in terms of the formation on their basis of various electro-optical and photonic planar devices such as optical switches, electro-optical modulators and optical logic devices. Nonlinear optical component in such kind of materials is chromophore – an organic complex with large molecular hyperpolarizability. Thin-film materials ordered by an external field demonstrate the quadratic optical nonlinearities, one-two orders of magnitude higher than the same solid-state inorganic crystal structures. Such a high nonlinearity allows reduce the operating modulators voltage by an order of magnitude [1, 2]. Moreover, the frequency dispersion of refractive index of the polymer structures is much less than crystalline counterparts and allows optical and radio waves propagate in-phase to a long distances, ensuring a wideband of microwave modulation.

Chromophore-Doped Polyimides Synthesis. The choice of polyimides as a backbone matrix was primarily due to their high glass transition temperature and, as a consequence, the expected high stability of the resultant polyimide-chromophore composition. We have synthesized a number of original polyimides, which allows the covalent addition of commercial DR (Disperse Red) dyes [3]. It allowed us to realize high admissible concentrations of chromophores in polyimide matrix preventing the migration, aggregation and crystallization processes.

Waveguide modulator elaboration. The lower gold electrode was deposited on the 250 μm silicon substrate, after which the polymer UV-cured layers (standard photoresist SU-8) were successively applied and processed via appropriate mask. The mask allowed us to create an array of both a phase and amplitude (Mach–Zehnder) modulator on one substrate (Fig. 1a). The widths of channels (from 2 to 5 μm) to be fabricated were calculated taking into account the refractive indices of the layers and the condition of the single-mode regime of channeling radiation inside the structure. Thicknesses of the lower and middle polymer layers, which form lower cladding, were 2 and 1 μm respectively. The resulting channels were filled with synthesized chromophore-doped polyimide (active waveguide core, spin coating at 600 rpm, layer thickness 1.5-2 μm), and then closed with an upper polymer coating. Commercial UV-cured polymer NOA 61 was used as an upper layer (layer thickness 5 μm). After these procedures, the upper metal (gold on chromium) electrode was deposited. The structures were poled through operating electrodes with a voltage of 75 V applied to each μm of the total thickness of the structure.

In result of the elaboration, we had an array of compact planar modulators with 2.5 cm length. Architecture of the array was designed in such way that a direct channel of the phase modulator of the same width was located next to each amplitude Mach-Zehnder modulator, and both modulators had a common control electrode. This solution ensures the identity of the transverse geometric dimensions of the waveguides and the degree of their poling. There are hard-to-control parameters of the Y-branch in Mach-Zehnder interferometer such as edge of arrow-like section of channels, total width of the channels in the section of their divergence, and the lack of balance of the interferometer arms. The presence of a phase modulator as the simplest structure near the Mach-Zehnder interferometer allows controlling the waveguide properties of the interferometers and obtain reliable information about the electro-optic properties of the active core.

Results. Our elaborated phase and Mach-Zehnder waveguide modulators were tested at zero operating frequencies (1 kHz) at 1310 nm. Lensed polarization maintaining fiber was used to insertion of the single-mode laser radiation. Modulated signal from output port was registered by objective with NA = 0.2 and photodiode. A typical modulation curve show on Fig.1b on background of the control

voltage pulses of triangular shape. The amplitude modulators in the array showed half-wave voltages Vπ from 24 to 38 V under the length of active part L = 1.3 cm depending on the modulator sample in the array and on input light polarization. Minimal value of the figure of merit of the device was 31 Vcm when linear polarization of the input light is normal to plane of the structure. Total optical losses to input-output and propagation did not exceed 20 dB.

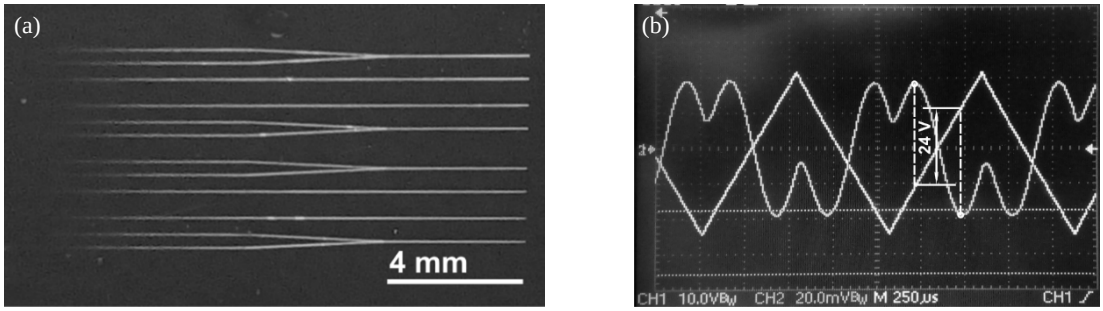

Fig. 1 (a) Photo of a fragment of modulators array. (b) A typical modulation curve.

Conclusion. The main result of this work is the elaboration of a planar amplitude modulator of the Mach-Zehnder type based on heat-resistant polymers and a successful demonstration of its modulation properties. The total length of the modulator was 2.5 cm, the length of the active part was 1.3 cm. The minimum half-wave voltage for the structures was 24 V.

Acknowledgments and funding. This work performed with the equipment of the Collective Use Center "High-resolution spectroscopy of gases and condensed media" based at the Institute of Automation and Electrometry of the Siberian Branch of the Russian Academy of Sciences (http://ckp-rf.ru/ckp/3046/).

The work was supported by the Russian Science Foundation (Grant No. 16-13-10156) in part of design and fabrication of the waveguide structures; waveguide and modulation properties of the structures studied under funding by the complex program of basic academic research (State Registration No. AAAA-A17-117060810014-9).

References

[1] L.R. Dalton, W.H. Steier, B.H. Robinson, et al., J. Mater. Chem. **9**, 1905 (1999).
[2] L.R. Dalton, P.A. Sullivan and D. H. Bale, Chem. Rev., **110**, 25 (2010).
[3] G.I. Nosova, I.G. Abramov, N.A. Solovskaya, et al., Polym. Sci. Ser. B, **53**, Issue1-2, 73 (2011).

Whistlers produced by laser plasma in a rarefied magnetized background

I.B. Miroshnichenko[1,2], V.N. Tischenko[1], I.F. Shaikhislamov[1,2], A.G. Berezutsky[1], Yu.P. Zakharov[1], A.A. Chibranov[1,2], M.S. Rumenskikh[1,2], M.A. Efimov[1,2]
[1]*Institute of Laser Physics SB RAS, Russia, Novosibirsk, Academician Lavrentyev Avenue, 15b*
[2]*Novosibirsk State Technical University, Russia, Novosibirsk, Prospekt K. Marksa, 20*
[3]*Novosibirsk State University, Russia, Novosibirsk, Novosibirsk, Pirogova Str., 2*
E-mail: mib383@gmail.com

One of the actual directions of space experiments is associated with the generation of low-frequency waves produced using HF radiation from heating stands (HAARP, Sura) [1-4] or space-based devices, for example, "Active cord" [5, 6]. The possibilities of using these methods in problems of ionospheric modification are limited by the low efficiency of generation of low-frequency waves. So in experiments [4], the ratio of the power of long-wave radiation to the output power of HAARP was of the order of ~ 100 mW / MW. With parametric generation, the ratio of the whistler magnetic field to the external magnetic field is in the range from 10^{-6} to 10^{-3} [6]. In laboratory experiments on a LAPD facility (USA), whistlers are studied, which are created as a result of the interaction of a laser plasma with a magnetized background plasma [7]. The comparatively low efficiency of whistler generation is apparently connected with the geometry of the thermal expansion of the plasma (across the external magnetic field).

In the Institute of Physics of the Siberian Branch of the Russian Academy of Sciences, the method of generating low-frequency waves, created as a result of resonance interaction by periodic bunches of a laser plasma with a magnetized background plasma, was first proposed at the KI-1 stand [8, 9]. And it is possible to generate three types of waves - slow magnetosonic, torsion Alfvén and whistler [10]. The efficiency of generation of the first two types of waves can reach up to ~ 50%.

In this paper we present the results of a numerical simulation of the whistler generation by a bunch of laser plasma on a supercomputer. The calculation parameters are close to the capabilities of the KI-1. The MHD model with axial symmetry relative to the external magnetic field was used. The Hall forces and the inertia of the electrons responsible for the generation of whistlers and torsion Alfvén waves were taken into account. The spherical geometry of the expansion of the bunch made it possible to generate with high efficiency all three types of waves that had axial symmetry and propagated along the axis of the magnetic power tube. In contrast to [7], a torsional Alfven wave was generated in which the plasma of the background rotates azimuthally and the wave carries the angular momentum.

It follows from the calculations that the whistlers are formed if the parameters of the bunches satisfy the set of the following conditions: the ion-plasma length in the background plasma is greater than L_{pi}> 0.3, the Larmor radius of the clusters is R_L <1, the plasma expansion velocity of the bunches substantially exceeds the velocity of the Alfvén waves and R_L / L_{pi}. All parameters are normalized to the dynamic radius R_d of the bunch, which depends on its energy and the magnetic field of the background. When these conditions are fulfilled, it follows from the calculations that the whistlers are effectively formed in a background plasma whose ion mass can differ by more than 10 times. Calculations were carried out for fully ionized hydrogen, helium, and argon. The intensity of the whistlers can be characterized by the ratio of the azimuthally magnetic field B_φ in the whistlers to the external magnetic field B_0. In the calculations and experiment, a record value of B_φ / B_0 ~ 0.1 - 0.25 was reached. The main part of the whistler wave packet is localized in a power tube whose radius is approximately equal to R_d. The intensity reaches a maximum near the axis at R_d ~ 0.1.

Fig. 1 shows the structure of B_φ / B_0 for the selected time. In the trail of the whistler packet, a low-frequency signal is formed, which is associated with the manifestation of the self-focusing effect (hypothesis). This allows us to simultaneously generate whistlers, the spectrum, which contains lines whose frequencies differ by more than an order of magnitude.

Thus, it is shown that, at optimal parameters, laser-plasma bunches can be generated by intense whistlers with the ability to control the spectrum, including obtaining VLF waves.

Acknowledgements. The reported research was funded by Russian Foundation for Basic Research and the government of the region of the Russian Federation, grant № 18-42-543019, № 18-32-00029, № 16-52-14006; Presidium of the Russian Academy of Sciences ("Basic Foundations of Dual-Use Technologies", Programme No. 31); SB RAS basic research project II.10 №0307-2017-0015 and RSF grant № 18-12-00080. Parallel computing simulations, were performed at the Computation Center of Novosibirsk State University, SB RAS Siberian Supercomputer Center, and Supercomputing Center of the Lomonosov Moscow State University.

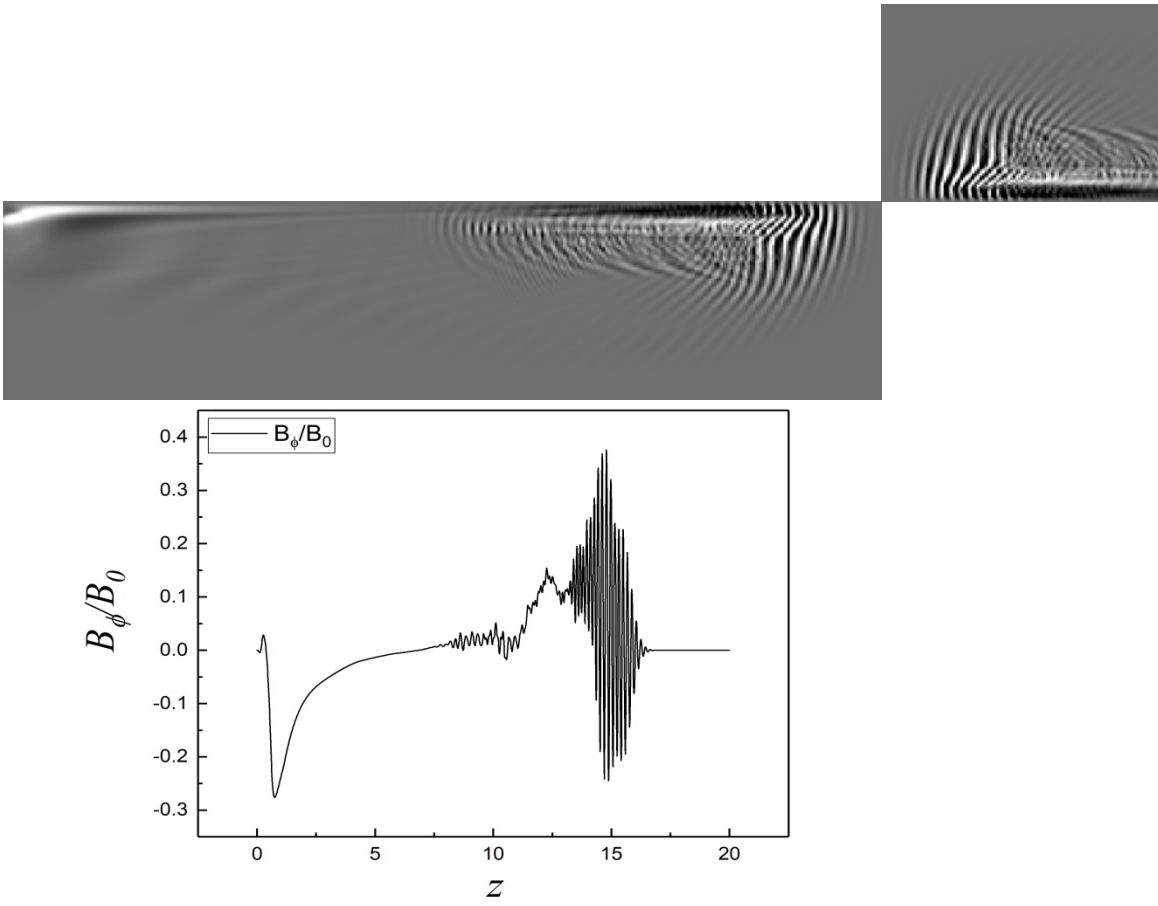

Fig. 1 a) structure of B_φ field: horizontal axis is z, vertical — r, plasma source locates on the symmetry axis at the left side of figure. b) B_φ field near the symmetry axis.

References

[1] V.L. Frolov, N.V. Bakhmet'eva, V.V. Belikovich et al., Phys. Usp. **50**, 315 (2007).
[2] G. A. Markov, A.S. Belov, Phys. Usp. **53,** 703 (2010).
[3] U.S. Inan, T. F. Bell, J. Bortnik, and J. M. Albert, J. Geophys. Res. **108**, SMP6 (2003).
[4] R. Barr, D. Llanwyn Jones, C.J. Rodger, Journal of Atmospheric and Solar-Terrestrial Physics **62,** 1689 (2000).
[5] A.S. Belov, G.A. Markov, L.L. Popova, Yu.V. Chugunov, Geomagnetism and Aeronomy. **49**, 187 (2009).
[6] M.E. Gushchin, S.V. Korobkov, A.V. Kostrov et al. Jetp Lett., **92**, 85 (2010).
[7] P. V. Heuer, M. S. Weidl, R. S. Dorst et al, Phys. Plasmas, **25**, 032104 (2018).
[8] V.N. Tishchenko, Yu.P. Zakharov, I.F. Shaikhislamov et al, JETP Letters, 104, 293 (2016).
[9] V.N. Tishchenko et al., Quantum Electronics, **47**, 849 (2017).
[10] P.A. Prokopov, Yu.P. Zakharov, V.N. Tishchenko et al, Solar-Terrestrial Physics. 2, 19 (2016).

Effect of terahertz radiation on the transport properties of albumin: in vitro investigation

E. Nemova[1], O. Cherkasova[2], and G. Dultseva[3]
[1]*Institute of Laser Physics SB RAS, pr-t ak.Lavrentieva 15B, Novosibirsk, Russia*
[2]*Institute of Chemical Kinetics and Combustion SB RAS, Institutskaya 3, Novosibirsk, Russia*
E-mail: endy@ngs.ru

Biopolymers functioning as transport agents enter reversible processes to form weakly bound complexes with the substances to be transported. Hydrogen bonding and steric hindrance are essential factors governing the possibility of reversible adsorption. This is why low-energy radiation, in particular within the terahertz range, may cause some detectable chemical consequences, though the radiation in this range cannot cause direct rupture of covalent bonds. We studied the effect of terahertz radiation on the formation of adsorption complexes between albumin, a globular protein playing several important functions including the transport function, and simple molecules such as molecular oxygen and nitrogen oxide. Both these species are biologically significant, so the changes in their binding by albumin may be of crucial importance for living organisms.

We studied the effect of terahertz laser radiation on conformational changes in bovine serum albumin (BSA) pronounced as subsequent changes in the interaction of BSA with oxygen and nitrogen oxide.

Conformational changes in BSA molecule induced by the terahertz radiation were studied by means of in situ spin probing. Paramagnetic centers were formed from a diamagnetic precursor of spin probe (dihydropyrazine dioxide) in the interaction on the reactive sites of BSA molecule. It was discovered that the oxidative ability of reaction centers increases in the irradiated BSA sample in comparison with non-irradiated one. Modeling suggested that possible candidates for reaction sites on which the nitroxide is formed are proline fragments and sulfohydryl groups of BSA molecule. The changes in the degree of precursor to spin probe transformation are the evidence of a conformational transition induced in BSA molecule by the terahertz radiation.

Oxygen adsorption on BSA may be competitive with respect to NO, while transportation of nitrogen oxide is an essential function of BSA. However, a special examination of this issue showed no dependence of the strength of binding in NO-BSA complex on oxygen concentration in solution.

The strength of binding in the BSA-NO complex was investigated using the rate of NO to NO_2 oxidation by atmospheric oxygen. The formation of nitrogen dioxide causes acidification of the local environment, which was measured with the help of pH-sensitive spin trap (pentamethyl-3-imidazoline-3-oxide). The acidity was found to be higher after the interaction of NO with THz-irradiated BSA. This means that the strength of binding in the BSA-NO complex decreases as a result of irradiation, and NO is more readily oxidized to form NO_2. A possible reason of this behavior may be conformational changes induced by THz radiation, causing some steric hindrance for more efficient binding.

The discovered consequences of BSA irradiation within the THz region, namely changes in BSA binding with oxygen and nitrogen oxide, provide evidence that THz raidation induces changes in BSA conformation. This is an example that rather weak action may cause observable chemical consequences. This phenomenon is to be studied in more detail because of the importance of the processes under investigation for protein-based transport in vivo.

Angle-susceptible sensing metasurface in terahertz regime

N. Nikolaev[1,2], S. Kuznetsov[3], and M. Beruete[4]
[1]*Institute of Laser Physics SB RAS, 15B, Academician Lavrentiev Ave., Novosibirsk, 630090, Russia*
[2]*Institute of Automation and Electrometry SB RAS, 1, Academician Koptyug Ave., Novosibirsk, 630090, Russia*
[3]*Rzhanov Institute of Semiconductor Physics SB RAS, Novosibirsk Branch "TDIAM", 2/1 Lavrentiev Ave., Novosibirsk, 630090, Russia*
[4]*Public University of Navarra, 31006, Pamplona, Spain*
E-mail: Nazar@iae.nsk.su

Nowadays thin-film coatings and structures are widely used in advanced industrial and scientific applications that makes the tasks of thin-film sensing highly demanded in practice. Last decade, stimulated by a progress in terahertz (THz) instrumentation, a keen interest has been attracted to the THz spectral range to develop its potential for detecting and measuring properties of thin films. The THz radiation can be an alternative to visible and IR waves when examining optically opaque coatings. Meanwhile, due to a relatively large wavelength λ, the conventional spectroscopic methods (TDS-, FDS-, FTIR-, BWO-based) are ill-suited for direct characterization of films with the thickness d of about 2–4 orders of magnitude smaller than λ. This problem can be solved with metamaterials, in particular, with plasmonic metasurfaces (PMSs) [1–3]. The plasmonic resonance exhibits high sensitivity of its spectral response to dielectric environment due to a strong field localization what makes possible measuring of analyte layers satisfying $d << \lambda$ condition.

Traditional approach of THz thin-film sensing with PMSs is based on detecting a frequency shift of the resonance when the analyte is deposited onto the PMS. In this work we present the idea to substitute THz spectral measurements for tracking the PMS response at a fixed wavelength upon changing the incidence angle θ of the exciting THz beam. This concept works well for the PMS with a narrowband resonance sensitive to θ.

The results of the numerical investigations and experimental study of such PMS designed as a single-layer array of hexagon-shaped annular slots with angle-susceptible resonant transmission near 0.85 THz are shown. The proposed approach paves the way to novel compact thin-film sensing devices utilizing the principle of single-wavelength multiangle photometry.

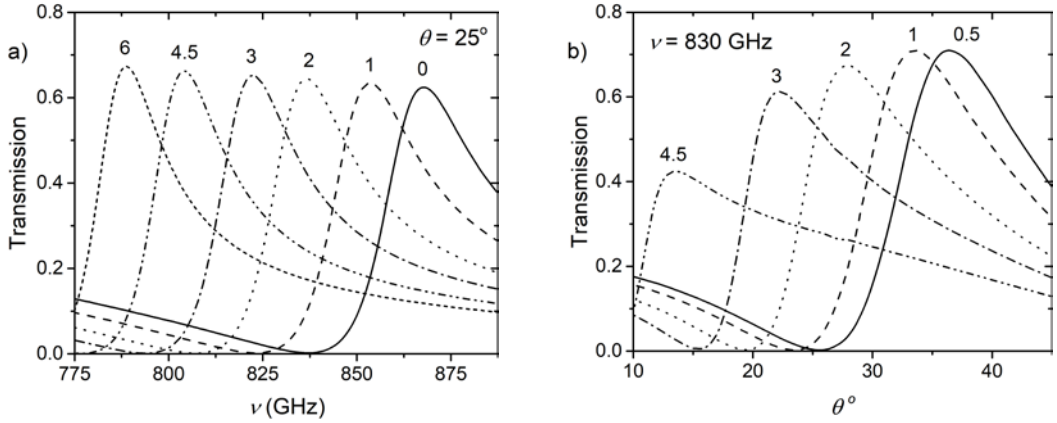

Fig. 1 (a) Transmission spectra for the PMS covered with the analyte of different thicknesses d simulated for three values of the incident angle θ. (b) PMS transmission at 830 GHz as the function of the incident angle θ modelled for different thicknesses d of the analyte overlayer. The numbers indicate the values of d in micrometers.

To illustrate the idea of replacing THz spectral measurements with tracking the PMS response at a fixed λ upon changing the incidence angle θ, the PMS transmission as a function of frequency ν (Fig.1 a) and θ (Fig.1 b) is plotted. The results correspond to the frequency of 830 GHz chosen for

example and a photoresist layer used as the analyte. The dielectric permittivity of the photoresist $\varepsilon = 2.7 - j \cdot 0.25$ was retrieved from direct transmission measurements of a 100 μm thick liquid cell.

The presented data remarkably demonstrate the expected effect of shifting the angular peak due to thickening the analyte. Note, the resonance peak amplitude decreases and its bandwidth increases when the analyte thickness d changes from 0.5 to 4.5 μm. This means that the method sensitivity degrades for the thicknesses larger than 4.5 μm. Nevertheless, the peak remains almost stable in amplitude for the thicknesses $d < 1$ μm and the angles of both maximum and minimum transmission can be used to evaluate the analyte thickness. Thus, the proposed approach is estimated to be promising for THz sensing of sub-μm-thick analyte layers, thereby capable of detecting the level of $d/\lambda \sim 10^{-3}$ at least.

The measurements were carried out in the Shared Equipment Center "Spectroscopy and Optics" of the Institute of Automation and Electrometry, SB RAS.

References

[1] Xu, W., Xie, L., & Ying, Y., Nanoscale **37**, 13864, (2017).
[2] Su, L., Mata-Contreras, J., Vélez, P., & Martín, F. Int. J. Antenn. Propag. **2017**, (2017).
[3] Al-Naib, I., & Withayachumnankul, W. (2017). J. Infrared Millim. Te. **38**, 1067, (2017).

Theory of the high-quality magneto-optical resonances observed in a buffer-gas-filled vapour cell

A. Novokreshchenov[1], D. Brazhnikov[1,2]
[1]*Institute of Laser Physics SB RAS, Novosibirsk, 630090, Russia*
[2]*Novosibirsk State University, Novosibirsk, 630090, Russia*
E-mail: aleksey-box@mail.ru

The electromagnetically induced absorption (EIA) resonance usually manifests itself as a steep increase in the absorption of a medium. This subnatural-linewidth resonance was first observed under a bichromatic laser field composed of two beams with opposite circular polarizations [1]. Then the effect was also studied under a single-frequency light wave accompanied by a static magnetic field (magneto-optical or so-called Hanle configuration) [2]. The main reason that seriously limits EIA use consists of the problem for obtaining the high-contrast and sufficiently narrow resonance. Therefore, getting high-quality EIA resonances will promote their application in many directions of quantum technologies.

A new scheme for observing the high-contrast magneto-optical EIA resonances was proposed in [3]. The idea consisted of exploiting two counter-propagating laser beams with mutually orthogonal linear polarizations to excite an open optical transition in the ^{87}Rb D_1 line. The proposed scheme of excitation and the optical transition chosen allows one using a buffer-gas-filled vapor cell to greatly improve the properties of the nonlinear signals. Recently we have used such the cell to check that idea [4]. In particular, the EIA signals registered in a probe-wave transmission reach an unprecedented contrast of about 135% with respect to the wide ("Doppler") absorption pedestal and 29% with respect to the residual level of background transmission. These contrast values correspond to a relatively small FWHM of about 7.2 mG (5.3 kHz). The width of the narrowest EIA resonance observed is about 2.1 mG (1.5 kHz). To our knowledge, such a large relative contrast at the kHz-width is the record result for EIA.

In spite of the success reached, any explicit and consistent theory of the high-quality EIA-resonances effect that would quantitatively predict the experimental data has yet been presented. Our current work is aimed to develop such the theory based on the standard quantum-mechanical density matrix approach. First, the results obtained agree well with the experimental data. Second, the theory helps us to understand potential abilities of the new observation scheme. For instance, we studied influence of a stray magnetic field on the properties of high-contrast EIA resonances. In particular, it is seen from Fig. 1 that the contrast of EIA with respect to magnitude of total absorption at the center of the resonance curve can be very high, but stray magnetic field can significantly limit its value.

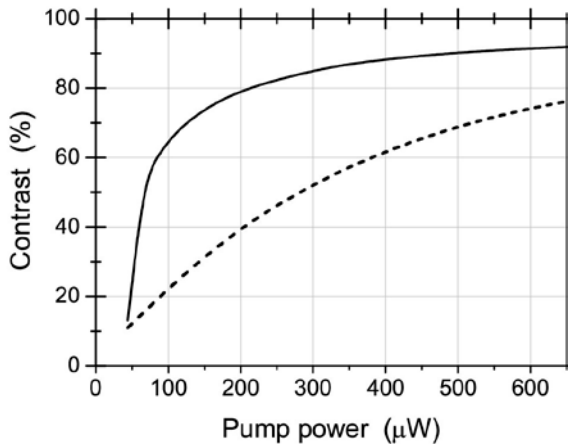

Fig. 1 The resonance contrast vs. pump wave power. It is defined with respect to the total absorption level. The transverse stray magnetic field is absent for the solid line and it equals to 10 mG for the dashed one.

An explicit analytical expression for the spectroscopic signal has been derived for the optical transition $F_g = 1 \rightarrow F_e = 1$ in the ^{87}Rb D_1 line. A new feature of the magneto-optical resonances has been revealed that consists of observation of a shift of the resonance center. An analytical expression for the shift has been also derived. It appears that the shift itself can serve as a basis for the new method of magnetic-field vector measurements.

The authors thank Russian Foundation for Basic Research (grant nos. 18-32-00707).

References

[1] A. Akulshin, S. Barreiro and A. Lezama, Phys. Rev. A **57**, 2996 (1998).
[2] Y. Dancheva et al., Opt. Commun. **178**, 103 (2000).
[3] D. Brazhnikov et al., Laser Phys. Lett. **11**, 125702 (2014).
[4] D. Brazhnikov et al., Laser Phys. Lett. **15**, 025701 (2018).

Optical vortex induced by light–matter interaction in fiber-coupled liquid crystal

S. Trashkeev[1,2], B. Nyushkov[1,2], and S. Shvetsov[3,4]
[1]*Novosibirsk State University, Pirogova str. 1, 630090, Novosibirsk, Russia*
[2]*Institute of Laser Physics, SB RAS, Ac. Lavrentyev's Prospect, 15B, 630090, Novosibirsk, Russia*
[3]*Lebedev Physical Institute, RAS, Leninsky Prospect, 53, 119991, Moscow, Russia*
[4]*Lomonosov Moscow State University, Leninskie Gory, 119991, Moscow, Russia*
E-mail: nyushkov@laser.nsc.ru

This paper reports on experimental research into the generation of optical vortex, i.e. light beam with the helical phase front, using disclination structure [1] induced in the fiber-coupled nematic liquid crystal (NLC) by light field of the fundamental fiber mode. Optical layout of our experimental setup was similar to the one used earlier [2, 3] to induce and study quadratic nonlinearity in NLC. In this layout a ~100-μm thick homeotropic NLC layer is deposited onto the end-face of a single-mode optical fiber. Such setup features relatively simple design, and makes it possible to effectively induce NLC disclinations with different strength due to high-gradient light field distribution at the fiber end-face. Moreover, the light-induced NLC disclination structure can be easily modified in the setup by changing fiber mode polarization state, NLC temperature, and by applying external electric field.

There are two key factors, which are in the basis of light-induced transformation of the NLC orientation structure and the consequent formation of the optical vortex in the proposed optical scheme. The first one is the light-induced Fredericksz effect [4], at which the NLC director (unit vector in the direction of the preferable orientation of NLC molecule long exes) tends to align along the light field, and the second one is the thermo-orientational effect [5], at which NLC director reorients in the direction of heat flow due to nonuniform light beam heating. The combination of these mechanisms can lead to the formation of a NLC disclination structure in the NLC layer, the geometric axis of which coincides with the axis of the light beam propagation. When the initial polarization is close to the circular one, this disclination leads to the appearance of a singularity of the light wave complex phase, which violates its symmetry and transforms the wave front into a spiral (helical) form [1]. Thus the optical vortex formation occurs during the light propagation through the self-induced NLC disclination (Fig. 1).

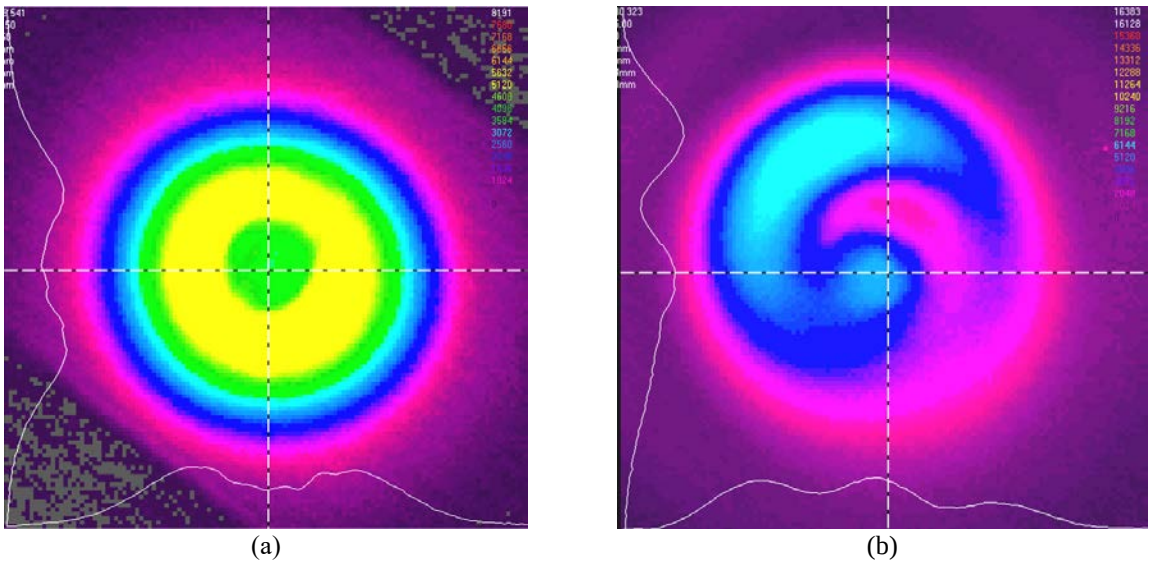

(a) (b)

Fig. 1 The transverse beam profiles (registered with a beam profiling camera Pyrocam): the optical vortex formed in the presence of external electric field (a); interference of the fundamental and vortex beams (b).

An erbium-doped fiber laser with a wavelength of ~ 1.55 μm served as a coherent light source in our experiments. Initial polarization state of the laser radiation coupled into the NLC was adjusted by

using fiber-optic polarization controllers in order to trigger and control transformation of the fundamental fiber mode to the optical vortex. In addition, the light-induced orientational structure in the NLC was tuned with the aid of external electric field applied transversely to the light beam axis. The thermoelectric converter was also used to control the NLC temperature.

The process of nonlinear light-matter interaction with the formation of the optical vortex had a threshold character. The threshold light power was strongly dependent on the thickness and temperature of the NLC layer and varied in the range of 10-30 mW. In general, when the initial light polarization was rather elliptical (the optimal polarization state was adjusted depending on the light intensity, the NLC thickness and temperature), the external electric field enabled formation of a light beam with a circular intensity distribution in its cross section (Fig. 1a). The profile of the formed beams was registered with the help of Pyrocam beam profiling camera. At a partial conversion, a characteristic pattern of interference between the fundamental and the vortex components of the light beam could be observed (Fig. 1b). The resulting interference pattern corresponds to the vortex with the charge $|m| = 1$, and therefore the topological charge of the NLC defect equals $|t| = ½$.

Thus, the possibility of efficient conversion of the fundamental fiber mode to an optical vortex in the microscopic NLC layer is demonstrated. The results of this study can possess a practical interest because of the expansion of the capabilities of optical telecommunication and metrological technologies by using of optical vortices with their specific features of intensity distribution, nonzero orbital momentum etc. [6].

This study was supported by the Russian Science Foundation (Project No. 18-72-00242).

S.T. and B.N. were supported by the Ministry of Education and Science (Project 5-100).

References

[1] R. Barboza, U. Bortolozzo, M. G. Clerc et al., Adv. Opt. Photonics **7**, 635 (2015).
[2] B. N. Nyushkov, S. I. Trashkeev, V. M. Klementyev et al, Quantum Electron. **43**, 107 (2013).
[3] S. I. Trashkeev, B. N. Nyushkov, "Thermal enhancement of optical harmonic generation in a fiber-coupled nematic liquid crystal", Laser Optics 2014-IEEE International Conference, 1 (2014).
[4] L. Csillag, I. Janossy, V.F. Kitaeva et al., Mol. Cryst. Liq. Cryst. **78**, 173 (1981).
[5] S. I. Trashkeev, A. V. Britvin, Tech. Phys. **56**, 747 (2011).
[6] S. Franke-Arnold, L. Allen, M. Padgett, Laser & Photon. Rev. **2**, 299 (2008).

Laser beam instrumental system (LBIS) landing aircraft

V.G. Oshlakov[1], Yu.V. Khokhlova[2], and S.M. Prigarin[2,3]
[1]*V.E. Zuev Institute of Atmosphere Optics SB RAS, pl. Academician Zuev, 1, 634055, Tomsk, Russia*
[2]*Novosibirsk State University, ul. Pirogova, 2, 630090, Novosibirsk, Russia*
[3]*Institute of Computational Mathematics and Mathematical Geophysics SB RAS, Prospekt Academician Lavrentyev, 6, 630090, Novosibirsk, Russia*
E-mail: oshlakov@iao.ru; julya_hohlova@mail.ru; sergeim.prigarin@mail.com

At present, is topical the problem of ensuring the landing of aircraft according of III c category, when the range of visibility on the runway, is close to zero. As you know, when boarding a plane decreases on a glide path to a height of 30 meters, and then goes to a decrease in the exponential trajectory (alignment path) to the touch of the runway. To solve this problem, it is necessary that at the beginning of the alignment path the course of the aircraft and the axis of the fuselage coincide with the glide path. The landing systems operating in the radio range are not principally possible to get the information that the pilot needs to do this. In LBIS planting the laser beam coincides in direction with the glide path and is 15 meters from it. Two photodetector blocks placed on the aircraft at a base distance from the beam images (the ray is visible due to scattering in the atmosphere) determine its position, and, consequently, the glide paths in the aircraft coordinate system. The phenomenon of multiple scattering of optical radiation worsens the contrast of the image of the laser beam and determines the tactical and technical characteristics of LBIS aircraft landing. **To study this phenomenon, we calculated body brightness (radiance angular distributions) of the optical field at glide path points by the Monte Carlo method**.

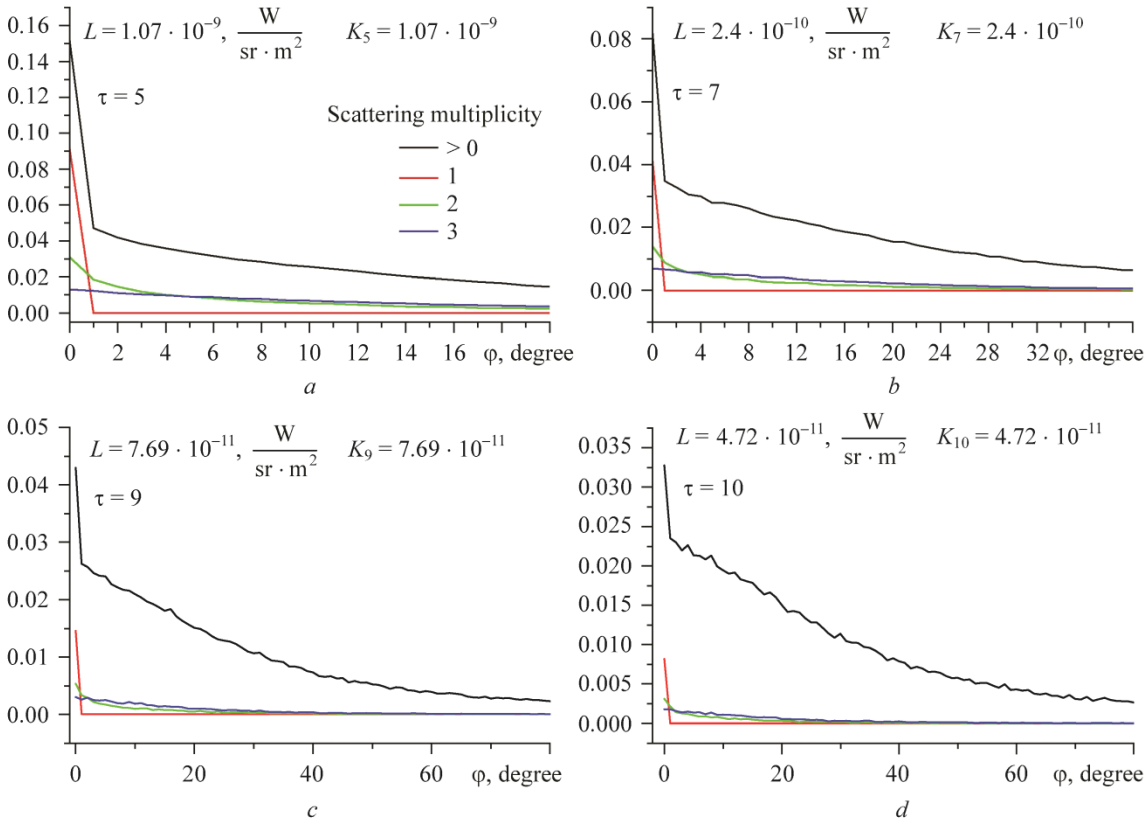

Fig. 1 Sections of brightness bodies.

The sections of the brightness bodies with a 75-degree sectional plane are shown in Fig. 1 (*a*, *b*, *c*, *d*) in accordance with the calculation scheme for the brightness bodies (Fig. 2). The fog is a model medium, the meteorological visibility range is 200 meters. The analysis of the figures has shown that the radiation of only the first and second scattering multiplicity has the expressed research area. The

radiation of the first scattering multiplicity makes it possible to determine the direction to the laser beam with an accuracy not worse than one degree up to $\tau = 10$. To increase the contrast of the image of the laser beam, it is necessary to cut the scattered radiation above the second multiplicity.

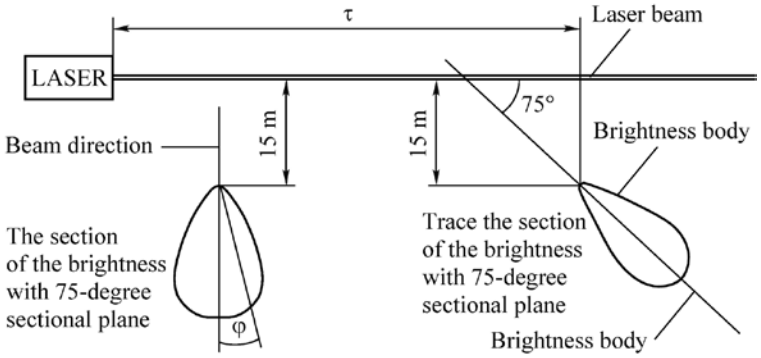

Fig. 2 Calculation scheme of brightness bodies.

References

[1] Patent RF No. 2322371. V.G. Oshlakov "Way of orienting moving vehicles by bight beam and its implementation". Paritet 1 February 2006.

[2] Oshlakov V.G., Tsvyk R.Sh., Soldatov A.N., Ilyushin Ya.A. Principles of construction of laser beam guidance system. Part I // Izv. vuzov. Fizika. 2013. **56**, No. 10/2. P. 84–93.

[3] Deimmerdjan D. Scattering of electromagnetic radiation by spherical polydisperse particles. Moscow: Mir, 1971. 300 p.

Pulsed optical pumping technique in application to rubidium compact atomic clocks

G. Osipenko, V. Baryshev, M. Aleynikov, I. Blinov
FSUE VNIIFTRI, Mendeleevo, 141570, Russian Federation
E-mail: osipenko.9494@mail.ru

Currently, a vital need exists for the compact (a mass of ~10 kg and a volume of ~10 l) quantum frequency standards (QFS's) possessing a short-term instability better than 5×10^{-13} (the averaging time 1 s) and a long-term instability at a level of 10^{-15} (the averaging time 10^5 s).

Such QFS's can be applied in radio navigation systems, as well as for synchronization of telecommunication networks and local time scales, including on-board ones. However, the existing microwave QFS's (including atomic beam tubes with magnetic selection of quantum states, atomic beam tubes with laser pumping, fountain-type clocks based on cold atoms, hydrogen frequency standards of active type, passive hydrogen frequency standards, and rubidium vapor cell frequency standards with lamp optical pumping) do not satisfy modern requirements to on-board QFS's for rapidly progressing global navigation satellite systems by at least some of such parameters as instability, mass and overall dimensions, energy consumption, reliability of operation.

The compact atomic clocks based on Rb gas cell with pulsed optical pumping and detection and with Ramsey interrogation in microwave cavity demonstrate improved frequency stability compared to that of existing lump-pumped Rb frequency standards and have the capacity to reach the stability level of the passive hydrogen masers [1–4]. The main physical advantage of the POP clocks is that the atomic clock transition is probed in the absence of optical radiation in the cell. This leads to the essential suppression of the light shift (ac Stark shift) which is the main source of frequency instability in optically pumped microwave frequency standards.

In the presented work we report the performance of the pulsed optically pumped Rb clock laboratory prototype. The Ramsey fringes with linewidth of 185 Hz, with no averaging on cycles at microwave frequency sweeping around clock transition frequency were obtained (Fig. 1). The study of the central fringe contrast in dependence on the pumping and detection laser pulses duration and intensity as well as on the cell temperature was conducted. The optimized central fringe contrast value exceeding 40% at cell temperature of 65 ^{0}C has been reached. We also report the achievement of the Rabi-Ramsey CPT resonances in lin||lin configuration of bichromatic laser radiation [5] in the same cell (Fig. 2). The magnetic sensitivity of the Rabi – Ramsey CPT transitions is studied. The perspectives of building atomic clock based on CPT will be discussed.

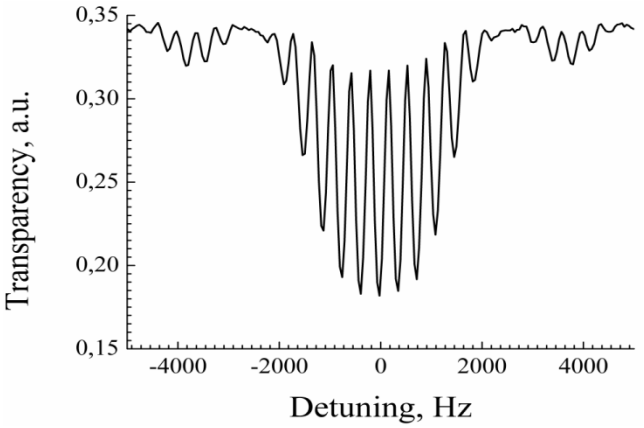

Fig. 2 Ramsey fringes with central fringe contrast over 40% achieved by implementing POP technique.

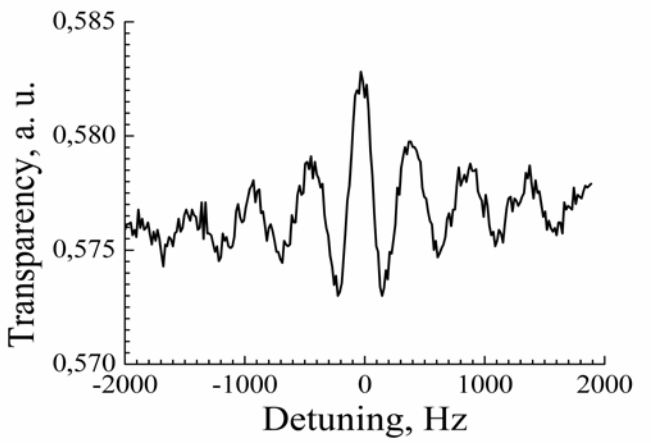

Fig. 3 Ramsey- CPT line without averaging on cycles.

References

[1] S. Micalizio, C. Calosso, A. Godone, and F. Levi, Metrologia, **49**, p. 425, 2012.
[2] S. Kang, M. Gharavipour, C. Afolderbach, F. Gruet, and G. Mileti, J. Appl. Phys., **117**, p. 104510, 2015.
[3] S. Micalizio, F. Levi, A. Godone, C. Calosso, B. Francois, R. Boudot, C. Afolderbach, S. Kang, M. Gharavipour, F. Gruet, G. Mileti, Journal of Physics: Conference Series, 723 (2016) 012015.
[4] V N Baryshev, M S Aleynikov, G V Osipenko, I Yu Blinov, QUANTUM ELECTRON, **48**, No. 5, 443, 2018.
[5] A. V. Taichenachev, V. I. Yudin, V. L. Velichansky and S. A. Zibrov, JETP Letters, **82**, No. 7, p. 398, 2005.

Yb-doped SrB_4O_7 -glass: A perspective laser material

A.A. Rybak[1,3], E.N. Galashov[2], V.V. Petrov[1-3], and E.V. Pestryakov[1]
[1]*Institute of Laser Physics SB RAS, 15b Ave. Ac. Lavrentyeva, Novosibirsk, 630090, Russia*
[2]*Novosibirsk State National Research University, 2 St. Pirogova, Novosibirsk, 630090, Russia*
[3]*Novosibirsk State Technical University, 20 Ave. K. Marksa, Novosibirsk, 630073, Russia*
E-mail: pefvic@laser.nsc.ru

Currently, among a number of known solid-state laser media, few have high parameters of optical, spectroscopic, thermophysical and generation properties, which determine their wide application in laser systems. In solid-state lasers and systems, in addition to crystals, glass and glass-ceramic media are actively used, allowing scaling of active elements to considerable sizes and increasing the output energy of laser radiation to a mega joule level [1].

Advantages of glasses include their high optical quality and the possibility of introducing high concentrations of ion-activators into the matrix, whose absorption and emission bands become wide due to the internal disorder of the glass structures. This makes them very promising for use in diode-pumped lasers [2]. It should also be noted that, due to the wide practical use of fiber lasers based on activated fused silica fibers, there has been a tendency to search for new glass matrices (borate, silicate, tungstate and others) of various compositions to enhance the efficiency of solid-state radiation sources of this type [2, 3].

Within the frame of this project Yb-doped strontium borate glasses $SrO\text{-}2B_2O_3$ (Yb:SBO-glass) with composite similar to a crystal tetraborate strontium - SrB_4O_7 have been synthesized by conventional melt-quenching technique. The physical and spectroscopic characteristics of glasses with $32SrO\text{-}65B_2O_3\text{-}3Yb_2O_3$ composition have been experimentally studied and perspective of their use in lasers and laser systems with diode pumping was defined.

The density of $32SrO\text{-}65B_2O_3\text{-}3Yb_2O_3$–glass samples ($\rho$=3.1 g/cm^3) was measured by hydrostatic weighing method and the concentration of Yb ($N_{Yb} = 3.8\cdot10^{20}$ cm^{-3}) in samples was calculated. The dispersion of the refractive index in the spectral range 400 – 1200 nm was defined by prism method. The refractive indices were determined using the method of measuring the minimum angle derivation of a light beam through the prism. The absorption and luminescence spectra of the Yb:SBO–glass samples were determined at room (300 K) and cryogenic (77 K) temperatures.

On the basis of the experimental data the absorption (σ_{abs}), emission (σ_{em}) and gain (σ_g) cross sections were calculated. The emission cross section was calculated by Füchtbauer-Ladenburg ratio and reciprocity method [3]. The position of the Stark levels of $^2F_{7/2}$ (ground) and $^2F_{5/2}$ (excited) electronic states of Yb^{3+}-ions were determined using the Yb:SBO glass absorption and emission spectra at temperature 77 K. The value of the radiative lifetime of the excited state on the $^2F_{5/2} \rightarrow {}^2F_{7/2}$ transition has been determined from the absorption spectra by using reciprocity method : $\tau_{rad} = 0.77$ ms. The spectra of gain cross-section - $\sigma_g(\lambda)$ determined as $\sigma_g(\lambda) = \beta\cdot\sigma_{em}(\lambda) - (1\text{-}\beta)\cdot\sigma_{abs}(\lambda)$ with the fraction on Yb ions in the upper manifold - β are presented on Fig. 1.

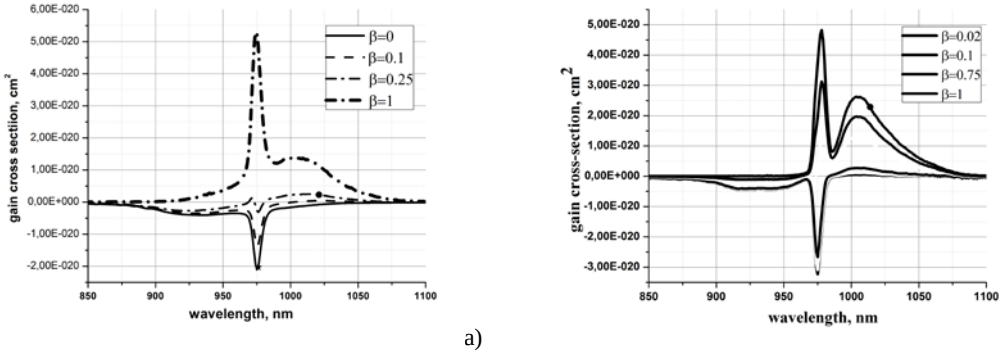

a) b)

Fig. 1 Gain cross section spectra of Yb:SBO–glass at 300 K (a) and 77 K (b).

The comparative analysis of the obtained data of laser properties with the data of known laser media was performed and the advantages of Yb:SBO glass were identified.

Results of research show promising of the use the Yb: SBO glass as active medium for diode pumped laser systems.

This work is supported in parts by RAS Presidium Program "Extreme light fields and their interaction with matter" and Government program (SB RAS).

References

[1] L.D. Deloach, S.A. Payne, L.L. Chase, L.K. Smith, W.L. Kway, W.F. Krupke. IEEE J. QE-**29**, 1179 (1993).
[2] L. Su, P. Zhou, J. Yu, H. Li, L. Zheng, F. Wu, Y. Yang, Q. Yang, and J. Hu, Opt. Express., **17**, 13554 (2009).
[3] G.E. Malashkevich, VV. Kouhar, E.V. Pestryakov, V.N. Sigaev, N.V. Golubev, E.Kh. Mamadzhanova, A.A. Sukhodola, Opt. Materials, **76**, 253 (2018).

The development of all-solid state laser system with high average and high peak power radiation

V.V. Petrov[1-3], G.V. Kuptsov[1,2], V.A. Petrov[1,3], A.V. Laptev[1], A.V. Kirpichnikov[1], E.V. Pestryakov[1]
[1]*Institute of Laser Physics SB RAS, 15b Ave. Ac. Lavrentyeva, Novosibirsk, 630090, Russia*
[2]*Novosibirsk State National Research University, 2 St. Pirogova, Novosibirsk, 630090, Russia*
[3]*Novosibirsk State Technical University, 20 Ave. K. Marksa, Novosibirsk, 630073, Russia*
E-mail: vpetv@laser.nsc.ru

The past two decades have seen rapid development in high power laser systems, which have enabled the study of nuclear and electronic dynamics by ultrafast X- ray spectroscopy with unprecedented time resolution ranging from nanoseconds to attoseconds [1].

At the ILP of SB RAS an all diode-pumped cryogenically cooled all solid state high intensity, high average power laser system is developed. The system operates at the repetition rates up to 1 kHz [2]. It consists of two optically synchronized channels: laser amplification channel and parametric amplification channel [3,4]. The laser amplification channel incorporates an all-diode pumped Yb:YAG 6-pass amplifier and all-diode pumped Yb:YAG multipass laser amplifier with closed-loop cryogenic cooling [5]. The second cryogenically cooled multipass amplifier has eight diffusion-bonded YAG-Yb:YAG (10 at.%) crystals. The crystals are shaped as thick disks with the diameter of 25 mm and diameter to thickness ratio of ~5. Total pump power of the second amplifier is 800 W. The channel is designed to produce at least 300 mJ pulses centered at 1030 nm with 1 kHz repetition rate, if seeded with 10 mJ pulses.

Closed-loop cryogenic cooling of disks has advantages such as efficiency, robustness, temperature stability and long-time operation time without additional actions such as replenishment, but also has disadvantage, namely vibration features due to pulsation of gas inside cold heads. Dissected copper heatsinks were designed to suppress angular vibrations caused by pulse tubes and maintain thermal conductivity to remove heat efficiently . Dissected heatsinks are consist of thermal bridge, based on flexible copper links, and a cooper cube mounted to base. This approach allowed to suppress long-term random displacements by two orders of magnitude to less than 10 urads for horizontal plane, and by three orders of magnitude to less than 3 urad in vertical plane for each heatsink in operation. Also, the angular cyclic wandering in short term was reduced by a factor of 3. Thermal properties of the dissected heatsinks were experimentally measured [6]. After the optimization of cooling system, we have obtained small-signal gain coefficient up to 1.5 per pass through active element, corresponding to total gain of 600.

Also, experiments targeted to determination of thermo-optical properties of the active elements of amplifier were carried out. The focal lengths of the thermal lenses in the active elements are modeled and experimentally evaluated. The characteristic focus obtained experimentally is about 10 m. Wavefront profiles after passing through the elements are experimentally measured and it is shown that the dominating aberration is defocus. An indirect measuring procedure of the average temperature of the pumped volume inside active element is experimentally implemented.

The results of this work are targeted to development of all solid state high intensity, high average power laser system. This work is supported in parts by RAS Presidium Program №6 "Extreme light fields and their interaction with matter" and Government program (SB RAS).

References

[1] S. Hädrich, J. Rothhardt, M. Krebs et al. // J. Phys. B: At. Mol. Opt. Phys. 49, 172002 (2016).
[2] V.V. Petrov, A.V. Laptev, G.V. Kuptsov et al. // Proc. of SPIE 10614, 106140U (2018).
[3] A.V. Kirpichnikov, V.V. Petrov, G.V. Kuptsov et al. // Proc. of SPIE 10614, 106149 (2018).
[4] G.V. Kuptsov, V.V. Petrov, V.A. Petrov et al. // IOP Conf. Series: JPCS 999, 012008 (2018).
[5] V.V. Petrov, G.V. Kuptsov, V.A. Petrov et al. // Quantum Electronics 48, 358 (2018).
[6] V.A. Petrov, G.V. Kuptsov, V.V. Petrov et al. // AIP Conf. Proc. 1893, 030121 (2017).

About measuring the forbidden $2^1S_0 - 2^3S_1$ transition frequency of helium by the method of stimulated Raman scattering

P.V. Pokasov[1], A.V. Taichenachev[1,2], E.V. Baklanov[1,2]
[1]*Institute of Laser Physics SB RAS, Pr. Lavrentyeva 15B, Novosibirsk, Russia*
[2]*Novosibirsk State University, ul. Pirogova 2, 630090, Novosibirsk, Russia*
E-mail: pokasov@laser.nsc.ru

We demonstrate the possibility of measuring the forbidden $2^1S_0 - 2^3S_1$ transition frequency (λ = 1557 nm) of a helium atom by the method of stimulated Raman scattering (SRS) through the intermediate 2^3P_1 level. The transition is important for the spectroscopy of the helium atom because it relates the singlet and triplet parts of the spectrum. The frequency of the pumping field (λ = 1083 nm) is close to the frequency of transition $2^3P_1 - 2^3S_1$. The frequency of the stimulated scattering (3561 nm) is close to the frequency of transition $2^3P_1 - 2^1S_0$.

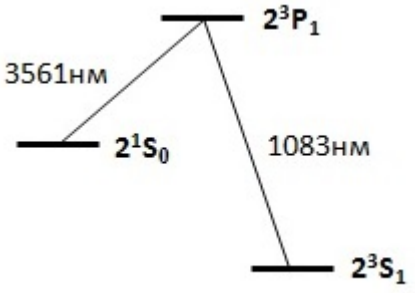

It is known that for lamda-schemes in the form of a line of stimulated scattering, there is a resonance with a homogeneous width of the transition line between the lower levels, which has been well studied theoretically and experimentally (see monograph [1]). Formally, this resonance is present in any problem with the lamda-scheme, but the greatest interest in it is associated with precision spectroscopy. Under the name of "a coherent population trapping resonance" (CPT resonance), it is used as a reference in compact commercial atomic clocks. At a temperature of cooled atoms on the order of 1 μK, we can neglect the motion of atoms and solve equations for the density matrix [2]. For the forbidden $2^1S_0 - 2^3S_1$ transition of helium, we present a solution of these equations and a formula for the SRS resonance. The influence of Doppler broadening, the recoil effect, and the field shift is considered. It was shown there that by using the SRS method it is possible to measure the frequency of the $2^1S_0 - 2^3S_1$ transition with an accuracy of about 1 kHz.

References

[1] Letokhov V.S., Chebotaev V.P. *Nelineinaya lazernaya spektroskopiya sverkhvysokogo razresheniya* (Nonlinear Ultrahigh- Resolution Laser Spectroscopy) (Moscow: Nauka, 1990), p. 512.
[2] E. Baklanov, P. Pokasov, A. Taichenachev, Quantum Electronics **48,** 464 (2018).

Polarized states of alkali with null effective gyromagnetic ratio

E. Popov, V. Bobrikova, K. Barantsev, and A. Litvinov
Peter The Great Polytechnic University, 195251, St.Petersburg, Polytechnicheskaya, 29, Russia
E-mail: enp-tion@yandex.ru

In the work we consider optical pumping of alkali atoms in a gas cell [1]. The main task is to suggest a method of preparing states of alkali atoms ensemble, in which spin polarization is non-zero and magnetization is absent. As we suppose, such states have unusual magnetic properties and may be interesting for inertial navigation and magnetometry [2,3].

Most schemes of pumping for creating of spin-polarization have single-frequency light with circular polarization. Such method of depopulation pumping allows creating one dark state on upper hyperfine level related to $^2S_{1/2}$ electron state. It is a zeeman level with max value of projection of the full angular moment of the atom to quantization axis. So, populating of the dark zeeman state leads to non-zero projection of angular momentum to quantization axis while alkali atoms interact with optical field. There were discussed of using a double frequency laser field for increase effeciency of spin polarization pumping in several previous works. But there were not suggest to using the second laser with different frequency of light for control of the magnetization in the gas cell.

Enter two new definitions:

- effective gyromagnetic ratio is the ratio of expectation value of operator $\hat{\mu}$ to expectation value of operator $\hat{M}$, where $\hat{\mu}$ is projection of magnetic moment to quantization axis, $\hat{M}$ is projection of full mechanical moment to quantization axis.

- g0-state is the state of ensemble of alkali atoms with effective gyromagnetic ratio approximated to zero. Magnetization of the atom ensemble is null, but spin polarization doesn't equal to zero in the state.

The idea of possibility of the existence of the g0-state is based on the difference between the signs of the gyromagnetic ratios of the two hyperfine levels belonged to $^2S_{1/2}$ electron state. Therefore magnetization created by atoms on the first hyperfine level can be compensated with magnetization created by atoms on the second hyperfine level. But in the case, spin-polarization created by atoms on the both hyperfine levels has been summed. We used double-frequency pumping and found the intensities of the fields under which vapor of an alkali was in g0-state. The fields had circular opposite polarization and was set to resonance with different transitions in D1 line of alkali. **Created by calculation maximum of the spin-polarization of the vapor of ^{87}Rb in the g0-state was 0.4.** The spin-polarization was calculated by formula (1):

$$\sum_{M=-F_1}^{F_1} M \left\langle F_1, M \left| \hat{\sigma}_g \right| F_1, M \right\rangle + \sum_{M=-F_2}^{F_2} M \left\langle F_2, M \left| \hat{\sigma}_g \right| F_2, M \right\rangle \quad (1)$$

$$F_1 = 1, \quad F_2 = 2 \quad (2)$$

In formulae (1,2) F_1 and F_2 are full angular momentums of the hyperfine levels of ^{87}Rb belonged to $^2S_{1/2}$ electron state, M is projection of the angular momentum to quantization axis, $\hat{\sigma}_g$ is density matrix of the atoms in $^2S_{1/2}$ electron state. Figure 1 shows the pumping scheme of alkali atoms.

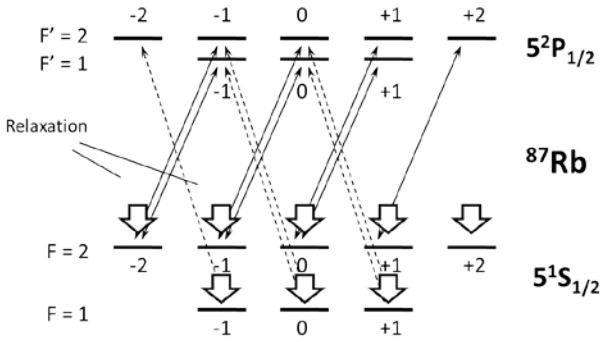

Fig. 1 Scheme of double-frequency pumping of the ^{87}Rb for preparing g0-state. Solid arrows demonstrate transitions, which are exceeded by the first field, dashed arrows demonstrate transitions, which are exceeded by the second field.

Dynamics of spin polarization can be surprise if state of the atomic ensemble is g0-state. With that suggested states are especially interested for physical applications, in which used electron paramagnetic resonance in alkali vapor and nuclear magnetic resonance in a noble gas [4]. Magnetization of the alkali in gas cell leads to shift of the magnetic resonance frequencies [5]. This effect adds some errors to devices based on magnetic resononce such as quantum sensor of rotation, quantum magnetometer and the frequency standards. Therefore new method of spin polarization pumping can improve characteristics of devices of quantum electronics.

This work was supported by the Ministry of Education and Science of the Russian Federation in the framework of the Federal Program "Research and Development in Priority Areas for the Russian Science and Technology Complex for 2014–2020" (agreement no. 14.578.21.0211, unique identifier RFMEFI57816X0211).

References

[1] W. Happer // Review of modern physics. V.44, P. 170 (1972).
[2] D. Budker, D. Kimball, "Optical magnetometry" Publ. by Cambridge University Press, 406 pages (2013).
[3] Fang J. C. and Qin J. // Sensors. V.12. P. 6331–6346 (2012).
[4] W. Happer, E. Miron, S. Schaefer, D. Schreiber, W.A. van Wijngaarden and X. Zeng, // Phys.Rev.A V.22 P.3092 (1984).
[5] T. Walker, Phys. Rev. A, 40(9), 4959 (1989).

High sensitivity laser pumped Caesium magnetic sensor for magnetoencephalography

A. Pazgalev[1], E. Ossadtchi[2], S. Dmitriev[1], V. Kartoshkin[1], M. Petrenko[1], and A. Vershovskii[1]
[1]*Ioffe Institute, 194021 St. Petersburg, Russia*
[2]*National Research University "Higher School of Economics", 101000 Moscow, Russia*
E-mail: anatoly.pazgalev@mail.ioffe.ru

Optically pumped quantum magnetic sensors provide the most sensitive up-to-date measurement of the magnetic field absolute value [1]. They are operating at room temperature and have a prominent perspective in a wide range of applications. After the pionering works by Dehmelt, and Bloom [2, 3] the electrodeless discharge lamps were used as a routine source for optical pumpinng. The last two decades made a change: diode lasers became available for pumping with unique combination of high power, narrow spectral line and flexibility of frequency control. High power provides a possibility to pump much more atoms, in comparison with lamp pumping, *i.e.* providing higher signal-to-noise ratio at the cost of accuracy. In many applications, sensitivity is more important than accuracy (long-term-stability). The medical applications, as magnetocardiography (MCG) [4] and magnetoencephalography (MEG) are such the case. These applications are traditionally the realm of superconductive quantum interferometer devices [SQUID]. Optically pumped magnetometers (OPMs) are supposed to be an alternative to SQUIDs [5–7].

Quantum sensor sensitivity depends on signal magnitude, its linewidth and principal noise. The magnetic resonance magnitude could be simply increased by total number of atoms, either the sensitive volume [5], or atomic density [7]. For small size sensors, the only choice is in increasing the density, *i.e.* vapour pressure related to the operating temperature. This solution has an apparent drawback, because the linewidth is also increased with density too, due to spin-exchange. The only exception is a magnetic sensor operating in a mode free of spin exchange (SERF mode) [8, 9], realizing high density Hanle magnetometer operating at near zero magnetic field. But such extreme conditions of homogeneous magnetic "vacuum" requires rather bulky and expensive magnetic shields or even magnetically shielded rooms, not suited for most of medical applications. Our goal is in developing a prototype of small compact and sensitive quantum sensor operating at Earth magnetic field range. Our approach utilizes the line-narrowing effect in highly polarized media firstly observed by W.Happer [10] and investigated, *e.g.* in [11].

The development of compact sensor suited for detection of magnetic field induced by brain neural activity is the field of active interest [12–14], it is a real challenge for technical physics and technology. The general trend of the technology is in development of compact sensors with reasonable loss of sensitivity, Chip-Scale Atomic Devices are the prominent examples. The magnetic sensor compactness opens a new fields of device applications. Such sensor could be placed more close to the magnetic field source, having gain in magnetometer response, since magnetic field is rapidly diminishes with distance; moreover small size means better spatial resolution in magnetic mapping task. The sensitive volume as small as 0.8 mm^3 was demonstrated [12] at the cost of reduced performance. Other important sensor features are sensitivity, dynamic range and immunity to interference and noise. Note, that the MCG/MEG magnetic signal is mostly located in a spectrum range from one to hundred Hz, so sensitivity is measured in this range.

We have developed a prototype of magnetic sensor with a volume of a part of cubic centimeter and measured its intrinsic sensitivity. The cubic cell with size of several mm was made of glass and filled with droplet of Caesium and buffer gas. The test of sensor sensitivity was performed in magnetic shield at Ioffe Institute Atomic Radio-spectroscopy Lab. Two identical cells were placed in a common thermostat heated to a temperature of about 90^0C. The cells were illuminated by circularly polarized light of pumping laser tuned to the one of Caesium D1-line hyperfine transition. The magnetic resonance was induced by AC-resonance field and probed by linearly polarized light of the second (probe) laser, tuned off the resonance. The optical power of the lasers, as well as their frequencies detuning, operating cell temperature, resonance driving AC-field magnitude, *etc*. were optimized to gain the best sensor sensitivity. The pumping light power was high enough to provide light narrowing

effect [10,11], making extra gain in sensor sensitivity. The magnetic field is stabilized either by external Rb-vapour magnetometer, placed close to the sensors, or by one of the sensors itself.

Fig.1a presents an example of in-phase and quadrature signals of the magnetic resonance, recorded by lock-in-amplifier with two cells constituting a gradiometer. Note, that both signals are almost completely coincide due to neatly balanced pumping and detection. With resonance linewidth and signal-to-noise ratio it is possible to estimate the principal sensitivity. We choose other, direct way of sensitivity measurement by applying a calibrating magnetic field and recording magnetometer response with lock-in-amplifier, as shown in Fig.1b.

Dark-noise and detecting light noise spectrum is shown in Fig.1c was recorded with the same set-up. Dark noise is well below detecting light noise. The noise spectra, were measured without applying resonance AC-field. It is worth to note, that magnetic gradient noise, not shown here, is typically is 10–30 times higher than principal sensor noise. Two beam pump-probe scheme allows us to reduce probe laser noise, due to balanced probe detection. The common magnetic field fluctuations were partly suppressed due to short base of gradiometer constituted of two sensors. The pumping light fluctuations were partly compensated by thoroughly balanced sensors pumping light level.

As a result we have demonstrated the possibility of achieving the sensitivity typical for the SERF device in a compact sensor with senivive volume less than half of cubic cm in a bias magnetic field of order 10 μT. The sensor size and its principal sensitivity opens the way to detect cortex brain activity in close proximity to the scalp, as supposed.

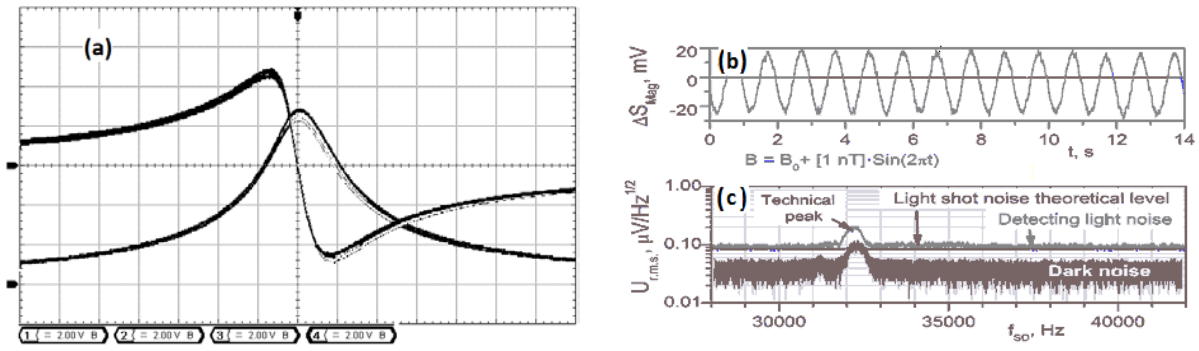

Fig. 1 Left: the measured magnetic resonance signals: vertical scale 2V/div, horizontal scale 500Hz/div. Right, a) magnetric sensor response to the 1 Hz-modulated magnetic field with amplitude 1000 pT applied to one sensor; b) spectra of dark noise and detecting light shot-noise. Resonance AC-field is not applied.

This work is funded by National Research University "Higher School of Economics" (HSE) within the framework of the cooperation agreement between HSE and Ioffe Institute. We express our gratitude to V. Velichansky and D. Chuchelov (Lebedev Institute, Moscow, Russia), for the available cells and fruitful discussions.

References

[1] M. V. Romalis et al., Nature, **422**, 596 (2003).
[2] A. Bloom, Applied Optics, **1**, 61 (1962).
[3] H. G. Dehmelt, Phys. Rev. **105**, 1924 (1957).
[4] A. Weis, et al., Sensors and Actuators A: Physical, **129**, 1 (2006).
[5] E. Aleksandrov et al., Tech.Phys. Letters, **12**, 749 (in russ.)(1987).
[6] A. Weis, G. Bison and Z. Grujić, Smart Sensors, Measurement and Instrumentation, **19**, 361 (2017).
[7] I. Savukov, Smart Sensors, Measurement and Instrumentation, **19**, 451 (2017).
[8] M. Romalis, at al., Phys. Rev. Lett. **89**, 130801 (2002).
[9] W. Happer, H.Tang, Phys. Rev. Lett. **31**, 273 (1973).
[10] N. D. Bhaskar, J. Camparo, W. Happer, et al., Rev. **23**, 3048 (1981).
[11] T. Scholtes et al., Phys. Rev. A, **84**, 043416 (2011).
[12] S. Knappe et al., Biomed. Opt. Express, **3**, 981 (2012).
[13] P. D. Schwindt, Opt. Express, **24**, 15403 (2016).
[1] [14] R. Jimenez-Martinez, S, Knappe, Measurement and Instrumentation, **19**, 523 (2017).

Femtosecond tapered diode-pumped Yb:KYW laser

A. Semenko, S.A. Kuznetsov, V.S. Pivtsov, S.N. Bagayev
Institute of Laser Physics SB RAS, Novosibirsk, Russia
E-mail: clock@laser.nsc.ru

A powerful single-mode diode laser (DBR TDL) is developed. The output characteristics of the DBR TDL laser are investigated. With the DBR TDL laser as a pumping source, a free running mode of a Yb:KYW laser is obtained and investigated. It is shown that a compact precision femtosecond frequency synthesizer based on a Yb:KYW laser can be created.

Study of genetic effects of terahertz radiation with Escherichia coli based genosensors

D. Serdyukov[1,2,4], O. Cherkasova[2], V. Popik[3], S. Peltek[4]
[1]*Novosibirsk National Research State University, Pirogova street 1, Novosibirsk, 630090, Russia*
[2]*Institute of Laser Physics of the Siberian Branch of the RAS, Prospekt Lavrentyeva 15B, Novosibirsk, 630090, Russia*
[3]*Budker Institute of Nuclear Physics of the Siberian Branch of the RAS, Prospekt Lavrentyeva 11, Novosibirsk, 630090, Russia*
[4]*Federal Research Center "Institute of Cytology and Genetics of the Siberian Branch of the RAS", Prospekt Lavrentyeva 10, Novosibirsk, 630090, Russia*
E-mail: Rna5s120@yandex.ru

The technologies based on the use of terahertz (THz) radiation (frequency range 10^{11} – 10^{13} Hz) are currently experiencing a boom in their development, finding application in numerous spheres of human activity. Against this background, the issue of the biological safety of THz radiation remains relevant, and this problem is largely associated with the non-thermal effects of THz radiation. It is known that the natural frequencies of vibrational-rotational transitions of water, small molecules and functional groups of large biomolecules, as well as the modes of the most important biopolymers (DNA, proteins, etc.), lie in the THz range [1, 2]. This circumstance causes non-thermal effects which had been experimentally demonstrated repeatedly [3–5].

Genosensors based on *Escherichia coli* (*E. coli*) cells are artificial genetic systems containing a promoter of sensitive gene-sensor that regulates the expression (production) of a fluorescent marker protein. The promoters of sensor genes are able to selectively react to certain factors of chemical or physical nature, and the genosensors themselves serve as a traditional tool for the analysis of such effects. With regard to THz radiation, the genosensors allow to analyze its effect directly on the activity of genes whose promoters are inserted in the artificial genetic systems.

In the laboratory of molecular biotechnologies of the Institute of Cytology and Genetics of the Siberian Branch of the RAS, Russia, studies are underway on the effect of THz radiation on living systems [6, 7]. Based on the RNA sequencing data obtained here, it was found that more than 50 genes in *E. coli* cells, including transcription factor genes, increased their activity at THz irradiation. Using the Gibson assembly method, the genosensor constructions based on the transcription factor gene promoters (namely, promoters of cadC, chbR, matA, tdcR, ydeO) had been assembled (Fig.). The made genosensors allowed to analyze the development of the response to THz radiation in time.

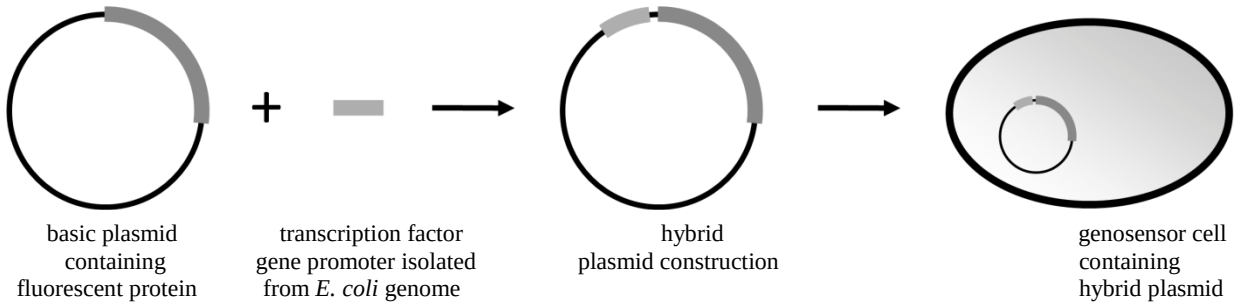

Fig. 1 The general scheme of the assembling *E. coli* genosensor based on a plasmid vector containing a gene of fluorescent protein.

The genosensor cells obtained were irradiated in wells of a 96-well plate in an amount of 50 μl (1.6 mm thick water layer) of the culture medium with the cells. The pulsed irradiation conditions were as follows: f = 2.3 THz, I = 0.08 W/cm^2, peak P ≤ 1 MW, pulse repetition rate 5.6 MHz, exposure time 30 min, sample heating under irradiation up to 37^o C. Control samples were incubated

in parallel in a thermostat at 37^{o} C for 30 min. After the irradiation, the fluorescence of the samples was analyzed on the multilabel plate reader for 4 hours.

At the THz irradiation, activation of the *E. coli*/pTdcR-yfp genosensor (it was assembled using the tdcR gene promoter and the basic plasmid containing the yellow fluorescent protein (yfp) gene) was demonstrated. So, in 6 irradiated samples, on average, fluorescence increased from 3600 (background value) to 4800 conv. units for 4 hours of observations. In 4 control samples the fluorescence value remained unchanged.

Thus, the THz radiation increases the expression of TdcR which is a DNA-binding regulatory protein serving as a trans-acting positive activator for the tdc operon of *E. coli*. The sensitivity of the other obtained genosensors to THz radiation is explored.

The non-thermal response of the prokaryotic genetic system to THz radiation can be traced in more detail by using the panel of the genosensors, some of which had been obtained in this work and some will have been obtained in further works. This is important for an in-depth understanding of the mechanisms of interaction between THz radiation and living systems. Among other things, this understanding will help resolve questions about its biosafety.

The irradiation experiments were performed on the Novosibirsk Free Electron Laser (Budker Institute of Nuclear Physics SB RAS).

References

[1] K. Johnson, J. Biol. Phys. **38**, 85 (2012).
[2] X. Yang, X. Zhao, K. Yang et al., Trends Biotechnol. **34**, 810 (2016).
[3] L. Zhao, Y. Hao, R. Peng, Mil. Med. Res. **1** (2014).
[4] V. Fedorov, Biophys. **62**, 324 (2017).
[5] V. Fedorov, D. Serdyukov, O. Cherkasova et al., J. Opt. Technol. **84**, 509 (2017).
[6] E. Demidova, T. Goryachkovskaya, T. Malup et al., Bioelectromagnetics **34**, 15 (2013).
[7] E. Demidova, T. Goryachkovskaya, I. Mescheryakova et al., IEEE Trans. Terahertz Sci. Technol. **6**, 435 (2016).

Metal halides vapor lasers with inner reactor

D. Shiyanov
Institute of Atmospheric Optics SB RAS, Tomsk, 634055, Academician Zuev square, 1, Russia, E-mail: qel@iao.ru
E-mail: qel@asd.iao.ru

In [1-3] we proposed a version of metal halide vapor lasers (MHVL) with an internal reactor (IR) and showed its reliability. IR means that the working substance is formed directly in the working zone of sealed GDT by using a halogen generator.

The results of an investigation of the energy characteristics of CuBr, CuCl, CuJ, $MnBr_2$, and $PbBr_2$ - lasers with IR and small active volume as a function of the buffer gas pressure, pumping power, pulse repetition rate (PRR), and wall temperature of the gas-discharge tube (GDT) are presented. The volume of the active zone of the examined GDT was 90 cm^3. Optimal operating conditions for lasers are determined using different halogen generators. In the first place, iodine in pure form. We also used halogen generators, working on the principle of a zeolite screen and dibromide (dichloride) copper.

The principle of operation of a MHVL with IR is as follows. When the halogen generator is heated, it enters the GDT channel, where it interacts with the working metal in the discharge, forming a metal halide molecule. Due to the electron impact, the dissociation of the metal halide molecule occurs and further excitation of the metal atom.

The main studies of the energy characteristics of copper, manganese and lead halides vapor lasers with capacitive pumping were performed at 25-35 kHz. In GDT with internal electrodes, the working capacitance was 500 pF, and the PRR 17.5 kHz with pumping powers of 600-650 W.

The dependence of the energy parameters on the pressure of the buffer gas showed that the range of optimum pressures of such systems for GDT with capacitive and conventional pumping is 20-30 torr, which corresponds to standard copper, manganese and lead halide vapor lasers. However, there are differences in the temperature dependence of the characteristics of these lasers. The minimum optimal operating temperatures of 500-600^{0}C are characteristic for a CuJ laser. For CuBr and CuCl lasers, the optimum lies in the region of 650°C. $MnBr_2$ laser has higher operating temperatures such as 750-770°C, and $PbBr_2$ laser too. These temperatures correspond to the effective salt formation in the discharge for each metal and halogen.

Within the framework of the studies, the maximum radiation power of the $MnBr_2$ laser with IR, total in the infrared and visible spectral range was 1 W. The main part of the radiation was on the line 534.1, 542 nm and 1.29 microns. In a $PbBr_2$ laser with a IR, the lasing power was 0.2 W on the 722.9 nm line.

An investigation of the frequency dependence of the output characteristics of MHVL with IR with internal electrodes has shown that for the metals under study the optimum is 15-25 kHz, which also corresponds to standard MHVL. In the case of GDT with capacitive pumping, the optimal PRR will depend on the capacitance of the electrodes. With a decrease in the capacitance of the electrodes, it is necessary to increase the PRR to provide the necessary pumping power.

It should be noted that the addition of hydrogen analogously to MHVL [21] introduces a delay in the development of the discharge (current and voltage), which creates favorable conditions for pumping the upper laser levels at the initial time.

Analyzing the work of the halogen generators, it should be noted that the zeolite-based generator works most effectively. Depending on the volume of the adsorbent and the concentration of the halogen contained in it, it ensures a reliable and long-time operation of the entire system. When working with copper dibromide and copper dichloride, the temperature of the halogen generator heater increases with increasing laser operating time. The use of iodine as a halogen generator leads to an unstable operating mode of the laser at the initial instants of time, since it has a high volatility. In the absence of discharge in the GDT, there is a certain vapor pressure of iodine, because at a temperature of 25^{0}C, the saturated vapor pressure of iodine is 0.31 mm Hg. Art.

Based on the obtained results, it can be concluded that the active elements of MHVL with IR have the following advantages over the known analogues:

1. When using capacitive pumping, a higher degree of purity of the discharge is provided, which ultimately leads to an increase in the service life of the active element.
2. There is the possibility of adjusting the vapor pressure of halogen with a low temperature of 20-150^{0}C, which is much lower than the temperature of containers with a metal halide in conventional MHVL 450-550^{0}C.
3. The time of the laser output to the operating mode is reduced.
4. Simplicity and safety in obtaining anhydrous halides.
5. It is possible to obtain any salts in one GDT.
6. Thanks to the sealed-off operation mode, unlike hybrid lasers, such a system becomes mobile.
7. With a rigid metal fixation, it is possible to operate the GDT in an upright position.

References

[1] D. Shiyanov, V. Sukhanov, G. Evtushenko, N. Tkachenko. Atmosp. and ocean. optics, **25**(8), 721 (2012) [in Russian].
[2] M. Trigub, D. Shiyanov, V. Sukhanov, G. Evtushenko. Atmosp. and ocean. optics, **27**(4), 321 (2014) [in Russian].
[3] D. Shiyanov, M. Trigub, V. Sukhanov, G. Evtushenko, V. Vlasov. Technical Physics, **60**(4) 571 (2015).

CuBr-laser with an efficiency of 2.7% in the double-pumping-pulse mode

A. Fedorov, D. Shiyanov
Institute of Atmospheric Optics SB RAS, Tomsk, 634055, 1, Academician Zuev square, Russia
E-mail: qel@asd.iao.ru

The double-pumping-pulse mode metal halide vapor laser excitation allows one to obtain high levels of radiation energy. In this case, the first pulse dissociates the metal halide molecules, and the second excites the metal atoms. The potential to achieve a several-fold increase in the laser efficiency by optimizing the excitation pulse parameters and matching it to the impedance of the active medium plasma produced by a dissociation pumping pulse was demonstrated in our earlier study [1].

In the present study, we consider the potential to enhance the energy characteristics and the efficiency of a CuBr laser through optimization of the pumping-pulse parameters in the mode of matched injection of the excitation energy into the active medium plasma.

The experimental setup and small active volume gas discharge tube was described in detail elsewhere [1, 2].

We have found that an increase in the energy density or the power of an excitation pulse affects the enhancement of the radiation energy or power with decreasing laser efficiency due to the mismatch of impedances of pumping sources. The maximum laser efficiency corresponded to the mode of matched injection of the excitation energy into the active medium plasma, which was defined by the dissociation pumping-pulse parameters. Therefore, we optimized the parameters of the sources of dissociation and excitation pumping pulses that produce the active-medium plasma and excite it.

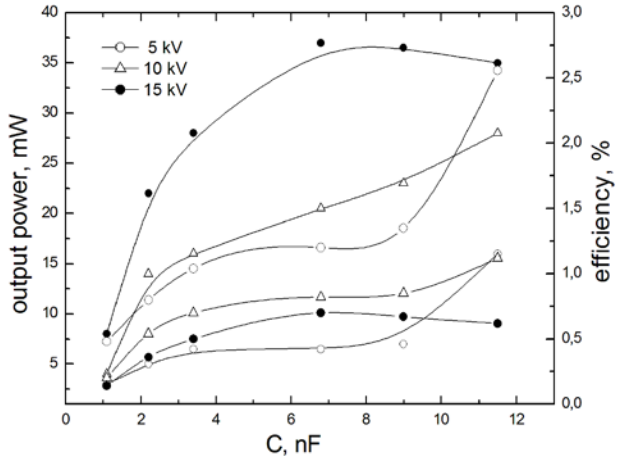

Fig. 1. Dependences of the average radiation power and the laser efficiency on the working capacitance of the dissociation pumping source and on the excitation pulse voltage at the active medium plasma for C_p = 1 nF and τ_d = 150 μs**.**

Figure 1 shows the dependences of the average radiation power and the laser efficiency on the working capacitance of the dissociation pumping-pulse source and on the active medium plasma voltage for the optimum capacitance (1 nF) of the excitation pulse source.

At the maximum excitation voltage (15 kV), the average radiation power rose steeply to 37 mW with an increase in the dissociation capacitance to 6.8 nF. As the capacitance grew further to 11.5 nF, the power decreased slowly to 35 mW. The laser efficiency behaved differently: it increased gradually to 0.7% at a dissociation capacitance of 6.8 nF and decreased slowly at higher capacitance values. This mode was observed at lower voltages at the active medium plasma. It turned out that the optimum plasma voltage is 5 kV. The dependences of the average radiation power and the laser efficiency in the matched mode differ from those obtained at the maximum excitation voltage of 15

kV. The average radiation power increased with the dissociation capacitance as the latter was varied from 1.1 to 3.3 nF. At a capacitance of 3.3–9 nF, the power remained almost constant (6.5 mW). When the capacitance was raised further to 11.5 nF, the radiation power rose sharply to 16 mW. The laser eff iciency demonstrated a similar variation pattern and was also maximized (2.6%) at a capacitance of 11.5 nF. This suggests that the optimum plasma-production conditions were established at a capacitance of 11.5 nF and a dissociation pulse energy density of 22 mJ/cm^3. The optimum radiation parameters (an average radiation power of 28 mW, a radiation energy of 0.56 mJ, and a laser efficiency of 1.1%) were obtained at an excitation voltage of 10 kV. By, setting the optimum voltage of 5 kV in the matched excitation mode (Ep= 0.4 mJ/cm^3 and Wp= 2 kW/cm^3), we have raised the laser efficiency to its maximum of 2.6% with an average radiation power of 16 mW, a radiation energy of 0.32 mJ, and a half-amplitude lasing-pulse duration of 40 ns. At the maximum excitation voltage of 15 kV (Ep= 2.7 mJ/cm^3 and Wp= 17 kW/cm^3), the average radiation power was 37 mW, the radiation energy was 0.7 mJ, and the laser efficiency was 0.7% at a lasing-pulse duration of 40 ns. At an excitation voltage of 10 kV (Ep= 1.6 mJ/cm^3 and Wp= 8 kW/cm^3), the average power was 28 mW, the radiation energy was 0.56 mJ, the laser efficiency was 1.1%, and the lasing-pulse duration was 30 ns. Thus, it was found that the maximum laser efficiency corresponded to minimum excitation pulse energies.

A further increase in the efficiency of the laser to 2.7% was achieved by including in the excitation circuit a saturating throttle. The inductance value of the saturating throttle varied from 15 to 70 μH. At a voltage of 10 kV, a maximum radiation power of 37 mW was obtained at a laser efficiency of 1.4% and an inductance of 30 μH, and a maximum laser efficiency of 2.7% with an average radiation power of 17 mW for a pulse amplitude of 5 kV excitation. In Fig. 3 shows the dependence of the average radiation power and laser efficiency on the saturation inductor value and the excitation pulse voltage. The maximum radiation parameters were observed for the optimum inductance of the saturating throttle of 30-40 μH. In this case, according to the oscillograms of the current and voltage pulses, there was an additional improvement in the matching of the impedances of the plasma of the active medium and the pump source. The optimum dissociating capacitance was 6.8 nF, and the excitation capacitance was 1 nF.

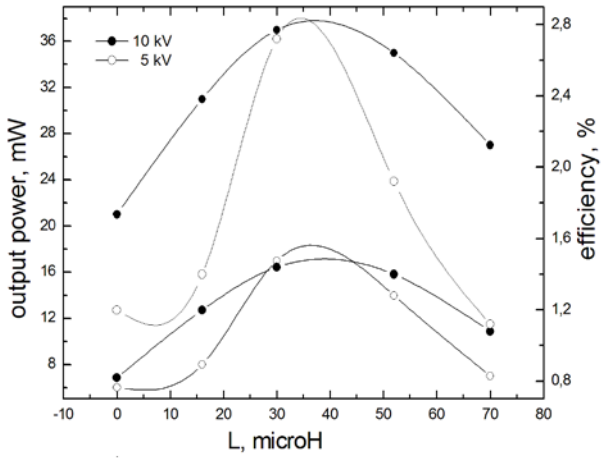

Fig. 2. Dependences of the average output power and laser efficiency on the inductance of the saturating throttle and the excitation pulse voltage for C_d = 6.8 nF, C_p = 1 nF and td = 150 μs.

Additional increase in laser efficiency can be associated with a change in the design of the electrodes. The use of ring electrodes will allow the formation of a volume discharge along the entire channel of the discharge tube.

References

[1] A.I. Fedorov, D.V. Shiyanov. Tech. Phys. Lett., **41**(8), 759 (2015).
[2] A.I. Fedorov, V.F. Fedorov, V.A. Dimaki. Atmosph. and ocean. optics. **25**(2), 198 (2012) [in Russian].

Features of orientational optical transition in dye doped nematic liquid crystalline polymers

I.A. Budagovsky[1], A.A. Kuznetsov[1], S.A. Shvetsov[1,2], M.P. Smayev[1,3], A.S. Zolot'ko[1], P.A. Statsenko[4], S.I. Trashkeev[4,5], A.Yu. Bobrovsky[2], N.I. Boiko[2], and V.P. Shibaev[2]

[1]*Lebedev Physical Institute, Russian Academy of Sciences, Leninsky Prospect, 53, 119991, Moscow, Russia*

[2]*Lomonosov Moscow State University, Leninskie Gory, 119991, Moscow, Russia*

[3]*Mendeleev University of Chemical Technology of Russia, Miusskaya sq., 9, 125047, Moscow, Russia*

[4]*Institute of Laser Physics, Siberian Division, Russian Academy of Sciences, Ac. Lavrentyev's Prospect, 13/3, 664033, Novosibirsk, Russia*

[5]*Novosibirsk State University, ul. Pirogova, 2, 630090, Novosibirsk, Russia*

E-mail: shvetsov@lebedev.ru

Doping nematic liquid crystal polymers (NLCPs) with an azobenzene dye increases the orientational optical response up to 4 orders of magnitude and allows one to observe the light-induced Freedericksz transition (LIFT) at microwatt light power levels [1, 2]. In addition, polymer-based mixtures possess very important advantage in comparison with low-molar-mass systems, i.e. high stability of the photoinduced orientation at room temperature due to its fixation in glassy state. Here, we present the results of our study about the effect of the light-beam spatial limitation on the director reorientation in NLCP with the presence of azobenzene dye additive.

NLCPs under study consist of a polyacrylic polymer with phenylbenzoate mesogenic side groups (PAA) doped with the bis-azobenzene dye KD-1 (0.05 wt %). Homogeneous mixture was placed into the glass cell (with the thickness L = 50 μm) providing planar orientation.

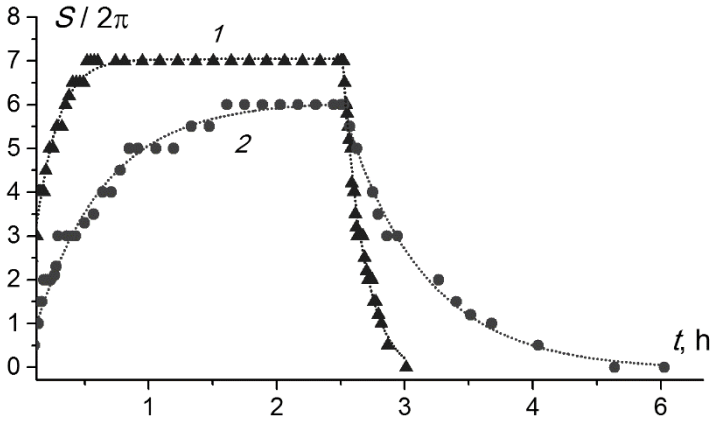

Fig. 1 Dynamics of light-induced phase shift S/2π for PAA+KD-1 (1) and PAA+5CB+KD-1 (2) at oblique incidence (α = 40°) of light beam (λ=473 nm, w0 = 75 μm) with the power of 20 μW and 50 μW, respectively.

At the normal incidence of the focused light beam on PAA+KD-1 cell, we observed the threshold aberrational self-defocusing, which indicates the manifestation of the LIFT. The LIFT threshold power varied in the range of 17–64 μW at variation of the light beam waist w_0 from 10 to 75 μm. At $w_0 < L$, the threshold light field $E_{th} \sim 1/w_0$; at $w_0 > L$, E_{th} decreases weakly with w_0. This behavior was previously observed for low-molar-mass NLCs and can be explained by a sufficient increase of elastic forces caused by director field inhomogeneity in the plane of NLCP film.

The obtained results suggest that the NLCP director evolution under nonuniform light fields can be described by continual elastic theory and a large variety of nonlinear optical phenomena inherent in low-molar mass NLCs can be observed in NLCPs at microwatt power.

Introduction of 5 wt % of low-molar-mass nematic 5CB to the PAA+KD-1 mixture results in faster orientation and relaxation dynamics as well as decrease in the light-induced response (Fig. 1). These effects are attributed to viscosity decrease due to the plasticization effect of low-molar-mass additive [2].

Numerical simulations of director field elastic deformation under light beam action in the stationary state as well as in the dynamic processes are performed.

The study was supported by the Russian Foundation for Basic Research, projects nos. 18-02-00986-a and 16-29-05140-ofi_m.

References

[1] I.A. Budagovsky, V.N. Ochkin, S.A. Shvetsov, et al, Phys. Rev. E **95**, 052705 (2017).
[2] I.A. Budagovsky, V.N. Ochkin, S.A. Shvetsov, et al., Mol. Cryst. Liq. Cryst. **647**, 100 (2017).

Laser cavity optical scheme optimization of a compact mechanically stable laser with intracavity filtration of transverse modes

P.A. Statsenko[1], S.I. Trashkeev[1,2], Y.S. Fedotov[1]
[1]*Institute of Laser Physics SB RAS, Novosibirsk, Russia*
[2]*Novosibirsk State University, Novosibirsk, Russia*
E-mail: PAStatsenko@laser.nsc.ru, sitrskv@mail.ru, fedotov.yurec@gmail.com

Numerical simulation and experimental testing of the optical scheme of a stable resonator with mode filtration based on graded reflectivity mirror for an Nd: YAG laser were carried out. To determine optimal profile of reflection coefficient of a mirror in the diffraction approximation the problem of determining eigenmodes of laser cavity was solved. Obtained results allowed realizing of cavity scheme supporting better beam quality maintaining other parameters of investigated Nd: YAG laser.

Currently there is a great demand for high-energy laser systems with pulse energy about hundreds joules and more. There are exist the most demand in medicine, cosmetology and in the field of precision material processing [1, 2]. These industries require high-energy environmentally stable lasers with high robustness, which does not require any systematic adjustments, having high beam quality for example, low divergence, Gaussian or super-Gaussian laser beam profile.

Environmental stability was easily achieved by direct coating of active crystal ends by dielectric mirrors. However, in this situation there are we have a short resonator with a large Fresnel number 100 ÷ 200 and consequently large number of transverse cavity modes proportional to the square of the Fresnel number. The generation of higher-order modes leads to a significant decrease of laser beam quality and makes application of such laser systems ineffective or even unacceptable. Further, we propose our method that makes it possible to substantially improve beam quality, but maintain or slightly decrease other parameters of obtained laser beam.

To solve this problem there are proposed to use filtering (to increase losses up to impossibility of generation) of higher-order modes. The design of solid-state systems as follows as one of the solutions could be use of "graded reflective mirror" having a variable reflection coefficient.

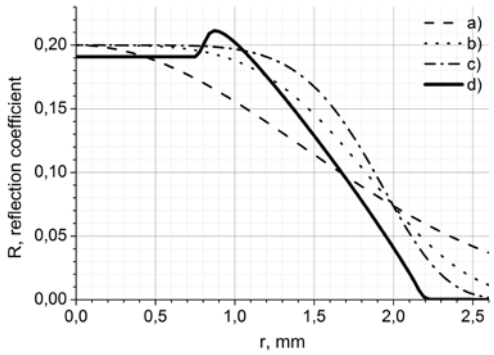

Fig. 1 Reflection coefficient dependence on the radius: R_0=0,2, a). n = 2; b). n = 4; c). n = 6; d). measured experimental profile.

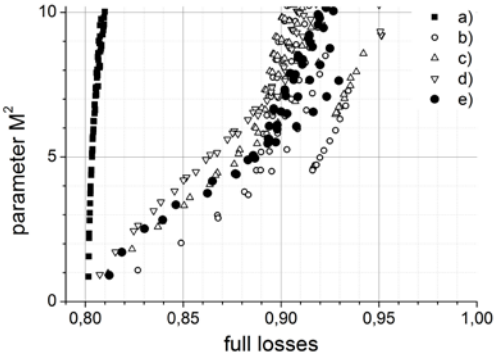

Fig. 2 Parameter M^2 dependence for mirror with different reflection coefficient, R_0=0,2. a) Continuous reflection coefficient; b). n = 2; c). n = 4; d). n = 6; e). measured experimental profile.

We observed a model of laser cavity with a graded reflective mirror which transmission profiles could be described by function $R(r) = R_0 \cdot \exp\left[-(r/w)^n\right]$, Fig. 1 The numerical simulation was based on the solution of the integral equation [3, 4], which describes in the diffraction approximation the mode composition of the radiation. A feature of the method is the ability to immediately determine a large number of modes in one calculation cycle. Figure 2 shows an example of a calculation showing the

dependence of the parameter M^2 on the loss for eigenmodes for different types of the reflection coefficient profile. As can be seen, the application of the graded reflective mirror introduces large losses for high-order modes, the curve of the parameter M^2 becomes flat and allows by changing transmission profile parameters of the mirror (R_0 и n) to more accurate choose a generation regime with minimum (necessary or prescribed) number of lower modes.

Based on performed calculations were made experiments (Fig. 3), where the shapes and divergences of laser beams were compared for a homogeneous planar and graded reflective mirrors (Fig. 1). In the second case, the maximum radiation energy slightly decreased (<10%), but the beam shape approached to Gaussian shape and the divergence was decreased.

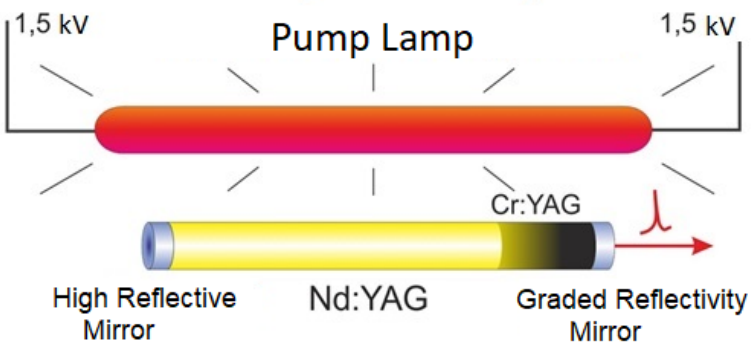

Fig. 3 Mechanically stable Nd:YAG laser cavity scheme.

As a result, it is shown that a gradient mirror in a resonator can be used as an analog of a diaphragm and allows filtering of eigenmodes and obtaining a laser beam with better quality with the radiation power maintaining. Proposed method is simple and allows not to violate the advantages of solid-state lasers (compactness, mechanical, temperature stability, etc.) and it provides an additional opportunity to form the given, more complex laser beam profiles.

References

[1] Carla Gregório Barbosa de Oliveira, et al. Laser assisted tattoo removal: a literature review. Surg Cosmet Dermatol 2013;5(4):28996.
[2]. A. F. Glova, A. Y. Lysikov, Drilling and cutting of thin metal plates in water with radiation of a repetitively pulsed Nd:YAG laser, Quantum Electronics(2011),41(10):906.
[3] A.E. Bu1yshev, G.A. Vedernikov, N.G. Preobrazhenskii, On calculation of laser resonator characteristics, Soviet Journal of Quantum Electronics(1980),10(5):623.
[4] Grachev G.N., Statsenko P.A., Trashkeev S.I. A software package for the calculation of resonator systems in the three-dimensional approximation. Collection of Works VI Int. Conf. Applied Optics, St. Petersburg, 2004, vol.3, p297-301.

Electron band structure analysis by intraband high-harmonic generation

E.A. Stepanov[1,2], A.A. Lanin[1,2], A.B. Fedotov[1,2], A.M. Zheltikov[1-3]
[1]*Physics Department, International Laser Center, M.V. Lomonosov Moscow State University, Vorob'evy gory, Moscow, 119992, Russia*
[2]*Russian Quantum Center, 143025, Skolkovo, Moscow region, Russia*
[3]*Department of Physics and Astronomy, Texas A&M University, 77843, College Station TX, USA*
E-mail: ea.stepanov@physics.msu.ru

High-order harmonic generation (HHG) in atomic gases is one of the key phenomena in strong-field laser–matter interactions, playing a central role in optical physics and rapidly growing attosecond technologies. HHG in bulk crystals is fundamentally different from that in the atomic case owing to the high density and periodic structure. When applied to solid materials [1 – 3], approaches of strong-field physics are subject to natural limitations, related to absorption and much lower laser damage thresholds of solids. As a reward, such solid-state extensions promise breakthroughs toward petahertz solid-state optoelectronics, open avenues toward attosecond science on the platform of solid-state materials, and suggest new all-optical methods for crystallographic analysis.

Here we study HHG in ZnSe polycrystalline film using mid-IR driver pulses within the wavelength range of 5.0 to 6.7 μm. In this wavelength region, a large group of below-the-bandgap high-order harmonics distinctly reflects, as our experiments show, an ultrafast dynamics of electron wave packets within the conduction and valence bands. We demonstrate that these harmonics directly relate to the nonlinearities of electron bands (Fig. 1), providing a tool for electron band structure analysis in bulk solids. The intensities of individual optical harmonics as functions of the driver intensity I_0 were used to retrieve the energy dispersion profile for one of the electron conduction bands of ZnSe and to show that the result of this retrieval is consistent with the first-principle analysis of the electron band structure of ZnSe.

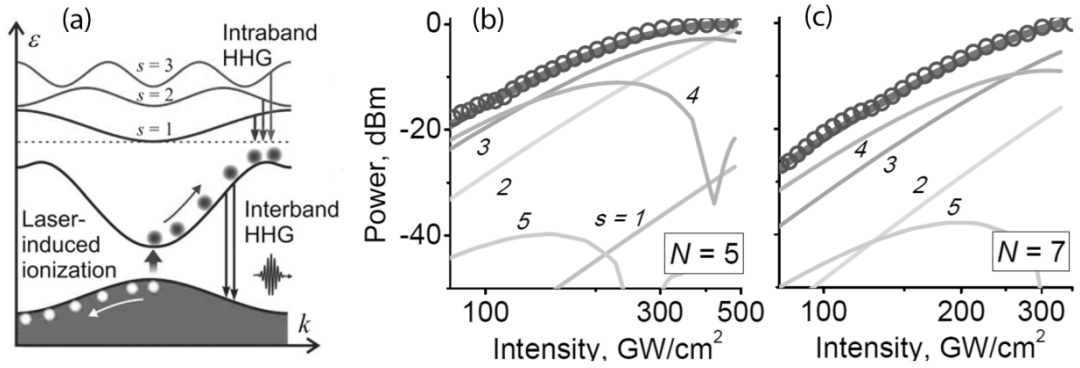

Fig. 1 (a) Inter and intraband HHG in a solid and electron band structure mapping. High-order harmonics are generated through the interband polarization involving electron-hole recombination, as well as through the modulation of the intraband current due to the nonlinearity of electron bands. (b,c) The power of optical harmonics with N = 5 (b) and 7 (c), generated by a laser driver pulse with a central wavelength of 5.0 μm in a 2-mm-thick ZnSe film as a function of the driver intensity I_0. Open circles show the experimental data. The solid lines show the intensity of the N^{th} harmonic generated by the s^{th} Fourier harmonic of the ΓL conduction band in ZnSe as predicted by the model of intraband HHG with s = 1-5.

The experimental were performed with a frequency-tunable source of ultrashort mid-IR pulses [4,5], which consists of two sequential stages of nonlinear-optical down conversion, involving optical parametric amplification in two cascaded BBO crystals, followed by difference-frequency generation

in an AgGaS2 crystal. With pulse width of 85 fs, and energy ranging from 7 μJ at central wavelength $\lambda_0 \approx 5.0$ μm to 5 μJ at $\lambda_0 \approx 6.7$ μm, the output radiation was focused by a 15x, 0.30-NA reflective objective onto a ZnSe sample, delivering field intensities up to 4 TW/cm^2. With such intensities a field-induced electron quiver motion can probe the entire Brillouin zone, even reaching the Brillouin-zone edges. Optical harmonics generated by such electrons as a part of their dynamics thus feature the signatures of electron band topology, enabling quantitative analysis of electron band anharmonicity.

This work was supported by the Russian Foundation for Basic Research (16-32-60163, 16-29-11799, 18-32-00782) and Foundation for the advancement of theoretical physics "BASIS".

References

[1] S. Ghimire, et al., Nature Phys. **7**, 138 (2011).
[2] G. Vampa, et al., Nature **25**, 462 (2015).
[3] M. Hohenleutner, et al., Nature **523**, 572 (2015).
[4] E. A. Stepanov, et al., Phys. Rev. Lett. **117,** 043901 (2016).
[5] A.A. Lanin, et al., Opt. Lett. **40**, 974 (2015).

Towards the development of transportable and portable ytterbium optical lattice clocks

D. Sutyrin[1], G. Belotelov[1], O. Berdasov[1,2], and S. Slyusarev[1]
[1]FSUE "VNIIFTRI", Mendeleevo, Moscow region, Russian Federation
[2]NRNU MEPhI, Moscow, Russian Federation
E-mail: sutyrin@vniiftri.ru

The recent progress in optical lattice clocks and in long-distance frequency transfer by optical fiber open the way for using measurements of the gravitational frequency redshift for geodesy. The remote comparison of frequencies generated by calibrated clocks will allow for a purely relativistic determination of differences in gravitational potential and height between stations on Earth surface. It requires high performance of optical frequency standards with precision calibration, which were in few labs demonstrated. Likewise, a more accurate and direct mean of optical frequency comparison is required for today's best clocks over quite long distance. For these reasons, it is quite necessary to develop the applicable optical clocks on ground and even in the space. It is preferable to develop a transportable optical clock in the first step, then portable one and, as synthesis of previous developments, to create an onboard space system. In addition to these performances, it should have the possibility of all the frequency shifts evaluation in every environment where it is placed [1], [2].

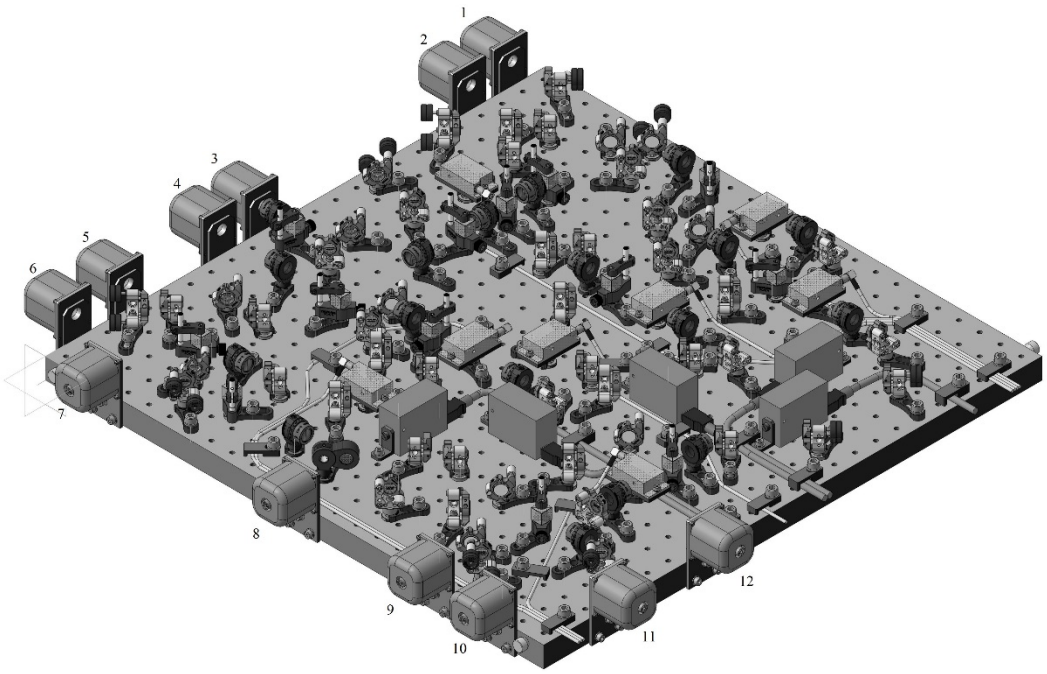

Fig. 1 Portable distribution breadboard for first and second stage cooling. Size 60 x 60 cm. Collimators: 1 – frequency stabilization output 556 nm , 2 – frequency stabilization output 399 nm, 3 – input 556 nm, 4 – input 399 nm, 5, 6, 7 – six-beam MOT output 556+399 nm, 8 – one-beam MOT output 556+399 nm, 9, 11 –2-D MOT output 399 nm, 10 – detection output 399 nm, 12 –Zeeman slower output 399 nm

We report on the design concept of transportable and portable ytterbium optical lattice clocks, which are developing at FSUE "VNIIFTRI". The work goal is to improve properties of optical clocks such as compactness, mass, power efficiency with preservation of typical for stationary optical clocks high relative frequency stability and accuracy level [3] and long-term continuous operation [4].

For the transportable optical clock version, we discuss physical principles and design solutions for the implementation of systems with the required characteristics. In particular, we present our step on way of the portable distribution breadboard for first and second stage magneto-optical trap (MOT) (Fig.1), a compact vacuum chamber and a new ceramics atomic oven development.

In case of the portable optical clock version, we use FEM methods to test the idea of mini MOT with one-beam instead of six-beam from the classical MOT [5]. In addition, we simulated intensity distribution of MOT beams for different types of one-beam reflectors such as conical hollow mirror and modified pyramidal funnel. Simulation showed that developed conical hollow mirror is suitable for the usage in one-beam MOT.

Considering both versions of optical lattice clocks, we calculate the compactness coefficient with respect to the stationary system. For example, a volume of system changed in 10 times in transportable version and in 20 times in portable. Power consumption changed in two times and size of laser cooling systems in 2000 times for the transportable version [4].

The results of the developments will serve as a basis for transportable optical frequency standards and for on-board precision navigation systems based on optical frequency standards.

References

[1] J. Grotti, et al., Nature Physics : 1 (2018).
[2] N. Poli, , et al., Applied Physics B 117.4: 1107-1116. (2014).
[3] B. Bloom, et al., Nature, 506(7486), 71. (2014).
[4] O. Berdasov, et al., QUANTUM ELECTRON, 48 (5), 431–437, (2018).
[5] W. He, PhD Thesis, The University of Birmingham.

Hyper-Ramsey spectroscopy of clock transitions in the presence of heating of single ion in a trap: the efficiency of suppression of probe-induced frequency shift

S. Kuznetsov[1], A. Taichenachev[1], V. Yudin[1],
N. Huntemann[2], Chr. Sanner[2], Chr. Tamm[2], E. Peik[2]
[1]*Institute of Laser Physics SB RAS, Novosibirsk, Russia*
[2]*Physikalisch-Technische Bundesanstalt, Braunschweig, Germany*
E-mail: taichenachev@laser.nsc.ru

In modern optical frequency standards based on ultracold atoms or ions strongly forbidden clock transitions (such as E3 transition in $^{171}Yb^{+}$ ion) are excited by a strong probe field. This leads to significant probe-field induced off-resonant AC Stark shift of the transition frequency. Several modifications of the Ramsey method have been proposed to suppress this shift [1,2]. Theoretical treatment of these methods is usually based on unitary evolution of pure quantum states under the action of a sequence of exciting pulses. Such approaches assume negligible relaxation and dephasing. These ideal conditions are not always realized in experiments. For example, one of possible imperfections is connected with a finite heating rate of ion in a Paul trap. In this paper we analyze the influence of ion heating on the efficiency of several generalized Ramsey schemes of suppression of probe-induced shifts in ion-based optical clocks.

We consider a two-level system interacting with a sequence of light pulses, taking into ac-count the vibrational degrees of freedom of the ion in a harmonic trap. The quantum kinetic equation for the ion density matrix can be written in the form

$$\frac{\partial}{\partial t}\rho = -\frac{i}{\hbar}[H_0,\rho] - \frac{i}{\hbar}[V,\rho] + \left[\frac{\partial}{\partial t}\rho\right]_{heating} \qquad (1)$$

where the Hamiltonian of the ion in a trap ($H_0 = -\hbar\delta|e><e| + \hbar\omega_v\left(a^{\dagger}a + \frac{1}{2}\right)$) and the interaction Hamiltonian ($V = \hbar\Omega_0|e><g|e^{ikx} + h.c$) are taken in the rotating wave approximation. The last term in eq.(1) describes the density matrix evolution due to heating of the ion: $\left[\frac{\partial}{\partial t}\rho\right]_{heating} = K(\bar{N}+1)\left[a\rho a^{\dagger} - \frac{1}{2}\{a^{\dagger}a,\rho\}\right] + K\bar{N}\left[a^{\dagger}\rho a - \frac{1}{2}\{aa^{\dagger},\rho\}\right]$, where K is a phenomenological constant, and an average equilibrium number of vibrational quanta $\bar{N} = \left(e^{\hbar\omega_v/k_BT} - 1\right)^{-1} \approx \frac{k_BT}{\hbar\omega_v} \gg 1$. For vibrational frequency 1 MHz and room temperature $\bar{N} \approx 10^7$. The experimentally measured heating rate $\nu = K\bar{N}$ usually lies in the range $1 - 10^3$ 1/s. Using numerical solution of eq.(1) we show that the finite heating rate limits the efficiency of all proposed generalized Ramsey schemes, mainly due to the reduction of effective Rabi frequency and decoherence caused by heating.

This work was supported by the Russian Scientific Foundation (project No. 16-12- 00052).

References

[1] V.I. Yudin et al., Phys. Rev. A 82, 011804 (2010); N. Huntemann et al., Phys. Rev. Lett. 109, 213002 (2012); T. Zanon-Willette et al., Phys. Rev. A 92, 023416 (2015); R. Hobson R., et al., Phys. Rev. A 93, 010501 (2016); T. Zanon-Willette et al., Phys. Rev. A 93, 042506 (2016); T. Zanon-Willette et al., Phys. Rev. A 96, 023408 (2017).
[2] For a review see T. Zanon-Willette et al., Progress and perspectives on composite laser-pulses spectroscopy for high-accuracy optical clocks, accepted for publication in Report on Progress in Physics (2018).

Project of the proof-of-principle experiment on THz generation in colliding laser wakefields

I. Timofeev[1], V. Annenkov[1,3], S. Avtaeva[2], K. Gubin[2], V. Khudyakov[1,3], V. Trunov[2], and E. Volchok[1,3]
[1]*Budker Institute of Nuclear Physics SB RAS, Novosibirsk, Russia*
[2]*Institute of Laser Physics SB RAS, Novosibirsk, Russia*
[3]*Novosibirsk State University, Novosibirsk, Russia*
E-mail: timofeev@ngs.ru

Filling of the "THz gap" (0.3-30 THz) via the creation of compact, tunable and high-power radiation sources is one of the most dynamically developing areas of modern science. Picosecond pulses of coherent terahertz radiation with electric fields >1 MV/cm and milijoule total energy are presently demanded either in fundamental physics for the control and manipulation of various collective degrees of freedom in condensed matter or in chemistry for stimulating surface reactions. Today, the most powerful (1-10 MW), energetic (tens of uJ) and narrow-band (<1%) THz pulses are produced by such large-scale and expensive accelerator facilities as free-electron lasers [1]. New ideas how to exceed these parameters using more compact generating schemes are actively proposed in both accelerator and laser communities.

The most frequently discussed laser schemes are based on the difference-frequency generation [2] and optical rectification [3] in nonlinear crystals. Despite the significant progress in these studies, energy and power of narrow-band THz pulses in such schemes are strongly limited by damage thresholds of a nonlinear medium. Moreover, the central pulse frequency cannot be tunable in the whole THz range due to opacity bands in crystals. To avoid these difficulties, we have recently proposed a new scheme based on nonlinear interaction of counterpopagating wakefields excited in a plasma by colliding laser pulses [4]. Each femtosecond laser pulse acts on plasma electrons through the ponderomotive force and enables to excite long-lived potential plasma oscillations if the laser duration is smaller than the period of these oscillations (Fig. 1). If transverse potential profiles of the colliding plasma waves differ from each other, their nonlinear interaction results in long-time (many periods of plasma oscillations) generation of electromagnetic waves at the doubled plasma frequency. Since the central frequency of the produced THz pulse is tied to the second harmonic of the plasma frequency, it can be easily tuned by the variation of plasma density. Since this nonlinear process proceeds in a uniform density plasma, the spectral line-width of the THz pulse can reach 1-2%. Plasma capabilities to sustain large electric fields allow to use petawatt-class laser drivers in such a scheme. Our particle-in-cell simulations have shown that such powerful drivers are able to produce gigawatt terahertz radiation with the record pulse energy 10 mJ.

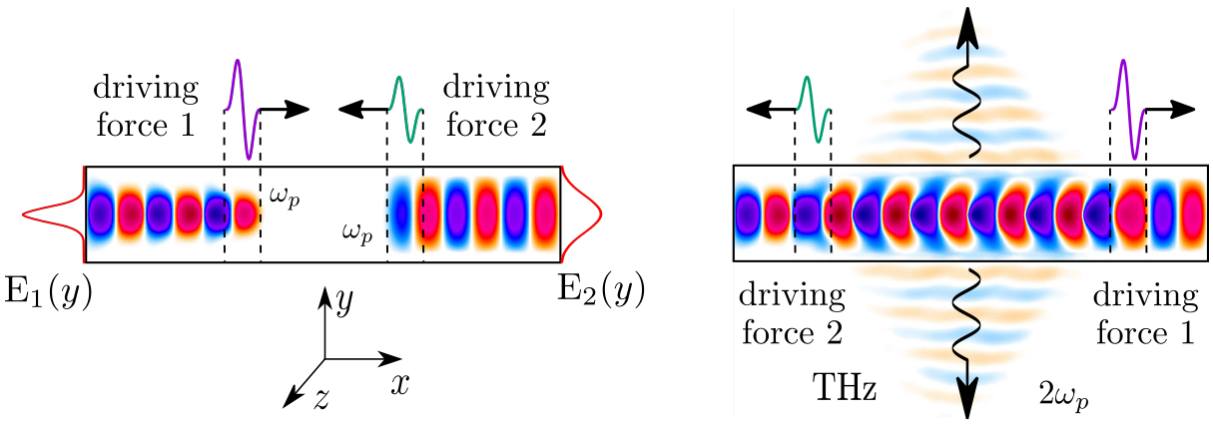

Fig. 1 The layout of the experiment on the collision of plasma wakes with differing amplitude profiles (two moments of time (before and after collision) are shown).

In order to prove the principal possibility of generating the second harmonic radiation by laser-induced colliding plasma wakes and verify our theoretical insights on this phenomenon, we propose to perform a laboratory experiment using the multi-TW laser system developed in the Institute of Laser Physics SB RAS. It is assumed that the primary laser pulse with the wavelength 830 nm and total energy 0.2 J will be divided into two pulses that will then be collided inside a supersonic gas jet. Although the proposed scheme is able to produce radiation at any frequency, it is suitable to demonstrate the effect at the frequency of CO_2 laser (28 THz). It means that the electron density of laser-ionized plasma should be equal to $2.5*10^{18}$ cm^{-3} and the optimal duration of laser pulses should be chosen as 39 fs. We have analyzed different overlapping schemes of colliding lasers and found that the optimal one is achieved when the first Gaussian laser pulse (containing 90% of energy) is focused into the spot with the diameter 40 um and the second one (10% of energy) is focused into the same focal plane, but with the less spot-size 14 um. If axes of colliding laser pulses coincide, our theory predicts the generation of a THz pulse with the peak power 38 MW and total energy 48 uJ which corresponds to the efficiency $2.4*10^{-4}$.

The case of head-on collision (Fig. 1), however, is not suitable for experimental implementation. To avoid the return of laser radiation to the amplification system, laser pulses will be collided at a small angle. We have generalized our theoretical model to the case of arbitrary collision angle and found that the THz power for given parameters reduces monotonically with the angle growth. It is shown that the angle 5^0 results in a power reduction of 20%.

Another important question discussed in this report is the choice of a gas. Radiation efficiency of the proposed scheme depends on the duration of THz emission which can be additionally limited by the effect of ion dynamics. Superposition of colliding oscillations form a standing plasma wave which modulates the ion density. It is obvious that heavy ions can solve the problem, but laser ionization of heavy gases cannot provide the uniform electron density necessary for the long life-time of excited plasma waves. According to this, nitrogen seems to be the most preferable gas. In this case, laser intensity is strong enough for the uniform 5-fold ionization of nitrogen in a large enough volume and the dynamics of nitrogen ions is slower than for ions of hydrogen and helium. We have carried out PIC simulations of THz generation in these three light gases and demonstrated that ion effects in nitrogen plasma lead to an additional power reduction of 20% compared to the case of infinitely heavy ions. The produced plasma channel with the modulated density can be also used for THz generation via the linear conversion of a plasma wake driven by a single laser pulse. Experimental realization of such a scheme capable of reaching higher efficiency 0.1% is also discussed.

This work is supported by RFBR grant 18-42-540010.

References

[1] N.A. Vinokurov, O.A. Shevchenko, Phys. Usp. **188**, 493 (2018).
[2] B. Liu, H. Bromberger, A. Cartella et al., Opt. Letters **42**, 129 (2017).
[3] C. Vicario, A.V. Ovchinnikov, O.V. Chefonov, C.P. Hauri, arXiv: 1608.05319 (2016).
[4] I.V. Timofeev, V.V. Annenkov, E.P. Volchok. Phys. Plasmas **24**, 103106 (2017).

Geometric phase in non-standard settings

V.A. Tomilin[1,2], T.S. Yakovleva[1,2], A.M. Rostom[1], L.V. Il'ichov[1,2]
[1]*Novosibirsk State University, 630090, Novosibirsk, Russia*
[2]*Instituite of Automation and Electrometry, 630090, Novosibirsk, Russia*
E-mail: 8342tomilin@mail.ru

Geometric (topological) phase $\varphi_{geom}(C)$ is a characteristic attributed to any curve C in a complex projective space of quantum states, i.e. to any quantum state evolution of an isolated system [1,2]. It was first defined for Hamiltonian evolution of a pure quantum state [1]. The present work is dedicated to expanding this concept to a broader range of physical situations – mixed states of open quantum systems, and the state change incorporating pre- and post-selection procedures (also known as two-state vector formulation of quantum mechanics [3]). First, we derive a general expression for geometric phase of open quantum system as a function of its history – a series of measurement outcomes generated during a system passage through a chain of Mach-Zehnder interferometers, given the arbitrary input state. This is a further development of operational approach to geometric phase introduced in [4,5]. In [4] a geometric phase was defined as a purely kinematic concept, analogous to [2]. The necessary step towards defining geometric phase for open quantum system is made by replacing a unitary evolution in each interferometer by interaction with the element of environment followed by measurement of some environment observable.

The scheme under consideration is shown in Fig. 1. The entrance interferometer numbered with (0) introduces a controllable phase shift θ to the state of spatial motion of the system, which is used for detecting geometric phase from the shift of interference pattern at the output of interferometer. All the interferometers to follow contain interaction with environment in a standard pre-defined state $|e\rangle$ in their vertical arm. The measurement of an observable related to the corresponding element of environment (possibly different for each element) is performed and its outcome i_n is recorded. The history I represents an ordered set of outcomes: $I = i_N \dots i_1$. Designating the states of horizontal and vertical motion with $|0\rangle$ and $|1\rangle$, respectively, and assuming that the initial state is fed to the horizontal input of (0)-th interferometer, the input state reads $\hat{\varrho}^{(in)} = \hat{\rho}^{(in)} \otimes |0\rangle\langle 0|$, where $\hat{\rho}^{(in)}$ is the initial internal state of the system. It is convenient to treat the evolution of the system in terms of intermediate states $\hat{\varrho}^{(n)}$ in which the system appears after passing the input beamsplitter of the (n)-th interferometer (Fig. 1). The corresponding internal states $\hat{\rho}^{(n)}$ get correlated with the states of spatial motion: $\hat{\varrho}^{(n)} = \sum_{\sigma,\sigma'=0,1} \hat{\rho}^{(n)}_{\sigma\sigma'} \otimes |\sigma\rangle\langle\sigma'|$.

The change of the internal state during propagation through an interferometer can be described with the help of operators $\hat{\mathcal{E}}_{i_n}(0) = \langle e^{(n)}_{i_n} \big| e\rangle, \hat{\mathcal{E}}_{i_n}(1) = \langle e^{(n)}_{i_n} \big| \hat{U} | e\rangle$, where $\hat{\mathcal{E}}_{i_n}(0)$ describes the interaction if the system goes via horizontal arm (no interaction, only measurement), and $\hat{\mathcal{E}}_{i_n}(1)$ describes it if the system goes vertically (interaction followed by measurement). Here $\left\{ | e^{(n)}_{i_n}\rangle \right\}$ is the basis of (n)-th observable's eigenstates. The geometric phase is extracted from the difference of detection probabilities at the output $D_- = Tr\left[\hat{\rho}^{(N+1)}_{11} - \hat{\rho}^{(N+1)}_{00}\right]$ and the final expression for it reads

$$\theta_{geom}(I) = \arg Tr\left[\sum_{\sigma=0,1} (\hat{\mathcal{E}}^{\dagger}_I(\sigma,1) - \hat{\mathcal{E}}^{\dagger}_I(\sigma,0)) \cdot (\hat{\mathcal{E}}_I(\bar{\sigma},1) + \hat{\mathcal{E}}_I(\bar{\sigma},0) \cdot \hat{\rho}^{(in)})\right] \qquad (1)$$

where $\bar{0} = 1, \bar{1} = 0$. The operators $\hat{\mathcal{E}}_I\left(\sigma^{(N)}, \sigma^{(1)}\right)$ explicitly depend on the measurement record I:

$$\hat{\mathcal{E}}_I\left(\sigma^{(N)}, \sigma^{(1)}\right) = \sum_{\sigma^{(N-1)}=0,1} \dots \sum_{\sigma^{(2)}=0,1} \hat{\mathcal{E}}_{i_N}\left(\sigma^{(N)}\right) \dots \hat{\mathcal{E}}_{i_1}\left(\sigma^{(1)}\right) \cdot (-1)^{\sigma^{(N)}\sigma^{(N-1)} + \dots + \sigma^{(2)}\sigma^{(1)}} \qquad (2)$$

This is the central result of the present work.

The obtained expressions were applied to the case of two-dimensional system (a qubit) and the same environment, as an illustration. The interaction $\hat{U}$ was chosen from the class of controlled two-quit operations. The values of the geometric phases corresponding to different measurement records were evaluated from (2) (see Fig. 1), and their certain features (particularly, inability to gain a non-trivial geometric phase for some input states and certain choices of $\hat{U}$) were explained.

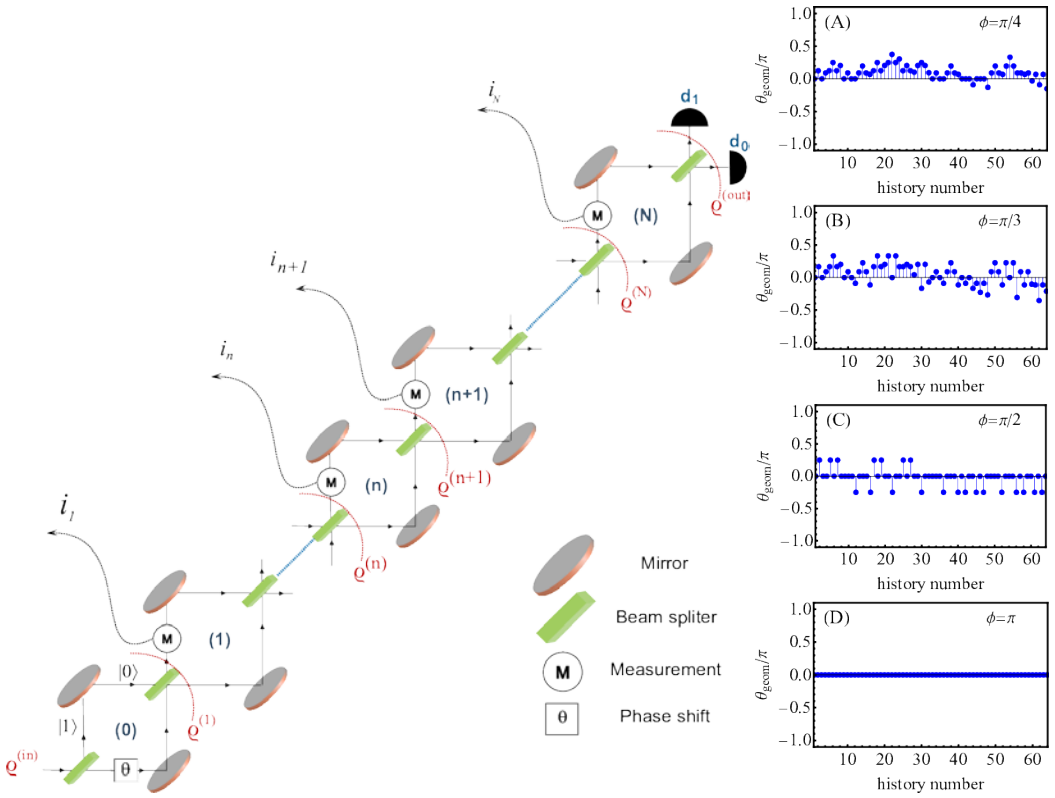

Fig. 1 (Left) The measurement scheme consisting of a chain of interferometers numbered from 0 to N. In the initial interferometer numbered (0) a controlled phase shift θ is inserted. In the subsequent interferometers the system interacts with the elements of environment prepared in a standard state, then a certain environment observable is measured, producing a series of measurement outcomes $i_1, \ldots, i_N$. Geometric phase acquired during propagation through the chain can be deduced from the detection probabilities in the output detectors d_0 and d_1. (Right) The results of the calculation of geometric phases for different measurement records for a qubit system interacting with qubit environment via controlled phase-shift ϕ (environment qubit is a taget, system qubit acts as control) for N=6, so the total number of different measurement histories is 2^6.

References

[1] M.V. Berry, Proc. R. Soc. A **392**, 45 (1984).
[2] M. Mukunda, R. Simon, Ann. Phys. **228**, 205 (1993).
[3] Y. Aharonov, P.G. Bergmann, J.L. Lebowitz, Phys. Rev. B **134**, 1410 (1964).
[4] E. Sjöqvist et al., Rhys. Rev. Lett. **85**, 2845 (2000).
[5] E. Sjöqvist, Acta Physica Hungarica B: Quant. Electron. **26**, 195 (2006).

Precision spectroscopy of cold magnesium atoms for an optical frequency standard

M. Tropnikov[1], A. Bonert[1], A. Goncharov[1-3], S. Kuznetsov[1], V. Baraulya[1], D. Brazhnikov[1,2], and O. Prudnikov[1]

[1]*Institute of Laser Physics SB RAS, pr. Acad. Lavrent'eva 15B, 630090, Novosibirsk, Russia*
[2]*Novosibirsk National Research State University, Pirogova 1, 630090, Novosibirsk, Russia*
[3]*Novosibirsk State Technical University, pr. Karla Marksa 20, 630092, Novosibirsk, Russia*
E-mail: makstropnikov@gmail.com

Frequency standards play an important role in various fields of science and technology: in fundamental physics, metrology, and navigation. The relative accuracy of a primary frequency standard based on a caesium fountain has probably reached its limit $\Delta\nu/\nu = 2*10^{-16}$ [1]. Further increase in the accuracy of frequency standards is associated with transition from the microwave range of the spectrum to the optical range and, hence, with the creation of optical frequency standards based on single ions or neutral atoms. Alkaline-earth and alkaline-earth-like atoms, such as Yb, Ca, Sr, Hg, and Mg, are among the main candidates for creating the optical frequency standards. The most accurate and stable optical frequency standards for today are optical frequency standards based on Sr and Yb atoms captured in the optical lattice. However, ^{24}Mg has some advantages over the other candidates such as the narrowest intercombination transition, the simplest structure of the electron shells, and the smallest frequency shift of the "clock" transition due to black body radiation. The presence of strong closed $^1S_0$–$^1P_1$ transition allows effective cooling and trapping of magnesium atoms in a magneto-optical trap. Creation of a frequency standard based on Mg atoms is possible using $^1S_0$–$^3P_1$ transition with the natural linewidth of 36 Hz. Sub-Doppler cooling of magnesium atoms and their localization in an optical lattice will later allow one to employ strongly forbidden $^1S_0$–$^3P_0$ transition and realize the frequency standard with the relative inaccuracy of 10^{-16}–10^{-17} [2]. In this paper, the possibility of obtaining the narrow reference lines using $^1S_0$–$^3P_1$ transition in creating the optical frequency standard is shown and the progress achieved in the frequency stabilization by observed resonances studies is presented.

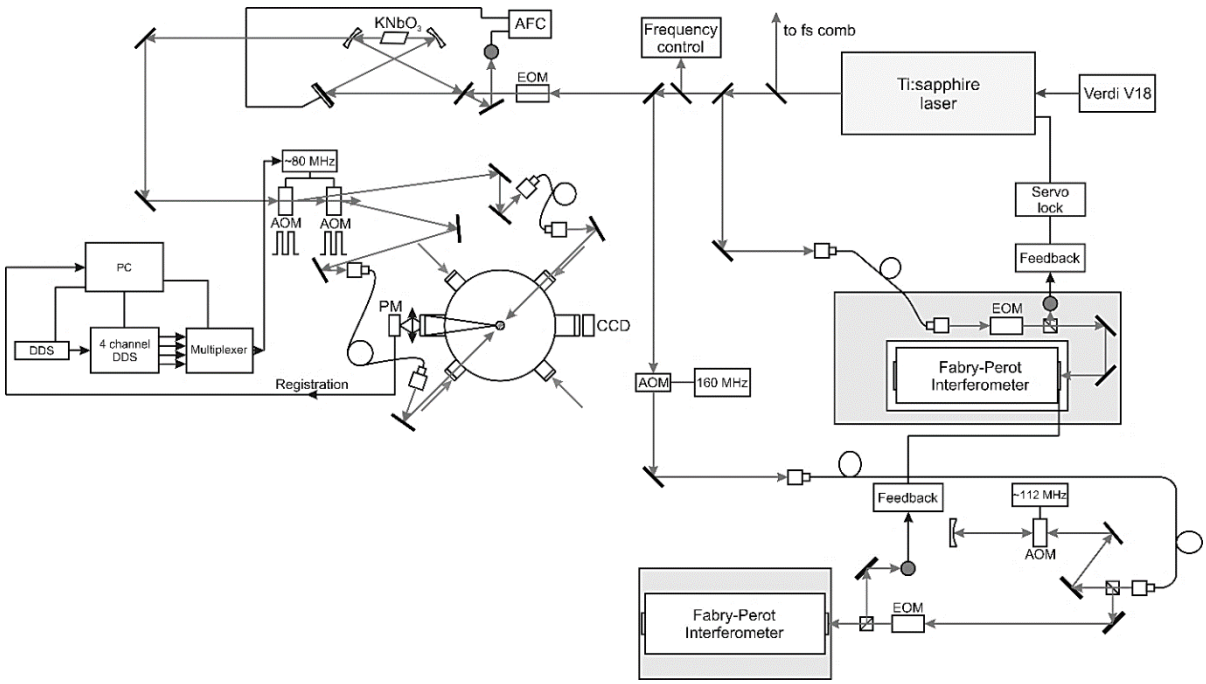

Fig. 1 Schematic of the experimental setup used for spectroscopy of the clock transition. Fs comb – femtosecond comb, $KNbO_3$ – nonlinear crystal in an external cavity, AFC – automatic frequency control, AOM – acousto-optic modulator, EOM – electro-optic modulator, DDS – 4-channel direct digital synthesizer, PM – photomultiplier tube, CCD – CCD camera.

The source of radiation for clock $^1S_0$–$^3P_1$ transition spectroscopy is a system based on Ti:sapphire laser pumped by 15-watt solid-state Verdi V18 laser with a two-stage system of frequency stabilization and a frequency doubling in a $KNbO_3$ crystal in an external cavity.

The frequency of the laser system radiation is stabilized by the two reference Fabry-Perot interferometers: with invar base and optical glass-ceramic base. The first interferometer provides the preliminary narrowing of the generation line of the Ti:sapphire laser, the second interferometer is used for correcting low-frequency perturbations of the first interferometer through automatic adjustment of its length by the piezoelectric actuator with an interferometer mirror installed on it.

The stabilized Ti:sapphire laser, which outputs about 1 W of power at 914 nm, is followed by cavity enhanced second harmonic generation inside a nonlinear $KNbO_3$ crystal that yields about 80 mW at 457 nm. Laser cooling and localization of magnesium atoms in a magneto-optical trap is carried out on the $^1S_0$–$^1P_1$ closed transition at 285 nm. Investigation of the $^1S_0$–$^3P_1$ transition of cold magnesium atoms localized in the MOT is performed by the method of fields separated in time (time-domain Ramsey–Borde atom interferometer) [3]. Two pairs of the light pulses formed from cw radiation of a highly stable laser system at 457 nm by acousto-optic modulators interact with a cloud of magnesium atoms. Pairs of pulses are transported into the magneto-optical trap through opposite windows via two fibers.

In recording narrow resonances, the radiation frequency of the laser system is tuned by a frequency synthesizer controlling AOM in the frequency stabilizing system of the second interferometer. The AOM frequency and pulse parameters were controlled by a multichannel timer, a multiplexer, and a computer-controlled four-channel direct digital synthesizer (DDS). The pulse duration τ was 4 μs and the time delay T for a pair of unidirectional pulses could be varied to achieve needed spectral resolution $\Delta\nu = 1/(8T_{eff})$, where $T_{eff} = (4/\pi)\tau + T$. The best to date spectral resolution, $\Delta\nu = 390$ Hz, was obtained at $T = 310$ μs. The fluorescence signal from a cloud of cold magnesium atoms on the resonance transition at 285 nm is detected by the photomultiplier. The Ramsey–Borde resonances in time-separated fields for $T = 310$ μs are shown in Fig. 2(a).

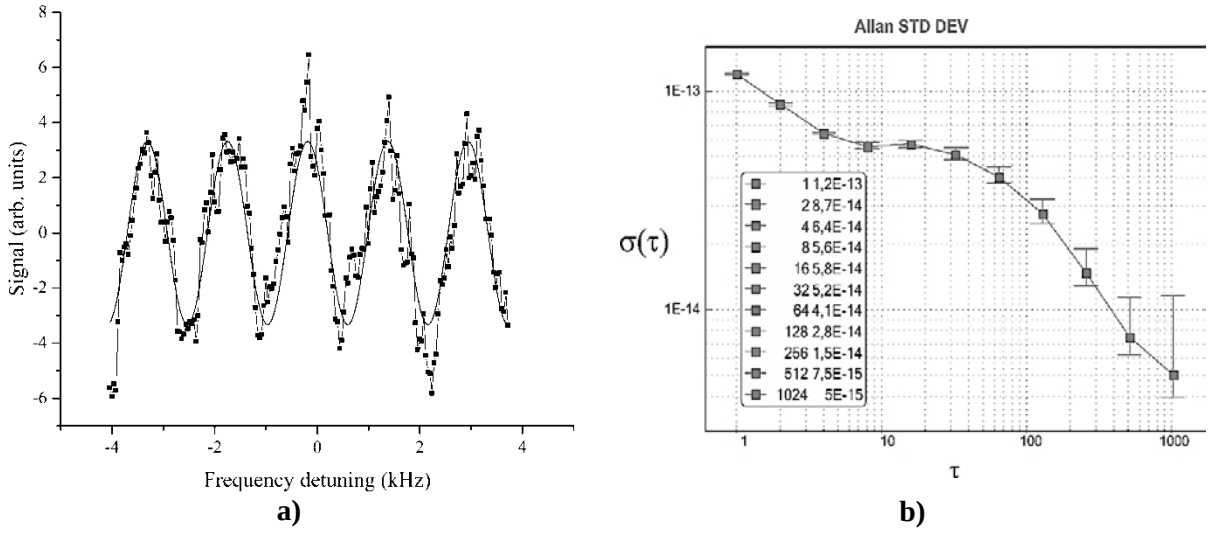

Fig. 2 (a) Resonances in time-separated fields for the delays between pulses T=310 μs. (b) Allan function characterizing frequency stability of the developed Mg frequency standard.

The clock laser frequency stabilization by the central fringe of observed resonances was performed. The optical frequency of the laser was tuned by varying the frequency of the double-pass AOM. The error signal for the stabilisation system was formed using a digital analogue of stabilisation with respect to the third harmonic of the modulation frequency. The calculated value was used to tune the AOM frequency in the second stabilization system. To determine the frequency stability for the radiation stabilized, some part of clock laser radiation at a wavelength of 914 nm was directed through an optical fiber to a femtosecond frequency comb, based on a Ti:sapphire laser. The

pulse repetition rate of the femtosecond comb was stabilized using the beat signal of one of its modes with a frequency standard based on an Yb:YAG laser. Fig. 2(b) shows the measured frequency stability of $5 \cdot 10^{-15}$ at averaging time $\tau = 1000$ s.

References

[1] F. Levi, D. Calonico, C. E. Calosso, A. Godone, S. Micalizio and G. A. Costanzo, Metrologia, **51(3)**, 270 (2014).
[2] A. N. Goncharov, A. E. Bonert, D. V. Brazhnikov, A. M. Shilov and S. N. Bagayev, Quantum Electronics, **44(6)**, 521 (2014).
[3] K. Sengstock, U. Sterr, G. Hennig, D. Bettermann, J. H. Müller, W. Ertmer, Opt. Commun., **103**, 73 (1993).

Modulation spectroscopy of CPT resonance displayed by polychromatic light

E.A. Tsygankov[1], D.S. Chuchelov[1,2], V.V. Vasiliev[1,2], M.I. Vaskovskaja[1,2], V.L. Velichansky[1-3], S.A. Zibrov[1,2], S.V. Petropavlovsky[4], V.P. Yakovlev[3]

[1]*OOO "Atomiks", 125315, Moscow, Russia*

[2]*P.N. Lebedev Physical Institute, Russian Academy of Sciences, 119991, Moscow, Russia*

[3]*National Research Nuclear University MEPhI (Moscow Engineering Physics Institute), 115409, Moscow, Russia*

[4]*National Research University Higher School of Economics, 101000, Moscow, Russia*

E-mail: selentinthebright@gmail.com

We present a theory of frequency modulation spectroscopy [1] of the CPT resonance, widely used in frequency standards [2, 3], where phase of the laser field is modulated by the law $a\sin(\Omega t + b\sin\omega_m t)$. Frequency Ω is close to the one half of the hyperfine splitting between levels of the ground state ω_g, therefore the two nearest to the carrier components of obtained polychromatic spectrum induce two-photon resonance: $2\Omega = \omega_g + 2\delta$ (see Fig. 1). The CPT resonance is displayed as a function of the detuning δ. Slow modulation at rate ω_m gives rise to the response in the absorption coefficient, which can be reduced to in-phase (M_S) and quadrature (M_Q) components. In general case their superposition $k \sim M_S \cos\omega_m t + M_Q \sin\omega_m t$, that provides the greatest sensitivity to the detuning is used to stabilize atomic clocks frequency.

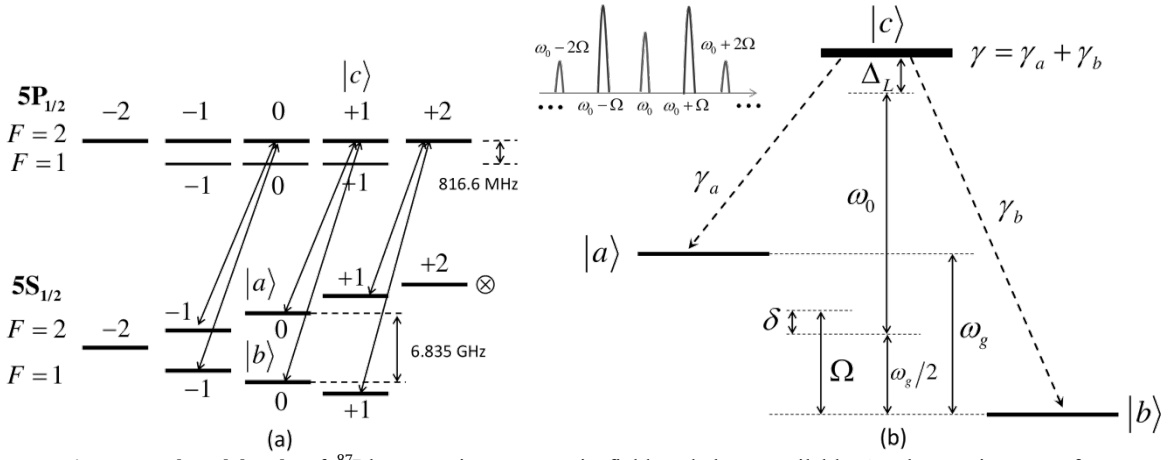

Fig. 1 Employed levels of ^{87}Rb atoms in a magnetic field and three available Λ-schemes in case of σ_+ polarized light. (b): The Λ-scheme for metrological 0-0 sublevels used as a model and the spectrum of optical field.

We considered equations for the atomic density matrix $\hat{\rho}(t)$ under the resonant approximation for optical transitions $|a>, |b> \leftrightarrow |c>$ at the next hierarchy of frequencies: $\omega_m \ll dE/2\hbar \ll \gamma \ll \Gamma \ll \Omega$, where $dE/2\hbar$ – Rabi frequency, γ – spontaneous decay rate of the upper state $|c>$, Γ – decoherence rate of the coherences ρ_{ca}, ρ_{cb}. The steady-state solution were obtained for amplitudes of the density matrix Fourier harmonics at the frequency Ω. Absorption coefficient is determined by zeroth Fourier harmonic of the upper state population ρ_{cc}. It slowly depends on time at the characteristic rate ω_m.

Analytical formulae are obtained for amplitudes M_S and M_Q, light shift μ and CPT resonance width λ. The solution includes the case of dynamical modulation regime: $\omega_m \gg \lambda$ and $b \gg 1$. Thus, the developed theory generalizes the results of work [4] to the case of optically thick media and polychromatic laser spectrum. Analytics are validated by direct numerical integration of initial density matrix equations. Theoretical results are compared with the experimental data obtained with ^{87}Rb atoms. They are in good agreement, see Fig 2.

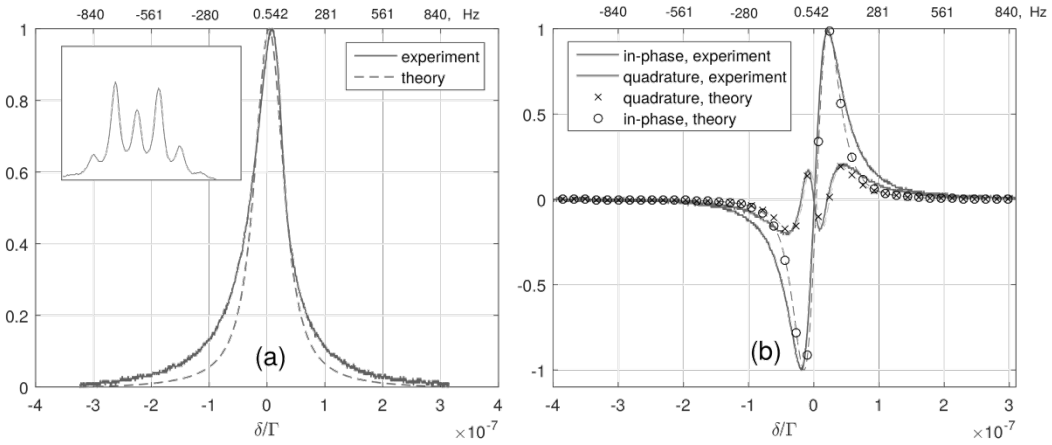

Fig. 2 a) Experimental and theoretical dependencies of transmission through the cell on frequency detuning; the inset demonstrates the spectrum of the incoming light centered at the carrier. b) The in-phase and quadrature signals. The frequency deviation about the central frequency 3 417 344 409 Hz is specified both in terms of relative detuning δ/Γ and directly in Hz on top of each graph. Theoretical curves are marked by circles and crosses only to help distinguishing the curves.

We consider a thick optical medium as a set of elementary thin media. In each of them most of the field components are constant but the first sidebands exponentially decay at a rate β as a functions of the thin medium position. The light shift of the CPT resonance for a thick optical medium is defined as a shift of the point δ that corresponds to minimum of the resonance profile averaged over the cell.

For a widely used VCSELs as a light source for CPT atomic clocks the spectrum under modulation differs from the spectrum arising from pure FM modulation or from a combination of FM and AM modulation because of nonlinear interaction between the components of electromagnetic field in active laser medium [5]. This effect results in spectrum asymmetry and non-zero amplitude of the carrier. However, the theory allows to calculate the light shift for arbitrary laser spectrum for a thick optical medium. It provides a way to select lasers and to find the optimum modulation regime for them.

The light shift of the CPT resonance is one of the major contributors to the instabilities of the atomic clocks [6, 7]. A smart technique for the light shift suppression for the double resonance effect in optically thick media utilizing quadrature response was proposed by Happer et al. in [8]. In Happer's method the in-phase signal is used to stabilize rf frequency and an additional feedback is used to control the laser frequency at the value at which both M_S and M_Q turn to zero simultaneously. A possibility of using a similar method for active light shift suppression of the CPT resonance for a case of thick optical medium, that is, to use quadrature response to control index of FM modulation is studied in this work.

We show that it is not possible to obtain the zero light shift of the CPT resonance by controlling the modulation index a by merging zeroes of the in-phase and quadrature responses: their zero-crossing points coincide for all modulation index in a thin optical medium; on the contrary, for a thick optical medium they differ, including the case of the zero light shift. A modified Happer's method can be used if feedback signal is formed as a difference of quadrature signal dependence on a and the fixed value of quadrature signal at zero light shift, which can be obtained in optical thick media and in the case of asymmetrical laser spectrum.

References

[1] G. Bjorklund, M. Levenson, W. Lenth et. al., Appl. Phys. B **32**, 145 (1983).
[2] V. Shah, J. Kitching, Adv. At. Mol. Opt. Phys. **59**, 21 (2010).
[3] J. Vanier. Appl. Phys. B, **81**, 421 (2005).
[4] V. Yudin, A. Taichenachev, M. Basalaev et. al., Opt. Express **25**, 2742 (2017).
[5] M. Vaskovskaya, V. Vassiliev, S. Zibrov et. al., Quant. El. **47**, 835 (2017).
[6] K. Svenja, R. Wynands, J. Kitching et. al., J. Opt. Soc. Am. B, **18**, 1545 (2001).
[7] D. Miletic, C. Affolderbach, M. Hasegawa et. al., Appl. Phys. B **109**, 89 (2012).
[8] B. McGuyer, Y. Jau and W. Happer, Appl. Phys. Lett. **94**, 251110 (2009).

The response of a diode laser with an external cavity to the microwave modulation of the pumping current

M.I. Vaskovskaya[1,3], D.A. Shiryaev[2], A.P. Bogatov[1], A.E. Drakin[1], S.A. Zibrov[1,3], V.V. Vassiliev[1,3], V.L. Velichansky[1-3]
[1]*P.N. Lebedev Physical Institute, Russian Academy of Sciences, Moscow, Russia*
[2]*National Nuclear Research University MEPhI, Moscow, Russia*
[3]*Atomiks Ltd., Moscow, Russia*
E-mail: dubniy105@mail.ru

Dynamically single-mode lasers are required for frequency standards based on the coherent population trapping (CPT). To suppress light shifts, their modulation spectra must have a high symmetry of the first sidebands and a significant part of the power in the higher sidebands. Not all commercially available vertical-cavity surface-emitting lasers (VCSEL) meet these requirements [1]. For a detailed comparison with the theory of CPT, in which the laser spectrum corresponds to the pure frequency modulation [2], it is of interest to explore a diode laser (DL) with an extended, spectrally selective cavity, because its control has more degrees of freedom.

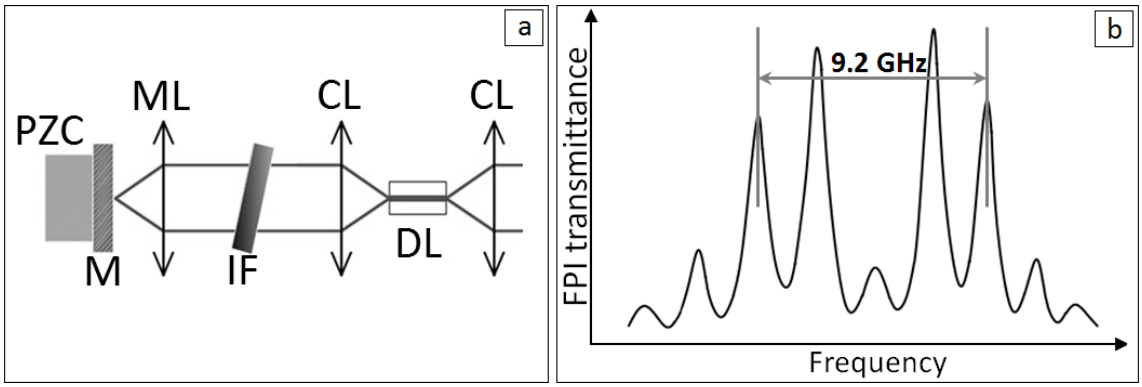

Fig. 1 a) Scheme of the extended-cavity diode laser with an additional selectivity: DL – diode laser, PZC – piezoceramic, M – mirrow, IF – interference filter, CL – collimating lens, ML – matching lens. b) Laser spectrum in case of HF (frequency=2.3 GHz) current modulation.

We used an external resonator with an interference filter (IF) and a cat's eye (Fig.1). A Sacher SAL2-0850-100 diode laser (DL) served as an active element. It's facet looking toward external cavity was AR-coated. The single pass efficiency and the FWHM of the transmission line of the IF were 0,77 and 121 GHz, respectively. All radiation emerging from AR coated facet (but coupling losses) returned back after filtering to the laser waveguide. The light for measurements was taken from another facet. It provided high level of feedback and dynamically stable single-mode operation under high frequency current modulation. The AC current was fed to the laser via bias-T. We displayed laser emission spectrum under modulation by means of scanning Fabry-Pérot interferometer (FPI) with 15 GHz free spectral range. Fig1 b) shows an example of such spectrum.

We found that modulation spectra of the described laser are closer to those arising under pure frequency modulation than spectra of VCSEL and allow for deeper carrier suppression, which was observed also in [3].

To determine frequency at which modulation is most effective we took the dependence of the carrier power on frequency of modulation. The first minimum of the carrier power where most of the power is in the sidebands corresponds to maximum efficiency of modulation and defines the resonant frequency. It is well known that frequency modulation of laser field is most effective at the frequency equal to the adjacent mode separation or it's multiple. We looked for it in this range and, indeed, maximum of efficiency occurs within this frequency range. However instead of one extremum we found two of them with high (ν_{HF}) and low frequencies (ν_{LF}). We observed it for different lengths of the cavity (L) in the range of 5.4 – 12.6 cm not only in the vicinity of c/2L frequency but also close to

c/L and 3L/2 frequencies. In all cases and for all sidebands light polarization was linear and did not change under modulation. It looks as if longitudinal mode become splitted. Fig.2 shows the dependence of the splitting on pumping current. The splitting increases with current and laser intensity. Typically . the rate of change of ν_{HF} frequency is greater than the absolute rate of change of $\nu_{LF.}$frequency

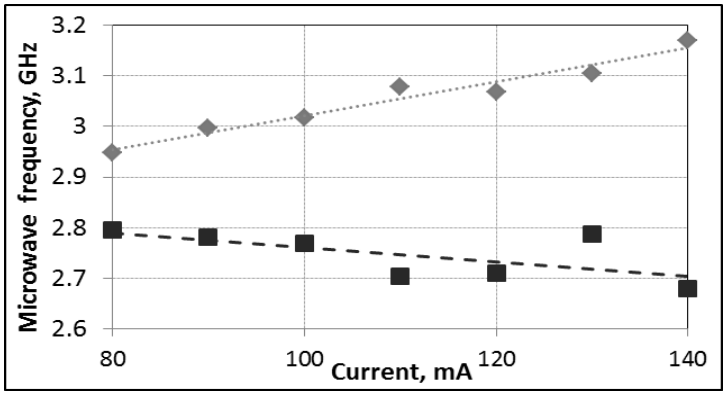

Fig. 2 Dependence of ν_{HF} (grey diamonds) and ν_{LF} (black squares) on laser current. Length of the cavity in this case was L=3.2 cm.

On looking for explanation we noticed very similar splitting of the modes described in [5] where the characteristic frequencies (the modes) were observed in the spectrum of laser's amplitude fluctuations. The ratio of the splitting to the free spectral range of the laser cavity is of the same order (0.1-0.05) in both cases. The dependencies on current are of the same type. However there is a great difference of the ways the resonance frequencies revealed themselves in presented work and in [5]. To find the resonance we tuned the frequency of the relatively strong field of the sidebands while in [5] the resonance response was probed by very weak field of amplified noise.

To be sure that the two phenomena have the same origin we also studied the spectrum of amplitude fluctuations with a fast photodiode and a spectrum analyzer. We found good coincidence of the splittings and the ν_{HF}, ν_{LF}. frequencies determined in both cases (by measuring fm modulation efficiency and by analyzing the amplitude noise spectra).

The simplified qualitative explanation of the effect is the following [6]. The beating of a strong field of the main operating mode with a small field of the neighboring mode in active region of laser at frequency of the order of reciprocal lifetime of electrons results in the oscillation of inversion. Due to strong amplitude-phase coupling it gives rise to modulation of refractive index. The gain in the neighboring mode is smaller than threshold gain so that diode laser cavity works for it as an interferometer. It's transmission varies with refractive index and produces small field in the neighboring mode with the opposite sign of the detuning with respect to the frequency of the main mode. A correct analysis of the small field evolution and stability implies consideration of the two coupled small fields. Two coupled equations for the small fields give two solutions for their attenuations and frequencies. Due to nonlinearity the frequencies are not equal. Their difference defines the splitting. Theory estimation of the splitting gives value close to experimental one.

We note that mentioned rigorous theory [5,6] describes also suppression of nonresonant noise in the vicinity of the frequencies involved in CPT which is important for it's application in metrology.

References

[1] M.I. Vaskovskaya, V.V. Vassiliev, S.A. Zibrov, et al, Technical Physics Letters, **44(1)**, 20, (2018).
[2] M. Zhu, L.S. Cutler, 32nd Annual Precise Time and Time Interval (PTTI) Meeting, 311, (2000).
[3] L. Hollberg, M. Ohtsu, Appl. Phys. Lett., **53**, 944, (1988).
[4] A. Waxman, M. Givon, G. Aviv, et al, Applied Physics B: Lasers and Optics, **95**, 301,(2009).
[5] A.P. Bogatov, et al, Sov J Quantum Electron, **16**:12, 1596, (1986).
[6] A.P. Bogatov, et al, Sov J Quantum Electron, **13**:9, 1221, (1983).

Study and optimization of atomic cell characteristics for CPT-clocks

M.I. Vaskovskaya[1,3], D.S. Chuchelov[1,3], A.B. Egorov[4], S.A. Zibrov[1,3], V.V. Vassiliev[1,3], V.L. Velichansky[1-3]

[1]*P.N. Lebedev Physical Institute, Russian Academy of Sciences, Moscow, Russia*
[2]*National Nuclear Research University MEPhI, Moscow, Russia*
[3]*Atomiks Ltd., Moscow, Russia*
[4]*A.M. Prokhorov General Physics Institute, Russian Academy of Sciences, Moscow, Russia*
E-mail: dubniy105@mail.ru

Nowadays, the main tasks in the development of frequency standards based on the effect of coherent population trapping (CPT) [1] are reducing the size and improving their long-term stability. To solve these problems, small atomic cells with carefully selected parameters of fabrication and filling are required.

Atomic cells for CPT standards are filled with alkali metal (in our case, it is ^{87}Rb) and a mixture of buffer gases (Ar+N_2). The gases in the mixture interact differently with the alkali metal, so the value of the central frequency of the CPT resonance and its temperature dependence are determined by the ratio of their partial pressures. In addition, the width of the CPT resonance depends on the total pressure of the buffer gases (under the condition that their collisional cross sections are close in value).

We produce cylindrical atomic cells (Ø=8mm, L=15mm) by laser welding in the following way. The glass tube is cut into work pieces of the desired length, and then windows made of sheet glass are welded to faces of work pieces by the CO_2-laser. We fill cells with metal and buffer gases through the hole made in the side surface of cylinder. The produced cells have a regular geometric shape of axial symmetry and good optical quality of the windows [2].

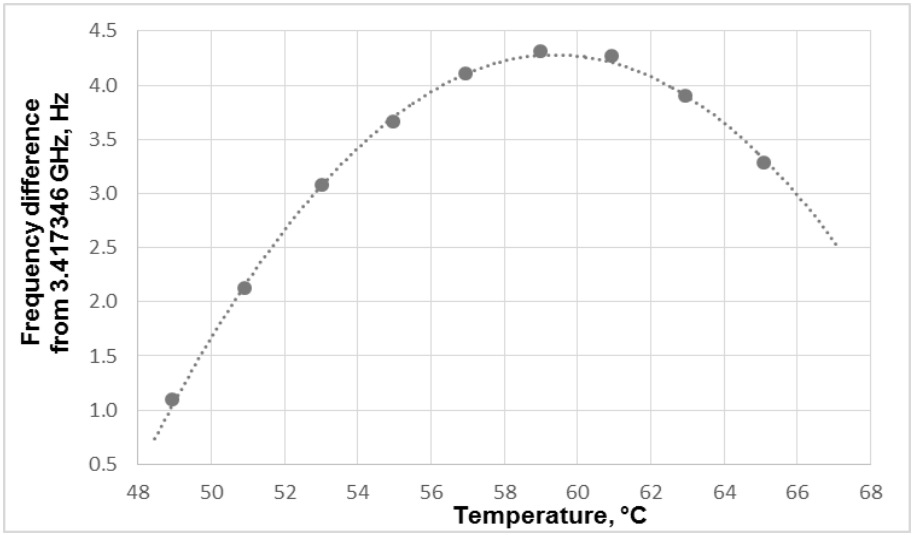

Fig. 1 Quadratic temperature dependence of frequency of CPT resonance observed in the cylindrical cell filled with ^{87}Rb and 74 Torrs of buffer gases mixture Ar and N_2. At the operating temperature corresponding to the top of the parabola a temperature change of 1 degree will cause a frequency change of 0.03 Hz.

The temperature dependence of the frequency of the CPT-resonance is determined by the formula

$$\nu(T) = \nu + P_s[\beta + \delta\,(T - T_0) + \gamma\,(T - T_0)^2], \quad (1)$$

where P_s is the cell sealing pressure, T_0 is the reference temperature, β,δ,γ are the coefficients found experimentally or in the available literature for each buffer gas [3,4]. In the case of a mixture of gases the coefficients β,δ,γ in (1) transform to the $\beta_m,\delta_m,\gamma_m$, which depend on the coefficients β,δ,γ for each of the gases and on the ratio of their partial pressures r. The coefficients δ for Ar and N_2 have different

signs, so, by choosing the right *r* it is possible to eliminate the linear dependence or to shift the vertex of a parabola to the desired temperature. Quadratic temperature dependence of frequency instead of linear one could improve the standard's stability. Typical temperature dependence of frequency of CPT resonance for our cell is shown on fig.1.

It is known that the stability of the frequency standard depends on the quality of the reference resonance *Q* and the value of the signal/noise ratio *S/N*. Both parameters should be maximized for the best stability of a standard [5]. *Q* is the ratio of the resonance frequency to its width. Thus, for high quality factor, a narrow resonance is needed. The ratio can be increased by increasing the resonance contrast under the condition of a constant noise level. Therefore, it is necessary to choose the operation mode of the standard in such a way that the contrast of the CPT resonance, which determines the useful signal, would be maximum.

We have found a method of filling the cells, which provides optimal values of width and contrast of the CPT resonance and quadratic temperature dependence. The first step was to find the value of the total pressure of buffer gases (for a given geometry of cells), at which the resonance width is minimal. After that, the dependence of the resonance contrast on the temperature (that is on the concentration of Rb atoms) was investigated. The last point was to choose such pressure ratio of buffer gases at which the temperature corresponding to the top of the temperature dependence coincided with the temperature at which the resonance's contrast is maximum.

The results on microwave frequency stabilization obtained with described cells as references confirm their quality.

References

[1] S. Knappe, V. Shah, et al., Appl. Phys. Lett., **85(9)**, 1460, (2004).
[2] D.I. Sevostyanov, A.V. Sivak et al., Electromagnetic waves and electronic systems, **20(8)**, 73, (2015), (published in Russian).
[3] J. Vanier, R. Kunski, et al., Journal of Applied Physics, **53**, 5387, (1982).
[4] O. Kozlova, S.Guérandel, E. Clercq, Phys. Rev. A, **83**, 062714 (2011).
[5] F. Riehle, "Frequency Standards: Basics and Applications", Wiley-VCH, (2006)

Efficient Tm-laser operation based on 5%Tm:KLu$(WO_4)_2$ with N_m and AT orientation

I.A. Vedin[1], S.N. Bagayev[1], V.A. Orlovich[4], S.M. Vatnik[1], N.V. Kuleshov[3], E.V. Smolina[1], A.A. Pavlyuk[2], N.V. Gusakova[3], S.V. Kurilchik[3,4], A.S. Yasukevich[3], V.E. Kisel[3], K.V. Yumashev[3], P.A. Loiko[5], V.I. Dashkevich[4]

[1]*Institute of Laser Physics, 13/3 Lavrentjeva Ave., 630090, Novosibirsk, Russia*
[2]*Institute of Inorganic Chemistry, 3 Lavrentjeva Ave., 630090, Novosibirsk, Russia*
[3]*Belarusian National Technical University, 65/17 Nezavisimosti Ave., 220013, Minsk, Belarus*
[4]*Institute of Physics, National Academy of Sciences of Belarus, 68 Nezavisimosti Ave., 220072, Minsk, Belarus*
[5]*ITMO University, Kronverkskiy Pr., 49, 197101, Saint-Petersburg, Russia*
E-mail: vedin@laser.nsc.ru, vatnik@laser.nsc.ru

Tm-doped potassium lutetium double tungstate oxides are well known for excellent laser properties. They have rather high gain cross-sections and would allow an efficient diode pumping by widely available laser diodes and bars emitting at 800…810 nm [1-2]. We have experimentally achieved efficient multi-watt lasing in N_m-cut and AT-cut slab-shaped laser crystals.

Lasing of AT-cut slabs with the same width (0.32 mm along the N_m-axis) and length (6.20 mm along the AT direction) but different heights (0.60, 0.75 and 0.95 mm) and one N_m-cut slab with the dimensions of 6.2(N_m) × 0.83(N_p) × 0.32(N_g) mm^3 were studied. The laser cavity was formed by a flat rear mirror, AR-coated IR-grade silica fused lens with a focal length of 20.0 mm and flat output coupler (OC), with the distance between the rear mirror and closest slab endface being less than 0.2 mm. The transmission T_{OC} of the OC is 10% and 19%. Figure 1a shows the dependence of the output laser power on the true CW diode pump power for one of the AT-cut slabs (with H = 600 μm) and the N_m-cut one. The Nm-cut slab demonstrates much weaker roll-over yielding up to 16.7 W of continuous-wave output at 1910 nm for 48.2 W of diode pump power. We believe that this roll-over was caused by heavy stress-induced distortions of the optical path in AT-cut slabs, see figure 1b. As a result, the laser cavity will become unstable at high pump powers, P > 30 W. From the other side, stress-induced distortions in the N_m-cut slab are about two times weaker than those of AT-cut slabs and it seems that they do not affect notably stability of the laser cavity. We guess that a minor roll-over in the laser output for N_m-cut slab can be explained by an increase in the average temperature of the slab under intense pumping.

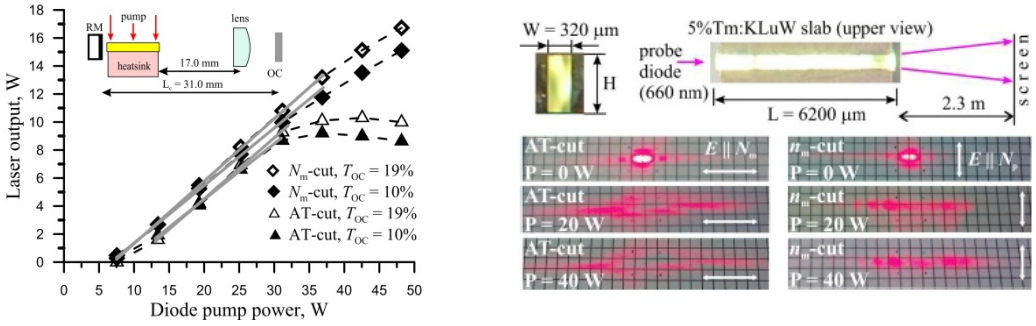

(a) (b)

Fig. 1 Input-output dependences of AT-cut (for H = 600 μm) and Nm-cut 5 at.% Tm:KLu$(WO_4)_2$ slabs for the laser cavity shown in the inset (a); Photographs of the diffraction patterns before and after switching on the CW pump (b).

We have demonstrated a multi-watts high-efficiency CW output of 16.7 W for N_m-cut Tm:KLu$(WO_4)_2$ slab well compared to other Tm^{3+}-doped double tungstate gain elements including thin disks, epitaxial structures, active waveguides and microchips.

References

[1] S.M. Vatnik, I.A. Vedin et al., Laser Physics Letters **9**, 765 (2012).
[2] X. Mateos, V. Petrov et al., IEEE J. Quantum Electron. **42**, 1008 (2006).

Oscillation performance of YAG ceramics with losses

I.A. Vedin[1], S.M. Vatnik[1], V.V. Osipov[2], K.E. Luk'yashin[2], R.N. Maksimov[2], V.I. Solomonov[2], Yu.L. Kopylov[3]
[1]*Institute of Laser Physics, Lavrentjeva ave. 13/3, 630090, Novosibirsk, Russia*
[2]*Institute of Electrophysics, Amundsen st. 106, 620016, Ekaterinburg, Russia*
[3]*Institute of Radio-engineering and Electronics, Mokhovaya st. 11/7, Moscow, 125009, Russia*
E-mail: vedin@laser.nsc.ru, vatnik@laser.nsc.ru

Significant progress in the synthesis of oxide laser ceramics has made it possible to produce large samples of Nd: YAG ceramics (up to 50 mm in diameter) with comparatively low losses and residual porosity [1] based on domestic pressing and sintering technologies [2]. Large-size laser ceramics is used not only as active elements of high-power diode-pumped lasers but also in power amplifiers and final amplification stages of high-power laser systems [3,4]. In this connection, evaluation of the influence of specific losses in ceramics on the amplification efficiency and the maximum possible energy output is of considerable scientific and practical interest and is the main aim of the present work.

In our past works, we report on optical properties and lasing of YAG ceramics synthesized at IREE (Fryazino) and IEP (Ekaterinburg). The studied samples of Nd :YAG optical ceramics had the form of disks with dimensions of Ø16 × 3.1 mm (IREE samples), as well as Ø 11 × 1.1 mm and Ø47 × 2.1 mm (IEP samples). The faces of disks were coated by dielectric films: the first face was coated by a broadband antireflection film at the pump (808 nm) and laser (1064 nm) wavelengths, and the second face was coated by a combined reflecting film consisting of a dense dielectric mirror (R > 99.8 % at l = 1064 nm) and an additional metallization layer to achieve a high reflection coefficient for the pump. The linear cavity (L = 20 mm) was formed by an external concave mirror and a rear mirror deposited on the active element from the side of the heat sink. Laser oscillation has been demonstrated for all samples under study, and the threshold and slope efficiency prove to be in a good qualitative agreement with the estimated ceramic losses. In particular, the best slope efficiency of 1%Nd:YAG (36%) and 1%Ho:YAG (40%) ceramics synthesized at IEP quite correlates with its low losses, 1.6×10^{-2}cm^{-1} and 5×10^{-2}cm^{-1}, respectively. We have shown that the value of losses ~ 1 % cm^{-1} seems to be an important milestone for "bad" or "good" ceramics in concern to their laser performance, see table 1.

Table 1. "Cold" losses (scattering, absorption) and slope efficiencies of YAG ceramics.

Sample number	Specific losses T_{loss} /H	Slope efficiency	Reference
Nd:YAG (IREE, IEP)	10…30 % cm^{-1}	5…10%	2008 – 2013 [5]
1% Nd:YAG (IEP)	6 % cm^{-1}	19%	2014-2016 [6]
0.8% Nd:YAG (IREE)	5 % cm^{-1}	21%	2014-2016 [6]
1% Nd:YAG (#1570 IEP)	**1.6 % cm^{-1}**	**36%**	**2017 [7]**
1% Ho:YAG (#1083 IEP), λ=2.1 μm	**5 % cm^{-1}**	**~40%**	**2017 [7]**

In this report we also present the analytical solution obtained using the rate equations describes the single-pass gain as a function of the optical material spectroscopic parameters, specific losses, and amplified radiation intensity. These results are of scientific and practical interest, in particular, for optimization of optical amplifiers and estimation of specific losses based on measurements of the gain of the optical material. Further improvement of the optical homogeneity of domestic ceramics remains a topical scientific and technical problem, which is of high priority for the development of high-efficiency multi-kilowatt solid-state laser systems.

References

[1] Bagayev S.N., Osipov V.V., Solomonov V.I., et al. Opt. Mater., 34, 1482 (2012).
[2] Bagayev S.N., Osipov V.V., Shitov V.A., et al. Atmos. Oceanic Opt., 25, 292 (2012).
[3] Li M., Hu H., Gao Q., et al. IEEE Photonics J., 9, 1504010 (2017).
[4] Chen Y., Fan Z., Guo G., et al. Opt. Mater., 71, 125 (2017).
[5] Vatnik S.M., Osipov V.V., Vedin I.A., et al., Quantum Electronics, vol. 43, 2013, p. 288.
[6] S.M. Vatnik, V.V. Osipov, K.E. Luk'yashin, et al., Quantum Electronics, vol. 44, 2014, p. 585.
[7] S.M. Vatnik, I. A. Vedin, Osipov, et al., Journal of Physics: Conference Series, v. 793, 2017.

Mass-defect effects in atomic clocks

V.I. Yudin[1-3] and A.V. Taichenachev[1,2]
[1]*Institute of Laser Physics SB RAS, Novosibirsk, Russia*
[2]*Novosibirsk State University, Novosibirsk, Russia*
[3]*Novosibirsk State Technical University, Novosibirsk, Russia*
E-mail: viyudin@mail.ru

We consider an influence of mass-defect on the frequency of atomic transitions. We have found that some well-known frequency shifts (such as gravitational and quadratic Doppler shifts) can be interpreted as consequence of mass-defect, i.e., without time dilation conception used in special and general relativity theories. Moreover, we show that the mass-defect leads to previously unknown shifts for clock based on trapped ions.

The main idea of our approach is following. Let us consider an arbitrary atomic transition between states $|g\rangle$ and $|e\rangle$ with unperturbed frequency $\omega_0 = (E_e^{(0)} - E_g^{(0)})\hbar$, where $E_e^{(0)}$ and $E_g^{(0)}$ are unperturbed energies of corresponding states (see Fig.1). Using the famous Einstein's formula: $E=Mc^2$, which connects the mass M and energy E of particle (c is the speed of light), we can find the rest masses of particle M_g and M_e in the states $|g\rangle$ and $|e\rangle$, respectively: $E_g^{(0)} = M_g c^2$ and $E_e^{(0)} = M_e c^2$. The fact that $M_g \neq M_e$ is an essence of so-called mass-defect in our case, where the connection between M_g and M_e is following:

$$M_e c^2 = M_g c^2 + \hbar\omega_0 \;\Rightarrow\; M_e = M_g + \hbar\omega_0 / c^2 \tag{1}$$

We show that the relationship (1) allows us in other manner to interpret some well-known systematic frequency shifts (so-called time dilation effects [1,2]. Moreover, our approach predicts new series of shifts previously unconsidered in scientific literature.

As the first example, let us show that the mass-defect allows us to formulate very simple explanation of the gravitational frequency shift even under classical description of the gravitational field (as classical potential U_G). Indeed, because the potential energy of the particle in the classical gravitational field is equal to the product MU_G (where $U_G<0$), then the energy of j-th state $E_j(U_G)$ is determined as following:

$$E_j(U_G) = M_j c^2 + M_j U_G = M_j c^2 (1 + U_G / c^2),\ (j = g, e) \tag{2}$$

Using Eqs.(1) and (2), we find the frequency of the transition $|g\rangle \to |e\rangle$ in the gravitational field:

$$\omega = \omega_0 (1 + U_G / c^2). \tag{3}$$

This expression coincides with the main order of well-known formula from the general relativity theory:

$$\omega = \omega_0 \sqrt{1 + 2U_G / c^2} \approx \omega_0 (1 + U_G / c^2) \tag{4}$$

in the case of $|U_G|/c^2 \ll 1$. We emphasize that the expression (4) was here derived without time dilation concept, which is taken as basis of Einstein's theory of relativity. Nevertheless, in deriving (4) we have used an equality of gravitational and inertial masses, $M_{grav}=M_{in}$, which is one of cornerstones of general relativity.

Other example is connected with shifts in the presence of confinement potential U(r), which is the same for both states $|g\rangle$ and $|e\rangle$. Such situation occurs either for clocks based on neutral atoms in optical lattice or for clocks based on trapped ions. In this case, we have the standard task about quantization of energy levels on translational degrees of freedom:

$$\hat{H}_j \left|\Psi_j\right\rangle = E_j^{(\mathrm{vib})} \left|\Psi_j\right\rangle,\ \hat{H}_j = \hat{\mathbf{p}}^2 / 2M_j + U(\mathbf{r}) \tag{5}$$

where Hamiltonian $\hat{H}_j$ and state $|\Psi_j\rangle$ describe the translational motion of the particle in the j-th internal state $|j\rangle$ ($j=g,e$), and $\mathbf{r}$ is coordinate of atomic center-of-mass. Thus, taking into account the

translational motion, the atomic wave function is described by the pair products $|j\rangle\otimes|\Psi_j(\mathbf{r})\rangle$. Because of mass-defect ($M_g\neq M_e$), the energy levels for lower and upper states differ: $\mathcal{E}_g\neq\mathcal{E}_e$. Consequently, the frequency ω between corresponding levels of trapped particle becomes different from unperturbed frequency ω_0 at the value $\Delta\omega$ (see Fig.1): $\Delta\omega=\omega-\omega_0=(\mathcal{E}_e-\mathcal{E}_g)/\hbar$. Let us estimate this value. For this purpose, we represent the Hamiltonian for upper state $\hat{H}_e$ in the following form:

$$\hat{H}_e=\hat{H}_g+\Delta\hat{H};\ \Delta\hat{H}=\frac{\hat{\mathbf{p}}^2}{2M_e}-\frac{\hat{\mathbf{p}}^2}{2M_g}=-\frac{\hbar\omega_0}{2M_eM_g}\hat{\mathbf{p}}^2, \tag{6}$$

where the operator $\Delta\hat{H}$ can be considered as small perturbation. In this case, using the standard perturbation theory, energy $\mathcal{E}_e$ can be presented as series $\mathcal{E}_e=\mathcal{E}_e(0)+\Delta\mathcal{E}_e(1)+...$, where $\mathcal{E}_e(0)=\mathcal{E}_g$, and the first correction is determined as average value $\Delta\mathcal{E}_e(1)=\langle\Psi_g|\Delta H|\Psi_g\rangle$. Using Eq.(6) and taking into account $M_g\approx M_e$, we obtain the following estimation of relative value of shift:

$$\frac{\Delta\omega}{\omega_0}\approx-\frac{1}{2c^2}\frac{\left\langle\Psi_g\left|\hat{\mathbf{p}}^2\right|\Psi_g\right\rangle}{M_g^2}. \tag{7}$$

It coincides with relativistic correction, which is well-known as quadratic Doppler shift due to the time dilation effect for moving particle [4]. Indeed, at the present time the following conventional explanation is usually used. In accordance with special relativity, the tick rate Δt in the moving (with velocity $\mathbf{v}$ coordinate system changes with respect to the tick rate $\Delta t'$ in motionless (laboratory) coordinate system by the law: $\Delta t=\Delta t'(1-\mathbf{v}^2/c^2)^{1/2}$. As a result, atomic oscillation with eigenfrequency ω_0 becomes perceived for external observer with other frequency: $\omega=\omega_0(1-\mathbf{v}^2/c^2)^{1/2}$. In nonrelativistic limit ($\mathbf{v}^2/c^2<<1$), we have: $\omega\approx\omega_0(1-\mathbf{v}^2/2c^2)=\omega_0[1-(\mathbf{p}/M)^2/2c^2]$ (where $\mathbf{p}$ is momentum of particle). Then, if we go over to the quantum consideration by the replacement $\mathbf{p}\to\hat{\mathbf{p}}=-i\hbar\nabla$, we obtain the expression for frequency shift (7).

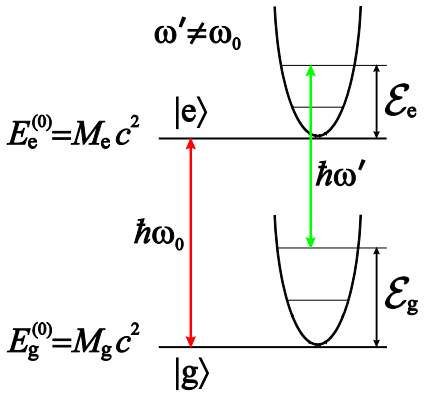

Fig.1. Scheme of atomic transition $|g\rangle\to|e\rangle$. Also it is shown the quantization of energy levels on translational degrees of freedom in confined potential $U(\mathbf{r})$, where $\omega\neq\omega_0$ due to mass-defect.

Thus, some well-known systematic shifts, previously interpreted as the time dilation effects in the frame of special and general relativity theories, can be considered as consequence of mass-defect concept. Furthermore, our approach has predicted a series of previously unknown shifts for ion clocks (it will be shown in our presentation). Obtained results have a principle importance for high-precision optical atomic clock and can be interesting for theoretical quantum mechanics.

V.I. Yudin was supported by the Ministry of Education and Science of the Russian Federation (No. 3.1326.2017/4.6) and Russian Foundation for Basic Research (No. 17-02-00570). A.V. Taichenachev was supported by the Russian Science Foundation (No. 16-12-00052).

References

[1] A. Einstein, Annal. Physik **17**, 891 (1905).
[2] C. W. Chou, D. B. Hume, T. Rosenband, and D. J. Wineland, Science **329**, 1630 (2010).

Possibility of cosmological gravimetry using high-precision atomic clocks

V.I. Yudin[1-3], A.V. Taichenachev[1,2]
[1]*Institute of Laser Physics SB RAS, Novosibirsk, Russia*
[2]*Novosibirsk State University, Novosibirsk, Russia*
[3]*Novosibirsk State Technical University, Novosibirsk, Russia*
E-mail: viyudin@mail.ru

According to the general theory of relativity [1], the clock tick rate in the gravitational field is slowed. As a result, the frequency of atomic transition experiences a gravitational redshift depending on the value of the gravitational potential. In the case of a spatially non-uniform gravitational potential, this effect leads to the following well-known relationship:

$$\frac{\omega(\mathbf{r}_1)-\omega(\mathbf{r}_2)}{\omega(\mathbf{r}_1)}=1-\frac{\omega(\mathbf{r}_2)}{\omega(\mathbf{r}_1)}=\frac{\varphi(\mathbf{r}_1)-\varphi(\mathbf{r}_2)}{c^2}, \qquad (1)$$

which describes the measured relative difference of the frequencies $\omega(\mathbf{r}_1)$ and $\omega(\mathbf{r}_2)$ for the same clock transition at two different spatial points $\mathbf{r}_1$ (observer) and $\mathbf{r}_2$ (emitter) with different gravitational ptetials, $\varphi(\mathbf{r}_1)$ and $\varphi(\mathbf{r}_2)$ (c is the light speed) [2,3]. In particular, formula (1) allows using high-precision atomic clocks to measure the difference of the gravitational potentials for various Earth's surface points, which can form a basis for the so-called chronometric geodesy (relativistic geodesy, chronometric leveling) [4].

We propose and substantiate a hypothesis according to which the following relationship [which is more exact than Eq.(1)] can be used:

$$\frac{\omega(\mathbf{r}_1)-\omega(\mathbf{r}_2)}{\omega(\mathbf{r}_1)}=(1+\alpha)\frac{\varphi(\mathbf{r}_1)-\varphi(\mathbf{r}_2)}{c^2}, \qquad (2)$$

where the parameter α does not depend on the type of atomic clock and has the meaning of a cosmological correction, which contains information on the cosmological gravitational action of the Universe on our planetary system. In particular, this correction can be interpreted as the value that is proportional to the cosmological gravitational potential Φ_{CP} at Earth's location point. We assume that the cosmological potential is formed by all matter of the Universe (including dark matter and dark energy) and that it is spatially uniform on planet scales. We also assume that the value of the gravitational-cosmological "background" Φ_{CP} is several orders of magnitude greater than the gravitational potential of our planet φ_E (where $|\varphi_E/c^2|\sim10^{-9}$ on Earth's surface). Thus, Eq.(2) can be a basis for cosmological gravimetry.

Our approach is based on "quasi-classical" explanation of the gravitational redshift for arbitrary atomic transition [5] as resulting from the "mass defect" (for quantum atomic states) in the presence of the classical (Newtonian) gravitational potential $\varphi(\mathbf{r})$, that is not within the framework of general relativity. In particular, the frequency at the point $\mathbf{r}$ is expressed by the following formula:

$$\omega(\mathbf{r})=\omega_0\left(1+\frac{\varphi(\mathbf{r})}{c^2}\right), \qquad (3)$$

where ω_0 is the unperturbed frequency of the atomic transition (clock transition) in the absence of gravitation.

If our hypothesis will be confirmed experimentally, this will open up new unique possibilities for investigation of the Universe. In particular, if $|\alpha|>10^{-5}$, then the cosmological gravitational contribution is much greater than the gravitational potential of the Galaxy. However, if experiments will show $|\alpha|<<10^{-5}$, then it can be considered as one of best and direct confirmation of general relativity, which predicts $\alpha=0$.

It should be noted that modern atomic clocks with a relative uncertainty of 10^{-18} make it possible to find, in earth-based experiments, the cosmological parameter α, if $|\alpha|>10^{-4}$ (for $|\mathbf{r}_1-\mathbf{r}_2|\sim100$ m). Analysis of some well-known experimental results (see in Ref.[3]) indirectly shows the possibility of $|\alpha|>10^{-3}$. Thus, the problem of verifying experiments becomes important.

V.I. Yudin was supported by the Ministry of Education and Science of the Russian Federation (No. 3.1326.2017/4.6) and Russian Foundation for Basic Research (No. 17-02-00570). A.V. Taichenachev was supported by the Russian Science Foundation (No. 16-12-00052).

References

[1] A Einstein, Annal. Physik **49**, 769 (1916).
[2] C. W. Chou, D. B. Hume, T. Rosenband, and D. J. Wineland, Science **329**, 1630-1633 (2010).
[3] T. Takano, M. Takamoto, I. Ushijima, N. Ohmae, T. Akatsuka, A. Yamaguchi, Y. Kuroishi, H. Munekane, B. Miyahara, and H. Katori, Nature Photonics **10**, 662 (2016).
[4] M. Vermeer, Chronometric levelling, Rep. Finnish Geodetic Inst. **83**, 1-7 (1983).
[5] V. I. Yudin and A. V. Taichenachev, Laser Phys. Lett. **15**, 035703 (2018).

Investigations of collisionless energy transfer to magnetised ionised background from super-Alfvenic laser plasma stream with ions of different masses

Yu.P. Zakharov[1], A.G. Ponomarenko[1], V.A. Terekhin[2], I.F. Shaikhislamov[1], V.G. Posukh[1], E.L. Boyarintsev[1], A.V. Melekhov[1], K.V. Vchivkov[1], A.A. Chibranov[1], M.A. Rumenskikh[1], A.G. Berezutsky[1], I.B. Miroshnichenko[1]

[1]*Institute of Laser Physics SB RAS, Av. Lavrentyeva, 13/3, 630090, Novosibirsk, Russia*

[2]*All-Russian Research Institute of Experimental Physics, Av. Mira, 37, 607188, Sarov, Russia*

E-mail: ki1z@mail.ru

The main problem of Collisionless Shock Wave (CSW) formation and collisionless interaction in general, between interpenetrating plasma flows moving across magnetic field consists in that at large Alfven-Mach numbers $M_{A0} = V_0/C_a \geq 4$ - 5 almost all known laminar and turbulent mechanisms of impulse transfer via electromagnetic fields become ineffective [1]. Exception is Magnetic Laminar Mechanism (MLM) the idea of which (Longmire C.L., 1963) and simplest structure of magnetic fields corresponding to spherical case [2] have been developed initially in USA while a physical model and mathematical background were later brought to practical verification in Russia [3]. And very soon a first experimental evidence of MLM was obtained [4] at the KI-1 facility of ILP, but it was need a decades of various efforts to prepare our scheme [5] and realize it to generate a perpendicular CSW for first time [6-8] and later quasi-perpendicular one [9], even more simple way than in USA [10].

Laser Plasma blob (LP)	***Definition and value***
LP front velocity and ion composition	$\mathbf{V_0} \approx 140$ km/s, $\mathbf{H^+/C^{+3}}$, $\langle m/z \rangle \approx 3$ a.m.u.
Effective Energy and number of electrons	$\mathbf{E_0} \approx 0{,}3 m_p \langle m/z \rangle \mathbf{N_0 V_0^2} \sim 300$J and $\mathbf{N_0} \sim 5*10^{18}$
Background Plasma (BP)	
Density / **composition**	$\mathbf{n_*} \approx 2*10^{13}$ cm^{-3}/ $\mathbf{He^+}$
Magnetic field	$\mathbf{B_0} = 200$ G
Electron temperature	$\mathbf{T_{e*}} \approx 5$ - 10 eV
Scales and Velocities	
Diamagnetic cavity radius of **LP** in **BP**	$\mathbf{R_*} = (3N_0/4\pi n_*)^{1/3} \approx$ **40** cm
Diamagnetic cavity radius of LP / vacuum	$\mathbf{R_b} = (3E_0/B_0^2)^{1/3} \approx$ **55** cm
Deceleration radius of spherical LP cloud	$\mathbf{R_m} = (3N_0 * \langle m/z \rangle / 4\pi n_* m_*)^{1/3} \approx$ **37** cm/"show-plough" model
Larmor gyroradius of **LP** and **BP** ions	$\mathbf{R_L} \approx$ **21** см, $\mathbf{R_L^*} \approx$ **28** cm determined by $\mathbf{V_0}$
Free path length of **LP** ions in **BP**	$\boldsymbol{\lambda i^{min}} \sim 500$ cm (Coulomb collisions)
Alfven velocity in **BP**	$\mathbf{C_A} = B_0/(4\pi n_* m_*)^{1/2} \approx$ **44** km/s
Most important similarity criteria	
Mach-Alfven number	$\mathbf{M_A} = V_0/C_A \approx$ **3,2** ($\geq$ **3**)
MLM - Parameter	$\boldsymbol{\delta_0} = R_*^2/ R_L R_L^* \approx$ **2,5** (> **1**)
Knudsen number	$\mathbf{Kn_i} = \lambda_i^{min} / R_* \sim$ **10** >> **1**
Thermal plasma beta	$\boldsymbol{\beta_e} = 8\pi n_* kT_{e*}/B_0^2 \sim$ **0,2** <<**1**

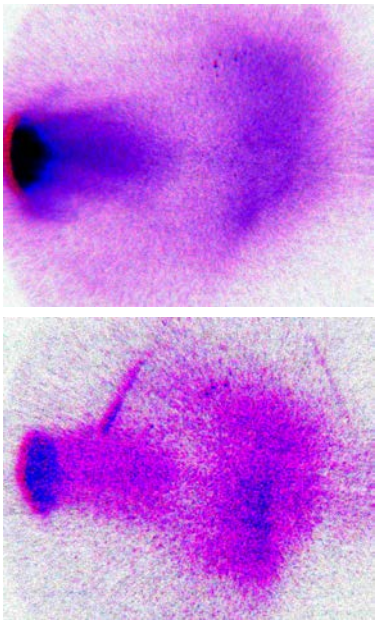

MEGA-BUW

a) Filter $\mathbf{H_\alpha}$ (**656,3** nm), #63

t = 5,1 μs

b) Filter **CIV** (**580,1** nm), #46

t = 5 μs

Fig. 1 Photos of Gated Optical Imager (GOI) for registration of Laser Plasma (LP) glow in a lines (**a**, **b**) during LP expansion into Helium He^+ Background Plasma (BP) with uniform magnetic field $B_0 = 200$ G (directed into the paper). Spots at the left – glow of laser target (C_2H_4) inside of black paper' buffle (∅11,5 cm of output). Laser beams falls from the right and for the same scale one can use a lower horizontal distances L between a tips of two tubes (with a probes). Here L = 49 cm for **a**) and 38 cm (**b**).

Nevertheless a lot of important features of MLM-interaction processes are still unclear, first of all the role of different ion masses (m/z) in LP-piston, because only in a «Linear Approximation» of initial LP-ions radial motion, one could obtain [11] a simple relation for calculation of effective $(m/z)_e$

as average <m/z>. To verify it in a general case we carried out a MEGA-BUW experiment (see **Table**) with a special type of He^+-BP to study the dynamics of various LP-ions by the registration of their luminosity in a lines by both: 2D-pictures of GOI-photos (**Fig. 1**, with interference filters) and a set of FEU-oscillograms [**Y**] from the various points along to target normal (focused to entrance slit of MDR-12). For comparison, a set of 2D-calculations by spherical hybrid model «Cloud» were done for experimental parameters while a data at axis perpendicular to $\mathbf{B_0}$ were chosen (see **Table** and **Fig. 2**).

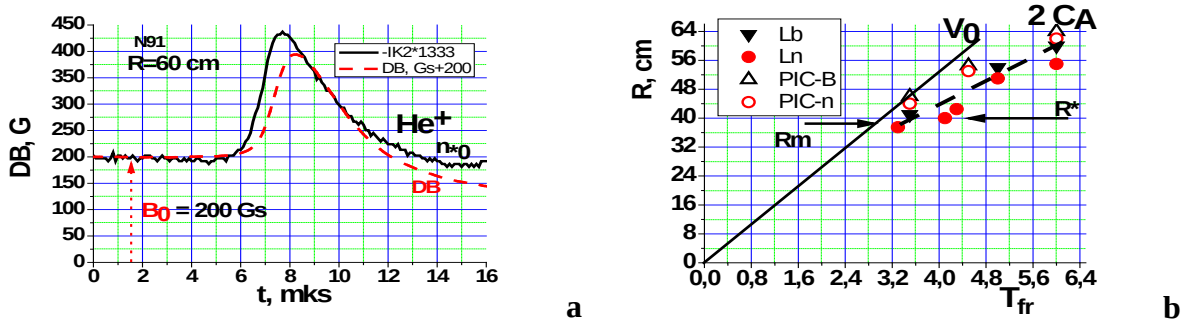

Fig. 2 a) Example of CSW as a joint oscillograms of background density (IK2) and magnetic field (DB) at distance R = 60 cm from the target; **b**) Joint R-t diagram of the fronts propagation both experimental (L_n and L_b) and model ones (PIC-B/n). Note that for the Y-scale of Fig. 2a, own LP-signal at KI2 (without BP, but also ×1333×1,5) is only 70 units of (DB, G).

According to GOI-data of Fig. 1a,b (and FEU-oscillograms [**Y**]), some LP-ions of a real (finite-size) blob, could propagate up to the distances 55÷60 cm (and even more, but with a scatter in time), while in the case of more ideal (spherical cloud) in hybrid runs one could see evidently, some effect of LP-ions capture (Fig. 3) inside of the region X ≤ 55 cm (across magnetic field). Finally note, that in spite of some differences in a set of new data MEGA-BUW, its main result on CSW-generation at the enough large both: MLM-parameter $\boldsymbol{\delta_0} = R_*^2/ R_L R_L^* \approx$ **2,5** (> **1**) and **BP-size** > $\mathbf{R_*}$ and $\mathbf{R_m}$, confirms, that previously found [11] definition of $\boldsymbol{\delta_0}$ via the average <m/z> of LP-ions was correct. Namely in a sense of η-values of their relevant electrons (see Fig. 3 with caption), because according to MLM-model [3] the BP energy gain is $W_*=K\delta_0 E_0$, where LP-energy (in Table) $E_0 \propto <m/z> \propto \Sigma\eta = (\eta_1+\eta_2+\eta_3)$.

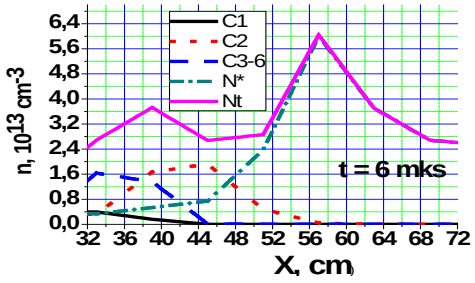

Fig. 3 Data of hybrid simulation on the distributions of electron density, corresponding to various plasma components along to target normal: C1 – H^+ (η_1 = 30% from the total number of LP-electrons, $N_0 \sim 10^{19}$) of LP, C2 – C^{+3} of LP (η_2 = 50%) and C^{+4} of LP (η_3 = 20%); N^* is the density of Background Plasma (BP) and Nt is the total plasma density (LP + BP). Note that for the given moment of calculations (6 μs), all LP- components have reached their limits in the radial X-direction, continuing their Larmor rotations, approximately inside of diamagnetic cavity of spherical «LP» – piston.

This work has been performed in the frame of program № 0307-2017-0015 of Fundamental studies of ILP SB RAS, and project 0307-2018-0022 of the Presidium RAS program.

References

[1] D. S. Spicer, R. W. Clark, S. P. Maran, Astrophys. J. **356**, 549 (1990).
[2] T.P. Wright, Phys. Fluids **14**, 1905 (1971).
[3] V.P. Bashurin, A.I. Golubev, V.A. Terekhin, J. Appl. Mech. and Tech. Phys. **24**, 614 (1984).
[4] V.M. Antonov V.P. Bashurin, A.I. Golubev, V.A. Zhmailo, Yu P. Zakharov, et al., Ibid **26**, 757 (1985).
[5] Yu P. Zakharov, IEEE Transactions on Plasma Science **31**, 1243 (2003).
[6] Yu P. Zakharov, et al., Modern Problems of Laser Physics (Sixth Intl. Symp., 25-31 August 2013, Novosibirsk, ILP) 193
[7] I. F. Shaikhislamov., Yu P. Zakharov, V. G. Posukh, et all, Plasma Physics Reports **41**, 399 (2015).
[8] Yu P. Zakharov, A.G. Ponomarenko, V.N. Tishchenko, V.A. Terekhin, et al., Quantum Electronics **46**, 399 (2016).
[9] Yu P. Zakharov, A.G. Ponomarenko V.A. Terekhin., et al., Journal of Physics: Conference Series **927**, #012078 (2017).
[10] D. B. Schaeffer, W. Fox, D. Haberberger, G. Fiksel et al., Physics of Plasmas **24**, #122702 (2017).
[11] Yu P. Zakharov, Dissertation PhD, Inst. Pure and Applied Mechanics, Novosibirsk (1988) In Russian.

New type of large scale laser plasma experiments for laboratory astrophysics

Yu.P. Zakharov[1], A.G. Ponomarenko[1], V.A. Terekhin[2], I.F. Shaikhislamov[1], V.G. Posukh[1], E.L. Boyarintsev[1], A.A. Chibranov[1], A.G. Berezutsky[1], I.B. Miroshnichenko[1], M.A. Rumenskikh[1]

[1]*Institute of Laser Physics SB RAS, Av. Lavrentyeva, 13/3, 630090, Novosibirsk, Russia*

[2]*All-Russian Research Institute of Experimental Physics, Av. Mira, 37, 607188, Sarov, Russia*

E-mail: ki1z@mail.ru

A lot of modern Laser Plasma Experiments (LPE) with the usual Laser Plasma (LP) range of energy $E_0 \sim 5 \div 10$ J were done [1, 2] in strong magnetic field $B_0 \geq 10 \div 30$ kG for simulation of various astrophysical phenomena at a small mm-scale of characteristic deceleration radius R_b of the problem. Here $R_b \approx (3E_0/B_0^2)^{1/3}$ is a main MHD-scale of the problem which determines a first stage of LP interaction with uniform field B_0, when according to ideal «Superconductive-Sphere» Model (SSM) of Raizer [3], expanding diamagnetic plasma cloud, doing exclusion of B_0 (from the cavity) should be stopped at R_b. But in a real LP (and other explosive-like plasmas) conditions, a fast non-MHD flute instability [4-6] could destroy plasma surface and diamagnetic current system, without plasma deceleration at expected MHD-time $T_b \sim R_b/V_0$ (for initial plasma expansion velocity V_0). During two decades of LPE [4, 6] with the vacuum B_0 at KI-1 facility of ILP, it was established for the first time, that level of ion magnetization criterium $\boldsymbol{\varepsilon_b} = R_L/R_b \leq 1$ determines the opportunity of MHD-type deceleration (across B_0) with its first stage at $t \sim T_b$. Here R_L is a directed ion Larmor radius ($\propto V_0$).

Futher dynamics of LP strongly depends upon the geometry of both LP expansion and magnetic field [6-9]. In particulare, during some earliest LPE of the authors at KI-1 and other facililities, with a flat (and even spherical) laser targets and in both strong uniform and dipole magnetic fields (~ 1÷10 kG), they had observed (as many others researches [10, 11]) a small jets (≥ cm) of LP, propagating transverse to fields up to rather large distances ~ 10 cm [12, 13]. Here we present first of all and for the first time a new, so called Super-Jet phenomena of huge size ~ 100 cm (along to target normal and across a rather weak uniform vacuum magnetic field $B_0 = 300$ G), revealed recently at KI-1. It became possible due to combined new experimental opportunities, which were realised last years at KI-1 laser facility, for simulation of various cosmophysical and astrophysical phenomena of explosive nature. Now its large scale chamber ∅1,2m*5m and new method [14] for generation of LP with effective energy $E_0 \sim$ kJ allow us to perform LPE at scale ~ m to simulate MHD-shocks [14, 15] and, for example, their impact onto a so called terrella [15], laboratory model of the Earth magnetosphere.

At the Fig. 1 a Photos of Gated Optical Imager (GOI) of Super-Jet at the two times, corresponding to stage of collaps its cavity with a probable Hall-effects (of inward magnetic field motion together with the plasma at near Alfven velocity). At the previous stage of cavity formation, its maximal size (Fig. 2) almost reach (see c) the theoretical size $R_b \approx 46$ cm for effective energy $E_0 \sim 300$ J of LP into derection along to target normal, while into derections transverse to it – up to comparable (but less) sizes both ≈ 16 cm (see at b, c the points of one half exclusion), at close times.

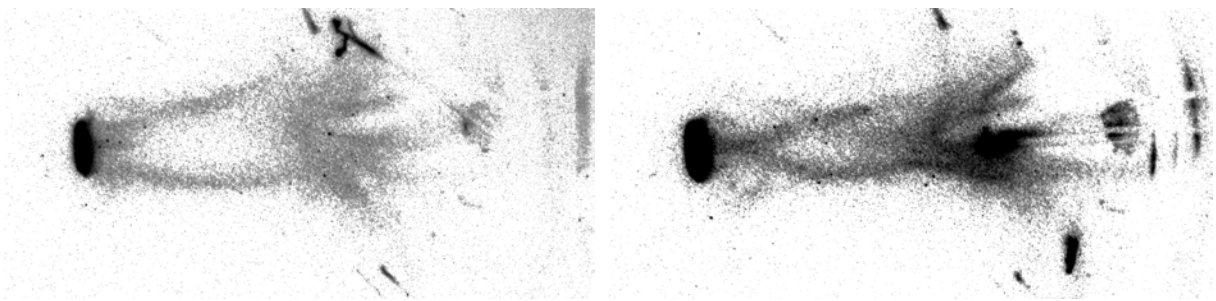

Fig. 1 Ctructure and dynamics of Super-Jet at KI-1 facility in vacuum uniform magnetic field (300 G, directed into paper), at the moments t=8,5 and 9 μs (at the left and right) and in the same scale of distance L=95 cm between a left black spot (∅11,5 cm, surrounding a laser target ∅2,5 cm from polyethylene) and extreme right reflection at the chamber wall. Near the head of Jet in both Photos one could see a lot of plasma diagnostics are seen (as well as a laser mirrors etc) and the more transparent region (between a left target and right head points) corresponds to collapsing cavity of Jet.

Therefore a Super-Jet data of both Fig. 1, 2 probably give us for the first time some example of the knowledge about the internal structure and dynamics of Jet-phenomena as a whole, because at present time a general theory of such-kind magnetised Jets (with along-velocity close to initial V_0) in vacuum is almost absent [16]. Mainly, probably, because a very small their size in laboratory study and very large distances from a real astrophysical (i.e. inter-galactic) jets. Exceptions may be only in magnetospheric [17] physics, as some intermediate case, with a relevant laboratory modelling [13].

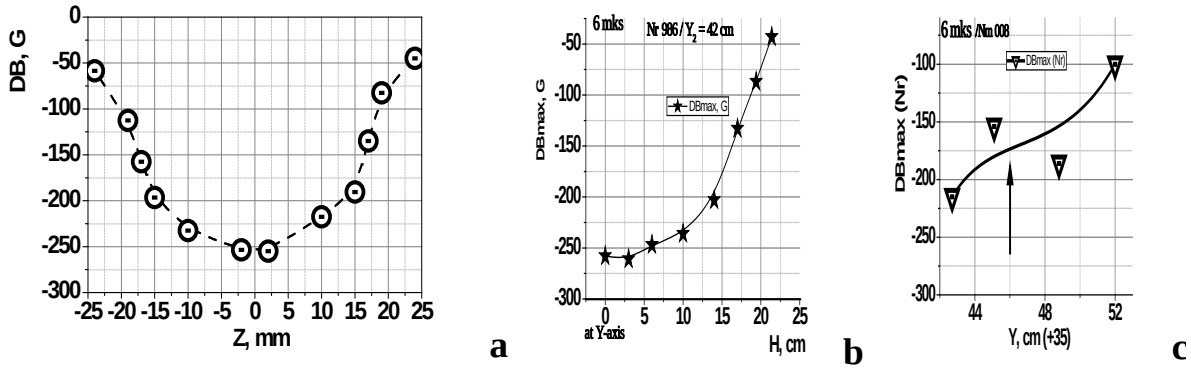

Fig. 2 Distributions of excluded magnetic field (main B_Z-component) inside of cavity (at the moment 6 μs of its maximal size, for directions of X-axis of plots see Photos at Fig, 1 and its capture): a – along to the initial B_{0Z}; b – along to vertical direction); c – along to Y – horizontal direction of plasma propagation (Row is in a point of theoretical R_b).

Another very important application of discussed new opportunities of KI-1 for Laboratory Astrophysics are the generation of magnetized and, especially, quasi-perpendicular [14] Collisionless Shock Wave (CSW) and a probable experiments on its interaction at the scale up to 3 m between a relevant positions of laser targets. As its result, a new simulative data about electron acceleration processes in explosive-type space phenomena coud be obtained.

This work has been performed in the frame of program № 0307-2017-0015 of Fundamental studies of ILP SB RAS, and project 0307-2018-0022 of the Presidium RAS Program.

References

[1] B. Albertazzi, A. Ciardi, M. Nakatsutsumi et al., Science **346**, 32 (2014).
[2] D. P. Higginson, G. Revet, B. Khiar et al, High Energy Density Physics **23**, 48 (2017).[
[3] Yu.P. Raizer**,** J. Applied Mechanics and Technical Physics N6, 19 (1963).
[4] Yu. P. Zakharov, A. M. Orishich, A. G. Ponomarenko, and V. G. Posukh, Sov. J. Plasma Phys. **12**, 674 (1986)].
[5] B. H. Ripin, E. A. McLean, C. K. Manka, et al Phys. Rev. Lett. **59**, 2971 (1987).
[6] Yu.P. Zakharov, V.M. Antonov, E.L. Boyarintsev, A.V. Melekhov, et al Plasma Physics Reports **32**, 183 (2006)
[7] V. M. Antonov, Yu. P. Zakharov, A. V. Melekhov, et al, J. Applied Mechanics and Technical Physics **42**, 649 (2001).
[8] Yu. P. Zakharov EEE Transactions on Plasma Science **31** 1243 (2003).
[9] A. G. Ponomarenko, Yu. P. Zakharov V. M. Antonov, et al, IEEE Transactions on Plasma Science **35** 813 (2007).
[10] A. N. Mostovych, B. H. Ripin, J. A. Stamper Phys. Rev. Lett. **62**, 2837 (1989).
[11] C. Plechaty, R. Presura, and A. A. Esaulov, Ibid, **111**, 185002 (2013).
[12] J. Wolowski, A. Kasperczuk, Yu. P. Zakharov, et al, Plasma Physics and Controlled Fusion**, 41**, A771 (1996).
[13] Yu. P. Zakharov, A.V. Eremin, A.M. Orishich, , et al, Advanes in Space Research, **29**, 1351 (2002).
[14] Yu P. Zakharov, A.G. Ponomarenko, V.N. Tishchenko, V.A. Terekhin, et al., Quantum Electronics **46**, 399 (2016).
[15] Yu P. Zakharov, A.G. Ponomarenko V.A. Terekhin., et al., Journal of Physics: Conf. Series **927**, #012078 (2017).
[16] V.S. Belyaev, G.S. Bisnovatyi-Kogan, A.I. Gromov,et all, Astronomy Reports, 2018, Vol. **62**, 162 (2018).
[17] E.V. Mishin, J. Geophysical Research, **118A**, 5782 (2013).

Investigation of mode-locking in diode laser with feedback on intermode frequency

V.M. Klementyev, E.A. Titov, V.F. Zakharyash
Institute of laser physics SB RAS, pr. Lavrent'eva 13/3, 630090, Russia
E-mail: valera@laser.nsc.ru

The results of experimental investigations of a semiconductor laser with an external cavity in which the active mode locking regime is obtained by feedback at the frequency of intermode beats are reported. These experiments are a continuation of the experiments started in [1]. The setup shown in Fig. 1 is used for the experiment. The radiation of semiconductor laser 1 is divided by a separation mirror into two beams supplied to photodetectors 3 and 8. The signal from photodetector 3 is supplied to microwave amplifier-limiter 4 and, by means of adjustable power amplifier with stabilization 5, comes to modulator circuit of semiconductor laser 6.

To record the parameters of radiation, the setup has optical spectrum analyzer 7 and intermode frequency spectrum analyzer 9. In the experiment, optical spectrum analyzer 7 is used to control the optical spectrum shape. Spectrum analyzer 9 is used to investigate the radio frequency beat spectrum of optical radiation.

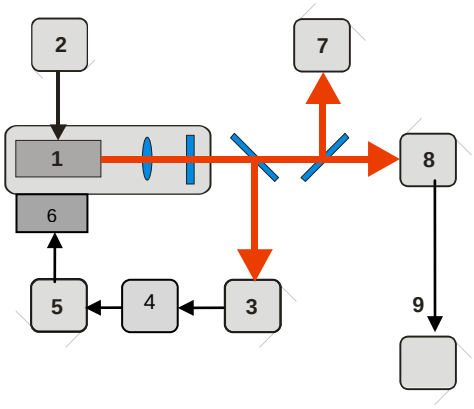

Fig. 1 1 – semiconductor laser; 2 –power supply; 3 –photodetector; 4 – microwave amplifier-limiter; 5 – adjustable power amplifier; 6 – modulator circuit of semiconductor laser .; 7 – optical spectrum analyzer ; 8 – photodetector; 9 - intermode frequency spectrum analyzer.

The coefficient of amplifier-limiter 4 is 75 dB at a frequency of 300 MHz with a band of 60 MHz. The output power of amplifier-limiter 4 is 5 mW. Adjustable power amplifier 5 (0.1 – 2 W) is based on an M687 10TL chip and includes a directional coupler with a detector and operational amplifier after it for power stabilization. Temperature stabilization of this chip is carried out by an independent system based on a Peltier element. In the free running mode (in the absence of laser current modulation), small signals of intermode beats with an amplitude of several dB and a spectrum width of about 50 MHz are observed.

When feedback is switched on, a qualitative change of the beat spectrum takes place. By amplifying the beat signal at a frequency of 300 MHz, matching the power of microwave amplifier 4, the constant component of the laser current, and the external cavity length, it is possible to obtain a mode locking regime at the pumping frequency (300 MHz) and, correspondingly, at the intermode frequency. This regime is shown in Fig. 2(a). Figure 2 (b) presents the form of intermode beats whose width at half-height is 200 Hz.

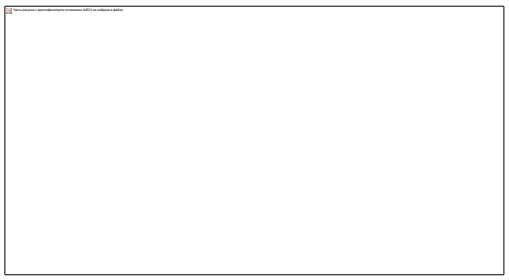

Fig. 2а

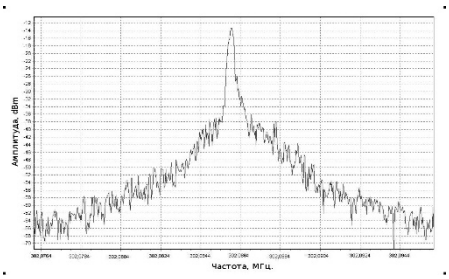

Fig. 2б

Fig. 3 shows the optical spectra of a semiconductor laser in the absence of feedback (red curve) and when feedback is switched on (gray curve). One can see in Fig. 4 that when feedback is switched on, mode locking takes place and, as a consequence, the optical spectrum of output radiation of the semiconductor laser broadens, as in [1].

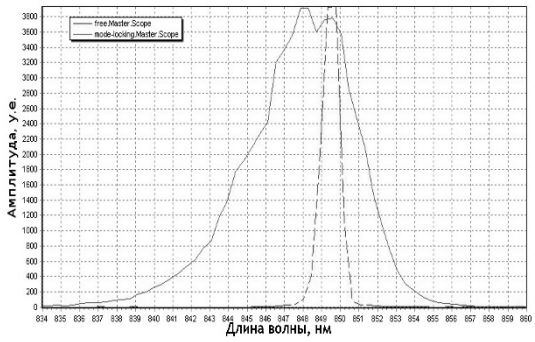

Fig. 3 The optical spectrum of a semiconductor laser in free running mode (dashed line) and under conditions of active mode locking.

In the future, it is necessary to investigate the effects of pulling and the role of a possible influence of delay of the feedback ring on the radiation noise and the stability of intermode beats. In subsequent experiments we plan to consider various feedback options and the effects of the compressed state of light in multimode oscillations.

The results obtained form the basis for the creation of small-size synthesizers and spectrometers of the radio-terahertz (THz) range with high resolution (10^{-11}-10^{-12}).

References

[1] С.Н.Багаев, А.В.Каширский.В. М.Клементьев ии др., Кв. электр. **35**, № 9, с. 821 (2005).

kW narrow linewidth all fiber laser

L. Zhang, N. Chen*, H. Zhao, K. Zhang, Y. Li, C. Zhu, D. Zhang, P. Gao, H. Zhang, Y. Liu, S. Zhou
Science and Technology on Solid-state Laser Laboratory, Beijing, 100015, China
E-mail: laser_2014@163.com, *cnj2222@163.com

In high power narrow linewidth fiber laser, Stimulated Brillouin Scattering (SBS) is the major power limitation factor. Through increasing the frequency number and frequency spacing, SBS threshold power multiplied. In this paper, tow stage sinusoidal phase modulation technology is used to control the frequency number and frequency spacing. Under tow stage sinusoidal phase modulation and three stage fiber amplified technology, the laser linewidth of 8GHz, power of 1kW and central wavelength of 1064.4nm, are achieved respectively. And the beam quality is $M_x^2 = 1.36$ and $M_y^2 = 1.3$.

Through theoretical simulation, we analyze the influence of frequency distribution on SBS. For equal intensity frequency, whether the frequency spacing equal or not, increasing the frequency number can improve the SBS threshold power. While, it's not the most effective method to improve the SBS threshold power by simply increasing the number of frequency. Frequency spacing should be increased so that there is no overlap between SBS gain spectrum of each frequency. Then the SBS threshold power can be most efficient to increase. We have validated the correctness of the above conclusion through experiment (Fig.1).

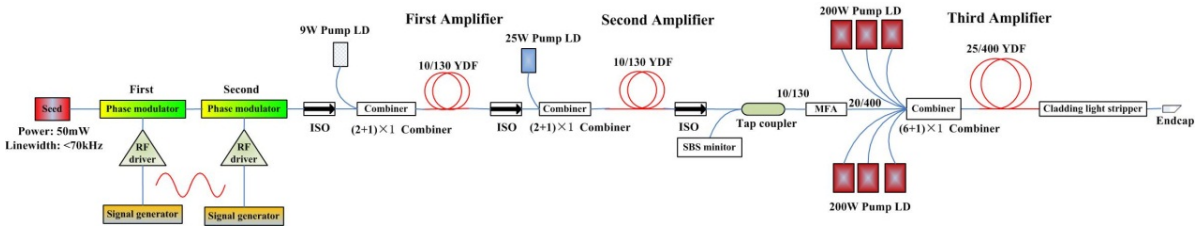

Fig. 1 Experimental schematic diagram.

The seed lasers with single frequency and multi-frequencies are amplified respectively. The results are showed as Fig.2, Fig.3 and Fig.4. As defined therein, when backscattered light increases nonlinearly, the according laser power is SBS threshold power. When the seed laser with single frequency is amplified directly, the SBS threshold power of the third amplifier stage is 77W (Fig.2 (a), Fig.3 (a)). When the seed laser is respectively modulated from single frequency to three frequencies (Fig.2 (b)), five frequencies (Fig.2 (c)) and twenty frequencies (Fig.2 (d)) with the frequencies spacing of 150MHz, after amplified, SBS threshold power of the third amplifier stage is 166W, 309W and 785W respectively (Fig.3 (a)). With the increasing of frequency number, SBS threshold power increases gradually. With the frequency spacing from 80MHz to 300MHz, the SBS threshold power increase gradually (Fig.3 (b)). While the frequency spacing changes from 300MHz to 350MHz, the SBS threshold powers are constant 200.8W. After 300MHz, the SBS threshold power reaches the biggest value under frequency number accordingly. The seed laser is modulated from one frequency to three frequencies with 3.5GHz frequency spacing by the first phase modulator. Then the three frequencies are modulated to sixty frequencies (Fig.2 (e)) with 150MHz frequency spacing by the second phase modulator (Fig.1). And the third amplifier stage produces laser power of 1000W under pump power of 1089W. The optical-optical efficiency and slope sufficiency is 91.8% and 94.7% respectively (Fig.4 (a)). In the experimental process, the SBS is not occurred (Fig.4 (b)). The pump power and laser power has a good linear ship. It shows that the higher laser power output can be got by increasing pump power.

With sixty frequencies, even 1000W output power, the measured linewidth is 8GHz (Fig.2 (e)).

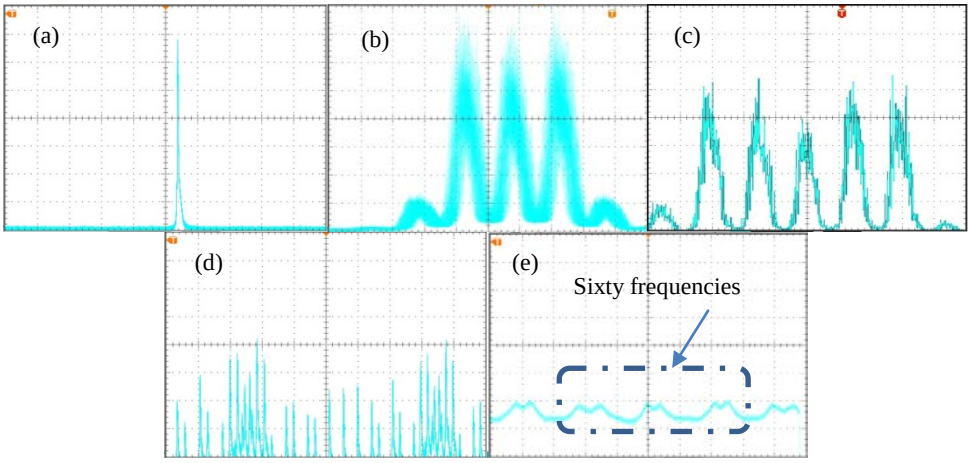

Fig. 2 The seed laser frequency spectrum distribution of (a) single frequency; (b) three frequencies; (c)five frequencies; (d) twenty frequencies; (e) sixty frequencies.

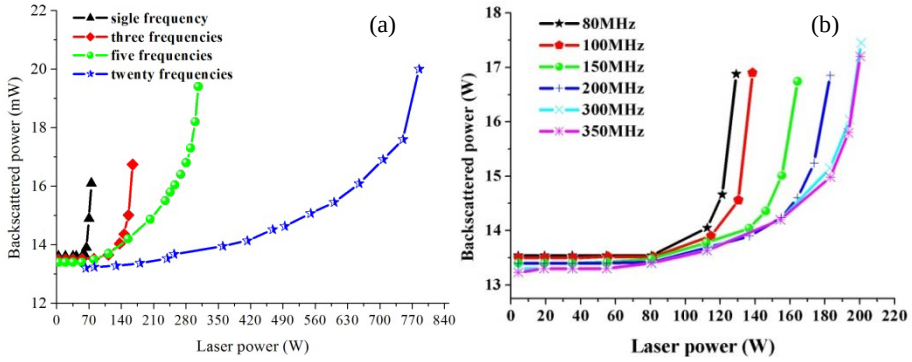

Fig. 3 Backscattered power variety with laser power under (a) different frequency number; (b) different frequency spacing with three frequencies.

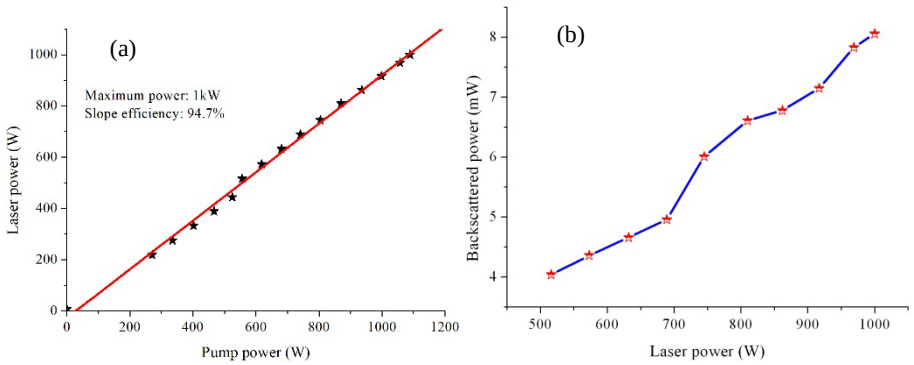

Fig. 4. At the third amplifier stage: (a) Laser power variety with pump power; (b) backscattered power variety with laser power.

Demonstration of Bessel-like beam with variable parameters generated using crossphase modulation

Q. Zhang, X. Cheng, J. Bai, B. He
Northwest University, China
E-mail: qianzhang_03@163.com

We propose a new method to generate Bessel-like beam using cross-phase modulation. It is demonstrated that the Bessel-like beam exhibits self-healing after encountering an obstruction on the beam path. The parameters of the Bessel-like beam are found to be easily adjusted by the pump beam power and sample temperature.

The influence of blood components on the optical properties of whole blood in terahertz frequency range

T. Zhang[1], P. Demchenko[1], M. Khodzitsky[1], Yu. Kononova[1,2], A. Babenko[1,2], E. Grineva[1,2]
[1]*ITMO University, Kadetskaya Liniya V.O. 3b, Russian Federation*
[2]*Almazov National Medical Research Center, Ul. Akkuratova 2, Russian Federation*
E-mail: tmzhang91@gmail.com

The concentrations of blood components play an important role in the diagnosis of blood diseases. The levels of glucose, bilirubin, creatinine and uric acid can simultaneously increase in one patient. For patients with disorders of carbohydrate metabolism, the deviation of the glucose level from normal level is characteristic. In addition, one of the complications of diabetes is diabetic nephropathy with a higher level of creatinine. Type two Diabetes mellitus is often accompanied by a growth of uric acid level, which causes gout [1]. An increase in the level of bilirubin rarely occurs in patients with diabetes, but such increase can be observed with concomitant liver pathological changes [2]. However, the measurement of bilirubin concentrations, as well as other biochemical parameters, is a challenge comparing with the existing measurement methods which are used in routine clinical practice [3]. This is due to the fat obtained from food, which serve as a source of triglycerides, and the growth of its concentration leads to measurement errors [3,4]. Therefore, a new measurement method therefore is necessary to be developed for quick and accurate blood components analysis.

THz radiation has been used in many research areas, such as detection of explosives, quality control, water concentration assessment, as well as medical diagnostics [5-7]. The photon energy in the THz frequency range is very low, so the radiation does not cause ionization in the biotissues [6,7]. Since THz radiation does not cause damage to biological objects, it has a good promise in biomedical applications. Thus, the investigation in blood components measurement methods in THz frequency range has its necessity. In order to qualitatively investigate and analyze the effects between the concentrations of glucose, bilirubin, creatinine, and uric acid in the terahertz (THz) frequency range for future quantitative analysis, the THz time-domain spectroscopy (TDS) was used.

In total 14 conditionally healthy participants aged 24 to 42 years provided their bloods for the experiment. All participants signed an informed consent to participate in the research. The research was approved by the Ethics Committee of the National Medical Research Center. V. A. Almazova.

The samples of whole venous blood were collected after 8-13 hours of fasting. The concentrations of the following biochemical components were measured in the serum: the level of total bilirubin using the colorimetric method, the level of creatinine using the pseudokinetic method. The level of glucose was determined in plasma using the enzyme method. The measurements were carried out by a Cobas c311 analyzer (Roche, Switzerland). Each blood sample were loaded in a special cell, which is shown in Figure 1(a). The groove for blood sample locates at the center of the cell with the depth of 75 μm (Fig. 1(b)).

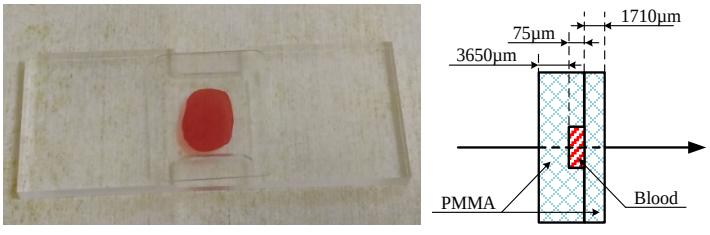

Fig. 1 The cell with blood (a) and the scheme of the cell (b)

A THz TDS in the transmission mode was used to carry out the analysis. For each blood sample, the waveform of THz pulse that passed through the empty cell is considered as the reference signal, while the waveform of THz pulse that passed through the cell with blood is counted as the sample signal. Afterwards, wavelet filtration was used to reduce the effect of noise on the result [8]. Then the Fourier transform was used to obtain its amplitude and phases, corresponding to the frequencies.

Finally, the optical properties such as the refractive index and the absorption coefficient were obtained using following formulas [9]:

$$a(v) = -2\ln\left[\frac{E_{sample}(v)}{E_{reference}(v)}\right]/d$$

$$n(v) = 1 + c\left[\phi_{sample}(v) - \phi_{reference}(v)\right]/[2\pi v d]$$

where a – absorption coefficient of the sample, n – refractive index of the sample, $E_{reference}$ and $\phi_{reference}$ – the amplitude and the phase of the reference signal, respectively. E_{sample} and ϕ_{sample} – the amplitude and the phase of the sample signal, respectively.

Since the maximum intensity of the THz signal is at the frequency of 0.4 THz, this frequency was chosen for further investigation. As a result, the correlations between the blood optical properties and the concentrations of the blood components were revealed. Since it has been proved that the glucose level affects the optical properties of the whole blood in the THz frequency range [10], in this experiment the samples, of which the glucose level varying in a narrow range, were chosen. The correlations between the optical properties and the concentrations of bilirubin, creatinine and uric acid with the glucose level ranging from 5.0 to 5.5 mmol / l are shown in Figures 2.

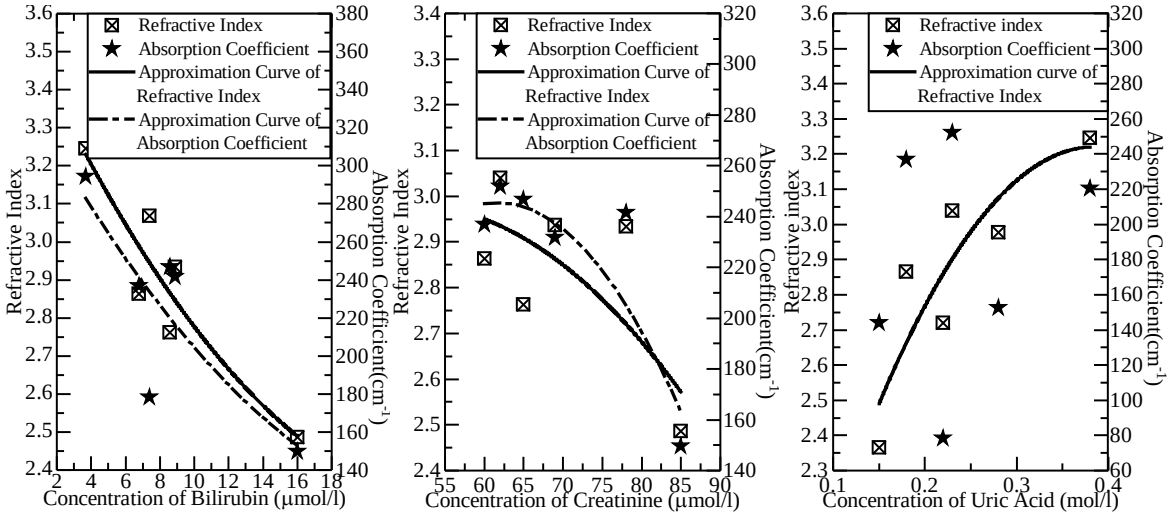

Fig. 2 The correlations between the optical properties and the concentrations of bilirubin, creatinine and uric acid

The results show that the refractive index and the absorption coefficient of blood decrease along with an increase in the concentration of bilirubin and creatinine, while the refractive index increase along with an increase in the concentration of uric acid. There is no correlation between the absorption coefficient and the concentration of uric acid. The results provide a prospect to consider the possibility of using THz TDS not only for determining the level of blood components, but also for determining the concentrations of other biological substances. However, because of the significant fluctuations in the concentrations of glucose, creatinine, uric acid under the influence of many factors (physical activity, nutrition, etc.) [3], quantitative measurement cannot yet be carried out. To establish a mathematical model of the correlation between the optical properties and the concentrations of the blood components, further researches on qualitative measurements of each component in THz frequency range are needed.

References

[1] A. Dehghan, A. Köttgen, Q. Yang, et al., Association of three genetic loci with uric acid concentration and risk of gout: a genome-wide association study. *The Lancet*, **372** (9654), 1953 (2008)
[2] J.M. Saudubray, G. Berghe, J. Walter, Inborn metabolic diseases. – 658 p. (2012).
[3] N. Naser, S. Naser, Clinical Chemistry Laboratory Manual. – 360 p. (1998).
[4] S. Klotzsch, J. McNamara, Triglyceride measurements: a review of methods and interferences. Clin Chem., **36**(9), 1605 (1990).
[5] A. Pawar, D. Sonawane, K. Erande, et al., Terahertz technology and its applications, *Drug invent. today*. **5**, 2 (2013).
[6] X. C. Zhang, J. Xu, Introduction to THz wave photonics. – 246 p. (2010).

[7] C. Reid et al. Terahertz time-domain spectroscopy of human blood, *IEEE Trans. Terahertz Sci. Technol* **3**(4), 363 (2013).
[8] G. Strang, T. Nguyen, Wavelets and Filter Banks. – 401 p. (1996).
[9] Dexheimer S. L. Terahertz Spectroscopy: Principles and Applications. – 360 p. (2007).
[10] S. Gusev, P. Demchenko, O. Cherkasova, et al. Influence of glucose concentration on blood optical properties in THz frequency range, Chinese Optics **11**(2), 182 (2018).

Study on removal of low thermal conductivity paint by high repetition rate pulsed laser

Z. Zhang, Y. Wang, and X. Lin
Institute of Semiconductors, Chinese Academy of Sciences
E-mail: zyzhang@semi.ac.cn

A high repetition rate pulsed laser was used to study the quantitative removal of low thermal conductivity resin based paint. Firstly, when we use a two-dimensional vibrating mirror system for laser cleaning, we have studied the selection of the scanning mode and the distribution characteristic of the light spot on the material surface and the calculation of the overlap rate. Secondly, the high repetition rate pulse laser is applied to the surface of the low thermal conductivity material and the temperature change of the material surface is simulated. High repetition rate pulsed laser ablation of gasifying low thermal conductivity materials has a linear correlation with the number of pulse on the material surface and the depth of ablation and gasification. Finally, based on the analysis results, we proved the existence of the linear correlation. This study provides theoretical and experimental support for the quantitative removal of lacquer by laser.

Passive coherent beam combination of three Nd:YAG lasers using cascaded Michelson-type compound cavities

P. Zhao, Z. Dong, J. Zhang, and X. Lin
Institute of Semiconductors, Chinese Academy of Sciences
E-mail: pfzhao@semi.ac.cn

High-power lasers (HPLs) with good beam quality have attracted great attention due to their widespread applicability in various areas such as material processing, scientific research, and military services. However, single-aperture HPLs are typically achieved with a trade-off on the beam quality. A coherent beam combination (CBC) of multiple lasers is a promising solution to increase the output power while improving the beam quality of laser sources. In the past two decades, significant attention has been paid to CBCs or phase-locking technology of multiple lasers using one of the following techniques: the Talbot cavity, Fourier cavity, Michelson cavity, grating cavity, master oscillator power-amplifier (MOPA) technique with active phase control, and multichannel laser cavity. However, side-by-side elements may cause a near-field intensity fill factor to be less than one and result in multiple lobes in the far field if the phase difference between adjacent elements is not zero. For example, single-lobe output techniques using the Talbot cavity involve in-phase mode selection and multimode suppression, and thus their implementation requires careful design. In these phase-locking techniques, precise and complex control of the phase of laser arrays is required. MOPA techniques based on the active phase correction are typical representatives of controlling the phase of each channel. The center wavelength of each individual amplifier channel is locked by optical injection from a master oscillator. In 2011, MOPA design made significant progress. Massachusetts Institute of Technology has demonstrated a coherent combined 4-kW output when it is operated at full power with a beam quality of 1.25 times of diffraction limit. To date, such an active phase-locking CBC technology is very promising, except that its feedback control technique is slightly complicated. The Michelson cavity-based techniques are also the representatives of the passive phase-locked method because they are characterized by self-organized phase locking. In general, a Michelson-type cavity is applied to the combination of two lasers; nevertheless, the beam-combination features are different from those of laser arrays because the output is common modes of two equivalent cavities, which do not produce interference fringes in the best state of adjustment.

In this paper, we present a coaxial multibeam passive coherent combination technique using cascaded Michelson-type compound cavities (CMTCCs) that can combine multiple lasers into a single beam rather than intersecting in the far field. In this new structure, the laser beam emitted from each laser element is forced to coaxially overlap with the same waist position, waist size, and divergence angle. The beam waist separation caused by the optical path difference (OPD) is eliminated by inserting a 4f optical system into the space of the adjacent laser elements. The 4f optical system is a telescope with finite conjugates one focal distance (f_1) to the left of the objective and one focal distance (f_2) to the right of the collector, respectively consists of a cascade of two Fourier transforms so that the object distance if twice of the focal length of the first lens and the image distance is twice of the focal length of the second lens. It is commonly used for image relay in Fourier Optics. At the same time, a CBC occurs when the laser elements are mutually injection locked, and the beam quality can be improved in the case of in-phase output when the phase differences among the laser beams are adjusted to zero at the coaxis. In this way, the total output power can be increased by summing the outputs of all the laser elements used with an improved beam quality. A proof-of-concept experiment shows that three 65 W Nd:YAG lasers with an M^2 factor of about 5.5 were coherently combined into a 124.4 W single lobed output improving the M^2 factor to 1.36. The central lobe accounted for 76% of the total power, corresponding to a total combined efficiency of 66.7%.

Superradiance by nitrogen ions in atmospheric filament

I.A. Zyatikov, N.G. Ivanov, V.F. Losev, and V.E. Prokop'ev
Institute of High Current Electronics SB RAS, 2/3 Akademichesky Avenue, Tomsk, 634055, Russia
E-mail: werop@sibmail.com

Cavity-free lasing of the nitrogen molecules and ions in plasma pumped by ultrafast laser is intensively studied [1-3]. By focusing a linearly polarized femtosecond laser pulse at 800 nm in ambient air or pure nitrogen and in the presence of the external seed operating at wavelength near 400 nm, one observes an intense directional and linearly polarized emission at 391.4 and/or 427.8 nm in the forward direction [4]. These wavelengths correspond to the transitions from $B^2\Sigma^+_u$ excited state to $X^2\Sigma^+_g$ fundamental state of singly ionized nitrogen molecules with vibrational quantum number $v = 0$ or $v = 1$. Recent time-resolved measurements have shown that these emissions are of the nature of superradiance, a kind of collective spontaneous emission [5].

The external seed is an analogue of the third and fifth harmonics of the pumping laser operating in the middle IR region. It has been demonstrated in [6] that in the case of self-seed the 391-nm lasing strongly depends from the pump laser wavelength. The air lasing occurs only when the high-order harmonic or the supercontinuum white light covers the wavelength of the corresponding transition. Recently it was shown that superradiance at $\lambda = 427.8$ nm can be obtained by pumping a cell with pure nitrogen by femtosecond laser beam with $\lambda = 950$ nm [7, 8]. Supercontinuum (SC) white light appears as the induced radiation that results in an exponential increase in the number of photons at laser transitions of molecular nitrogen ions [9, 10].

In spite of a large number of experimental studies in this field, it is still incompletely clear how population inversion and lasing occur in the filament plasma at the above transitions in molecular nitrogen ions. In this work, we demonstrate that coherent light amplification at the electron transition of N_2^+ ions can indeed be induced in a plasma filament without seed.

The laser radiation of Start-480 fs-complex, which is a part of THL-100 laser system, was used for filament formation. Beams of the output radiation at 940-950 nm had diameters of 1 cm, pulse length of 50 fs, and energy up to 15 mJ. The filament was formed in a focused beam in air and the glow spectrum was measured along the pumping radiation propagation direction and across it using the spectrometer Ocean Optics HR4000 (resolution of 0.03 nm; 250-425 nm wavelength range). The temporal behavior of molecular nitrogen ions radiation was recorded with the spectrometer (Acton SpectraPro SP-2300, resolution of 0.27 nm) and the streak camera (Hamamatsu, Universal Streak Camera C10910, time resolution of 2 ps). In order to set the reference point in time and establish the temporal resolution of the streak camera, the duration of second harmonic (SC) was measured simultaneously with the superradiance.

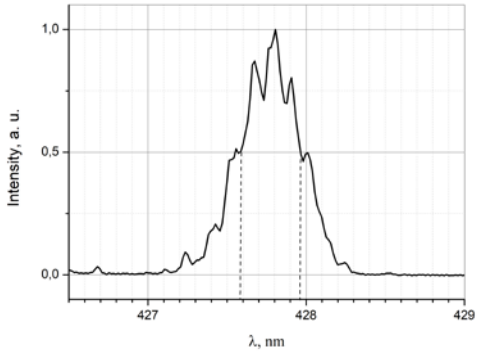

Fig. 1 Spectrum of radiation propagating along the pumping direction.

Short duration is one of the important parameter of superradiance at wavelength of 427.8 nm. In our conditions, the spectral width of this line was about 0.4 nm at half maximum of the intensity (Fig. 1). If we take into account that the maximum spectral resolution of the streak camera is 0.2 nm for an optical grating period of 1200 grooves/mm, then, according to the uncertainty principle for

Gaussian beams $\Delta\nu\Delta t \geq 0.441$, the real spectral width is 0.2 nm and the pulse length is no less than 1.34 ps.

In respect that temporal resolution of streak camera, the real pulse duration value is less than 1.4 ps and approximately coincides with the lower boundary (1.34 ps) (Fig. 2(a)). Fig. 2(b) shows the spontaneous emission of molecular nitrogen ions measured across the filament. It can be seen from this figure, that there is a delay between the intensity maxima of the second harmonic and the 427.8 nm emission. This means that the spontaneous emission arises later than the femtosecond pumping pulse. The same result was obtained by other authors [2]. The question about the reason for the appearance of this delay remains open.

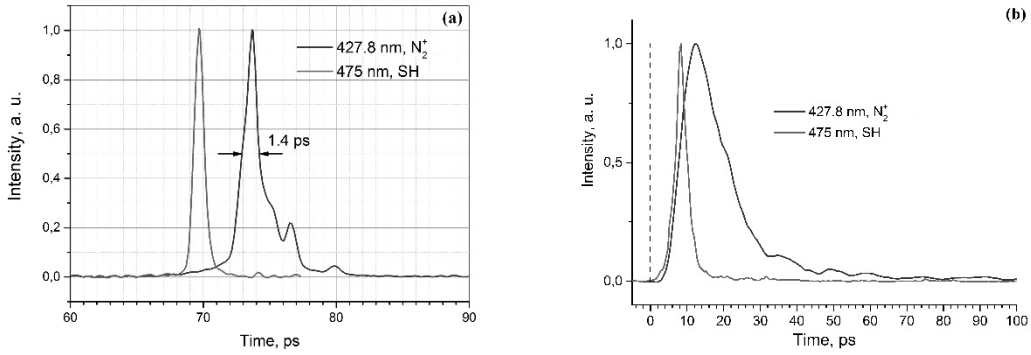

Fig. 2 (a) Superradiance pulse of 427.8 nm lasing signal. (b) Spontaneous emission of N_2^+ ions propagating across the pumping direction.

Our experiment stood out for occurrence of 427.8 nm superradiance with the use of 950 nm pump radiation only. The photon energy for this pump wavelength is 1.3 eV; hence, multiphoton ionization at the upper laser level (18.7 eV) requires 15 photons; the energy exceeds the level $B^2\Sigma^+_u$ (v = 0) by 0.88 eV in this case. When operating with λ = 800 nm [1-6, 9, 10], 13 photons are required, which provides for total energy of 20.15 eV and excess over the upper laser level by 1.45 eV. This means that the resonance energy transfer to the upper laser level is more efficient for 950 nm than for 800 nm.

The SC is one of the conditions for superradiance appearance in our case. At long-focal-length, the SC is axial and at short-focal-length the SC is conical [11]. In our experiment, the focal length was 13.7 cm and the SC was conical. The photons of this conical SC, which occurs in the filament, are, probably, act as the seed photons and launch the superradiance at molecular nitrogen ion transitions.

Thus, the 427.8 nm superradiance was produced in atmospheric air by molecular nitrogen ions by pumping with femtosecond radiation pulses at the central wavelength of 950 nm. The spectrum line width and the pulse duration were experimentally measured taking into account resolution of the streak camera. According to these measurements, the real pulse duration of superradiance is in the range of 1.34 - 1.4 ps. It is noteworthy that the pulse duration measured by other authors was tens of picoseconds [2, 12]. It was shown that the population inversion at $B^2\Sigma^+_u$ - $X^2\Sigma^+_g$ transition of molecular nitrogen ion occurs by multiphoton excitation of N_2^+ ($B^2\Sigma^+_u$) state with energy of 18.7 eV.

References

[1] Y. Liu, P. Ding, N. Ibrakovic et al., PRL **119**, 203205 (2017).
[2] X. Zhong, Z. Miao, L. Zhang et al., Phys. Rev. A **96**, 043422 (2017).
[3] M. Lei, C. Wu, A. Zhang et al., Opt. Express **25**, 4535 (2017).
[4] J. Yao, S. Jiang, W. Chu, et al., PRL **116**, 143007 (2016).
[5] G. Li, C. Jing, B. Zeng et al., Phys. Rev. A **89**, 033833 (2014).
[6] Q. Luo, W. Liu, and S. Chin, Appl. Phys. B **76**, 337 (2003).
[7] V. Prokopev, N. Ivanov, D. Krivonosenko, and V. Losev, Rus. Phys. J. **56**, 1274 (2014).
[8] N. Ivanov, V. Losev, V. Prokopev, and K.A. Sitnik, Atmospheric and Ocean Optics **29**, 385 (2016).
[9] Y. Liu, Y. Brelet, G. Point et al., Opt. Express **21**, 22791 (2013).
[10] T. Wang, J. Ju, J. Daigle et al., Laser Phys. Lett. **10** (12), 1 (2013).
[11] Z. Xu, X. Zhu, Y. Yu et al., Scientific Reports **4**, 3892 (2014).
[12] W. Chu, G. Lie. H. Xie et al., Phys. Lett. **11**, 015301 (2014).

SCIENTIFIC EQUIPMENT
COMPANY GROUP

WWW.SPEGROUP.RU
Novosibirsk, Inzhenernaya str., 4a, office 212
+7 (383) 330-82-95, sales@spegroup.ru

MANUFACTURING, RESEARCH & DEVELOPMENT EQUIPMENT

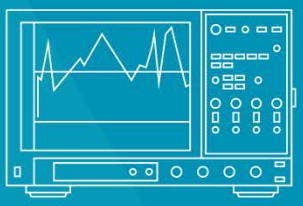

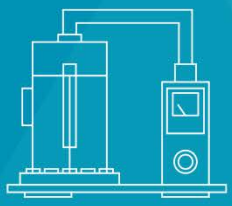

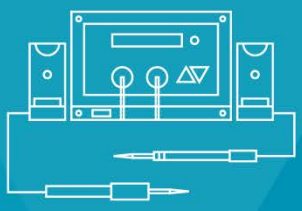

MAJOR ACTIVITIES:

- Radiophysics and Electronics
- Electricity and Magnetics
- Environmental monitoring
- Testing and Quality Control
- Microscopy
- Sample Preparation
- Furnaces and Drying Ovens
- Soldering and assembly components
- Laboratory furniture and supplies
- Vacuum equipment
- Systems for frame-by-frame and video recording of processes
- Microelectronics
- Photonics
- Chemical and structural analysis
- Water and Gas Preparation
- Chemical Reagents
- Spectrometry
- Particle size measuring
- Chromatography
- 3D scanning and printing
- Analytical equipment for geology
- Biotechnology

The *Nauchnoe Oborudovanie* group of companies was founded in 1999. It is one of the biggest suppliers of scientific and industrial equipment in Siberia and in the Far East with core activities covering provision of research institutes and industrial enterprises with high-tech equipment.

We analyze the customer's problem and select appropriate equipment to deal with a specific challenge. We supply instruments, provide technological and methodological support as well as warranty and post-warranty service. From delivering a single product to fulfilling complete enterprise supply programs, *Nauchnoe Oborudovanie* always meets its commitments and has gained the reputation of so reliable partner that some customers entrust us with complete equipping of their laboratories including both instruments and consumables.

Highly skilled technical specialists with their own research experience who constantly improve their professional level make our team. We regularly get acquainted with the new equipment and approaches in instrument engineering, and attend international exhibitions and training seminars organized by the manufacturers. We can offer the most advanced solutions for any customers' task. The existing working relationship with many laboratories of SB RAS allows inviting field experts to satisfy the customer's unique needs. Moreover, we conduct workshops providing our customers with an opportunity to try the latest equipment.

We have established partnership relations with many the world's leading manufacturers of scientific and technological equipment, both in Russia and abroad. Besides, we have our own engineering department; if necessary, we can develop and produce an instrument to solve the customer's problem.

The institutes of the Siberian Branch of the Russian Academy of Sciences focused on the fundamental research, many industrial enterprises, engineering companies, higher education institutions of the Siberian and Far Eastern regions are among our customers.

In addition to supply and production of equipment, we are engaged in the promotion of the scientific developments with commercial potential of institutes of the Russian Academy of Sciences in the foreign markets, and organize joint projects of the SB RAS institutes with different organizations to develop specific technological and knowledge-based solutions.

We see our goal to create and maintain long-standing mutually beneficial relationships with each customer.

Contact us:

Russia, Novosibirsk, Inzhenernaya str., 4a, office 212

Tel./fax: +7 (383) 330-82-95

E-mail: sales@spegroup.ru

www.spegroup.ru